OLEFIN OLIGOMERIZATION REACTIONS: THEORETICAL STUDIES USING CYCLOMETALLATED PALLADIUM(II) CATALYSTS AND EXPERIMENTAL STUDIES ON PLATINUM(II) ANALOGUES

Feng Zheng

A thesis submitted in fulfilment of the requirements for the degree of Doctor of Philosophy

Department of Chemistry
University of Cape Town

Supervisors:
Prof. John R. Moss (deceased 31 May 2010)
Assoc. Prof. Alan T. Hutton
Prof. Selwyn F. Mapolie (Stellenbosch University)
Dr. Cornie G.C.E. van Sittert (North-West University)

July 2012

DECLARATION

I know the meaning of plagiarism and declare that all of the work in this thesis, save for that which is properly acknowledged, is my own.

……..

Feng Zheng

July 2012

ACKNOWLEDGEMENTS

I would like to express my sincere thanks to the following people:

My supervisors, Associate Professor Alan Hutton, Professor Selwyn Mapolie and Dr Cornie van Sittert, for their guidance and encouragement, and for the invaluable advice and knowledge that contributed so greatly to this project.

The analytical staff at the University of Cape Town: Mr Pete Roberts and Mr Noel Hendricks for NMR spectra, Mr Piero Benincasa for elemental analysis, and Dr Hong Su for X-ray structure determinations. The mass spectrometry staff at the University of Stellenbosch, for mass spectra.

Dr Werner Janse van Rensburg for all the discussions and invaluable advice with the problems relating to DFT study. Dr Gregory Smith for his help in the lab. Dr Emma Hager for taking the time to read my thesis.

My colleagues and friends in the Organometallic/Transition Metal Research group, for their friendship and assistance over the years. Thank you all!

All my friends and family who have supported and encouraged me throughout the years of research and the writing of this thesis. Special thanks to my Mother, Ms Bao'E Zheng and to my husband, Dr Jiang Wu, as well as my little Vicky, for their love and for believing in me.

I wish to express gratitude to c* change DST-NRF Centre of Excellence and UCT for financial support.

Lastly, I would like to acknowledge my late supervisor, Professor John Moss, whose enthusiasm for and love of organometallic and transition metal chemistry first sparked my own interest.

ABSTRACT

Ethylene oligomerization reactions catalysed by cyclometallated palladium(II) *N*-benzylidenebenzylamine complexes were studied theoretically. Density functional theory (DFT) calculations are reported on the interaction of various MAO models with the methylated pre-catalyst. The neutral MAO dissociation process is shown to remain the major interaction that takes place in the Pd/MAO interactions. On the other hand, the formal methyl abstraction process could be also feasible if more energy is provided. Therefore, the relative energies were calculated for intermediates and transition states for both Cossee-type and metallacycle mechanisms. The Cossee-type mechanism was found to be more likely due to the favourable thermodynamics calculated with each uptake of ethylene compared to the metallacycle mechanism. From the DFT results, the difficulty of forming the *trans*-methylpalladium(II) species **III-s** (where PPh_3 is *trans* to the N atom) is the key factor resulting in the low activity of the ethylene oligomerization reactions. The high energy barrier for the *cis/trans* isomerization process prior to ethylene uptake results in the formation of ethylene dimers as the predominant products.

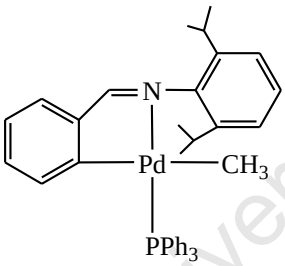

III-s

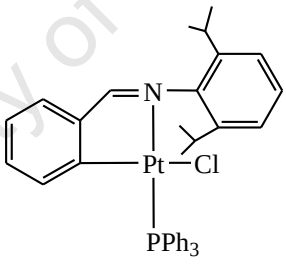

C4

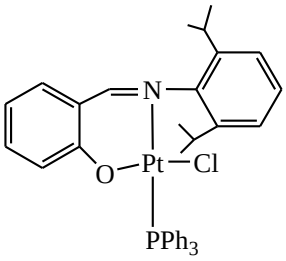

C5b

On the experimental side, cyclometallated platinum(II) PPh_3 complexes were synthesized as model complexes of the palladium pre-catalysts from dmso-ligated precursors. The methylation reaction of the *trans* platinum(II) complex **C4** was found to be consistent with the DFT-calculated methylation reaction of the analogous palladium pre-catalyst, i.e., the *cis*-methylplatinum(II) complex was produced as the major product. In addition, the salicylaldimine (N^O) platinum(II) analogues (e.g. **C5b**) were synthesized because salicylaldimine palladium(II) complexes are well established as pre-catalysts in ethylene oligomerization/polymerization. The influence of both N^C and N^O ligands in the platinum(II) complexes was investigated by analysis of their spectroscopic and structural properties, and various reactivity studies were undertaken. The N^C platinum(II) complexes

were found to be generally more stable than their N^O analogues from both thermodynamic and reactivity points of view. Cyclic voltammetry results for the 1,1'-bis(diphenylphosphino)ferrocene (dppf) complexes of these ligands confirmed that the N^C ligand is a better electron-donor ligand compared to the related N^O ligand, which could explain the DFT prediction of the formation of dimers as major products in ethylene oligomerization reactions.

ABBREVIATIONS

Å	angstrom
acac	acetylacetone
Ar	aromatic
atm	atmosphere
BMI	butylmethylimidazolium
br	broad
ca.	approximately
calc	calculated
COD	cycloocta-1,5-diene
δ	chemical shift
°	degrees
℃	degrees Celsius
CV	cyclic voltammetry
DCM	dichloromethane
DFT	density functional theory
DMSO	dimethyl sulfoxide
d	doublet
dd	doublet of doublets
ddd	doublet of doublet of doublets
dppf	1,1'-bis(diphenylphosphino)ferrocene
dt	doublet of triplets
EASC	ethylaluminum sesquichloride
EI-MS	electron impact mass spectrometry
ESI-MS	electrospray ionization mass spectrometry
Eq	equation
Equiv	equivalent(s)
Et	ethyl

Et_2O	diethyl ether
FT-IR	Fourier transform infrared spectroscopy
g	gram(s)
GC	gas chromatography
h	hour(s)
Hz	Hertz
^{i}Pr	isopropyl
IR	infrared
J	coupling constant
MHz	megaHertz
Me	methyl (CH_3)
m	multiplet
M.p.	melting point
m/z	mass to charge ratio
MAO	methylaluminoxane
MMAO	modified methylaluminoxane
min	minute(s)
mL	millilitres
mmol	millimoles
Mn	number average molecular weight
NMR	nuclear magnetic resonance
PE	polyethylene
PES	potential energy surface
Ph	phenyl
ppm	parts per million

ppy	deprotonated 2-phenylpyridyl
py'	4-(5-nonyl)pyridine
q	quartet
RT	room temperature
s	singlet
sh	square-hexagonal
sept	septet
ss	square-square
tlc	thin layer chromatography
t	triplet
tt	triplet of triplets
^{t}Bu	tertiary-butyl
THF	tetrahydrofuran
TMA	trimethylaluminum
TOF	turnover frequency
wt	weight

TABLE OF CONTENTS

Declaration i

Acknowledgements ii

Abstract iii

Abbreviations v

Table of Contents viii

Chapter 1

Recent Developments with Palladium-Catalysed Ethylene Dimerization and Oligomerization 1

1.1 Introduction 1

1.2 Palladium Catalysts for Ethylene Oligomerization 3

1.2.1 Complexes with N^N chelates 15

1.2.1.1 α-Diimine ligands 15

1.2.1.2 Iminopyridine ligands 16

1.2.1.3 Bis(*N*-heterocycle)methane ligands 18

1.2.1.4 Phenanthroline and bis(azaferrocene) ligands 19

1.2.2 Complexes with P^N chelates 20

1.2.2.1 Phosphino- and phosphaalkene-imine ligands 21

1.2.2.2 Phosphino-pyridine ligands 23

1.2.2.3 Phosphino-oxazoline and -quinoline ligands 24

1.2.3 Complexes with P^O chelates 25

1.2.4 Complexes with N^O chelates 29

1.2.5 Complexes with other ligands 30

1.3 General Factors Affecting Oligomerization Reactions 32

1.4 Mechanisms of Palladium-Catalysed Ethylene Oligomerization/Polymerization 33

1.4.1 Overall mechanism 33

1.4.2 Chain initiation, propagation and isomerization: NMR spectroscopic approach and computational insights 36

1.5 Conclusions 41

1.6 Aims and Objectives of the Thesis 42
1.6.1 Aims 42
1.6.2 Specific objectives 43
1.7 References 45

Chapter 2
DFT Insight into Role of MAO in Catalyst Activation and a Probe into Possible Mechanisms for Cyclometallated Palladium-Catalysed Oligomerization 52

2.1 Introduction 52
2.2 Functional Validation and Ligand Dissociation in Palladium Complex 60
2.2.1 Functional validation 60
2.2.2 Pd-ligand bond dissociation energies 61
2.3 The Role of MAO in the Activation of Pd Pre-catalyst 64
2.3.1 Palladium model and MAO models 65
2.3.1.1 Palladium model 65
2.3.1.2 MAO models 65
2.3.2 Palladium complexes in the presence of MAO models 67
2.3.2.1 $(AlOMe)_6$-TMA model 67
2.3.2.2 $(AlOMe)_9$-TMA models 69
2.3.2.3 Discussion on Pd-MAO interactions 71
2.4 Possible Mechanisms for Cyclometallated Palladium-Catalysed Ethylene Oligomerization 73
2.4.1 Mechanism A: Cossee-type pathway 74
2.4.1.1 Chain growth initiation 75
2.4.1.2 Chain transfer 87
2.4.1.3 Chain propagation: ethylene dimerization and trimerization 90
2.4.2 Mechanism B: metallacycle pathway 98
2.4.2.1 Exploration of crucial elementary steps in the mechanism 100
2.4.3 Discussion on the theoretical studies of a possible mechanism 112
2.4.3.1 The entire catalytic reaction course: comparison between Cossee-type and metallacyclic mechanisms 112

2.4.3.2 Discussions on Cossee-type mechanism 117
2.5 Conclusions 119
2.6 References 121

Chapter 3
Dimethylsulfoxide Platinum(II) Complexes of *N*-benzylidenebenzylamine and *N*-salicylidenebenzylamines: Spectroscopic and Structural Investigations of the Influence of Chelate Ligands 127

3.1 Introduction 127
3.2 Results and Discussion 130
3.2.1 Synthesis and characterization of dmso platinum(II) complexes 130
3.2.1.1 Cyclometallated platinum(II) complex of (benzylidene)(2,6-diisopropylphenyl)amine 130
3.2.1.2 Platinum(II) complexes of salicylidenebenzylamines 131
3.2.1.3 IR spectroscopy and mass spectrometry 133
3.2.1.4 NMR spectroscopy 138
3.2.1.5 Crystal structures 140
3.2.1.6 Thermal analysis 147
3.3 Conclusions 149
3.4 References 151

Chapter 4
Phosphine Platinum(II) Complexes: Spectroscopic, Structural, Reactivity and Electrochemical Investigations of the Influence of Chelate Ligands 154

4.1 Introduction 154
4.2 Results and Discussion 155
4.2.1. Reactions with phosphines 155
4.2.1.1 IR spectroscopy and mass spectrometry 159
4.2.1.2 NMR spectroscopy 161
4.2.1.3 Crystal structures 166
4.2.2 Methylplatinum(II) complexes 172

4.2.2.1 Methylplatinum(II) complex of N^C chelate ligand 173
4.2.2.2 Methylplatinum(II) complex of N^O chelate ligand 174
4.2.2.3 IR, NMR spectroscopy and mass spectrometry 175
4.2.2.4 Crystal structure 179
4.2.2.5 Discussion 180
4.2.3 Cyclic voltammetry studies of ferrocene-containing complexes 184
4.2.4 *Cis*-to-*trans* isomerization of Pt(N^O) complex 186
4.2.4.1 Kinetic studies 187
4.2.4.2 DFT studies 189
4.3 Conclusions 192
4.4 References 195

Chapter 5
Conclusions 198

5.1 Conclusions 198
5.2 References 202

Chapter 6
Experimental Details 203

6.1 General Remarks 203
6.2 Instrumentation 203
6.3 Preparation of the Platinum(II) Complexes 204
6.4 Isomerization Kinetics (**C5a→C5b**) 214
6.5 X-ray Structure Analysis 214
6.6 Computational Methods 215
6.6.1 Hardware 215
6.6.2 Software 215
6.7 Reference 217

CD-Rom
Support information 1 (for theoretical studies)

Support information 2 (for Experimental studies)

CIF files of X-ray structures

Chapter 1

Recent Developments with Palladium-Catalysed Ethylene Dimerization and Oligomerization

1.1 Introduction

α-Olefins in the range $C_4 - C_{20}$ are widely used as co-monomers in the polymerization of ethylene to give linear low-density polyethylene (LLDPE)[1] or for the preparation of detergents and synthetic lubricants.[2–4] There are four main processes that can produce α-olefins: (i) the cracking of paraffins, (ii) the dehydrogenation of paraffins, (iii) the dehydration of alcohols, and (iv) the oligomerization of ethylene.[5] These reactions can be classified as either elimination reactions (i-iii) or chain-growth reactions (iv). The first three processes have become less important for the preparation of α-olefins with the result that the oligomerization of ethylene has become the main source of α-olefins in industry.[6] Therefore, there is considerable current academic and industrial interest in catalytic ethylene oligomerization. The search for new catalysts for the oligomerization of olefins has received much attention over recent years.

The first transition metal catalysts for oligomerization of ethylene were developed by Ziegler and Natta. Linear α-olefins were produced by the Ziegler (Alfen) process which consists of a controlled oligomerization of ethylene in the presence of $AlEt_3$ at 90–120 ^oC at a monomer pressure of 100 bar.[7–9] Since then, transition metal catalysed dimerization and oligomerization of mono-olefins and the related organometallic chemistry have been extensively studied, and some of the comparative data on activity and selectivity is summarized in Table 1.1.[10]

Table 1.1 Comparative characteristics of activity and selectivity of transition metal complexes in the reaction of dimerization and oligomerization of olefins.[10]

	I	II	III	IV	V	VI	VII	VIII		
3	Na	Mg	Al	Si	P	S	Cl			
4	K	Ca	Sc	Ti	V	Cr	Mn	Fe	Co	Ni
	Cu	Zn	Ga	Ge	As	Se	Br			
5	Rb	Sr	Y	Zr	Nb	Mo	Tc	Ru	Rh	Pd
	Ag	Cd	In	Sn	Sb	Te				
6	Cs	Ba	La	Hf	Ta	W	Re	Os	Ir	Pt

High activity, low selectivity

Moderate activity, low selectivity

Low activity and selectivity

High activity and selectivity

Low activity, high selectivity

Currently catalysts used for commercial production of linear α-olefins are either compounds of early transition metals such as titanium tetrachloride in combination with alkylaluminium activators or late transition metal compounds, especially, nickel(II) complexes bearing bidentate mono-anionic ligands (the SHOP process).[11–15] Further research has been focused on late transition metal catalysts as alternatives for olefin oligomerization due to the fact that these complexes generally exhibit reduced activities for olefin insertion relative to early metal catalysts. In this case β-hydride elimination typically competes with chain growth, resulting in the formation of dimers and oligomers.[10] Late transition metals such as iron and cobalt,[16] nickel[17] and palladium (Table 1.2) in conjunction with chelating ligands have been found to be effective catalysts for the oligomerization of olefins.

Among the known systems, palladium complexes have generally been less applied in olefin oligomerization presumably due to their relatively low activity. However, since palladium chloride was considered as a catalyst for the dimerization of ethylene in various solvents,[18] a variety of palladium complexes has been reported, which are potentially capable of catalyzing the oligomerization reactions. In the next section of this chapter, we review palladium complexes with various ligand systems and their use as catalyst precursors for the oligomerization of olefins. In order to have a better understanding of the behaviour of

palladium catalysts in the oligomerization reactions and possibly to improve their performance, a range of reaction parameters were also evaluated in this chapter.

1.2 Palladium Catalysts for Ethylene Oligomerization

Active palladium ethylene oligomerization catalysts can be generated from neutral or cationic catalyst precursors bearing a range of ligand systems with coordination modes such as bidentate N^N, P^N, P^O etc. (Table 1.2). The applications of these chelate ligands in the oligomerization and polymerization of α-olefins and of ethylene in particular, have recently been reviewed in detail.[19–22] The significant steric and electronic asymmetry of these heteroditopic ligands can possibly have a considerable impact on controlling the selectivity in oligomerization reactions occurring at metal centres.[23,24] Another advantage of these ligands is the ease and flexibility of synthesis. Many of these ligands were synthesized following classical condensation methods.

Neutral Pd^{II} dichlorides and methyl(chloro)palladium complexes are generally prepared (unless otherwise specified) by treatment of $[PdCl_2(COD)]$ or the more labile $[PdCl_2(MeCN)_2]$, and [PdMeCl(COD)] with the appropriate bidentate ligands in CH_2Cl_2 or Et_2O, respectively to give yellow-orange solids with a square-planar coordination geometry.[25–29] Monocationic derivatives in the form of $[(L\text{^}L)PdMe(NCMe)]^+X^-$ [$X^- = BF_4^-$, PF_6^-, SbF_6^-, BAr'_4^-, $B(Ar_F)_4^-$, where Ar' = 3,5-$(CF_3)_2$-(C_6H_3)] were prepared by addition of the appropriate halide abstraction reagents to their neutral methyl(chloro) precursors (Eq. 1.1). The obtained complexes maintain the nearly ideal or distorted square-planar geometries around the metal centre.[30–32]

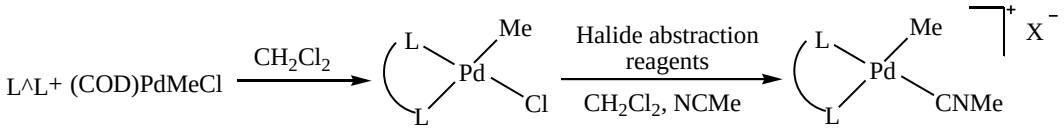

($X^- = BF_4^-$, PF_4^-, SbF_6^-, BAr'_4^-, BAr_{F4}^-) (Eq.1.1)

After the initial observation by Keim,[33] it has become clear over the last decade that careful tuning of ligand properties and choice of appropriate co-catalysts can lead to either oligomers or polymers. Modifications of the steric and electronic properties of the donor function of the chelate ligands are expected to influence the coordination chemistry and catalysis. However,

despite extensive research, the influence of a ligand on catalytic properties of a transition metal complex is still very hard to predict.[34] Many investigations have been reported on the effect of ligand systems or environments in palladium complexes in ethylene oligomerization reactions, e.g., the effect of systematic changes of the backbone in a series of closely related ligands,[35] the effect of changes in chelating properties,[36] etc. An overview of the catalytic results obtained with various Pd^{II} complexes is provided in Table 1.2.

Table 1.2 Palladium complex-based catalytic systems for ethylene oligomerization reactions**.**

Catalytic systems	Reaction conditions	Products	Activity/remarks	Ref
N^N ligands				
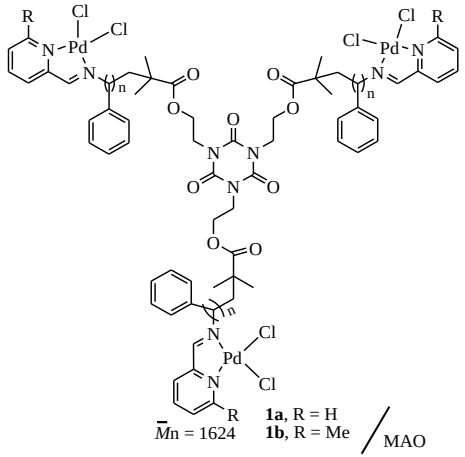 $\bar{M}n$ = 1624 **1a**, R = H **1b**, R = Me / MAO	T = 10 & 30 ^{o}C, P = 5 atm, t = 1 h, Solvent = Toluene (50 ml), Amount of catalyst = 5 μmol, Al:Pd = 1500	Butenes (27.5 – 34.4%) and hexenes(54.9 – 64.1%) and a small amount of higher olefins (7 – 10.8%)	Substantially high activities up to 42.66 x 10^{7} g (mol Pd x h x atm)$^{-1}$	37
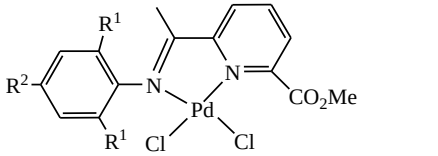 **2a**, R^1 = Me, R^2 = H **2e**, R^1 = F, R^2 = H **2b**, R^1 = Et, R^2 = H **2f**, R^1 = Cl, R^2 = H **2c**, R^1 = i-Pr, R^2 = H **2g**, R^1 = Br, R^2 = Me **2d**, R^1 = Me, R^2 = Me / MAO	T = 20 ^{o}C, P = 8 atm, t = 1 h, Solvent = Toluene (150 ml), Amount of catalyst= 5 μmol, Al:Pd = 1000	Butenes in mixture with polyethylenes (PEs)	Moderate activities up to 180 g (g of Pd x h x bar)$^{-1}$	38
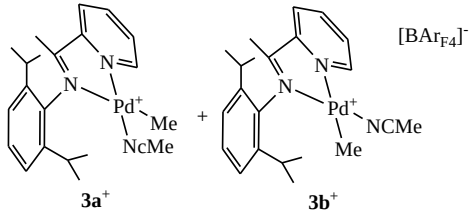 **3a**$^{+}$ **3b**$^{+}$ $[BAr_{F4}]^{-}$	T = 30 ^{o}C, P = 6 atm, t = 18 h, Solvent = CH_2Cl_2 (60 ml), Amount of catalyst= 40 μmol	Light oligomers (C_4-C_{20})	Moderate activities up to 160g (g of Pd x h x bar)$^{-1}$. Efficient long-lived catalyst	30

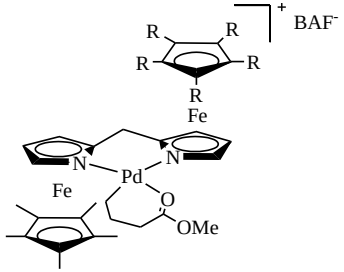 **4a**, R = Me; **4b**, R = Ph	T = 20 – 120 °C, P = 3.4 – 34 atm, t = 2,5 & 24 h, Solvent = Toluene (70 ml), Amount of catalyst = 6, 11 – 14 μmol	Oligomers with molecular weight (M_n) in the range of 200-600 g/mol and branching density from 20 to 60 br./1000 carbons.	Moderate activities with maximum TOF = 2080 h^{-1}.	39
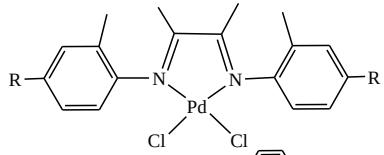 **5a** (G0) **5b** (G1) **5c**: R = H / MAO	T = 40 °C, P = 0.99 atm, t = 1 h, Solvent = Toluene (30 ml), Amount of catalyst = 20 μmol, Al:Pd = 400	Higher carbon oligomers (C_{10}, C_{12}, C_{14+}).	Yields up to 148 mg oligomers.	40
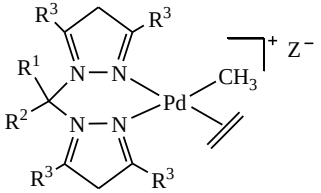 **6a**, $R^1 = R^2$ = Me, R^3 = H **6b**, R^1 = H, R^2 = Si(*p*-tol)$_3$, R^3 = H **6c**, $R^1 = R^2 = R^3$ =H **6d**, $R^1 = R^2$ = H, R^3 = Me **6a-c**, Z = $B(C_6F_5)_4$; **6d**, Z = SbF_6	**6a**: T = 23 °C, P = 1 atm, t = 22 h, Solvent = CH_2Cl_2 (30 ml), Amount of catalyst = 30 μmol **6b**: T = -10 & 25 °C, P = 2.7 & 30 atm, t = 18 h, Solvent = CH_2Cl_2 (20 ml) Amount of catalyst = 30 μmol	Linear internal C_8 - C_{24} olefins (*ca.* 0.1 branches per 2 carbons) for **6a**. Branched C_6-C_{20} internal for **6b**. A mixture of 1-butene and *cis*- and *trans*-2-butenes for **6c-d.**	TOF = 13 x 10^{-3} s^{-1} Catalysts generated in situ.	25, 41, 42
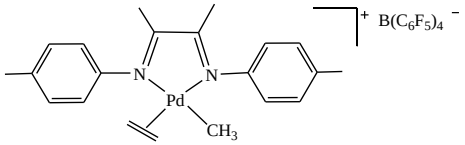 **7**	T = -60 °C, P = *ca.* 96 μmol, Solvent = CD_2Cl_2 (0.7 ml), Amount of catalyst = 16 μmol	1-butene, *cis*- and *trans*-2-butenes. 1-butene:2-butene = 1:6, *cis*-2:*trans*-2 = 1:2		42

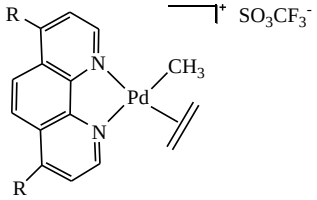 **8a**, R= H **8c**, R = butoxy **8b**, R = CH3 **8d**, R = octyloxy	T = 20 °C P = 5 atm, t = 5 h, Solvent = CH_2Cl_2 (5 ml), Amount of catalyst = 0.19 mmol	Butenes, hexenes and longer alkenes up to C_{20}.	Catalysts generated *in situ*.	43
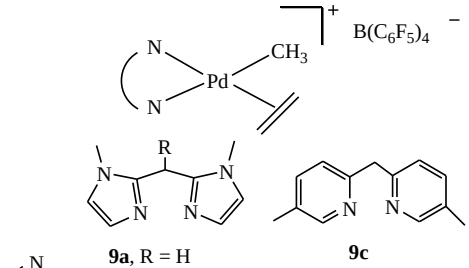 **9a**, R = H **9b**, R = nHex **9c** 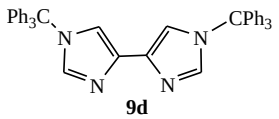 **9d**	T = -60 °C, P = *ca*. 4 -10 equiv, Solvent = CD_2Cl_2 (0.7 ml), Amount of catalyst = 16 - 31 μmol	A mixture of 1-butene and *cis*- and *trans*-2-butenes.	Catalysts generated *in situ*.	42
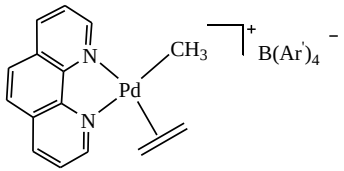 **10**	T = -25 °C, t = *ca.* 5 min, excess ethylene Solvent = $CDCl_3$ (0.7 ml), catalyst = 10 mg	Butenes (*trans*-2 > *cis*-2 > 1).	Catalyst generated *in situ.*	44
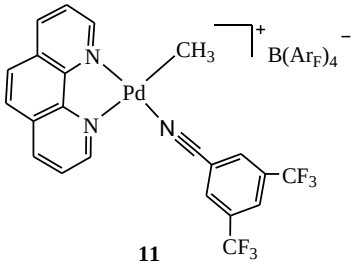 **11**	T = 25 °C, P = 13.6 atm, t = 1 h, Solvent = CH_2Cl_2 (100 ml), Amount of catalyst = 97 μmol	Butenes	Low activity	45

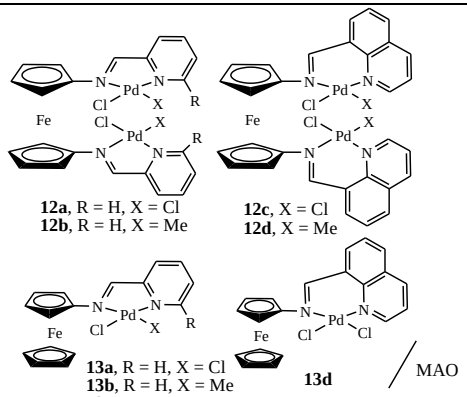 **12a**, R = H, X = Cl **12b**, R = H, X = Me **12c**, X = Cl **12d**, X = Me **13a**, R = H, X = Cl **13b**, R = H, X = Me **13c**, R = Me, X = Me **13d** / MAO	T = 25 °C, P = 0.99 atm, t = 60 min, Solvent = Toluene (100 ml), Amount of catalyst = 10 μmol, Al:Pd = 100		Inactive	26
P^N ligands				
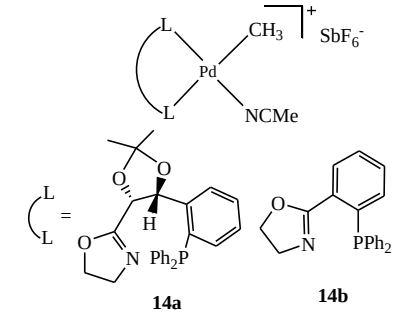 **14a** **14b**	T = 25 °C, P = 13.6 atm, t = 1 h, Solvent = CH_2Cl_2 (100 ml), Amount of catalyst = 97 μmol	A statistical (Schulz-Flory) distribution of olefins up to C_{24} for **14a**, and only C_4 olefins for **14b**.	Moderate activities up to 1.57×10^4 (mol C_2H_4) x (mol Pd x h)$^{-1}$	45
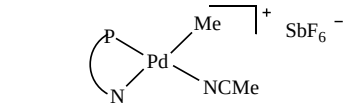 **15a**, n = 1, $R^1 = R^2 = CH_3$ **15b**, n = 1, $R^1 = R^2 = {}^iPr$ **15c**, n = 2, $R^1 = R^2 = CH_3$ **15d**, n = 2, $R^1 = R^2 = {}^iPr$ **15e**, n = 2, $R^1 = OCH_3$, $R^2 = H$ **15f**, n = 3, $R^1 = R^2 = {}^iPr$ 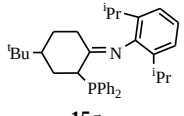 **15g** 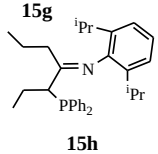 **15h**	T = 70 °C, P = 29.6 atm, t = 2 h, Solvent = CH_2Cl_2 (20 ml), Amount of catalyst = 50 μmol	$C_{12} - C_{34}$ oligomers with a Schulz-Flory distribution	Moderate activities up to TOF = 1337 h^{-1}.	46

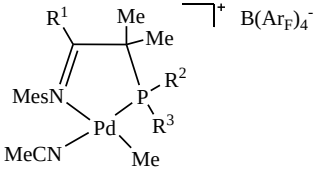 **16a**, R^1 = H, R^2 = Mes, R^3 = Me **16b**, R^1 = Ph, R^2 = Mes, R^3 = Me **16c**, R^1 = Ph, R^2 = R^3 = Me **16d**, R^1 = Ph, R^2 = R^3 = Ph (Mes = 2,4,6-trimethylphenyl)	T = 80 °C, P = 394.8 atm, t = 3 & 15 h, Solvent = Toluene (100 ml), Amount of catalyst = 10 μmol,	Branched oligomers with M_n up to 660 g mol^{-1}.	**16a-b**: low catalytic activity (TOF = 510 h^{-1} for **16a**, 110 h^{-1} for **16b**; **16c-d**: inactive	47
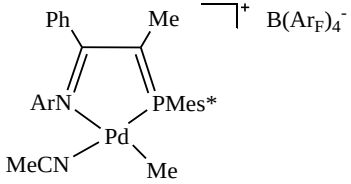 **17a**, Ar = 2,6-di-*i*-propylphenyl; **17b**, Ar = 2,4,6-trimethylphenyl (Mes* = 2,4,6-tri-*tert*-butylphenyl)	T = 26 °C, P = 27.2 atm, t = 3 & 15 h, Solvent = CH_2Cl_2 (100 ml), Amount of catalyst = 10 μmol	Oligomers with M_n in the range of 180 to 670 g mol^{-1}.	Low activity up to TOF = 97 h^{-1}	36
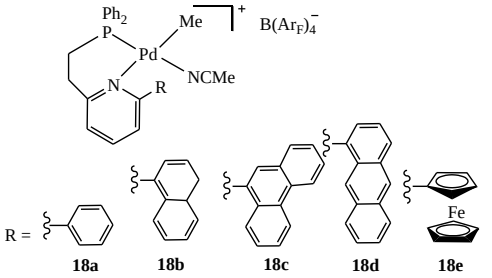 **18a** **18b** **18c** **18d** **18e**	T = 30 °C, P = 9.9 atm, t = 2 h, Solvent = Toluene (25 ml), Amount of catalyst = 100 μmol	C_4 – C_6 olefins	Low activity TOF = 3.1 (mol C_2H_4) x (mol Pd x h)$^{-1}$.	48
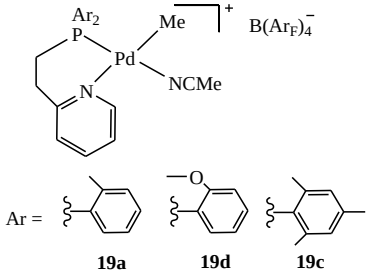 **19a** **19d** **19c**	T = 30 °C, P = 9.9 atm, t = 2 h, Solvent = Toluene (25 ml), Amount of catalyst = 100 μmol	Butenes (41 – 63%) and a significant amount of higher olefins.	Low activities up to 25 (mol C_2H_4) x (mol Pd x h)$^{-1}$	27

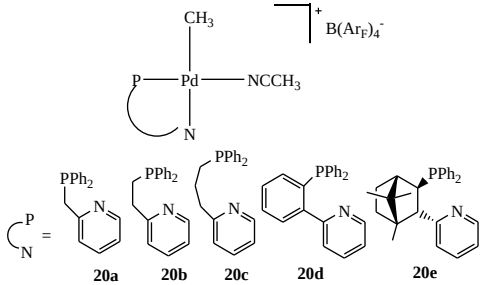 **20a** **20b** **20c** **20d** **20e**	T = 30°C, P = 9.9 atm, t = 2 h, Solvent = Toluene (25 ml), Amount of catalyst = 100 μmol	Short-chain oligomers (C_4-C_{10}) with C_4 as major products.	Low activity up to 16 (mol C_2H_4) x (mol Pd x h)$^{-1}$	35
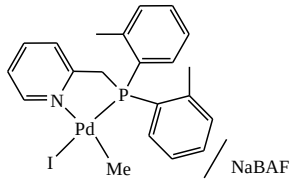 **21**	T = 25 °C, P = 9.9 & 59.2 atm, t = 1 h, Solvent = CH_2Cl_2 (30 ml), Amount of catalyst = 50 μmol	C_8 to C_{32} oligomers along with olefins with a chain length C_n > 32 (<1%).	Low activity	28
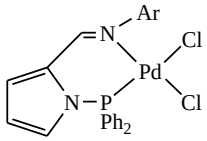 **22a-d**, R = Ph **23a-d**, R = NPr^i_2 **a**, Ar = Ph **b**, Ar = 3,5-Me_2-C_6H_3 **c**, Ar = 2,4,6-Me_3-C_6H_2 **d**, Ar = 2,6-$^iPr_2$-C_6H_3	T = 25 °C Amount of catalyst = 50 μmol, MAO: P = 0.99 atm, t = 30 min, Solvent = Toluene (100 ml), [Al]: [Pd] = 500. $EtAlCl_2$: P = 9.9 atm, t = 3 h, Solvent = Toluene (20 ml), [Al]: [Pd] = 4.5.		Inactive	29
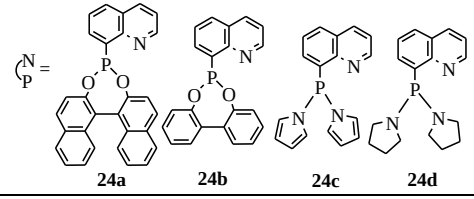 **24a** **24b** **24c** **24d**	Using triisobutylaluminium ($^iBu_3Al$) at 7.9 – 59.2 atm, and up to 80 °C		Inactive	31

P^O ligands			
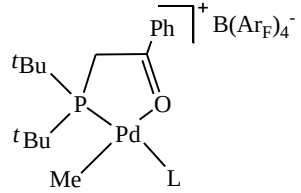 **25a**, L = Et_2O **25b**, L = NCMe	T = 25, 60, 80 °C, P = 1, 13.6 atm, t = 3 h, Solvent = Toluene (100 ml), Amount of catalyst = 3.88 & 10 μmol	Oligomers with M_n in the range of 280 to 400 g mol^{-1}.	Moderate activity, TOF up to 2 x 10^4 h^{-1}	49
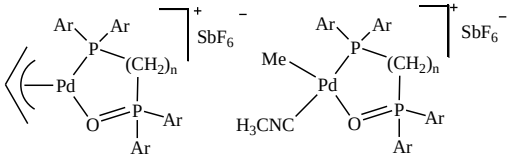 **26a**: n = 1, L = dppmO **26b**: n = 2, L = dppeO **26c**: n = 1, L = dtolpmO **27a**: n = 1, L = dppmO **27b**: n = 2, L = dppeO **27c**: n = 1, L = dtolpmO	T = 70 °C, P = 29.6 atm, t = 2 h, Solvent = CH_2Cl_2 (20 ml), Amount of catalyst = *ca*. 0.05 mmol	C4 – C12 oligomers with a Schulz-Flory distribution, in which butenes are the major products (65 – 85%)	Moderate activity, TOF up to 8.97 x 10^3 h^{-1}	50
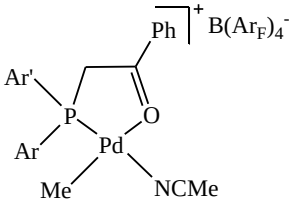 **28a**, Ar, Ar' = C_6H_5 **28b**, Ar, Ar' = 2,4,6-$(CH_3)_3C_6H_2$ **28c**, Ar = 2,4,6-$(CH_3)_3C_6H_2$; Ar' = C_6H_5	T = 25 °C, P = 13.6 atm, t = 0.5 & 1 h, Solvent = Toluene (105 ml), Amount of catalyst = 3.24 μmol	Mainly butenes and a small amount of hexenes	Moderate activity, TOF up to 8.8 x 10^3 h^{-1}, short catalyst lifetime	51
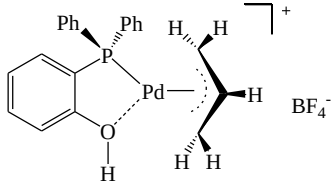 **29**	T = 70 & 100°C, t = 1 h, [ethylene] = 528 or 560 mmol Solvent = Toluene (260 ml), Amount of catalyst t= 10 μmol, Al:Pd = 500.	Mainly butenes, 10% of hexenes and trace amounts of octenes.	Moderate activity, TOF up to 4.29 x 10^3 h^{-1}	52

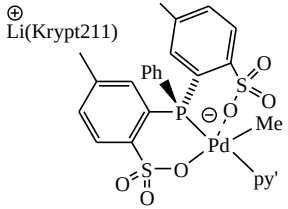 **30**	T = 25 °C, P = 5.4 atm, t = 24 h, Solvent = Toluene (70 ml), Amount of catalyst = 6, 11 – 14 μmol	$C_4 – C_{18}$ oligomers with a Schulz-Flory distribution (β = 0.69).	good yield (2.25 g)	53
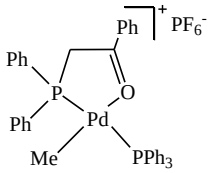 **31a** 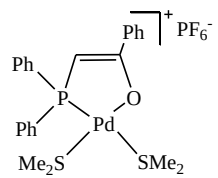 **31b**	T = 85 °C, P = 54 atm, t = 3 h, Solvent = CH_2Cl_2 (20 ml), [**29a**] = 0.23, 0.26 mmol, [**29b**] = 0.33 mmol	Butenes	Low activity, TON up to 164 h^{-1}	54
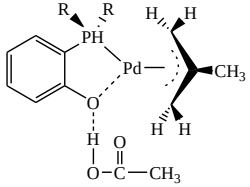 **32a**, R = Ph **32b**, R = *c*Hex 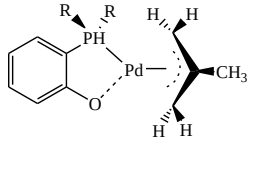 **32c**, R = Ph **32d**, R = *c*Hex	T = 70 °C, t = 1 h, [ethylene] = 528 or 560 mmol Solvent = Toluene (260 ml), Amount of catalyst = 10 μmol, Al:Pd = 500.		Inactive	52
N^O ligands				
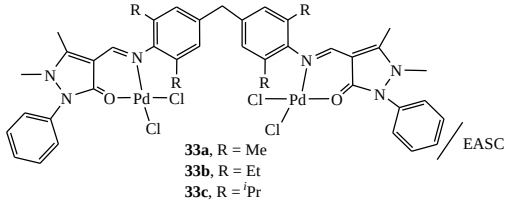 **33a**, R = Me **33b**, R = Et **33c**, R = ^{i}Pr	T = 30 & 50°C, P = 1.3 bar, t = 30 min, Solvent = Toluene (80 ml), Amount of catalyst = 5 μmol, Al: Pd = 300	$C_4 – C_{20}$ oligomers, nearly 75% butane, 5%-10% C_6 and C_8, traces of higher olefin content	Up to 1308 x 10^3 g (mol Pd x bar x h)$^{-1}$	55

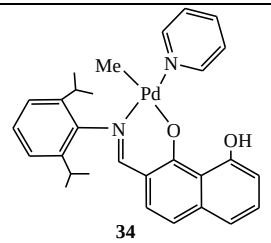 **34**	T = 90 °C, P = 300 psi, t = 2 h, Solvent = Toluene (5 ml), Amount of catalyst = 30 μmol	Oligomers with M_n less than 700 g mol $^{-1}$	15.8 x 10^3 g (mol Pd x h)$^{-1}$	56
Other ligands				
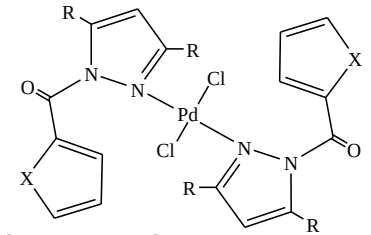 **35a**, R = Me, X = O **35b**, R = Me, X = S **35c**, R = ^{t}Bu, X = O **35d**, R = ^{t}Bu, X = S **35e**, R = Ph, X = S / $EtAlCl_2$	T = 25°C, P = 5 atm, t = 120 min, Solvent = Toluene (50 ml), Amount of catalyst = 9.0 μmol, Al: Pd = 500	C_{10} and C_{12} oligomers	Moderate activity up to 1.1 x 10^6 g (mol Pd x h)$^{-1}$	57
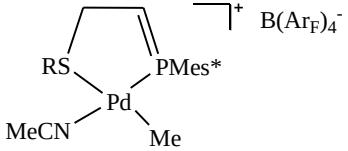 **36a**, R = 2,4,6-tri-*i*-propylphenyl **36b**, R = *t*-butyl (Mes* = 2,4,6-tri-*tert*-butylphenyl)	T = 26 °C, P = 27.2 atm, t = 3, 15 h, Solvent = CH_2Cl_2 (100 ml), Amount of catalyst = 10 μmol	Oligomers with M_n in the range of 180 to 215 g mol $^{-1}$ for **32a**, and a mixture of internal butenes for **32b**	Moderate activity, TOF up to 4.3 x 10^3 h^{-1}	36
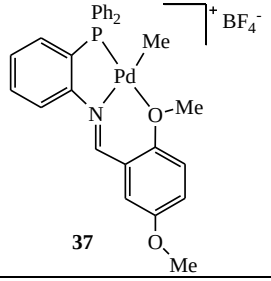 **37**	T = 0, 30, 70 and 110 °C, P = 10.2, 20.4 & 34 atm, t = 12 & 24 h, Solvent = CH_2Cl_2 (30 ml), Amount of catalyst= 30 mg	C_6 – C_{16} oligomers	Low activities up to 49.5 x 10^{-3} g mmol^{-1} h^{-1}	32

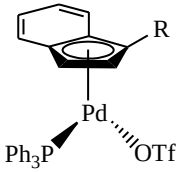 **38a**: R = H **38b**: R = Me	Ethylene: t = *ca*. 5 min, Solvent = $CDCl_3$ (1 ml), catalyst = 20 mg ; Styrene: t = 15 h, Solvent = $CDCl_3$ (1 ml), Styrene = 1 mmol catalyst = 10 mg; Substituted styrenes: t = 15 h, Solvent = $CDCl_3$ (1 ml) Substituted styrene = 50 – 70 equiv	Dimerization and/or trimerization of ethylene, styrene and *p*-fluorostyrene; oligomerization of *p*-amino- and *p*-methylstyrene; or polymerization of *p*-methoxystyrene.	58
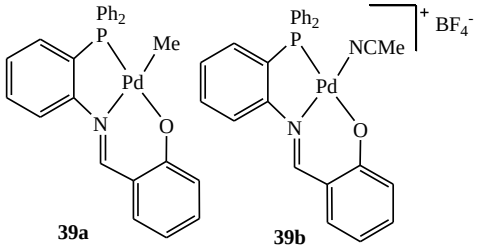 **39a** **39b**	T = 30 ^oC, P = 34 atm, t = 24 h, Solvent = CH_2Cl_2 (30 ml), Amount of catalyst = 30 mg	Inactive	32

1.2.1 Complexes with N^N chelates

1.2.1.1 α-Diimine ligands

α-Diimine complexes have been widely applied in ethylene oligomerization/polymerization reactions. These complexes were found to catalyze the polymerization of ethylene. By reducing the steric bulk of the ligand backbone, in particular the *ortho* substituents (R^1) on the aryl rings of the ligands (**L_1**), the oligomerization of ethylene was favoured.[59–61]

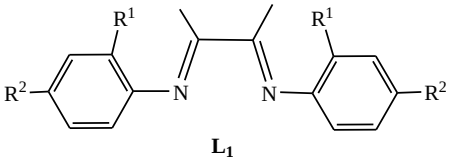

L_1

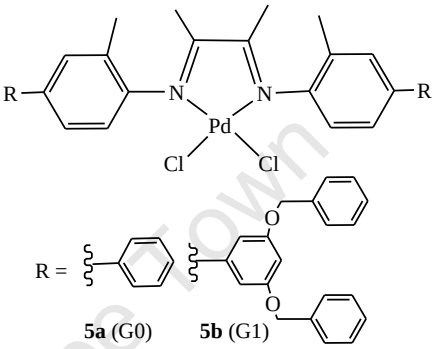

5a (G0) **5b** (G1)

5c: R = H

The effect of substituents in the *para*-position (R^2) was studied by Moss *et al.*[40] Different sizes of dendritic wedges (G0 and G1) were introduced into the aryl ring of the α-diimine ligands on the *para*-position (R^2). The corresponding Pd^{II} complexes **5a** and **5b**, along with a literature complex **5c** (R^2 = H), showed activity towards ethylene oligomerization when using MAO as a co-catalyst. Higher carbon oligomers (C_{10}, C_{12}, C_{14+}) were detected. The activity and product distribution, however, were not related to the size of the *para*-substituents, R^2.

Cationic complex **7** was generated *in situ* according a similar procedure showed in Scheme 1.2 (section 1.2.1.3). When excess ethylene was treated with **7**, a mixture of 1-butene and *cis*-, *trans*-2-butenes formed (1-butene:2-butene = 1:6, *cis*-2-butene:*trans*-2-butene = 1:2).[42]

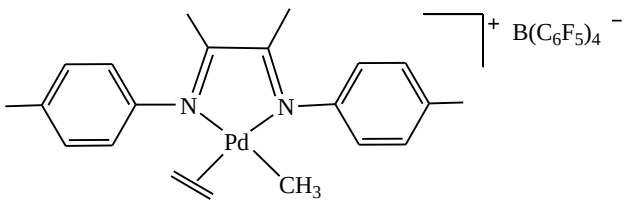

7

1.2.1.2 Iminopyridine ligands

Iminopyridine ligands might be considered to be structurally related to both diimine and pyridyl diimine ligands, and the olefin polymerization/oligomerization behaviour of the late transition metal complexes was investigated recently.[21]

Pd^{II} complexes bearing asymmetrical (imino)pyridines (**2** and **3**) have been reported to catalyze the oligomerization of ethylene.[30,38]

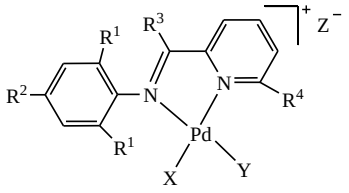

	R^1	R^2	R^3	R^4	X	Y	Z
2a	Me	H	Me	CO_2Me	Cl	Cl	NA
2b	Et	H	Me				
2c	^{i}Pr	H	Me				
2d	Me	Me	Me				
2e	F	H	Me				
2f	Cl	H	Me				
2g	Br	Me	Me				
3a & 3b	^{i}Pr	H	Me	H	Me	NCMe	BAr_F
40a	^{i}Pr	H	H	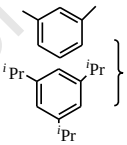	Cl	Cl	NA
40b	^{i}Pr	H	H				

Cationic complex $\mathbf{3}^{+}BAr'_4{}^{-}$ catalysed the oligomerization of ethylene with production of light oligomers ($C_4 - C_{20}$) and activity up to 160 g (g of Pd x h x bar)$^{-1}$, and is regarded as an efficient long-lived catalyst.[30] Upon activation with MAO, neutral Pd^{II} dichlorides **2a-g** produces butenes and polyethylenes (PEs) with oligomerization activities up to 180 g (g of Pd x h x bar)$^{-1}$. The dimerization activity decreased with increasing size of the alkyl substituents (R^1) (**2a** > **2b** > **2c**) or decreasing the eletronegativity of the alkyl substituents (R^1) (**2e** > **2f** > **2g**).[38] On the other hand, when bulky groups were introduced into the pyridine ring, the sterically encumbered palladium complexes **40** showed good activity towards ethylene polymerization [up to 2.0 x 10^4 g (mol Pd x h x bar)$^{-1}$] when activated with MAO and MMAO.[62]

Gibson and co-workers prepared a series of pyridyl- and quinolyl-N-substituted ferrocenyl and ferrocenediyl ligands and their mono- and di-nuclear palladium complexes **12** and **13**.[26]

However, there was no activity towards ethylene oligomerization for these Pd^{II} complexes upon activation by MAO.

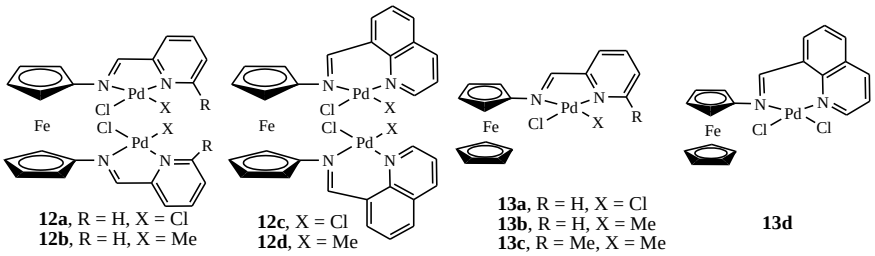

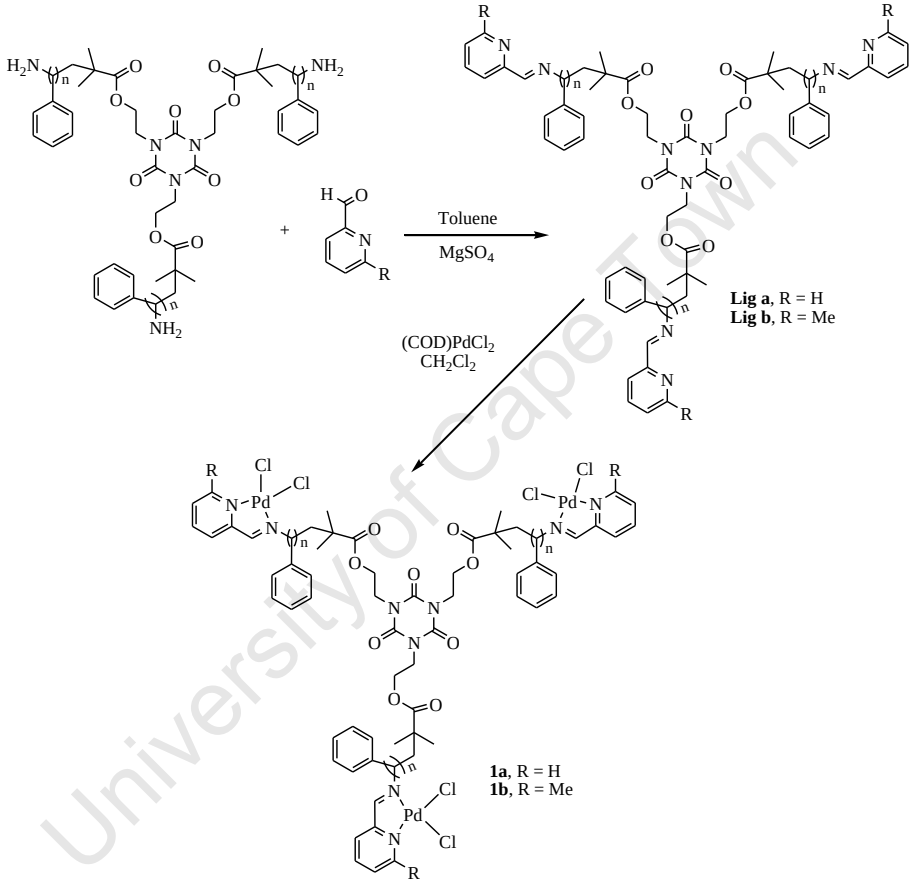

Scheme 1.1 Synthesis of tri-nuclear polymeric macroligated palladium(II) complexes.

Furthermore, multi-nuclear macroligated pyridylimine-based Pd^{II} complexes were prepared by Kim and co-workers.[37] The pyridylimine ligands were functionalized at the chain ends of a multi-arm synthetic star polymer and subsequently reacted with $(COD)PdCl_2$ to generate the corresponding macroligated Pd^{II} complexes **1** (Scheme 1-1). **1** showed substantially high activity (up to 42.66 x 10^7 g x (mol Pd x h x atm)$^{-1}$) towards ethylene oligomerization on activation with MAO, producing C_4 and C_6 compositions as major products.

1.2.1.3 Bis(*N*-heterocycle)methane ligands

Bis(*N*-heterocycle)methane donor ligands represent another group of N^N chelates whose complexes are employed in ethylene oligomerization[39,41–42] and polymerization reactions.[19,59(b),63] The chemistry of (N^N)Pd(Me)(H_2C=CH_2)$^+$ complexes incorporating bis(pyrazoyl)methane ligands, **6** and **9**, was studied by Jordan and co-workers.[25,41,42] Most of these species undergo ethylene insertion at low temperature and dimerize ethylene to butenes at room temperature, except cation **6a**, which oligomerizes ethylene to predominantly linear internal C_8 to C_{24} olefins.

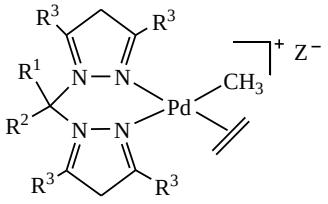

6a, $R^1 = R^2 = Me$, $R^3 = H$
6b, $R^1 = H$, $R^2 = Si(p\text{-tol})_3$, $R^3 = H$
6c, $R^1 = R^2 = R^3 = H$
6d, $R^1 = R^2 = H$, $R^3 = Me$
6a-c, Z = $B(C_6F_5)_4$; **6d**, Z = SbF_6

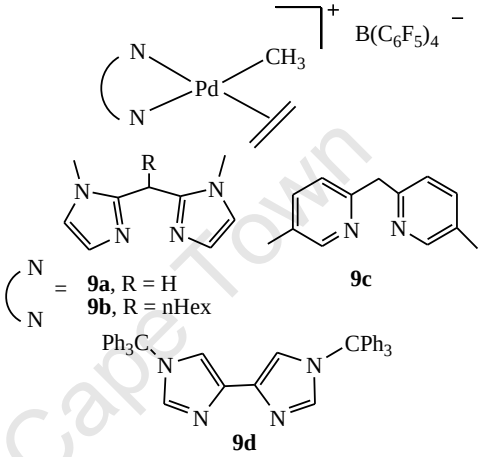

9a, R = H
9b, R = nHex
9c
9d

It has been shown (Scheme 1.3) that the dimerization of ethylene by (N^N)PdR^+ systems proceeds *via* an insertion/β-H elimination mechanism. The catalyst resting state is the (N^N)Pd(Et)(ethylene)$^+$ species (**Pd-1**).[42,44]

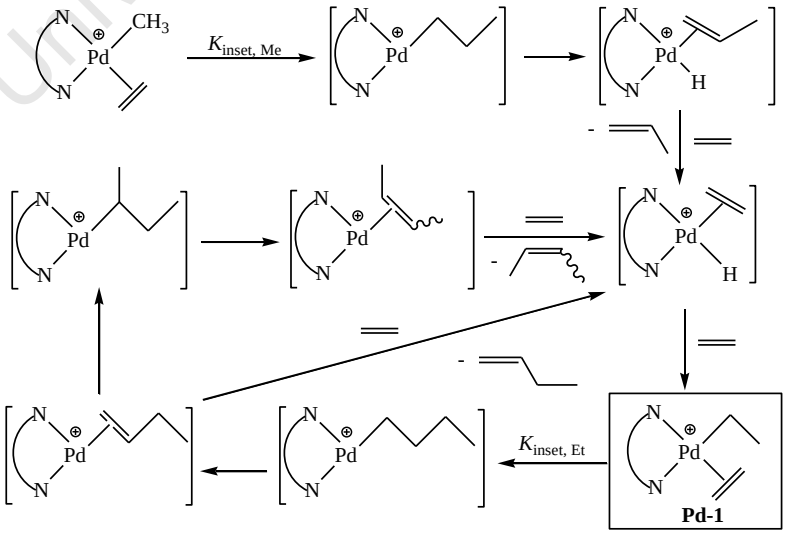

Scheme 1.2 Possible mechanism for ethylene dimerization.

1.2.1.4 Phenanthroline and bis(azaferrocene) ligands

The phenantroline-based Pd (**8a-d, 10**) cations containing sterically small N^N ligands were reported to catalytically dimerize ethylene to form butenes.[43,44] These catalysts appear to be unstable and are generated *in situ* from addition of ethylene to their cationic precursors in methylene chloride at -25 ^{o}C (Scheme 1.3).

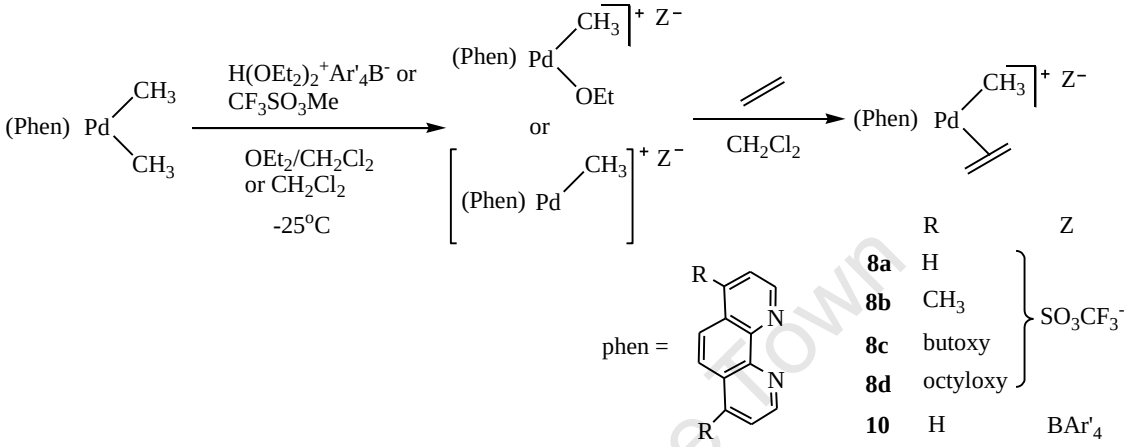

Scheme 1.3 Synthesis of phenatroline-based palladium (II) complexes.

When using **10** as catalyst, a mixture of butenes was formed with a composition of *trans*-2-butene (60-65%) > *cis*-2-butene (30-35%) > 1-butene (5-10%). The formation of hexenes and longer olefins up to C_{20} were observed besides butenes when using **8a-d** as catalyst.

Recently, an air-stable complex **11**, of the same type as **10**, was synthesized by Brookhart and co-workers. The treatment of (Phen)PdMeCl with $NaB(Ar_F)_4$ (Ar_F = fluorinated aryl) and 3,5-bis(trifluromethyl)benzonitrile in methylene chloride at room temperature yielded the desired product **11** (Eq. 1.2), which catalytically dimerized ethylene as expected.[45]

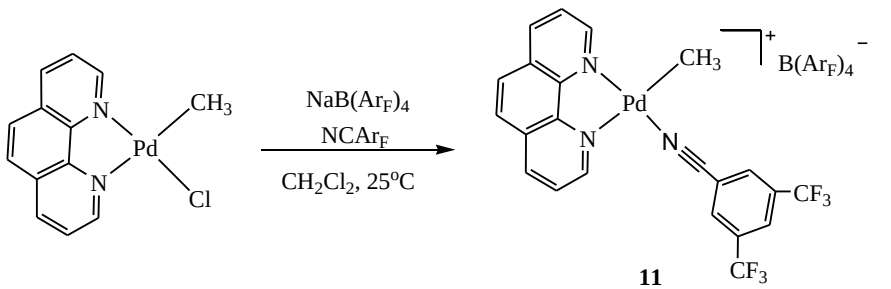

11 (Eq. 1.2)

Bisazaferrocene ligands comprise a different type of bidentate nitrogen ligand which have bulky pentamethyl or pentaphenyl cyclopentadiene (Cp* or Cp^{o}) rings above and below the coordination plane. Their C_2-symmetrical and asymmetrical cationic Pd^{II} complexes **4** were reported by Salo and Guan[39] to oligomerize ethylene giving oligomeric PEs with M_n in the range of 200 – 600 g mol^{-1} and branching density from 20 to 60 br./1000 carbons.

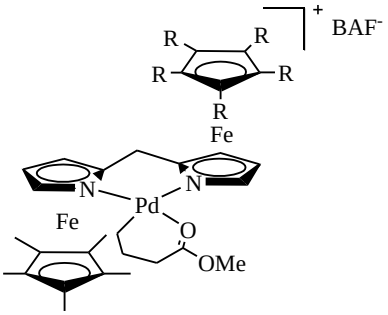

4a, R = Me; **4b**, R = Ph

The asymmetrical complex **4b** was found to be less active and less thermally stable than the symmetrical analogue **4a**, and both are significantly less productive than the α-diimine counterparts.

1.2.2 Complexes with P^N chelates

Unsymmetrical bidentate ligands with nitrogen and phosphorus donor atoms (P^N ligands) have attracted considerable attention in the field of transition metal catalysis.[23,64] Nitrogen donor atoms in most P^N bidentate ligands reported in the literature are often bound to an aromatic system or are in the form of an amino- or imino-group. The P^N chelates are particularly interesting because of the difference in *trans*-effect of the different donor and acceptor properties of the two coordinating groups in the ligand. An advantage of these ligands can be the improved thermal stability during catalysis; for example nickel complexes with P^N ligands often show much higher thermal stability than related N^N ligand complexes.[47,65] P^N ligands are known to bind to Pd in a unique way: the soft P atom coordinates very strongly to Pd whereas the hard N donor is relatively weakly bound.[66] These features might be exploited in tuning the reactivity of Pd complexes in olefin coupling reactions. Until now, many efforts have been made to investigate this observation. In ethylene oligomerization reactions, active palladium catalysts bearing P^N ligands have been reported

(see Table 1.2),[28,45,46] however, low or no activity is often observed with such complexes (see Table 1.2).[29,31,36,48]

1.2.2.1 Phosphino- and phosphaalkene-imine ligands

The phosphino-imine ligands of type **L_2** developed by Shell,[67] Feringa *et. al.*[68] and Rush *et. al.*[69] with varying R groups on either the phosphorus- or nitrogen-bound phenyl substituent, have been recently applied in palladium-catalysed oligomerization/polymerization of ethylene.

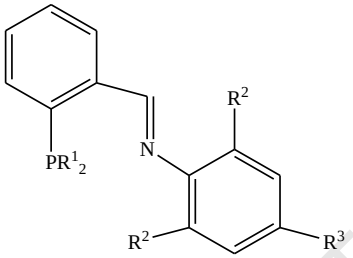

L_2-a, R^1 = Ph, R^2 = R^3 = H
L_2-b, R^1 = Ph, R^2 = Me, R^3 = H
L_2-c, R^1 = Ph, R^2 = ^{i}Pr, R^3 = H
L_2-d, R^1 = *p*-CH_3OPh, R^2 = ^{i}Pr, R^3 = H
L_2-e, R^1 = *m*-CH_3OPh, R^2 = ^{i}Pr, R^3 = H
L_2-f, R^1 = *o*-CH_3OPh, R^2 = H, R^3 = Cl
L_2-g, R^1 = *o*-CH_3OPh, R^2 = R^3 = H
L_2-h, R^1 = *o*-CH_3OPh, R^2 = ^{i}Pr, R^3 = H

The Pd^{II} triflate and *p*-toluenesulfonate complexes bearing ligands **L_2**[67] and an *in situ* catalytic system comprising palladium acetate, one equivalent of **L_2** and two equivalents of *p*-tolyl-sulfonic acid catalyze the oligomerization of ethylene.[69] The product distribution shifted from short to medium chain oligomers when the steric bulk of either the R^1 or R^2 substituents were increased. The use of electron-releasing groups for R^3 considerably increased the reaction rate.

Besides studying the effects of different R groups on P- and N-bound phenyl substituents, the effect of different backbones connecting those donor groups has been studied as well.[46] Cationic Pd^{II} complexes of the type **15** with cyclic α-diphenylphosphino-ketoimines showed moderate catalytic activities in ethylene oligomerization and produced oligomers in the range of C_{12} to C_{34} with a Schulz-Flory distribution. Activity in propene and 1-butene oligomerization was also observed.[46] By increasing the steric bulk of the substituent on the imine, or by using ligands with cyclohexylidene or cycloheptylidene backbones instead of cyclopentylidene, a drop in catalytic activity was reported.

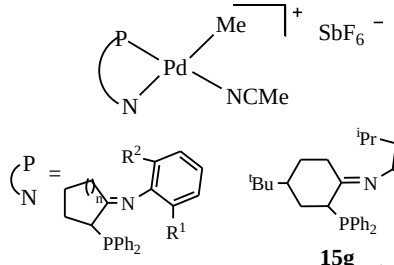

15a, n = 1, $R^1 = R^2 = CH_3$
15b, n = 1, $R^1 = R^2 = {}^iPr$
15c, n = 2, $R^1 = R^2 = CH_3$
15d, n = 2, $R^1 = R^2 = {}^iPr$
15e, n = 2, $R^1 = OCH_3$, $R^2 = H$
15f, n = 3, $R^1 = R^2 = {}^iPr$

15g

15h

Considering that the use of non-enolizable imine donors should be beneficial to catalyst thermal and chemical stability, Brookhart and co-workers examined the synthesis, structure and catalytic properties of various Pd^{II} complexes with bulky phosphine-[47] and phosphaalkene -imine[36] ligands (**16** and **17**)

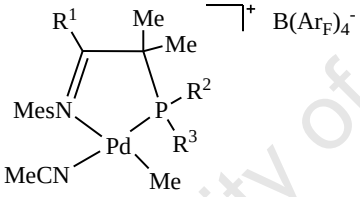

16a, $R^1 = H$, $R^2 = Mes$, $R^3 = Me$
16b, R^1 = Ph, $R^2 = Mes$, $R^3 = Me$
16c, $R^1 = Ph$, $R^2 = R^3 = Me$
16d, $R^1 = Ph$, $R^2 = R^3 = Ph$

(Mes = 2,4,6-trimethylphenyl)

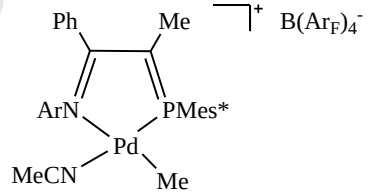

17a, Ar = 2,6-di-*i*-propylphenyl;
17b, Ar = 2,4,6-trimethylphenyl
(Mes* = 2,4,6-tri-*tert*-butylphenyl)

If the bulky mesityl (Mes) substituent was introduced on phosphorus, complexes **16a-b** oligomerized ethylene giving branched oligomers with M_n up to 660 at 80 °C. The catalytic activity of the aldimine-derived catalyst **16a** was substantially higher than that of ketimine-containing **16b**. In contrast, diphenyl- and dimethyl-substituted complexes **16c-d** showed inactivity towards ethylene oligomerization.[47]

By incorporating the phosphaalkene functionality into one arm of bidentate ligands, Pd^{II} complexes **17a-b** were obtained in a similar way to **16b**.[36] The complexes displayed moderate activity in the oligomerization of ethylene at 26 °C. An increase in turnover number with a concurrent drop of oligomer molecular weight (from 670 to 300) was observed when the steric bulk of ligand was decreased.

Pyrrolyl-substituted phosphine-containing ligands have also been found to be catalytically active.[70] However, Pd^{II} complexes of types **22** and **23** bearing variously-substituted *N*-pyrrolylphosphino-imine ligands proved inactive for ethylene oligomerization and polymerization.[29]

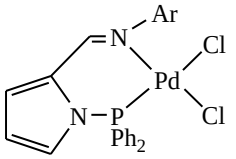

22a-d, R = Ph **23a-d**, R = NPr^i_2

a, Ar = Ph
b, Ar = 3,5-Me_2-C_6H_3
c, Ar = 2,4,6-Me_3-C_6H_2
d, Ar = 2,6-$^iPr_2$-C_6H_3

1.2.2.2 Phosphino-pyridine ligands

Palladium complexes bearing phosphino-pyridine ligands have been employed in many catalytic reactions including ethylene oligomerization.[27,28,35,48] The molecular structures of neutral and cationic methylpalladium complexes show that the methyl coordinates *cis* with respect to the phosphine due to the larger *trans* influence of phosphorus compared to nitrogen. Similar to phosphino-imines, there are three types of modifications that can be applied on these ligands (Figure 1.1). These could then be incorporated into palladium complexes and applied in catalysis. These modifications include changing the (i) substituent on pyridine (**18**),[48] (ii) phosphorus-bound aryl group (**19**, **21**)[27,28] and (iii) ligand backbone (**20**).[35] These modifications can be applied to other ligand systems as well during the ligand design.

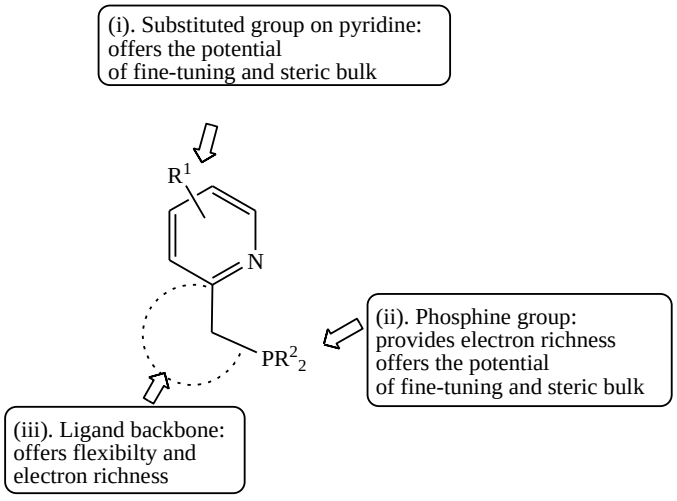

Figure 1.1 Ligand design and diversity (example for phosphino-pyridine ligands).

Cationic Pd^{II} complexes **18** are typical examples of type (i) modification, i.e. the ligands differ in the steric bulk of the aromatic substituent at the pyridine 6-position. However, these complexes showed poor activity in ethylene oligomerization with almost negligible TOFs.[48] The coordinated pyridine-phosphine ligands in complexes **19** differ with respect to the aryl groups at the phosphine, which are 2-tolyl, 2-anisyl and mesityl for **19a**, **19b** and **19c** respectively.[27] These complexes all displayed very low activity. Contrast to this, complex **21**, the neutral analogue of **19a**, showed moderate activity for ethylene oligomerization after activation with a borate salt such as $NaBAr_{F4}$. Oligomers in the range of C_8 to C_{32} were detected.[28]

It is necessary to investigate the effect of systematic changes of the backbone in a series of closely related ligands and to study the effect of changes in chelating properties when metal complexes bearing these ligands are used in catalysis. With this purpose complexes such as **20** and their nickel analogues prepared by Kamer and co-workers[35] were tested for ethylene oligomerization. These cationic methylpalladium complexes showed a very low activity to give mainly butenes as product.

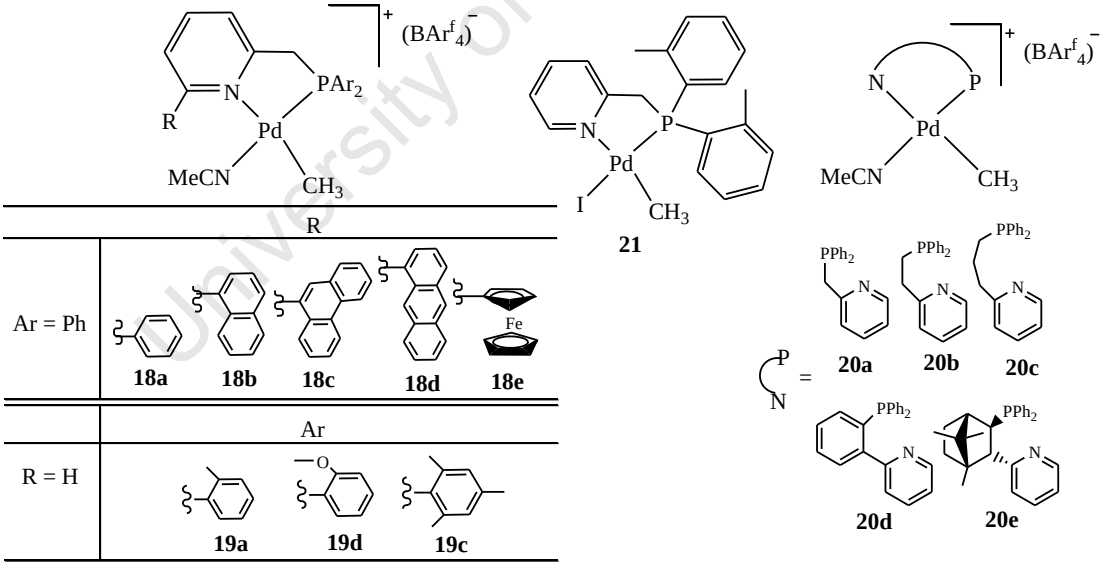

1.2.2.3 Phosphino-oxazoline and -quinoline ligands

Phosphino-oxazoline palladium complexes have seldom been used in the oligomerization of ethylene, although the cations **14** were found to be active for ethylene oligomerization.[45] **14a** has a unique axial Pd···H interaction, which was revealed by the X-ray structures of its neutral analogue **41** and the previously reported palladium dichloride complex **42**.[71] This interaction

was observed to provide sufficient steric bulk and resulted in oligomerization of ethylene by **14a** producing a Schulz-Flory distribution of α-olefins ranging from C_4 to C_{24}. In contrast to this, **14b**, which had similar electronic properties to **14a** but lacks the axial C-H···Pd interaction, yielded strictly butenes.

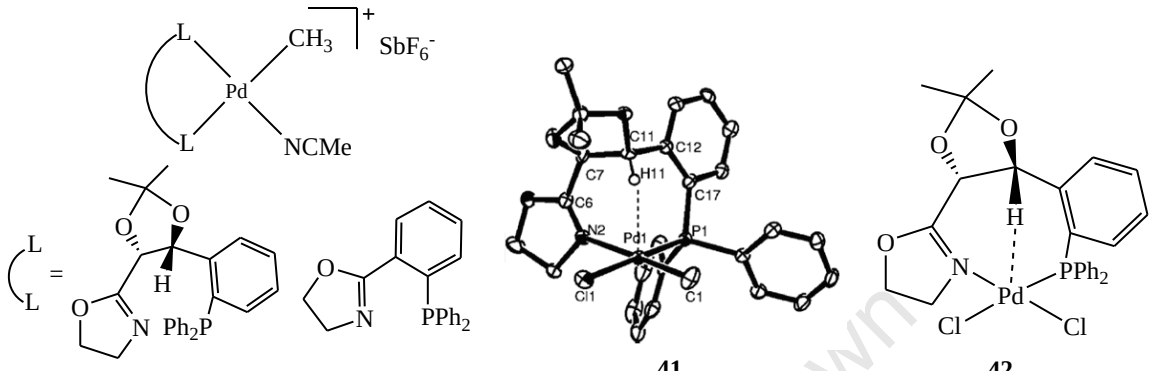

14a **14b** **41** **42**

Consiglio and co-workers prepared four ligands with 8-substituted quinoline as a backbone in order to change the properties of the (P^N) ligands. However, their palladium complexes **24** were inactive for ethylene oligomerization using triisobutylaluminium at 8-60 bar and up to 80 ^{o}C.[31]

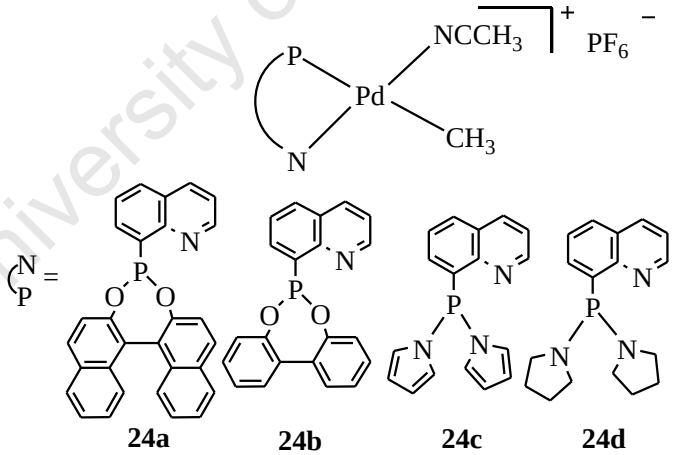

24a **24b** **24c** **24d**

1.2.3 Complexes with P^O chelates

The Shell Higher Olefin Process (SHOP), developed by Keim, is one of the well-known catalytic processes in homogeneous catalysis.[7] This technology makes use of neutral nickel(II) complexes bearing a bidentate mono-anionic (P^O) ligand (Figure 1.2).[12,72]

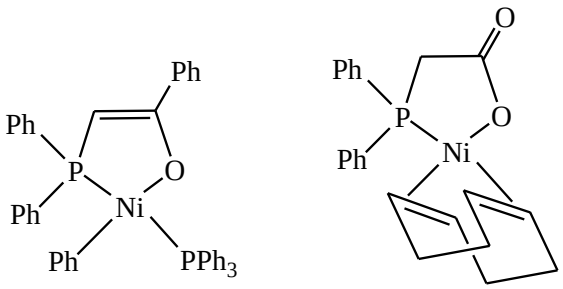

Figure 1.2 Representation of two SHOP catalysts bearing P^O ligands

The first palladium analogues of neutral SHOP-type nickel catalysts were reported by Braunstein and co-workers in 1996.[73,74] The cationic palladium analogues, **25**, **28** and **31**, were subsequently developed and examined for their reactivity towards olefin oligomerization.[49,51,54]

Palladium complexes **25a-b** based on the phenacyl-di-tert-butylphosphine ligands were found to oligomerize ethylene to an amorphous material (TOF = 2 x 10^4 h^{-1}, $M_n \approx 350$) in which the degree of branching decreases with increasing ethylene concentration.[49] Cationic palladium methyl acetonitrile complexes **28a-c** with phenacyl-diarylphosphine ligands showed modest activity (TOF up to 1.3 x 10^4 h^{-1}) for oligomerization of ethylene but displayed short catalyst lifetimes. **28a** and **28c** generated butenes, while **28b** formed a mixture of butenes and hexenes at high ethylene pressure.[51] The effect of adducts (L) in these complexes was also found to have an important role in the catalytic activity. The more labile ether complex **25a** is typically more reactive than the acetonitrile adduct,[49] while complex **31a**, which is a PPh_3 adduct, showed much lower activity (TON = 164 h^{-1}) towards ethylene dimerization.[54] A similar activity to **31a** was found for the palladium phosphino enolate complex **31b**.

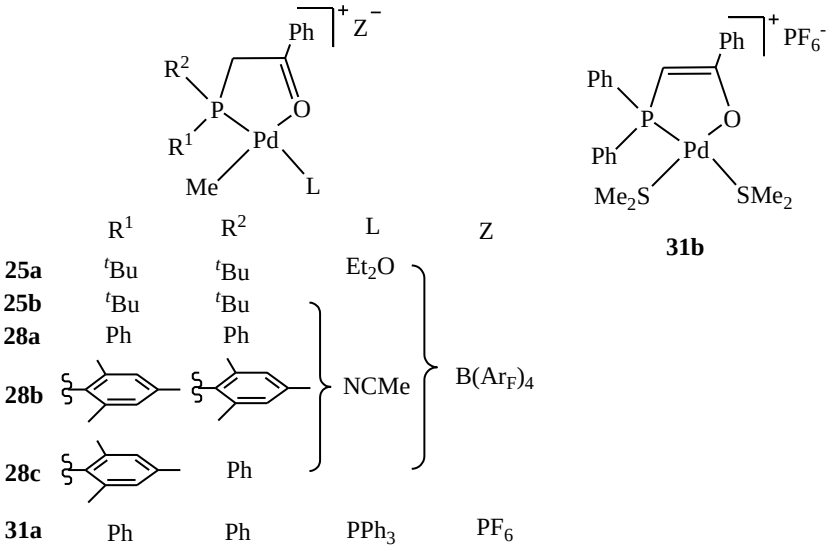

The allylpalladium phosphinophenol tetrafluoroborate **29**, demonstrated moderate activity (reaching a maximum of 4.29 x 10^3 mol C_2H_4 mol^{-1} Pd h^{-1}) toward ethylene oligomerization, forming a mixture of butenes and smaller amounts of hexenes. Heating was necessary to initiate the catalytic reaction. The methylalylpalladium phosphinophenolate acetic acid conjugates **32a-b** and the neutral complexes **32c-d** did not catalyse the oligomerization of ethylene.[52]

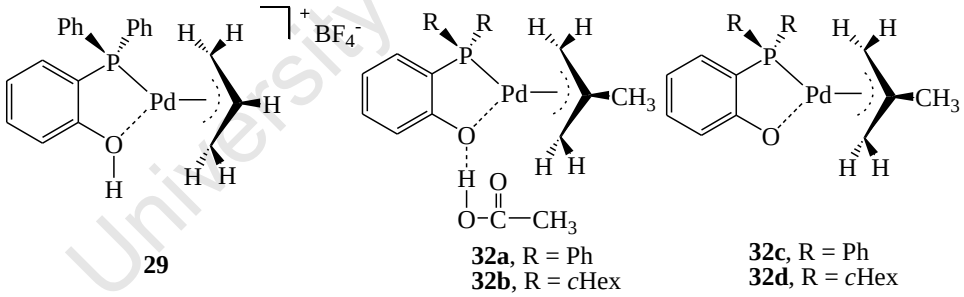

Cationic allyl and methyl palladium complexes **26** and **27** with the monoxides of diphosphine ligands dppm, dppe and dtolpm were prepared by Suranna and co-workers, and used in the catalytic oligomerization of ethylene to form $C_4 - C_{12}$ oligomers.[50] It was found that not only the coordination mode of the ligand but also the catalytic results were dependent on the backbone. The selectivity to linear α-olefins of five ring chelates (dppmO, dtolpmO) was higher than six-membered rings (dppeO), and the values of Schulz-Flory distribution were rising in the order: dppmO < dtolpmO < dppeO. Moreover, the cationic methyl complexes were more active than their allyl analogues.

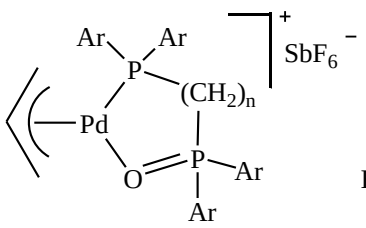

26a: n = 1, L = dppmO
26b: n = 2, L = dppeO
26c: n = 1, L = dtolpmO

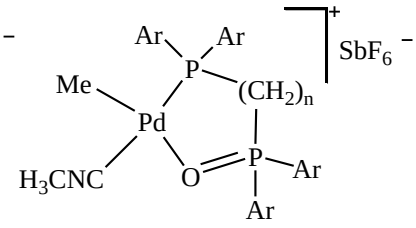

27a: n = 1, L = dppmO
27b: n = 2, L = dppeO
27c: n = 1, L = dtolpmO

dppmO = bis(diphenylphosphino)methane-monoxide
dppeO = 1,2-bis(diphenylphosphino)ethane-monoxide
dtolpmO = bis(di *o*-tolylphosphino)methane-monoxide

The palladium complex [Li(Krypt211)[(OPO)PdMe(Py')] (**30**) was obtained using the method shown in Scheme 1.4.[53] The corresponding ligand reacts with [PdMeCl(COD)] to yield $\{Li[(Li\text{-}OPO)PdMe(Cl)]\}_n$ **43** followed by addition of $AgPF_6$ yielding **44**. The reaction of **44** with py' (py' = 4-(5-nonyl)pyridine) gives a self-assembled tetranuclear complex $\{Li[OPO]PdMe(py')\}_4$ (**45**), which reacts with the cryptand Krypt211 yielding **28**. The $[OPO]^{2-}$ ligand of **28** binds to Pd as a P^O chelator. The precursors **43 – 45** behaved as catalysts for ethylene polymerization, while **30** produced only ethylene oligomers in good yield. This could be due to the free $ArSO_3^-$ group in **30** which could facilitate chain transfer.

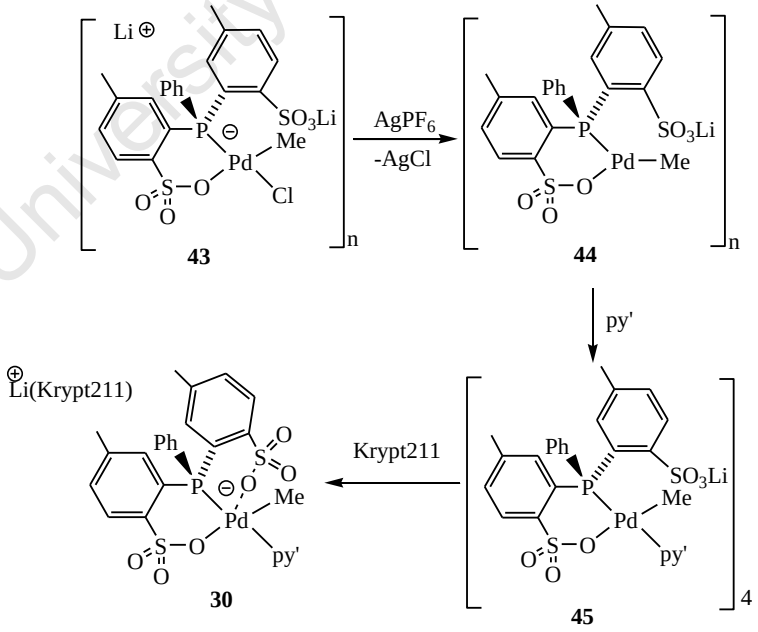

Scheme 1.4 Synthesis of [Li(Krypt211)[(OPO)PdMe(py')] **30**. PF_6 anion is omitted from compounds **44**, **45** and **30**.

1.2.4 Complexes with N^O chelates

Complexes containing both relatively hard oxygen and relatively soft nitrogen donor atoms can also offer interesting and unique bonding properties that may have a direct influence on catalytic reactions. Nickel catalysts with N^O chelating ligands, modelled after the P^O ligands used in SHOP-type catalysts (e.g. Figure 1.2), have been well defined.[75] In contrast, their palladium analogues have seldom been reported in olefin oligomerization and polymerization reactions except in some DFT studies. In these studies propylene polymerization catalysed by palladium complexes with the "Grubbs ligand" (Figure 1.3) was investigated.[76]

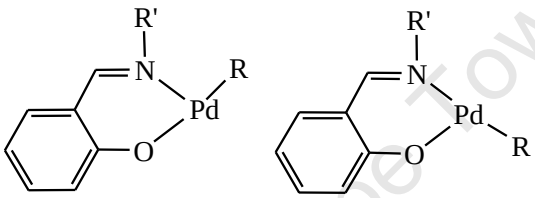

R = Ph, Me; R' = H, *t*-But

Figure 1.3 Active catalyst structures of Grubbs complexes in propylene polymerization

It was only quite recently that the N^O ligated palladium complex **34** was reported to catalyze ethylene oligomerization and produced oligomers with molecular weights (M_n) less than 700. The activity increased with increasing reaction temperature but without the addition of co-catalyst, BPh_3.[56]

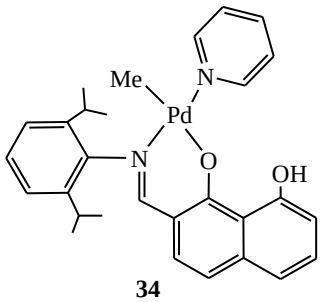

34

Budagumpi and co-workers synthesized binuclear palladium complexes having N^O ligands, **33a-b**, according to Scheme 1.5.[55] All the complexes were reported to efficiently oligomerize ethylene in combination with EASC (ethylaluminum sesquichloride). The selective production of ethylene dimers and trimers along with small amount of higher olefins at

moderate activities was observed. Their activities increased with the increasing size of the R group in the ligands, i.e. Me < Et < ^{i}Pr.

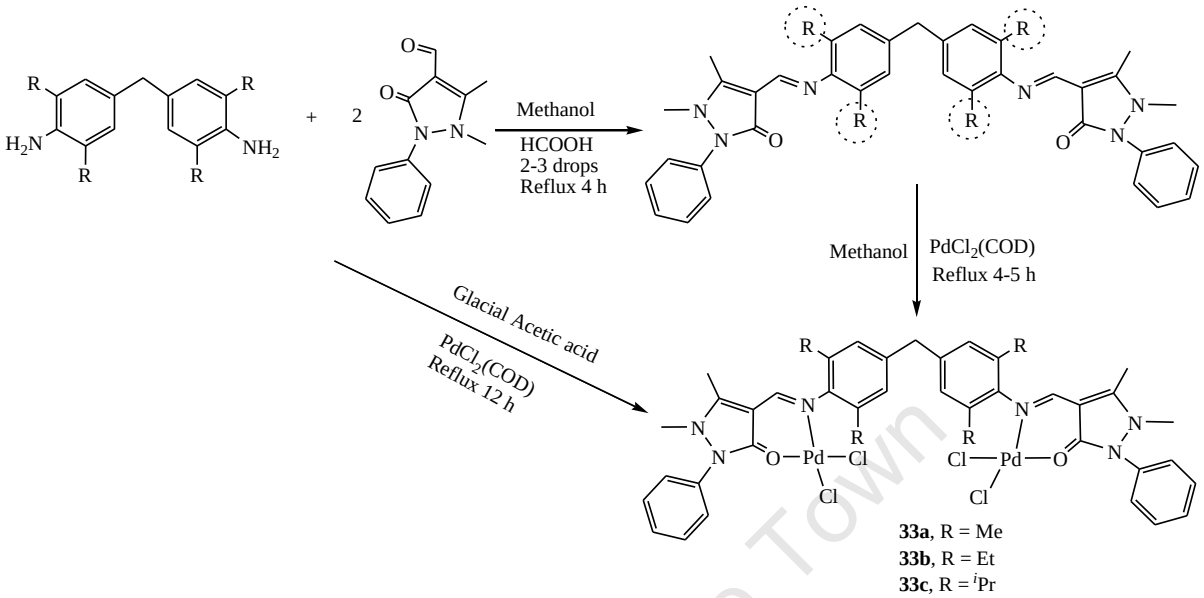

33a, R = Me
33b, R = Et
33c, R = ^{i}Pr

Scheme 1.5 Synthesis of binuclear palladium complexes having N^O ligands **33a-b**.[55]

1.2.5 Complexes with other ligands

Besides the N^N ligands mentioned above, mono-pyrazolyl nitrogen donor ligands have been found to be tuneable to modify electronic and steric effects. Pyrazolyl and pyrazole Ni(II) and Pd(II) have been found to be good catalysts for ethylene polymerization.[77] For ethylene oligomerization reactions, palladium complexes bearing furoyl and thiophene carbonyl linker pyrazolyl groups such as in **35** were reported.[57] The nature of the ligands appeared to have an effect on both the catalyst activity and product distribution. For example, **35e**, with the less electron-donating phenyl group, showed the highest activity and the catalysts with furoyl linkers gave higher percentages of the C_{12} than C_{10} oligomers.

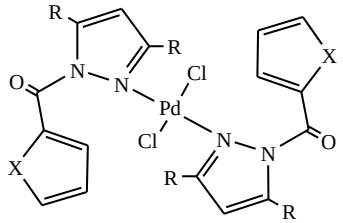

35a, R = Me, X = O
35b, R = Me, X = S
35c, R = ^{t}Bu, X = O

35d, R = ^{t}Bu, X = S
35e, R = Ph, X = S

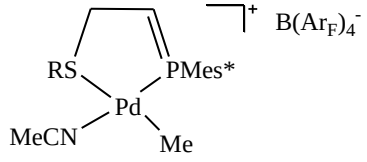

36a, R = 2,4,6-tri-*i*-propylphenyl
36b, R = *t*-butyl
(Mes* = 2,4,6-tri-*tert*-butylphenyl)

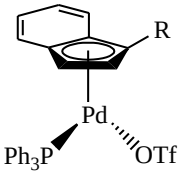

38a: R = H
38b: R = Me

phosphaalkene-sulfide based palladium complexes **36** were prepared in order to compare the catalytic behaviour with their phosphinidine-imine analogues **17**.[36] Higher catalytic activity was observed in these P^S ligated complexes. The *tert*-butyl-substituted complex **36b** produced a mixture of internal butenes, mainly *cis*-2-butene (2:1 of *cis/trans*), while the tri-isopropylphenyl-substituted catalyst **36a** produced oligomers with M_n = 215 at a moderate rate (TOF = 4300 TO/h).

Ind ligands (Ind = indenyl and its substituted derivatives) are another alternative type of ligand for utilization in late-transition metal catalytic systems.[78] For example, Ni-Ind complexes have been applied in the oligo- and poly-merization of olefins.[79] The indenyl-palladium complexes **38** with a triflate moiety were prepared by reacting their corresponding Pd-Cl derivatives with AgOTf.[58] These complexes were found to isomerize 1-hexene, dimerize ethylene and styrene, dimerize and trimerize *p*-fluorostyrene, oligomerize *p*-X-styrenes (X = NH_2, Me) and polymerize *p*-methoxystyrene.

In order to study ligand effects of tridentate versus bidentate coordination on ethylene oligomerization, palladium complexes containing P^N^O donors **37** and **39** were prepared by Liu and co-workers.[32]

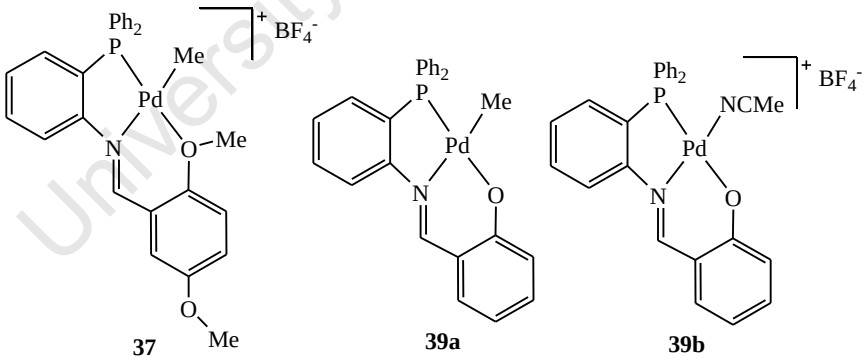

37 **39a** **39b**

Complex **37** catalysed the conversion of ethylene into oligomers (C_6-C_{16} depending on the ethylene pressure), while complexes **39a-b** were found to be inactive. The hemilabile ether donor in **37** played an important role during ethylene oligomerization and was easily replaced by a weakly coordinated ligand such as acetonitrile. The degree of oligomerization using **37**, however, is poor when compared to that for the Pd^{II} unsymmetrical diimine systems (**3a-b**) reported by Kress and co-workers.[30]

1.3 General Factors Affecting Oligomerization Reactions

It has been demonstrated that using different heteroditopic ligands or varying substituents on the ligands has the potential for controlling the catalytic properties (Section 2.2). The influence of reaction conditions on selectivity, oligomer molecular weight distribution and yields is also significant. There are many factors that need to be investigated during ethylene oligomerization reactions. This section provides an overview on the effect of these factors on catalytic results.

Solvent. The most commonly used solvents in ethylene oligomerization reactions are the relatively non-polar solvents, toluene and dichloromethane (see Table 1.2), although the choice of other solvents has been considered in some reports. The palladium dichloride complex **2d** showed higher activity for ethylene dimerization in dichloromethane than in toluene.[38] The same phenomenon was observed for cationic complexes **8a-b** and **31a**. The influence of the solvent was examined by reacting **8** in CH_2Cl_2, ether, THF or acetonitrile[43] and **31a** in CH_2Cl_2, the molten salt, (BMI)PF_6 (BMI = butylmethylimidazolium) or MeOH, respectively.[54] Dichloromethane was superior in both cases.

Reaction temperature. With increasing temperature, the ethylene oligomerization catalytic activity[30,32,45,49,57] and the amount of products[40,32] increases, while the Schulz-Flory value[32,40] decreases. The effect of reaction temperature on the nature of the oligomers produced is also very obvious. A distribution of higher olefins was always obtained at higher temperature for catalyst **37** (C_{12}-C_{16} olefins at 70 and 100 ^oC and C_6-C_{10} olefins at 0 ^oC).[32] In contrast to this, the percentage of higher oligomers increased at lower temperature for catalysts **1** and **6b**.[32,37]

Al/Pd ratio. Ethylene oligomerization by neutral palladium complexes requires the use of aluminium containing co-catalysts such as $AlEt_3$, methylaluminoxane (MAO) and modified MAO (MMAO) (MMAO = MAO containing 25 % isobutyl groups). It is observed that palladium catalysts commonly required a high amount of co-catalyst for activation towards oligomerization (Al/Pd = 400 – 1500) and an increase in Al/Pd ratio results in a general increase in oligomer yield and activity.[37,38,57]

Ethylene pressure. Increasing the ethylene pressure, generally leads to an increase in catalytic activity being observed.[30,32,39,41,45,46,49,57] An increase in the reaction pressure also increases the

selectivity towards higher oligomers[57] and α-olefins[39,46] i.e. an increase in the Schulz-Flory α-value.[46]

Reaction time. Oligomerization activity is generally observed to initially increase with prolonged reaction time,[32,36,47,51] until it reaches a maximum, after which it decreases with reaction time.[37,45,57]

1.4 Mechanisms of Palladium-Catalysed Ethylene Oligomerization/Polymerization

1.4.1 Overall mechanism

Basically, the mechanism for olefin oligomerization is the same as that of ethylene polymerization. Both oligomerization and polymerization reactions catalysed by palladium can be represented by the overall mechanism shown in Scheme 1.6. It involves three main processes beyond initiation: (1) chain propagation, (2) chain isomerisation, and (3) chain transfer.[80] In the case of ethylene oligomerization, chain transfer by β-elimination has to occur much faster than chain growth in order to limit the chain length.[81]

In oligomerization/polymerization catalysed by palladium complexes, the chain initiation (Route 1) proceeds via coordination of an olefin to the open site of the square-planar metal centre (**Pd-4**) followed by direct insertion of the coordinated olefin into the Pd-R bond without the formation of any intermediate (Cossee-Arlman mechanism).[82] For acyclic olefins, alkyl-olefin complexes of type **Pd-4** have been observed as the resting states by NMR spectroscopy, while the alkyl cations **Pd-5** exist as stable β-agostic species in the absence of excess olefin or other Lewis bases.[83] Repetition of the above steps results in the growth of a linear oligomer/polymer chain (**Pd-5** → **Pd-6** → **Pd-7**) (chain propagation, Route 2). This reaction is fast and first order in ethylene concentration. Complex **Pd-5** can also produce the branched β-agostic species **Pd-11** involving an olefin hydride intermediate, **Pd-10** (chain isomerisation, Route 3). The branched alkyl cation **Pd-11** can continue with "chain walking" by β-elimination and reinsertion with opposite regiochemsity, producing longer branches. Alternatively, **Pd-11** can be trapped with ethylene, and subsequent insertion produces an oligomer/polymer chain containing a methyl branch along the backbone. Routes 4 – 7 are the chain transfer (termination) pathways, although the precise mode of chain transfer is not yet

completely understood. Reaction 4 is slow and occurs by an associative displacement of the unsaturated chain from the olefin hydride complex **Pd-10**. The transfer rate is independent of the ethylene concentration (zero order in olefin); Molecular weights however increase with increasing monomer concentration. This route is applicable in the SHOP system.[84] A similar pathway showed in route 7, involves the associative displacement of an olefin from **Pd-10** by a solvent molecule.[45]

Routes 5 and 6 represent two possibilities which could not be distinguished. Route 5 shows a slow reaction of **Pd-10** with ethylene (**Pd-13**) leading to an alkene terminated polymer chain and a new metal ethyl initiator.[84] In Route 6, chain transfer may occur from the alkyl olefin resting state, **Pd-6**, via intramolecular hydrogen transfer to ethylene forming a new growing ethyl chain as well. This route was suggested by computational studies by Ziegler.[85] Since the ethylene complex **Pd-6** and the olefin hydride complex **Pd-10** are in equilibrium with the β-agostic alkyl complex **Pd-5**, a first order dependence in ethylene concentration for the chain transfer processes 5 and 6 can be observed, but the molecular weight distribution of the polymers/oligomers remains the same.

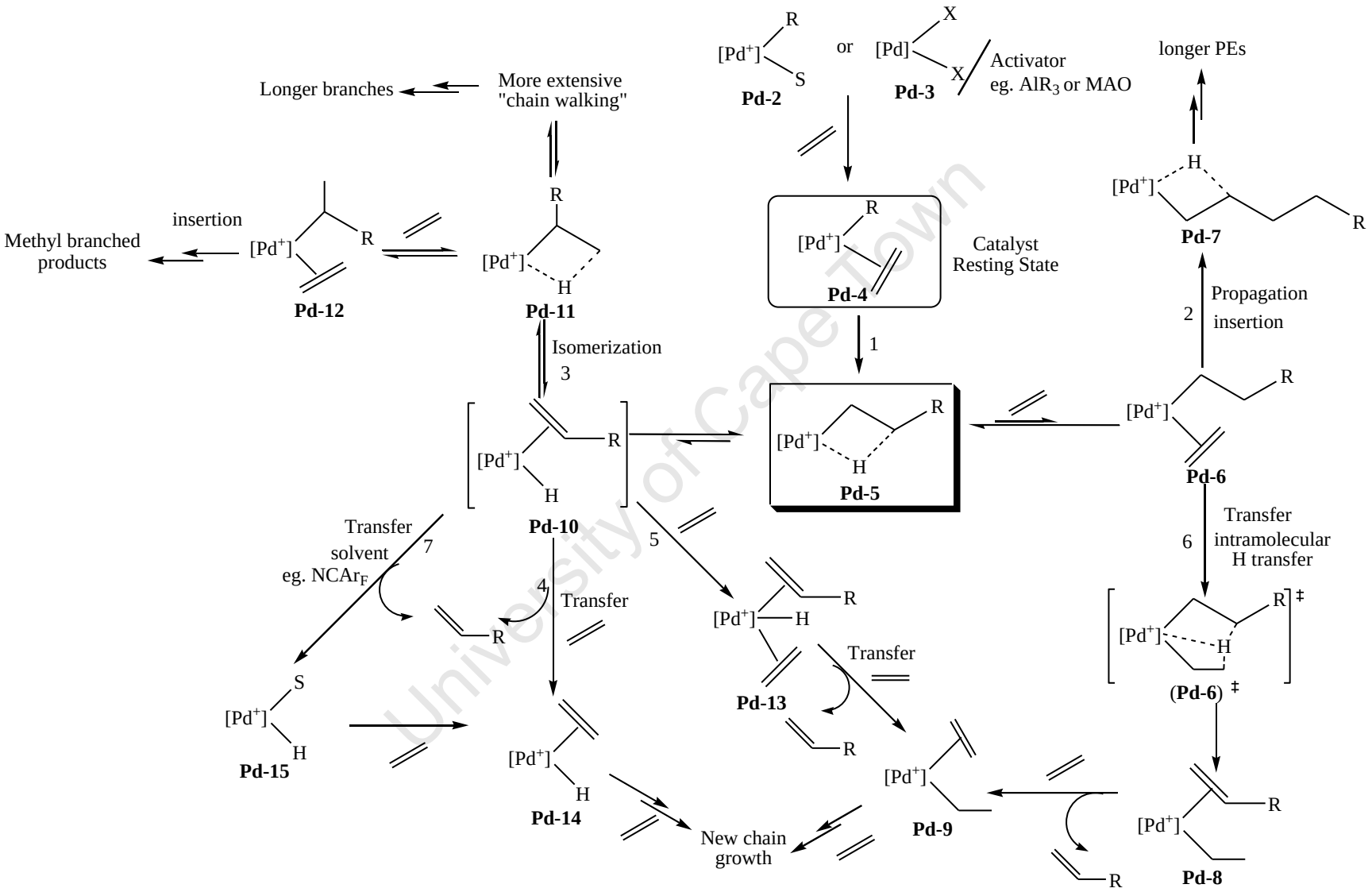

Scheme 1.6 Proposed mechanisms for palladium-catalysed ethylene oligomerization/polymerization (ligand is omitted).

1.4.2 Chain initiation, propagation and isomerization: NMR spectroscopic approach and computational insights

Many mechanistic investigations of ethylene oligomerization/polymerization catalysed by well-defined palladium catalysts have been reported, including NMR spectroscopic studies complemented by theoretical calculations. Mechanistic details of these catalyst systems are summarized in Scheme 1.7.

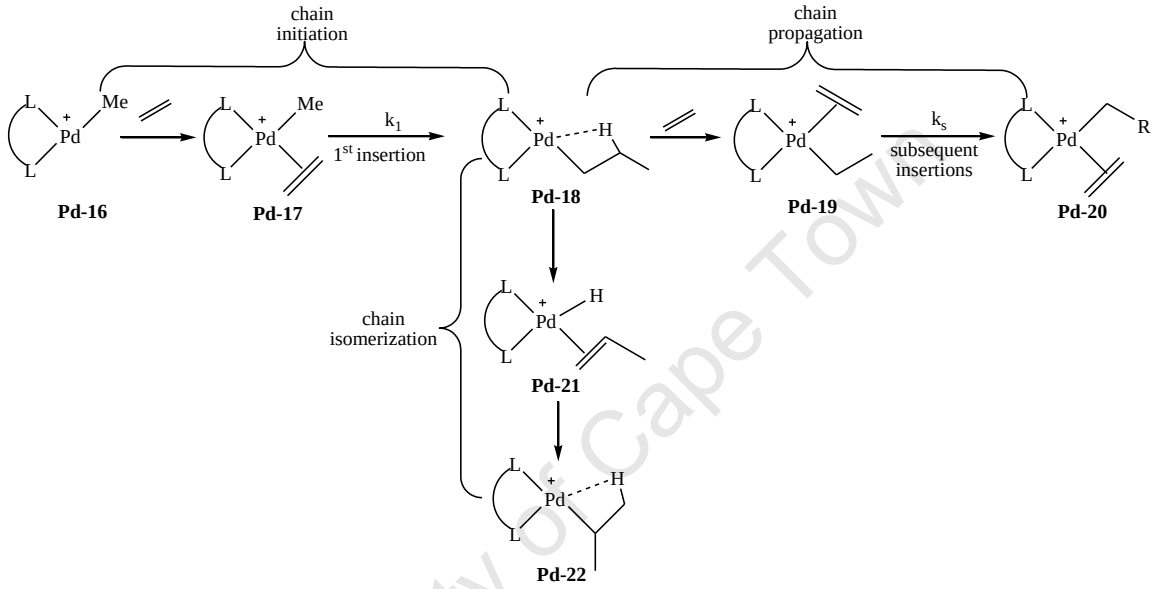

Scheme 1.7 NMR studied mechanistic details in ethylene polymerization reactions.

The initiation reaction includes olefin coordination and insertion. Characterization of catalyst resting states, **Pd-17**, and measurement of insertion barriers were investigated by using low-temperature NMR spectroscopy by Brookhart's group as well as other groups (Table 1.3). The ensuing first insertion of ethylene into the Pd-methyl bond is reported to be first order in catalyst, and the rate for this step was determined by monitoring the decrease of the integral for the Pd-*Me* signal in the NMR spectrum.

Chain propagation is the reaction of olefin coordination and insertion giving a linear polymer. The rate for subsequent insertions for chain growth was determined from the turnover frequency based on the decreasing signal for free ethylene in solution by ^{1}H NMR spectroscopy (Table 1.3). This rate was found to be zero order in ethylene. As shown in Table 1.3, the ethylene insertion barriers for the complexes with symmetrical ligands (e.g. **L_3 – L_9, L_{20} – L_{26}**) are found to be lower than those with asymmetrical ligands (e.g. **L_{17} – L_{19},**

L_{27} – L_{34}). This could be due to the fact that the asymmetrical ligands possibly provide less stabilization in the transition state than symmetrical ligands. In this case a larger ground/transition state energy difference can be expected for the asymmetrical bidentate ligands.[47]

The effects of substituents on these barriers were also observed. For α-diimine-palladium complexes, increasing the bulk of the *ortho* substituents on the aryl groups of α-diimine ligands **L_4** to **L_8** was observed to lower the barrier to insertions and an increase in TOF.[80] For the palladium complexes containing bidentate phenacyl-diarylphosphine ligands **L_{27} – L_{34}**, a decrease in the donor ability of either the diaryl phosphine ligand or the keto group were observed and results in a decrease the insertion barrier. An increase in the donor ability of either group increased the insertion barrier. This is consistent with the general notion that increasing the electrophilicity of the metal centre should decrease the insertion barrier.[51]

Table 1.3 Kinetic data for Pd-catalysed insertion of ethylene

Ligand	Temp (°C)	First insertion		Subsequent insertion		Ref
		k_1 (x 10^3 s^{-1})	$\Delta G_1^{\ddagger}$ (kcal/mol)	k_s (x 10^3 s^{-1}) [c]	$\Delta Gs^{\ddagger}$ (kcal/mol)	
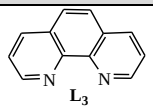 **L_3**	-20	(2.8 ±0.2) x 10^{-1}	18.5 ±0.1[a]	(4.7 ±0.2) x 10^{-2}	19.4 ±0.1	1
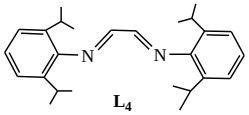 **L_4**	-30	1.9	17.2	0.88	17.5	
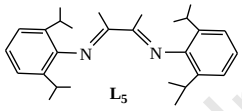 **L_5**	-30	1.7	17.2	3.4	16.9[b]	
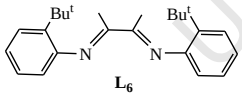 **L_6**	-26	0.83	17.8	0.67	18.0	80
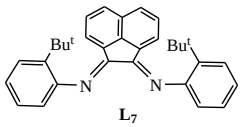 **L_7**	-14	2.1	18.3	0.71	18.8	
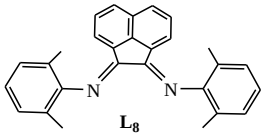 **L_8**	-20	0.63	18.4	0.42	18.6	
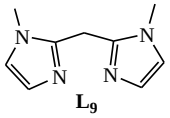 **L_9**	-10	1.2(1) x 10^{-1}		1.0(1) x 10^{-1}		42
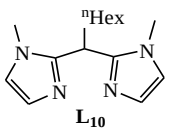 **L_{10}**	-10	1.6(1) x 10^{-1}				

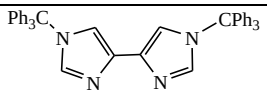 **L_{11}**	-10	$1.0(1) \times 10^{-1}$		$0.48(5) \times 10^{-1}$		42
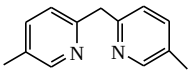 **L_{12}**	-10	$9.0(9) \times 10^{-1}$		$2.0(2) \times 10^{-1}$		
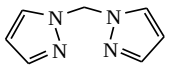 **L_{13}**	-10	$3.6(3) \times 10^{-1}$		$2.0(2) \times 10^{-1}$		
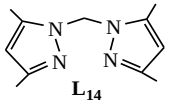 **L_{14}**	-10	$13(1) \times 10^{-1}$		$7.0(7) \times 10^{-1}$		42
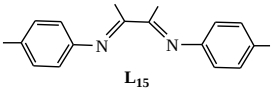 **L_{15}**	-10	$39(4) \times 10^{-1}$		$12(1) \times 10^{-1}$		
	-30	$3.9(4) \times 10^{-1}$				
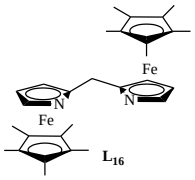 **L_{16}**	-14	2.49×10^{-2}	20.6	1.3 (9.5 °C)	20.2	39
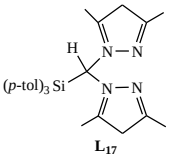 **L_{17}**	-10	3.3(3)	18.3			41
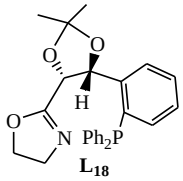 **L_{18}**	-10	1.63×10^{-1}	19.9	1000 (25 °C)	17.5	
	-15	1.00×10^{-1}	19.8			45
	-21	5.3×10^{-2}	19.6			
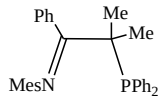 **L_{19}** (Mes = 2,4,6-trimethylphenyl)	23	3×10^{-3}	24.8(3)			47
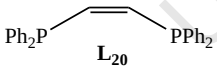 **L_{20}**	-36	4.2×10^{-1}	17.4(2)	0.83	17.2(2)	
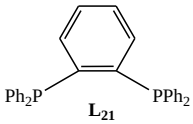 **L_{21}**	-41	8.1×10^{-1}	16.8(2)	1.6 (-35 °C)	16.9(2)	
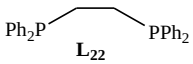 **L_{22}**	-42	1.9×10^{-1}	17.4(1)	1.6 (-29 °C)	17.3(1)	89
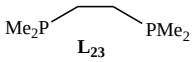 **L_{23}**	-40	0.35×10^{-1}	18.3(1)	1.3 (-23 °C)	17.9(2)	
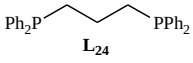 **L_{24}**	-45	4.9×10^{-1}	16.6(1)	5.5 (-36 °C)	16.3(1)	
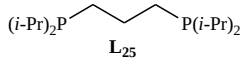 **L_{25}**	-44	1.02	16.5(1)			
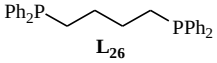 **L_{26}**	-40	7.8×10^{-1}	16.8(1)	2.5 (-35 °C)	16.6(1)	

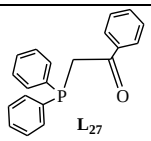 **L_{27}**	-20	1.27(3) x 10^{-1}	19.2			
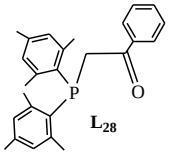 **L_{28}**	-20	1.29(5) x 10^{-1}	19.2			
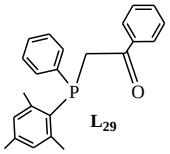 **L_{29}**	-20	7.2(2) x 10^{-2}	19.5			51
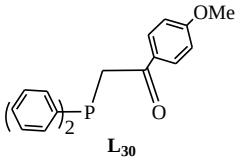 **L_{30}**	-6.3	1.68(9) x 10^{-1}	20.2			
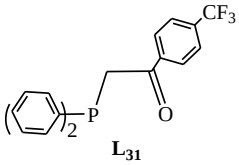 **L_{31}**	-27.7	9.6(2) x 10^{-2}	18.7			
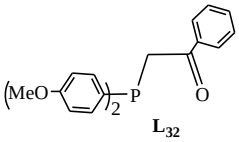 **L_{32}**	-10.2	6.7(1) x 10^{-2}	20.3			
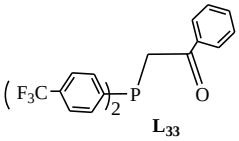 **L_{33}**	-27.7	2.9(1) x 10^{-1}	18.2			
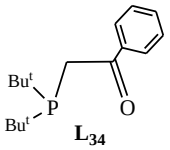 **L_{34}**	-78	4.3 x 10^{-2}	21.4	2.1 x 10^{-2} (0 °C)	21.8	49

[a] $\Delta H_1^{\ddagger}$ = 18.5 ± 0.6 kcal/mol & $\Delta S_1^{\ddagger}$ = -3.7 ± 2.0 eu in a temperature range from -25 to 29 °C.
[b] $\Delta H_s^{\ddagger}$ = 14.2 ± 0.1 kcal/mol & $\Delta S_s^{\ddagger}$ = -11.2 ± 0.8 eu in a temperature range from -40 – 0 °C.
[c] TOF

According to the study by Burns and Jordan,[42] increasing the electrophilic character (*N*-heterocycle = imidazole < pyridine < pyrazole) and the steric bulk of the (N^N)Pd unit leads to moderate (up to *ca.* 10-fold) increase in ethylene insertion rates of $(N^N)Pd(R)(ethylene)^+$ species.

Barriers to insertion in $(N^N)Pd(olefin)R^+$ species have been theoretically addressed by Morokuma[86,87] and Siegbahn.[88] There is reasonable quantitative agreement between the calculated barriers and experimentally measured barrier (see Table 1.4). For model systems of the type $(HN=C(H)C(H)=NH)Pd(olefin)R^+$, the insertion barriers of initial ethylene insertion

were in the range of 16.2 to 16.7 kcal/mol according to different calculations. Moving to the system bearing bulky *ortho*-disubstituted aryl groups and with a substituted backbone, $\mathbf{L_5}$, an insertion barrier of 14.1 kcal/mol was reported by Morokuma.[87] In this case the experimental barrier was measured to be 17.2 kcal/mol.[80]

The isomerisation reaction is suggested to arise from so called "chain walking". This involves rapid β-hydride elimination from a normal metal alkyl intermediate; **Pd-18** giving a hydridometal-olefin complex **Pd-21** followed by reinsertion of the olefin into the metal-hydride bond provides iso-alkylmetal species **Pd-22**, and subsequent chain growth from the iso-alkylmetal complex. Theoretical calculations have been reported for β-agostic n-propyl and isopropyl Pd-α-diimine compounds and it was found that the β-agostic isopropyl species was favoured by 0.5 to 2.0 kcal/mol (see Table 1.4).[87] The chain isomerisation barriers were calculated to be *ca.* 5 kcal/mol for the "model" system.[86–88] It was however found to be 0.2 kcal/mol for the "real" system (with $\mathbf{L_5}$).[87] This is consistent with the suggestion by Brookhart[59(b)] that increase steric bulk of the diimine ligand leads to an increase in branching.

Table 1.4 Theoretical data for Pd-catalysed insertion of ethylene and chain isomerization

Ligand	Method	First insertion	Subsequent insertion	Chain isomerization	Ref
		ΔG (kcal/mol)	ΔG (kcal/mol)	ΔG (kcal/mol)	
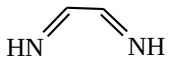 model	B3LYP/BSI	16.7	17.5	5.8	86
	B3LYP/MM3	16.2		5.4	87
	B3LYP/LANDL2DZ	16.4	18	4.8	88
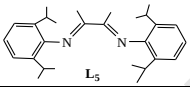	B3LYP/MM3	14.1 (17.2*)		0.2	87

* Measured by low-temperature NMR spectroscopy.[80]

In the NMR spectroscopy study, Brookhart and co-workers[80] did not directly observed a β-agostic n-propyl species. On the contrary, the static spectra obtained below *ca.* -110 ^{o}C were consistent with a β-agostic isopropyl species. ΔG for the n-propyl/ isopropyl equilibrium was determined to be *ca.* 1.2 – 1.3 kcal/mol, which is in agreement with the theoretical values.

1.5 Conclusions

Due to the fact that the demand for linear α-olefins in the $C_4 – C_{10}$ range is growing fast, the catalytic oligomerization of ethylene has attracted much research interest. This has led to an effort to identify and fine-tune the parameters that influence the activity and selectivity of suitable catalysts. In this chapter, we have reviewed palladium complexes with various chelating ligands such as N^N, P^N, P^O, N^O, etc., and their use as catalysts or catalyst precursors for homo-oligomerization of ethylene.

These comparative studies showed that changing the coordination properties of ligands by simple modification of the ligand architecture and the incorporation of various substituents can result in beneficial effects on ethylene oligomerization reactions. For example, within the family of P^N ligands, variables include the basicity of the N-donor moiety, from pyridines to less basic oxazolines, and the stereoelectronic properties of the phosphorus donor, from a phosphine to a phosphinite or phosphonite type. Moreover, effects of varying reaction parameters such as the kind of solvent, reaction temperature and time, ethylene pressure and catalyst composition, i.e., Al/Pd ratios, have been found to influence the catalytic activity, selectivity, Schulz-Flory distribution and product yields.

Both experimental and theoretical studies of palladium-catalysed ethylene oligomerization/polymerization have been reported. In one sense, these studies can be divided into two distinct classes: 1) the adjustment of ligands, co-catalyst, and solvent in an attempt to improve the existing technology, and 2) the search for alternative catalysts.

As far as highly active palladium catalysts are concerned, these are relatively rare. This means that research into improving the production of specific short-chain α-olefins through more active, selective, and stable palladium catalysts will continue to attract attention. The search for new transition metal catalysts for olefin oligomerization/polymerization, which includes the synthesis of new functional ligands, their coordination chemistry, and the systematic study of the catalytic properties of their metal complexes, will retain its important position in the area of α-olefins production.

1.6 Aims and Objectives of the Thesis

1.6.1 Aims

Among the palladium catalysts for ethylene oligomerization, complexes containing nitrogen donor ligands are the most reported in the literature (see Table 1.2). In an attempt to search for new palladium catalysts with nitrogen donor ligands, a series of new cyclometallated palladium complexes bearing *N*-benzylidenebenzylamines, **I**, were synthesized by Mungwe and Swarts in Mapolie's group at Stellenbosch University recently.[91] *N*-benzylidenebenzylamines combine with palladium as bidentate ligands through a cyclometallation method. These kinds of complexes have been extensively used in Suzuki and Heck coupling reactions. In order to expand their utility, they have been tested in another C-C linkage reaction, ethylene oligomerization, in the presence of an aluminum co-catalyst such as MAO or MMAO. However, low or no activity was observed. On the other hand, they have also been tested in phenylacetylene polymerization. In this case, they showed reasonable catalytic activity.[92]

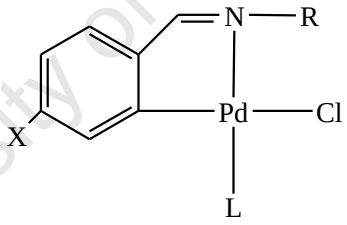

X = H, Cl, Br, Me
R = 2,6-di-^{i}Pr, Ph, Pr
L = PPh_3, PMe_3

I

In order to adjust efficiently the catalyst system and improve the catalytic activity for ethylene oligomerization, it is important to investigate and understand why the current catalyst system has low or no activity. With the aim to gain insight into the potential problems which may exist in the current cyclometallated palladium catalyst system (**I**), theoretical and experimental studies have been carried out in this project.

1.6.2 Specific objectives

The catalytic mechanisms of above type of cyclometallated palladium complexes in coupling reactions are well understood. For ethylene oligomerization reactions, however, there is still debate about the possible mechanisms. To reach the aim of the theoretical study, the following objectives were proposed:

1. use molecular modelling as a tool to study the interaction of the cyclometallated palladium precatalyst with co-catalyst MAO, i.e., catalyst activation process,
2. study the possible mechanisms of their ethylene oligomerization reactions, and
3. identify a possible reason why the cyclometallated Pd systems show low activity for ethylene oligomerization.

The results of these investigations are described in Chapter 2.

Salicylaldimines (N^O), a class of Schiff-base ligands, have a similar nature to the currently studied *N*-benzylidenbenzylamines (N^C). Both are mono-anionic heteroditopic ligands. Palladium complexes containing N^O and N^C chelate ligands are both known to catalyze C-C bond formation reactions such as the Suzuki and Heck reactions.[93] On the other hand, N^O chelating ligands such as "Salicylaldiminato", known as "Grubbs ligand", have been incorporated with transition metals and applied in ethylene polymerization reactions.[75(a)-(b)] Several (N^O) ligated palladium complexes were investigated as catalysts for ethylene oligomerization (**33**, **34** in Table 1.2) and polymerization.[94] In contrast, there are no related applications of the (N^C) ligated transition metal complexes. In view of this, a series of comparative studies was proposed to be carried out on platinum complexes bearing N^C and N^O ligands to investigate their different chemistry. The use of platinum is due to its similar chemistry to palladium. Platinum complexes, however, have enhanced kinetic and thermodynamic stability and are thus easier to study.[95] The platinum analogues could be model complexes for the palladium catalysts.

The aim of the experimental study is thus to investigate the influence of chelate ligands in the platinum complexes and to study their reactivity. The following objectives were set to reach these aims:

4. synthesis of dimethylsulfoxide (dmso) ligated platinum(II) complexes of *N*-benzylidenebenzylamine and *N*-salicylidenebenzylamines;
5. carry out spectroscopic and structural investigations, especially to investigate the

influence of chelate ligands in the above complexes;

6. carry out various reactivity studies on the above dmso ligated platinum(II) complexes to investigate the influence of chelate ligands, namely:
    a. reactions with phosphines
    b. methylation reactions
    c. isomerization reactions
    d. electrochemical studies

The results obtained in investigating objectives 3 and 4 are reported and discussed in Chapter 3 and the results related to objective 5 are reported and discussed in Chapter 4.

1.7 References

1. D. E. James, *Encyclopaedia of Polymer Science and Engineering*; H. F. Mark, N. M. Bikales, C. G. Overberger and G. Menges, Eds.; Wiley-Interscience: New York, 1985; Vol. 6, pp. 429-454.
2. A. H. Tullo, *Single-Site Success: Novel Catalysts are Expanding Beyond the Polyolefin Markets that Nurtured Them*. C&EN August, 2000, Vol. 7, pp. 35-46.
3. D. Vogt, *Oligomerization of Ethylene to Higher Linear α-Olefins in Applied Homogeneous Catalysis with Organometallic Compounds*; B. Cornils and W. A. Hermann, Eds.; VCH: New York, 1996.
4. G. R. Lappin and J. D. Sauer, *Alphaolefins Applications Handbook*; Marcel Decker Inc.: Berkeley, CA, 1989. Vol. 1, pp. 245-258.
5. W. Keim, A. Behr and G. Schmitt, *Grundlagen der Industriellen Chemies Technische Produkte und Prozesse, 1. Auflage*; Otto Salle Verlag GmbH and Co.: Frankfurt am Main, Germany, 1986; pp. 126-150.
6. A. M. Al-Jarallah, J. A. Anabtawi, M. A. B. Siddiqui, A. M. Aitani and A. W. Al-Sa'doun, *Catal. Today*, 1992, **14**, 1.
7. J. Skupinska, *Chem. Rev.*, 1991, **91**, 613.
8. D. Vogt, *Applied Homogeneous Catalysis with Organometallic Compounds*, VHC, New York, 1996.
9. G. V. Parshall and S. D. Ittel, *Homogeneous Catalysis: The Applications and Chemistry of Catalysis by Soluble Transition Metal Complexes*, John Wiley and Sons, New York, 1992.
10. G. P. Belov, *Russ. J. Appl. Chem.,* 2008, **81**, 1655.
11. M. Peuckert and W. Keim, *Organometallics*, 1983, **2**, 594.
12. W. Keim, A. Behr, B. Limbacker and C. Krüger, *Angew. Chem. Int. Ed.*, 1978, **17**, 466.
13. W. Keim, A. Behr and G. Kraus, *J. Organomet. Chem*., 1983, **251**, 377.
14. M. Peuckert and W. Keim, *J. Mol. Catal*., 1984, **22**, 289.
15. W. Keim and R. P. Schulz, *J. Mol. Catal*., 1994, **92**, 21.
16. Example references: (a) J. Wang, W. Li, B. Jiang and Y. Yang, *J. Appl. Polym. Sci*., 2009, **113**, 2378; (b) L. Xiao, R. Gao, M. Zhang, Y. Li, X. Cao and W.-H. Sun, *Organometallics*, 2009, **28**, 2225; (c) M. Zhang, R. Gao, X. Hao and W.-H. Sun, *J. Organomet. Chem*., 2008, **693**, 3867; (d) C. Wallenhorst, G. Kehr, H. Luftmann, R. Frohlich and G. Erker, *Organometallics*, 2008, **27**, 6547; (e) S. Jie, S. Zhang and W.-H. Sun, *Eur. J. Inorg. Chem*., 2007, 5584.

17. (a) J. Yu, X. Hu, Y, Zeng, L. Zhang, C. Ni, X. Hao and W.-H. Sun, *New J. Chem*., 2011, **35**, 178; (b) D. Schaarschmidt, J. Kuehnert, S. Tripke, H. G. Alt, C. Goerl, T. Rueffer, P. Ecorchard, B. Walfort and H. Lang, *J. Organomet. Chem*., 2010, **695**, 1541; (c) K. Song, H. Gao, F. Liu, J. Pan, L. Guo, S. Zai and Q. Wu, *Eur. J. Inorg. Chem*., 2009, 3016.
18. Y. Kusunoki, R. Katsuno, N. Hasegawa, S. Kurematsu, Y. Nago, K. Ishii and J. Tsutsumi, *J. Bull. Chem. Soc. Jpn*., 1966, **39**, 2021.
19. S. D. Ittel, L. K. Johnson and M. Brookhart, *Chem. Rev*., 2000, **100**, 1169.
20. V. C. Gibson and S. K. Spitzmesser, *Chem. Rev*., 2003, **103**, 283.
21. C. Bianchini, G. Giambastiani, L. Luconi and A. Meli, *Coord. Chem. Rev*., 2010, **254**, 431.
22. F. Speiser, P. Braunstein and L. Saussine, *Acc. Chem. Res*., 2005, **38**, 784.
23. P. Braunstein and F. Naud, *Angew. Chem., Int. Ed*., 2001, **40**, 680.
24. K. N. Gavrilov, O. G. Bondarev, R. V. Lebedev, A. A. Shiryaev, S. E. Lyubimov, A. I. Polosukhin, G. V. Grintselev-Knyazev, K. A. Lyssenko, S. K. Moiseev, N. S. Ikooikov, V. N. Kalinin, V. A. Davankov, A. V. Korostylev and H.-J. Gais, *Eur. J. Inorg. Chem*., 2002, 1367.
25. S. Tsuji, D. C. Swenson and R. F. Jordan, *Organometallics*, 1999, **18**, 4758.
26. V. C. Gibson, C. M. Halliwell, N. J. Long, P. J. Oxford, A. M. Smith, A. J. P.White and D. J. Williams, *Dalton Trans*., 2003, 918.
27. J. Flapper, H. Kooijman, M. Lutz, A. L. Spek, P. W. N. M. van Leeuwen, C. J. Elsevier and P. C. J. Kamer, *Organometallics*, 2009, **28**, 3272.
28. G. Müller, M. Klinga, P. Osswald, M. Leskelä and B. Z. Rieger, *Naturforsch., B: Chem. Sci*., 2002, **57**, 803.
29. C. E. Anderson, A. S. Batsanov, P. W. Dyer, J. Fawcett and J. A. K. Howard, *Dalton Trans.*, 2006, 5362.
30. S. P. Meneghetti, P. J. Lutz and J. Kress, *Organometallics*, 1999, **18**, 2734.
31. D. Sirbu, G. Consiglio and S. Gischig, *J. Organomet. Chem*., 2009, **691**, 1143.
32. P.-Y. Shi, Y.-H. Liu, S.-M. Peng and S.-T. Liu, *Organometallics*, 2002, **21**, 3203.
33. W. Keim. *J. Mol. Catal*., 1989, **52**, 19.
34. (a) C. Gennari and U. Piarulli, *Chem. Rev*., 2003, **103**, 3071; (b) N. Fey, J. N. Harvey, G. C. Lloyd-Jones, P. Murray, A. G. Orpen, R. Osborne and M. Purdie, *Organometallics*, 2008, **27**, 1372.
35. J. Flapper, H. Kooijman, M. Lutz, A. L. Spek, P. W. N. M. van Leeuwen, C. J. Elsevier and P. C. J. Kamer, *Organometallics*, 2009, **28**, 1180.
36. O. Daugulis and M. Brookhart, P. S. White, *Organometallics*, 2002, **21**, 5935.

37. S. Abraham, C.-S. Ha and I. Kim, *Macromol. Rapid Commun*., 2006, **27**, 1386.
38. W. Zhang, W.-H., Sun, B. Wu, S. Zhang, H. Ma, Y. Li, J. Chen and P. Hao, *J. Organomet. Chem*., 2006, **691**, 4759.
39. E. V. Salo and Z. Guan, *Organometallics*, 2003, **22**, 5033.
40. B. Blom, M. J. Overett, R. Meijboom and J. R Moss, *Inorganica Chimica Acta*., 2005, **358**, 3491.
41. M. P. Conley, C. T. Burns and R. F. Jordan, *Organometallics*, 2007, **26**, 6750.
42. C. T. Burns and R. F. Jordan, *Organometallics*, 2007, **26**, 6276.
43. S. Strömberg, M. Oksman, L. Zhang and K. Zetterberg, *Acta Chem. Scand*., 1995, **49**, 689.
44. (a) F. C. Rix and M. Brookhart, *J. Am. Chem. Soc*., 1995, **117**, 1137; (b) F. C. Rix, M. Brookhart and P. S. White, *J. Am. Chem. Soc*., 1996, **118**, 4746.
45. M. D. Doherty, S. Trudeau, P. S. White, J. P. Morken and M. Brookhart, *Organometallics*, 2007, **26**, 1261.
46. W. Keim, S. Killat, C. F. Nobile, G. P. Suranna, U. Englert, R. Wang, S. Mecking and D. L. Schröder, *J. Organomet. Chem*., 2002, **662**, 150.
47. O. Daugulis and M. Brookhart, *Organometallics*, 2002, **21**, 5926.
48. J. Flapper, P. W. N. M. van Leeuwen, C. J. Wlsevier and P. C. K. Kamer, *Organometallics*, 2009, **28**, 3264.
49. W. Liu, J. M. Malinoski and M. Brookhart, *Organometallics*, 2002, **21**, 2836.
50. I. Brassat, W. Keim, S. Killat, M. Mötjratj, P. Mastrorilli, C. F. Nobile and G. P. Suranna, *J. Mol. Catal. A: Chem*., 2000, **157**, 41.
51. J. M. Mlinoski and M. Brookhart, *Organometallics*, 2003, **22**, 5324.
52. J. Heinicke, M. Köhler, N. Peulecke, M. K. Kindermann, W. Keim and M. Köckerling, *Organometallics*, 2005, **24**, 344.
53. Z. Shen and R. F. Jordan, *J. Am. Chem, Soc*., 2010, **132**, 132.
54. J. Andrieu, P. Braunstein, F. Naud and R. D. Andams, *J. Organomet. Chem*., 2000, **601**, 43.
55. S. Budagumpi, Y. Liu, H. Suh and I. Kim, *J. Organomet. Chem*., 2011, **696**, 1887.
56. Y. Chen, S. Mandal and A. Sen, *Organometallics*, 2010, **29**, 3160.
57. S. Ojwach, M. G. Tshivhase, I. A. Guzei, J. Darkwa and S. F. Mapolie, *Can. J. Chem*., 2005, **83**, 843.
58. C. Sui-Seng, L. F. Groux and D. Zargarian, *Organometallics*, 2006, **25**, 571.
59. (a) C. M. Killian, L. K. Johnson and M. Brookhart, *Organometallics*, 1997, **16**, 2005; (b) L. K. Johnson, C. M. Killian and M. Brookhart, *J. Am. Chem. Soc*., 1995, **117**, 6414.

60. G. J. P. Britovsek, S. P. D. Baugh, V. C. Gibson and D. F. Wass, *Angew. Chem. Int. Ed*., 1999, **38**, 428.

61. B. L. Small and M. Brookhart, *J. Am. Chem. Soc*., 1998, **120**, 7143.

62. T. Irrgang, S. Keller, H. Maisel, W. Kretschmer and R. Kempe, *Eur. J. Inorg. Chem*., 2007, 4221.

63. (a) C. T. Burns and R. F. Jordan, *Organometallics*, 2007, **26**, 6737; (b) S. Mecking, L. K. Johnson, L. Wang and M. Brookhart, *J. Am. Chem. Soc*., 1998, **210**, 888; (c) D. J. Temple, L. K. Johnson, R. L. Huff, P. S. White and M. Brookhart, *J. Am. Chem. Soc*., 2000, **122**, 6686.

64. (a) P. Braunstein, *J. Organomet. Chem*., 2004, **689**, 3953; (b) G. Chelucci, G. Orru and G. A. Pinna, *Tetrahedron*, 2003, **59**, 9471; (c) P. Espinet and K. Soulantica, *Coord. Chem. Rev*., 1999, **195**, 499; (d) P. J. Guiry and C. P. Saunders, *Adv. Synth. Catal*., 2004, **346**, 497; (e) G. Helmchen and A. Pfaltz, *Acc. Chem. Res*., 2000, **33**, 336; (f) G. R. Newkome, *Chem. Rev*., 1993, **93**, 2067.

65. Z. B. Guan and W. J. Marshall, *Organometallics*, 2002, **21**, 3580.

66. (a) E. Drent, P. Arnoldy and P. H. M. Budzelaar, *J. Organomet. Chem*., 1993, **455**, 247; (b) G. P. C. M. Dekker, A. Buijs, J. Elsevier, P. W. N. M. van Leeuwen, W. J. J. Smeets, A. L. Spek, Y. F. Wang and C. H. Stam, *Organometallics*, 1992, **11**, 1937.

67. E. van den Beuken, E. Drent and B. L. Feringa, WO 98/42440, 1998 (Shell International Research).

68. E. K. van den Beuken, W. J. J. Smeets, A. L. Spek, B. L. Feringa, *Chem. Commun*., 1998, 223.

69. S. Rush, A. Reinmuth, W. Risse, J. O'Brien, D. R. Ferro and I. Tritto, *J. Am. Chem. Soc*., 1996, **118**, 12230.

70. (a) K. G. Moloy and J. L. Petersen, *J. Am. Chem. Soc*., 1995, **117**, 7696; (b) H. Brunner and H. Weber, *Chem. Ber*., 1985, **118**, 3380; (c) P. G. Cozzi, N. Zimmermann, R. Hilgraf, S. Schaffner and A. Pfaltz, *Adv. Synth. Catal*., 2001, **343**, 450. (d) S. C. van der Slot, J. Duran, J. Luten, P. C. J. Kamer and P. W. N. M. van Leeuwen, *Organometallics*, 2002, **21**, 3873; (e) A. D. Burrows, R. W. Harrington, M. F. Mahon, M. T. Palmer, F. Senia and M. Varrone, *Dalton Trans*., 2003, 3717; (f) C. D. Andrews, A. D. Burrows, J. M. Lynam, M. F. Mahon and M. T. Palmer, *New J. Chem*., 2001, **25**, 824; (g) H. Brunner, B. Reiter and G. Riepl, *Chem. Ber*., 1984, **117**, 1330.

71. S. Trudeau and J. P. Morken, *Tetrahedron*, 2006, **62**, 11470.

72. W. Keim, B. Hoffmann, R. Lodewick, M. Peuckert, G. Schmidt, J. Fleischhauer and U.

Meier, *J. Mol. Catal*., 1979, **6**, 79.

73. J. Andrieu, P. Braunstein, F. Naud, R. D. Adams and R. Layland, *Bull. Soc. Chim. Fr.*, 1996, **133**, 669.
74. J. Andrieu, P. Braunstein and F. Naud, *Dalton Trans.*, 1996, 2903.
75. (a) C. Wang, S. Friedrich, T. R. Younkin, R. T. Li, R. H. Grubbs, D. A. Bansleben and M. W. Day, *Organometallics*, 1998, **17**, 3149; (b) T. R. Younkin, E. F. Connor, J. I. Henderson, S. K. Friedrich, R. H. Grubbs and D. A. Bansleben, *Science*, 2000, **287**, 460; (c) F. A. Hicks and M. Brookhart, *Organometallics*, 2001, **20**, 3217; (d) J. C. Jenkins and M. Brookhart, *Organometallics*, 2003, **22**, 250; (e) F. A. Hicks, J. C. Jenkins and M. Brookhart, *Organometallics*, 2003, **22**, 3533; (f) M. J. Rachita, R. L. Huff, J. L. Bennett and M. Brookhart, *J. Polym. Sci., Part A: Polym. Chem*., 2000, **38**, 4627; (g) T. Dohler, H. Gorls and D. Walther, *Chem. Commun*., 2000, 945; (h) D. Walther, T. Dohler, N. Theyssen and H. Görls, *Eur. J. Inorg. Chem*., 2001, 2049.
76. (a) Y. Liu, M. Zhang, M. G. B. Drew, Z.-D. Yang and Y. Liu, *J. Mol. Struct.: THEOCHEM*, 2005, **726**, 277; Y. Liu, M. G. B. Drew and Y. Liu, *J. Mol. Struct.: THEOCHEM*, 2007, **821**, 30.
77. (a) S. Tsuji, T. R. Younkin, D. C. Swenson and R. F. Jordan. *Organometallics*, 1999, **18**, 4758; (b) K. Li, J. Darkwa, I. A. Guzei and S. F. Mapolie, *J. Organomet. Chem*., 2002, **660**, 108; (c) S. M. Nelana, J. Darkwa, I. A. Guzei and S. F. Mapolie, *J. Organomet. Chem*., 2004, **689**, 1835; (d) I. A. Guzei, K. Li, G. A. Bikzhanova, J. Darkwa and S. F. Mapolie. *Dalton Trans*., 2003, 715.
78. (a) T. M. Frankom, J. C. Green, A. Nagy, A. K. Kakkar and T. B. Marder, *Organometallics*, 1993, **12**, 3688; (b) M. P. Gamasa, J. Gimeno, C. Gonzalez-Bernardo, B. M. Martin-Vaca, D. Monti and M. Bassetti, *Organometallics*, 1996, **15**, 302; (c) J. M. O'Connor and C. P. Casey, *Chem. Rev*., 1987, **87**, 307.
79. (a) R. Vollmerhaus, F. Bélanger-Gariépy and D. Zargarian, *Organometallics*, 1997, **16**, 4762; (b) M.-A. Dubois, R. Wang, D. Zargarian, J. Tian, R. Vollmerhaus, Z. Li and S. Collins, *Organometallics*, 2001, **20**, 663; (c) L. F. Groux and D. Zargarian, *Organometallics*, 2001, **20**, 3811; (d) L. F. Groux, D. Zargarian, L. C. Simon and J. B. P. Soares, *J. Mol. Catal. A*, 2003, **193**, 51; (e) L. F. Groux and D. Zargarian, *Organometallics*, 2003, **22**, 3124; (f) L. F. Groux and D. Zargarian, *Organometallics*, 2003, **22**, 4759; (g) H. Sun, W. Li, X. Han, Q. Shen and Y. Zhang, *J. Organomet. Chem*., 2003, **688**, 132; (h) W.-F. Li, H.-M. Sun, Q. Shen, Y. Zhang and K.-B Yu, *Polyhedron*, 2004, **23**, 473; (i) M. Jimenez-Tenorio, M. C. Puerta, I. Salcedo, P. Valerga, S. I. Costa, L.

C. Silva and P. T. Gomes, *Organometallics*, 2004, **23**, 3139; (j) H. M. Sun, Q. Shao, D. M. Hu, W. F. Li, Q. Shen and Y. Zhang, *Organometallics*, 2005, **24**, 331; (k) D. Gareau, C. Sui-Seng, L. F. Groux, F. Brisse and D. Zargarian, *Organometallics*, 2005, **24**, 4003.

80. D. J. Tempel, L. K. Johnson, R. L. Huff, P. S. White and M. Brookhart, *J. Am. Chem. Soc*., 2000, **122**, 6686.
81. S. Bhaduri and D. Mukesh, *Homogeneous Catalysis: Mechanisms and Industrial Applications*. Wiley-Interscience: New York, 2000, pp. 138-147.
82. (a) P. Cossee, *J. Catal*., 1964, **3**, 80; (b) E. J. Arlman and P. Cossee, *J. Catal*., 1964, **3**, 99.
83. (a) S. A. Svejda, L. K. Johnson and M. Brookhart, *J. Am. Chem. Soc.*, 1999, **121**, 10634; (b) M. Brookhart, M. L. H. Green and L.-L. Wong, *Inorg. Chem*., 1988, **36**, 1; (c) D. J. Tempel and M. Brookhart, *Organometallics*, 1998, **117**, 2290; (d) F. M. Conroy-Lewis, L. Mole, A. D. Redhouse, S. A. Litster and J. L. Spencer, *J. Chem. Soc., Chem. Coummun.*, 1991, 1601.
84. P. W. N. M. van Leeuwen, *Homogeneous Catalysis: Understanding the Art*. Kluwer Academic Publishers, The Netherlands, 1999, pp. 175 – 191.
85. (a) L. Deng, P. Margl and T. Ziegler, *J. Am. Chem. Soc.*, 1997, **119**, 1094; (b) L. Deng, T. K. Woo, L. Cavallo, P. M. Margl and T. Ziegler, *J. Am. Chem. Soc.*, 1997, **119**, 6177.
86. D. G. Musaev, M. Svensson, K. Morokuma, S. Stromberg, K. Zetterberg and P. E. M. Siegbahn, *Organometallics*, 1997, **16**, 1933.
87. R. D. J. Froese, D. G. Musaev and K. Morokuma, *J. Am. Chem. Soc*., 1998, **120**, 1581.
88. S. Stromberg, K. Zetterberg and P. E. M. Siegbahn, *J. Chem. Soc., Dalton Trans*., 1997, 4147.
89. F. C. Rix and M. Brookhart, *J. Am. Chem. Soc.*, 1995, **117**, 1137.
90. J. Ledford, C. S. Shultz, D. P. Gates, P. S. White, J. M. DeSimone and M. Brookhart, *Organometallics*, 2001, **20**, 5266.
91. (a) N. W. Mungwe, M.Sc. thesis, *The synthesis of the cyclometallated palladium complexes and their applications in olefin oligomerization and in phenylacetylene oligomerization/polymerization*, University of Western Cape, 2008; (b) A. J. Swarts, M.Sc. thesis, *Mononuclear and multinuclear palladacycles as catalyst precursors*, Stellenbosch University, 2010.
92. N. Mungwe, A. Swarts, S. F. Mapolie and G. Westman, *J. Organomet. Chem*., 2011, **696**, 3527.
93. For N^O ligands: (a) Y. Liu, M. G. B. Drew and Y. Liu, *J. Mol. Struct.: THEOCHEM*, 2007, **809**, 29; (b) J. Cui, M. Zhang and Y. Zhang, *Inorg. Chem. Commu.*, 2010, **13**, 81.

For (N^C) ligands: e.g. (a) J. Dupont, C. S. Consorti and J. Spencer; *Chem. Rev*., 2005, **105**, 2527; (b) V. V. Dunina and O. N. Gorunova; *Russ. Chem. Rev.*, 2004, **73**, 309.

94. E.g.: I. Kenichi, W. Akira and K. Kaoru. Manufacture of salicylideneamine-based transition metal complex polymerization catalysts. *Jpn. Kokai Tokkyo Koho*, (2001), 13 pp. CODEN: JKXXAF JP 2001072654 A 20010321 CAN 134:237968 AN 2001:194781

95. (a) F. R. Hartley, *The Chemistry of Platinum and Palladium*, Applied Science Publishers Ltd, London, 1973, pp. 331 – 334; (b) A. Garoufis, S. K. Hadjikakou, N. Hadjiliadis, *Metallotherapeutic Drugs and Metal-based Diagnostic Agents*; M. Gielen, E. R. T. Tiekink, Eds; John Wiley & Sons Ltd, England, 2005, pp. 339 – 415.

Chapter 2

DFT Insight into Role of MAO in Catalyst Activation and a Probe into Possible Mechanisms for Cyclometallated Palladium-Catalysed Oligomerization

2.1 Introduction

Transition metal-catalysed ethylene oligomerization has been one of the dominant synthetic routes to α-olefins.[1] Two possible oligomerization mechanisms have been proposed for this process and these will be discussed later. A substantial number of transition metal ethylene oligomerization catalysts show high activity but very poor selectivity for linear α-olefins, usually forming products with either a Schulz-Flory or Possion distribution.[2] These product distributions are due to similar propagation and termination rates in the polymerization mechanisms proposed by Cossee and Arlman,[3] which was discussed in detail in Chapter 1. In contrast to this, another reaction mechanism, shown in Scheme 2.1 (the so-called metallacycle mechanism),[4] can apply to systems producing exclusively a single group of olefins such as, e.g., 1-hexene or 1-octene.[5]

The metallacycle mechanism (Scheme 2.1) was shown experimentally[6] and by using DFT calculations[7–12] to be a consequence of two molecules of ethylene coordinating to the active species **A** and forming intermediate **B**. The two coordinated ethylene entities in **B** react by an oxidative coupling reaction to form a metallacyclopentane **C**. At this stage, insertion of a third molecule of ethylene forming a metallacycloheptane **D** can be observed. 1-Hexene is liberated by reductive elimination from **D**, or another ethylene molecule inserts in **D** to form a larger size metallacycle. Although polyethylene is likely the result of polymerization via the Cossee-Arlman pathway, the formation of polyethylene following an extended metallacyclic pathway should, however, not be excluded. This is particularly true considering the experimental results with chromium-based catalysts,[13–15] where polyethylene is sometimes observed as a product.

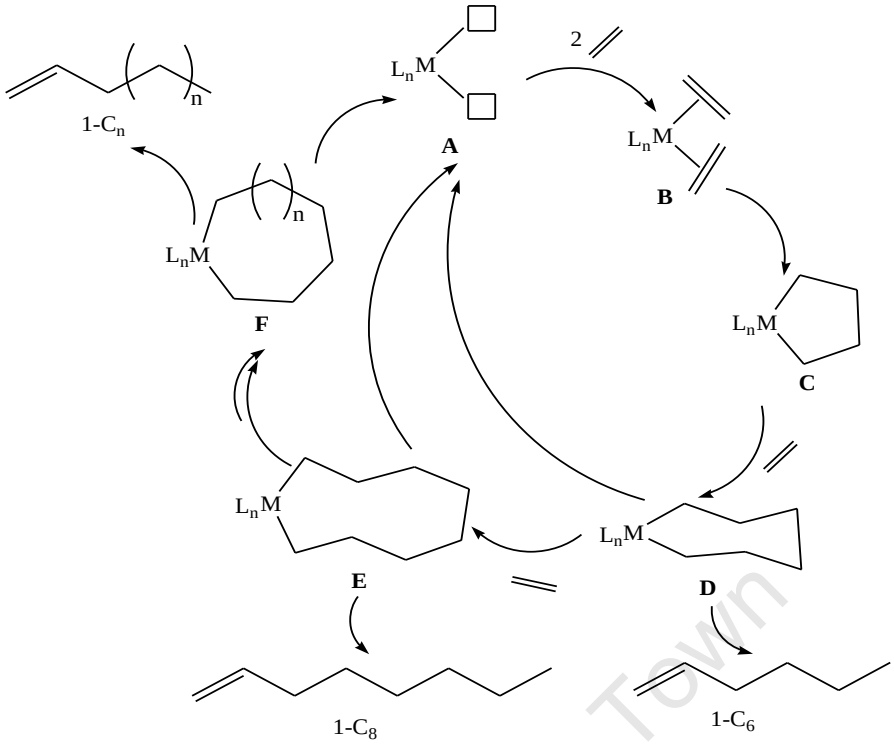

Scheme 2.1 Metallcycle mechanism for catalytic ethylene trimerization, tetramerization and polymerization.

In principle, a metallacycle mechanism offers the potential of catalyst tuning toward lighter $C_{2n}H_{4n}$ oligomers (trimerization and tetramerization), without concomitant 1-butene formation. This is not possible when a Cossee-Arlman mechanism is operative, as a shift to lower carbon numbers necessarily increases the percentage of 1-butene. Many studies have been carried out to elucidate the mechanism of chain growth and to investigate the effects of ligand modification on olefin selectivity in olefin oligomerization/polymerization reactions. The mechanism of chain growth has been shown to be ligand dependent in various transition metal catalyst systems.

The original Cossee-Arlman mechanism was proposed for the $TiCl_3$-based heterogeneous catalyst as shown in Scheme 2.2.[16] When the cyclopentadienyl ligand bearing a hemilabile pendant arene substituent was introduced, the resultant cationic half-sandwich complexes of titanium were found to be transformed from ethylene polymerization catalysts into selective ethylene trimerization catalysts, producing 1-hexene.[17] Computational studies suggest that the pathway for ethylene trimerization occurs through a metallacyclic mechanism that involves Ti(II) and Ti(IV) intermediates (Scheme 2.3). [9–11]

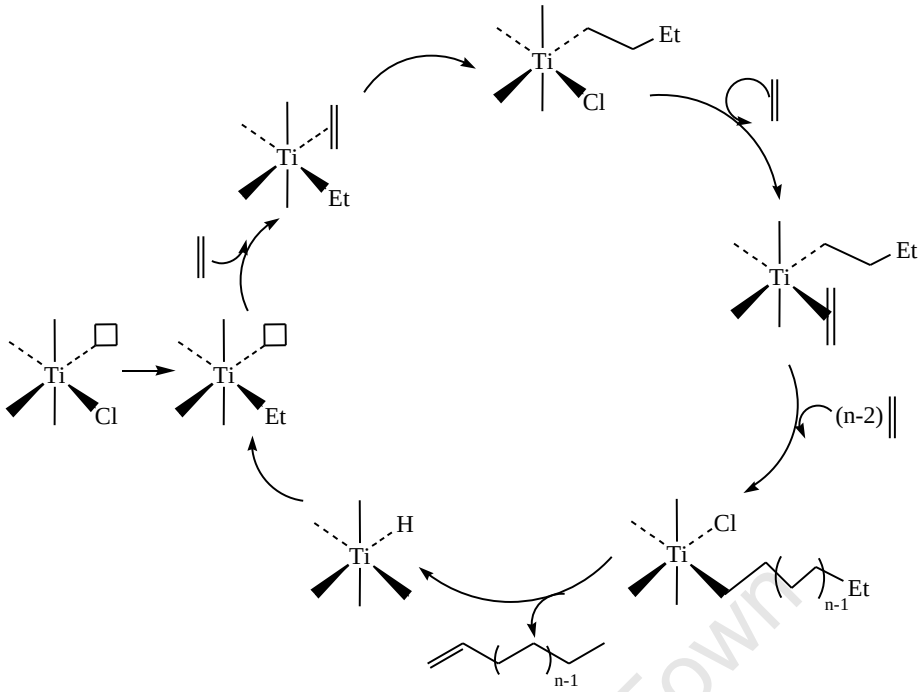

Scheme 2.2 Catalytic cycle for Ti-catalysed ethylene polymerization proposed by Cossee and Arlman.[16]

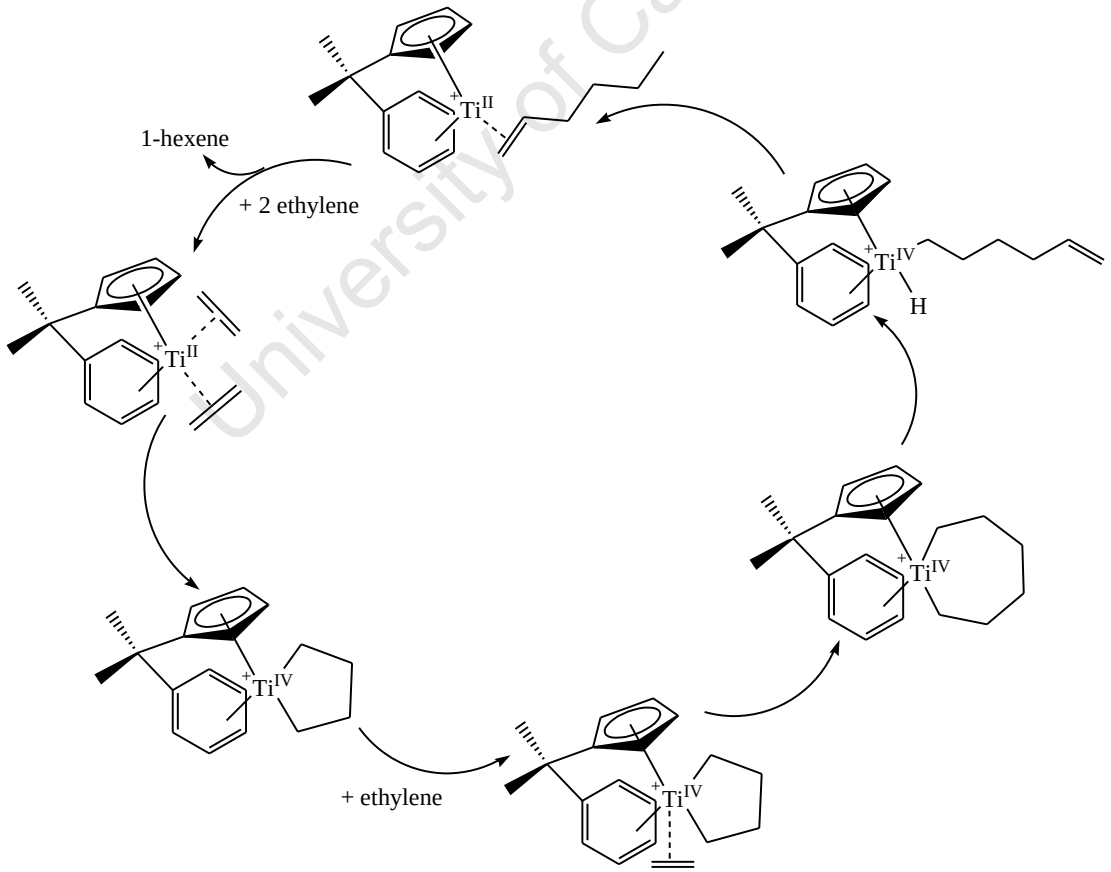

Scheme 2.3 Catalytic cycle for Ti-catalysed ethylene trimerization involving metallacycle intermediates.[17]

By using Cr catalysts, the selective trimerization of ethylene to 1-hexene[18] and the more recent tetramerization to 1-octene[19] has opened a new phase in oligomerization of ethylene. The mode of selective 1-hexene and 1-octene generation relies on a metallacyclic mechanism (Scheme 2.1), which has been supported by the use of deuterium labelling techniques. For example, catalytic trimerization of a 1:1 mixture of C_2D_4 and C_2H_4 using the Cr-PNP-based catalytic systems leads to a 1-hexene isotopomer distribution of only C_6H_{12}, $C_6H_8D_4$, $C_6H_4D_8$ and C_6D_{12}.[20] The lack of observing H/D scrambling provides unequivocal support for the metallacycle mechanism.[20] For the Cr catalysts which give high activity in oligomerization forming Schulz-Flory distributions of LAOs, the mechanism of chain growth was indicated to be ligand dependent by way of deuterated experiments. These experimental facts clearly indicate that ethylene oligomerization using Cr-based pre-catalysts **Cr-1** and **Cr-2** (Figure 2.1), which incorporate CNC-pincer carbene ligands, occurs via an extended metallacycle mechanism.[14] The change to a bidentate ligand in complexes **Cr-3** and **Cr-4** led to a switch in the mechanism of oligomer growth, from metallacycle to Cossee-Arlman type mechanism.[14]

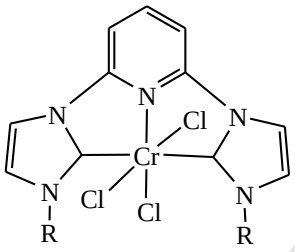

Cr-1, R = ^{i}Pr
Cr-2, R = 2,6-^{i}Pr$_2$C$_6$H$_3$

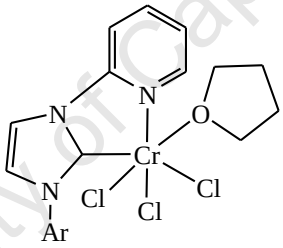

Cr-3

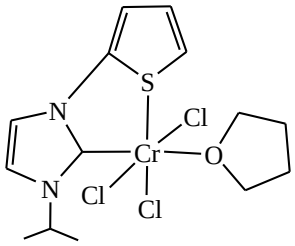

Cr-4

Figure 2.1

The same applies to the nickel-catalysed ethylene oligomerization/polymerization reactions. In spite of the more commonly proposed Cossee-Arlman mechanism,[21–23] reaction mechanisms, which resemble the concerted coupling are also observed for nickel.[24] Some olefin 2+2 dimerization reactions catalysed by nickel systems, developed by Grubbs,[24(a)] involve the oxidative coupling of the two olefin fragments by Ni(0), followed by the decomposition of the nickellacyclopentane complex by reductive elimination (Scheme 2.4).

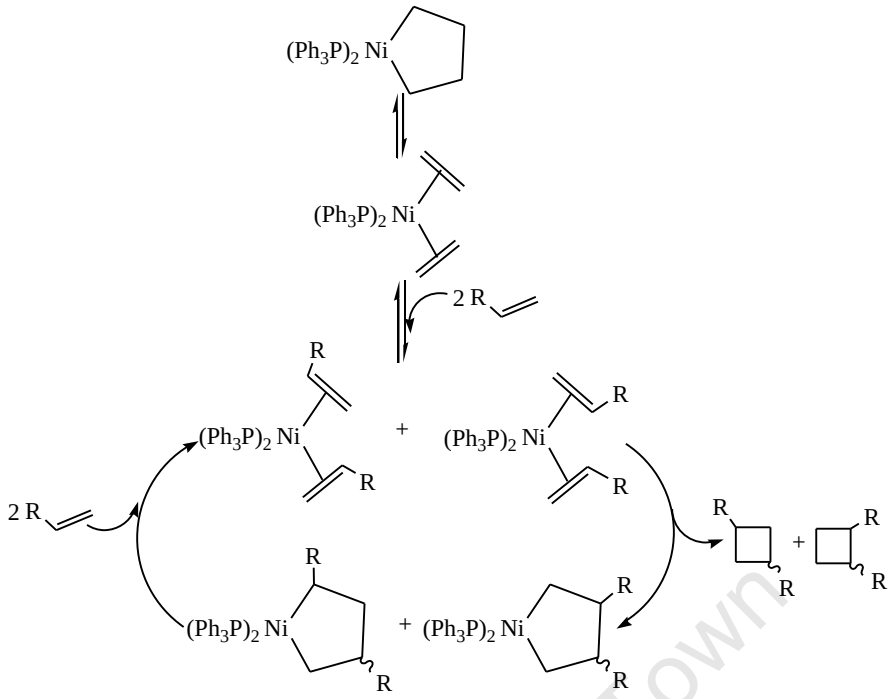

Scheme 2.4 Catalytic cycle for Ni-catalysed olefin dimerization involving metallacycle intermediates.[24]

With these findings, identifying whether a particular catalyst operated via a linear chain growth (Cossee-type) mechanism or a metallacycle mechanism is of more than academic interest. Deuterium labelling techniques could be used to distinguish between the two mechanisms in a relatively straightforward way, as mentioned above. Computational (DFT) methodologies could be used to rationalize some of the key experimental observations and to predict the possible reaction mechanism.

Recently, Bhaduri and co-workers[25] provided theoretical calculations on the mechanism of Cr-catalysed ethylene trimerization. Both Cossee and metallacycle mechanisms were compared, in which the metallacycle mechanism was found to be the most favoured path with cationic Cr intermediates, while the Cossee pathway was followed with neutral intermediates.

Among the palladium catalysts for olefin oligomerization reactions, the complexes containing heteronitrogen donor ligands are the most reported in the literature (see Chapter 1). In an effort to search for new palladium catalysts with a nitrogen donor ligand, a series of new cyclometallated palladium complexes bearing *N*-benzylidenebenzylamines (**I**) have recently been synthesized by Mungwe *et al*.[26]

Cyclometallated palladium complexes have been extensively utilized in Suzuki and Heck coupling reactions and the mechanism of catalytic coupling reactions are well understood.[27] However as catalysts in ethylene oligomerization, there is still debate about the possible mechanism. In order to expand their utility, the catalytic activity of these complexes (**I**) towards olefin oligomerization has been investigated in the presence of methylaluminoxane (MAO) or modified methylaluminoxane (MMAO) (Scheme 2.5). However, low or no activity was observed.

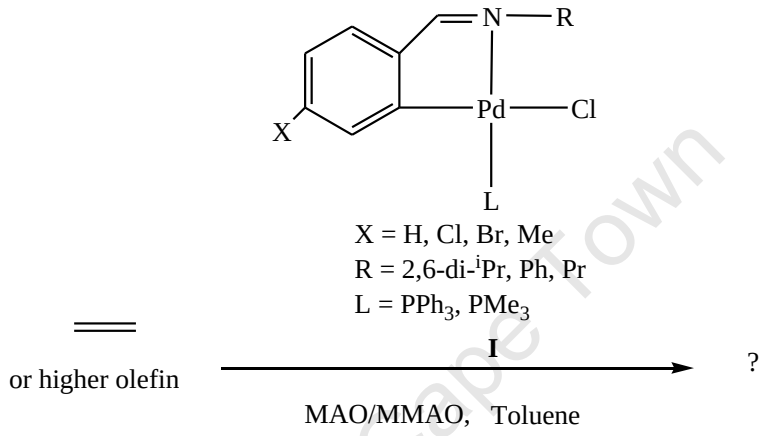

Scheme 2.5

The fundamental understanding of the reaction mechanisms by means of computational studies is important, since it can predict catalytic activity and selectivity in ethylene oligomerization, and, more importantly, it can provide useful insight into the potential problems which may exist in the current cyclometallated palladium catalyst system **(I)**. It could possibly be applied to the efficient modification of ligands to improve this class of complexes or the design of new alternative complexes as active catalysts.

In the current DFT study, MAO was chosen as the model co-catalyst. As one of the most widely used co-catalysts in transition metal-catalysed ethylene oligomerization, MAO is thought to generate the active species from the catalyst precursor.[28] MAO is widely known to play a significant role in several aspects: i) alkylation of the catalyst precursor, ii) generation of a cationic complex, iii) stabilization of cationic complexes acting as counterions, and iv) reactivation of deactivated sites.[29] For the dihalide transition metal catalyst precursors, the active species can be achieved by treating the precatalyst with an alkylating reagent followed by alkyl-abstraction,[30] in which MAO can perform both alkylation and alkyl-abstraction processes as shown in Scheme 2.6. It is generally accepted that an anionic co-catalyst

fragment [RX^-] and a cationic metal fragment [LnM^+] are generated from the alkyl abstraction process by the co-catalyst, which in combination represents the active catalytic system as an ion-pair denoted by [LnM^+][RX^-].[31]

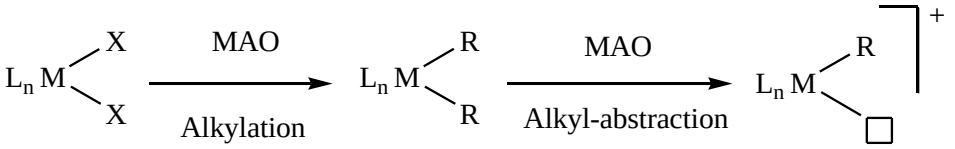

Scheme 2.6 The role of MAO in activation of a dihalide transition metal catalyst.[30]

The possible interactions of palladium complex **Ia** (**I** where X = Me, R = 2,6-di-^{i}Pr, L = PPh_3) with MAO are represented in Scheme 2.7. After alkylation, the methyl functionality on the Pd complex could bridge three-coordinate Al moieties in MAO yielding a formally coordinated Pd-MAO species **II**. Similar structures have been reported in the DFT studies of zirconocene/MAO[32] and chromacycloheptane/MAO interactions.[33] It is well known that Cp_2ZrCl_2 rapidly reacts with MAO to yield the monomethylated complex $Cp_2Zr(Me)Cl$ and that the addition of excess MAO leads to the fully methylated complex Cp_2ZrMe_2.[34] This led to our hypothesis that a Pd-Me complex **III** could be generated from **II** by dissociation of a MAO fragment. On the other hand, the generation of ion-pair complexes, in which a cationic transition metal complex is paired with an anionic co-catalyst fragment, is widely accepted in, for example, metallocene-catalysed polymerization.[1] By means of DFT, a number of studies on catalyst/co-catalyst interactions argue that the interaction of the co-catalyst with the metal occurs via a bridging methyl group.[35] This interaction generates a catalyst/co-catalyst "dissociated" ion-pair complex after abstraction of a methyl group from an appropriate methylated catalyst precursor. A similar possibility of this interaction from **II** to generate a "dissociated" ion-pair species **IV** could as well be considered in our case.

From the Pd-Me species **III**, ethylene could coordinate to the palladium centre via ligand exchange with PPh_3 or via a vacant site after dissociation of the N atom of the bidentate ligand dissociation followed by a Cossee-type mechanistic pathway. While two ethylene molecules could coordinate to the metal centre after ligand dissociation from **IV**, an oxidative coupling reaction could also take place on the Pd(II) centre to give Pd(IV) metallacyclic intermediates, i.e., a metallacycle pathway.

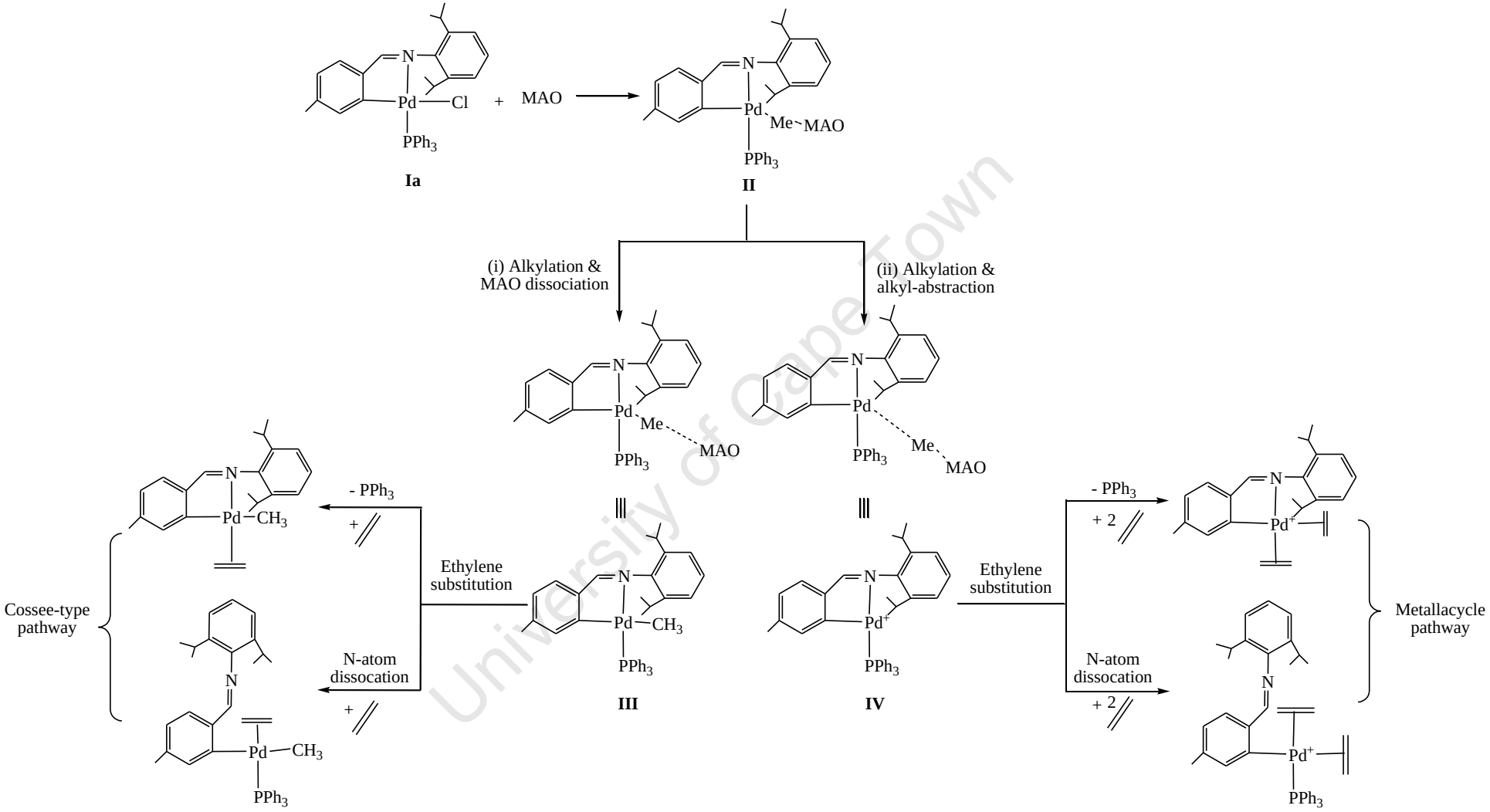

Scheme 2.7 Catalyst/co-catalyst interactions and possible active species.

The work reported in this investigation was undertaken with a view to gain fundamental understanding of the mechanism of chain growth and to predict the catalytic activity by using DFT methods. We address the following specific questions: Firstly, do theoretical calculations on Pd/MAO interactions reveal the role of MAO in Pd-catalysed ethylene oligomerization, i.e., which is the preferred step after the alkylation step, MAO dissociation or alkyl-abstraction? Secondly, we will attempt to identify the possible mechanism by analysing the results of DFT calculations in terms of the reaction energetics. That is, is a Cossee-type mechanism or a metallacycle mechanism the preferred one for chain growth? Thirdly, and also the most importantly, to determine using DFT calculations a possible reason why the cyclometallated Pd system gave low activity when tested for ethylene oligomerization.

A full exploration of all the possible mechanistic pathways was not considered in the current study, as that would require considerable computional cost. The mechanisms we proposed and subjected to calculation were therefore focussed on the specific reaction pathways based on those proposed in the literature. The pathways not modelled are considered not important to the entry reaction profle and relatively expensive in computer time.

2.2 Functional Validation and Ligand Dissociation of Palladium Complex

2.2.1 Functional validation

The cyclometallated palladium complex **Ia** has been synthesized and used as the pre-catalyst in ethylene oligomerization.[26 (b)] As stated by some authors, "accurate molecular geometries are prerequisite for reliable quantum-chemical computations".[36] Consequently, we investigated the performance of four GGA density functionals available in the DMol^3 code in the Materials Studios Software (Accelrys)[37] and the basis set of DNP in reproducing four structures derived from the single-crystal X-ray diffraction structure of the cyclometallated palladium complex **Ia** (where R = Me). The calculated bond distances and angles of the optimized structure are summarized in Table 2.1 for purpose of comparison. The average deviation of the calculated values is the smallest for bond distances for PW91 and bond angles for PBE. But due to the fact that the bond distance average deviation for PBE is close to double that of PW91, the functional method PW91 was considered to represent the most accurate structure and was thus used for further calculations. It is important to note that there will be deviations between experimentally measured and calculated values, because

experimental values were measured in the solid state, while calculations were performed in vacuum. We conclude that DMol^3/PW91/DNP reproduced the most accurate molecular geometry of **Ia**, and this was used in all subsequent calculations reported.

Table 2.1 Comparative calculated and experimental data on selected bond distance (in Å) and angles (deg) in complex **I**

	Experimental[i]	**PW91**	**PBE**	**RPBE**	**B3LYP**
N-Pd-Cl	91.921	92.026	92.710	93.637	92.008
Cl-Pd-P	92.124	92.307	91.408	90.431	91.569
P-Pd-C	96.310	96.064	96.588	97.590	97.345
C-Pd-N	80.765	79.794	79.760	79.414	79.331
AD[ii]	0	0.376	0.697	1.150	0.778
Pd-Cl	2.364	2.397	2.403	2.431	2.443
Pd-N	2.105	2.259	2.164	2.206	2.205
Pd-C	2.008	2.081	2.078	2.092	2.114
Pd-P	2.252	2.342	2.340	2.376	2.400
AD[ii]	0	0.088	0.064	0.094	0.108

[i] see Ref. 26 (b).

[ii] Average deviation from experimental values.

2.2.2 Pd-ligand bond dissociation energies

Many of the important mechanistic steps in homogeneous catalytic cycles involve the addition or loss of ligands, in particular phosphine ligands.[38] M-P bond dissociation energies in several transition metal complexes have been studied both theoretically and experimentally.[39] During ethylene oligomerization, it is generally accepted that exchange of weakly coordinated ligands such as PPh_3 for ethylene should be facile.[31] On the other hand, the nitrogen atom of the hemilabile imine ligand could potentially dissociate as well. This is due to the notion that a hemilabile ligand provides a free coordination site 'on demand' in the presence of competing substrates.[40] In this sense, Pd-P and Pd-N bond dissociation in **Ia** could occur during ethylene oligomerization reactions (Figure 2.2). The Pd-ligand bond dissociation energies were therefore compared to obtain insight into the possible coordination site for incoming ethylene in **Ia**.

Figure 2.3 shows the plots of the potential energy for two Pd-ligand bond dissociation processes of complex **Ia**. For the Pd-P bond dissociation, the reaction coordinate is plotted relative to the breaking Pd-P bond distance. The starting structure has a Pd-P bond distance of 2.432 Å and was followed through the transition state (TS, a structure with highest energy having a Pd-P bond distance of 5.125 Å) all the way to a structure with Pd-P bond distance of 6.271 Å. It should be noted that an isomerization process occurred spontaneously when the Pd-P bond was elongated to 5.125 Å, in which the structure has the chlorine atom in the *cis* position relative to the cyclometallated carbon atom, remaining in the same position after optimization. The potential energy profile for Pd-N bond dissociation is plotted along the breaking Pd-N bond distance. Elongation of the Pd-N distance from 2.207 in the starting structure to 4.385 Å, went through the transition state (TS, a structure with highest energy and having a Pd-N bond distance of 3.141 Å).

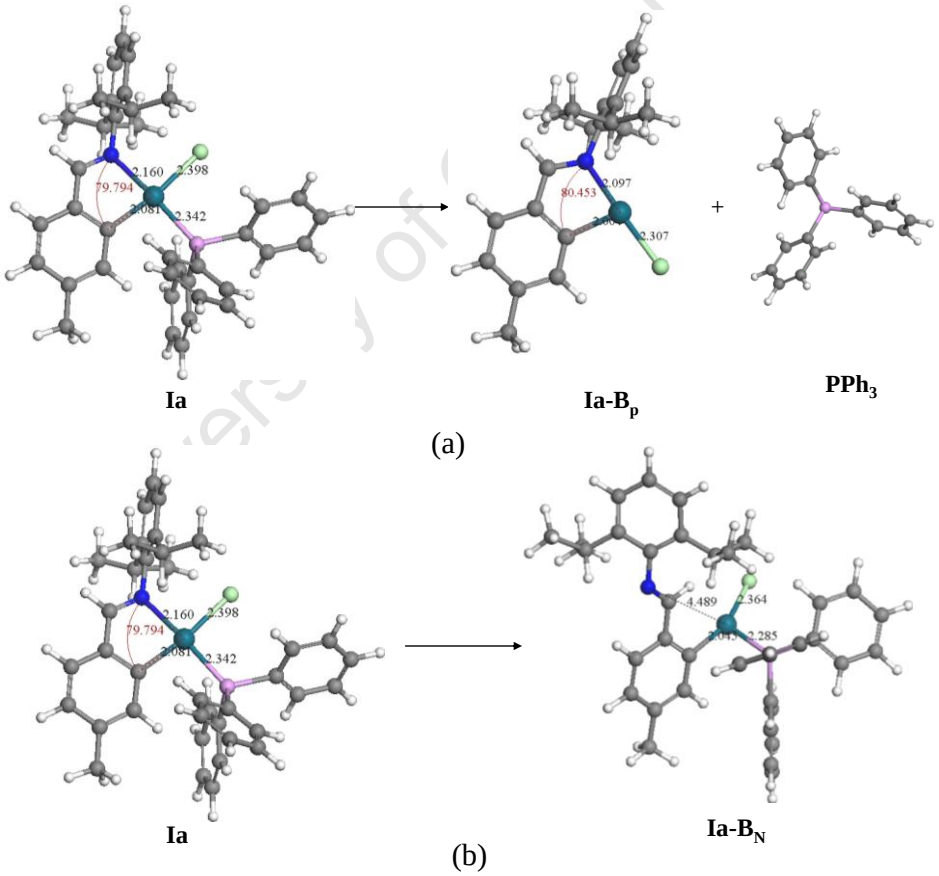

Figure 2.2 (a) Pd-P bond dissociation (**Ia** to **Ia-B$_P$**) and (b) Pd-N bond dissociation (**Ia** to **Ia-B$_N$**) in complex **Ia**.

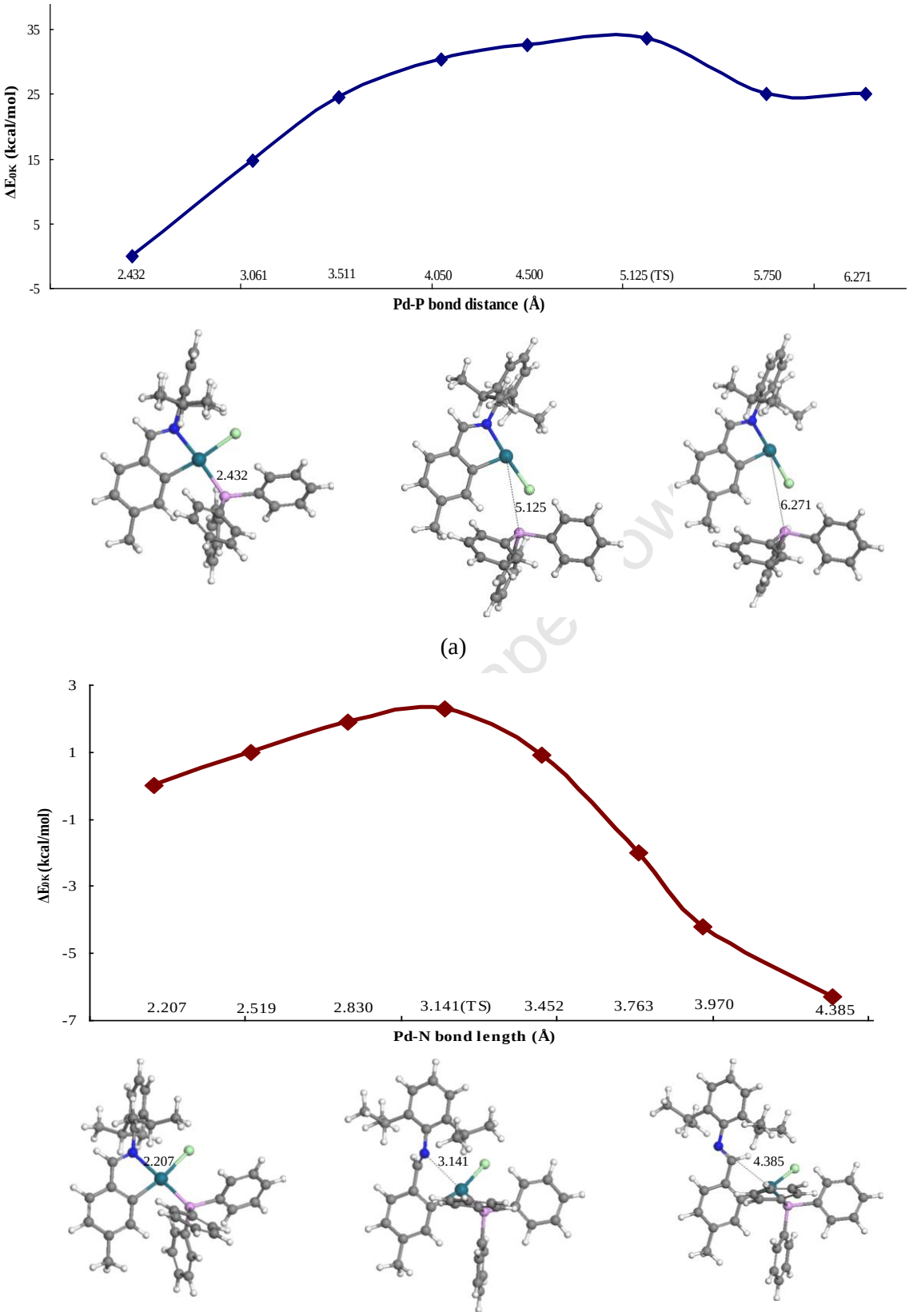

Figure 2.3 Potential energy surface (PES) of Pd-ligand bond dissociation in **Ia**: (a) Pd-P bond dissociation, (b) Pd-N bond dissociation.

The two primary transition states obtained from the potential energy surface (PES) scan were then subjected to TS optimization giving the formal transition states with one imaginary frequency, **TS(Ia-B_N)** and **TS(Ia-B_p)**, respectively, with calculated energies in kcal/mol expressed as Gibbs free energies ($\Delta G_{298.15K}$) [a] at 298.15 K and 1 atm (Figure 2.4). As compared with Figure 2.3, Figure 2.4 clearly shows that the entropy corrections significantly influence the relative energies upon moving from 0K to 298K.

The Pd-N bond dissociation energy in **Ia** is calculated to be 7.4 kcal/mol less favourable than the Pd-P bond dissociation energy as shown in Figure 2.4. This implies that the exchange between an ethylene molecule and PPh_3 is more likely in the cyclometallated palladium complex **Ia** during the oligomerization reactions.

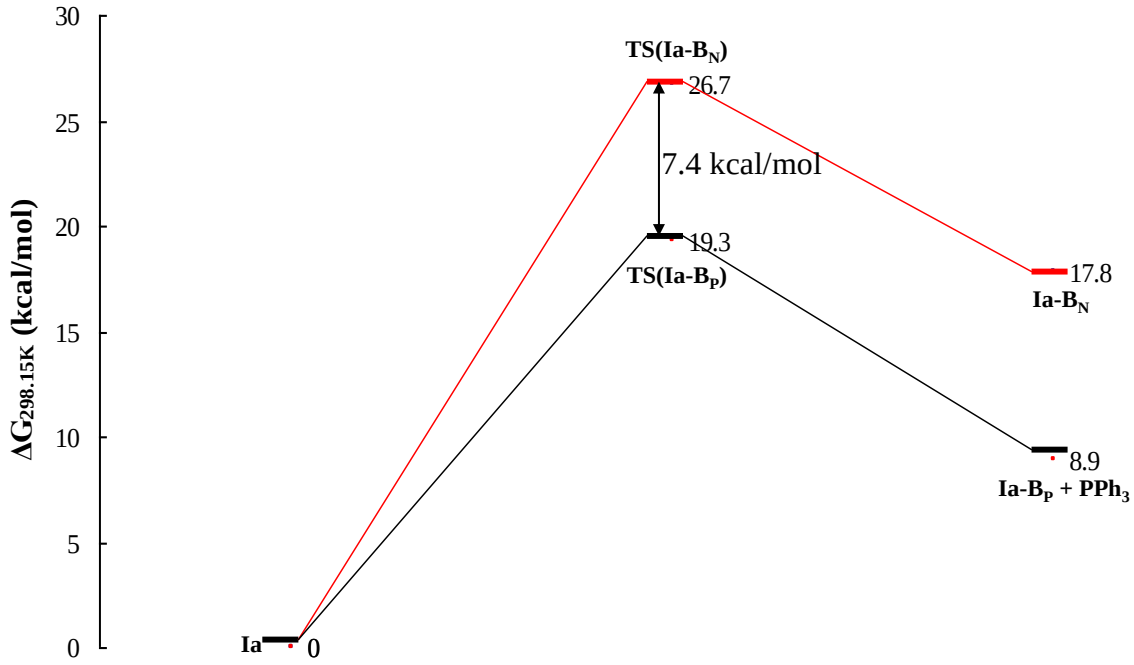

Figure 2.4 Calculated Gibbs free energies ($\Delta G_{298.15K}$) at 298.15 K and 1 atm in kcal/mol for the dissociation of PPh_3 or the dissociation of N-atom.[b]

2.3 The Role of MAO in the Activation of Pd Pre-catalyst

A number of theoretical studies focusing on co-catalyst interaction with transition metal

[a] The calculated Gibbs free energies were corrected from (ΔE_{0K}) by adding frequency calculation and entropy gain in the gas phase at 298 K and 1atm.
[b] All energies are reported relative to the respective '**Ia**' and balanced with the energies of free ligand, where necessary.

catalysts have been reported.[32,33,41] It is generally accepted that the interaction of the co-catalyst with the metal occurs via a bridging methyl group, and this interaction has been envisaged for "activated" MAO, i.e., TMA-expanded MAO, with a methylated catalyst precursor or intermediate.[32,33] As shown in Scheme 2.7 (p. 59), the interaction of the palladium complex with MAO could take place via two routes, i.e. (i) alkylation followed by MAO dissociation and (ii) alkylation followed by alkyl-abstraction. In an attempt to assess the role of MAO in the activation of the palladium precatalyst, the two interactions were compared using DFT calculations.

2.3.1 Palladium model and MAO models

2.3.1.1 Palladium model

It is believed that the methylation of catalyst precursors prior to ethylene oligomerization is an important first stage for catalyst activation when MAO is used as co-catalyst. To simplify the DFT calculation, the methylated-palladium complex shown in Figure 2.5 was chosen in the current study, as representative of the catalyst precursor during ethylene oligomerization. This is required for direct comparison with complexes explicitly containing different MAO models.

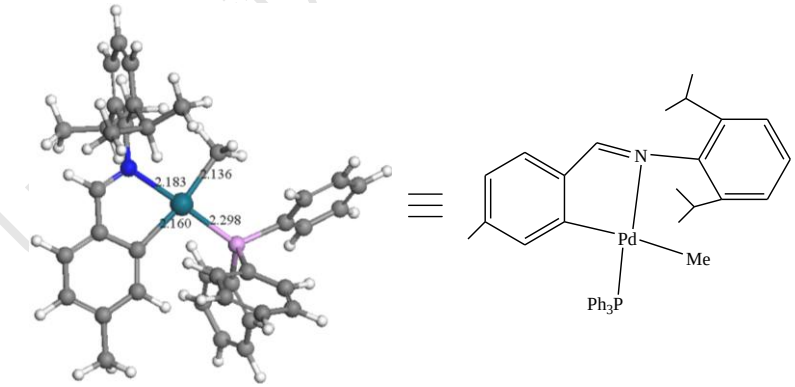

III

Figure 2.5 Optimized geometry for methylated palladium complex **III**.

2.3.1.2 MAO models

The interaction of MAO with the palladium complex most likely involves a bridging methyl group that is shared by the palladium and appropriate MAO models. Although the exact structure of MAO is not known, theoretical models of MAO have been reported based on some important evidence from a number of experimental studies.[42,43] It has been concluded

that "classic" MAO models, $(AlOMe)_n$, are three-dimensional cage structures which consist of three-coordinate oxygen and four-coordinate aluminium.[41(c),42,44,45] However, they cannot be regarded as being significantly Lewis acidic due to the fact that there are only four-coordinate aluminium centres contained in the structures. "True" MAO models, in which residual trimethylaluminum (TMA) in MAO is incorporated in the structure of "classic" MAO, have been constructed according to the following general reaction: [41(c),43]

$$(AlOMe)_n + n/3\ TMA \longrightarrow (AlO_{0.75}Me_{1.5})_{n+n/3} \qquad \text{(Eq. 2.1)}$$

This was suggested by several NMR studies.[46] Furthermore, calculations performed by Zurek and Ziegler[41(c)] suggest that less TMA should be present, as they found that incorporation of TMA into "classic" MAO to yield a Me:Al ratio of 1.5 is energetically unfavourable. "TMA-expanded" MAO models, i.e., $(AlOMe)_n$ (where n = 6, 9) activated by one TMA unit, were used in Zurek and Ziegler's and some other studies.[33,41(c),44] In addition, it was shown that the incorporation of TMA leads to the cleavage of the most reactive square-square (*ss*) Al-O bond for all "classic" MAO cage structures studied, except for $(AlOMe)_9$. The interaction of a TMA dimer with the $(AlOMe)_9$ cage results in cleavage of both a square-hexagonal (*sh*) and a square-square (*ss*) Al-O bond, for which the cleavage of the *sh* Al-O bond was calculated to be more energetically favourable.[41(c)]

In the current study, three TMA-expanded MAO models, i.e. $(AlOMe)_6$-TMA-*ss* (**MAO3**), $(AlOMe)_9$-TMA-*sh* (**MAO4**) and $(AlOMe)_9$-TMA-*ss* (**MAO5**) were considered (Scheme 2.8). These MAO models were reported by Janse van Rensburg *et al*. in a theoretical study that involves MAO interactions with chromacycloheptane intermediates during ethylene tri- and tetramerization.[33]

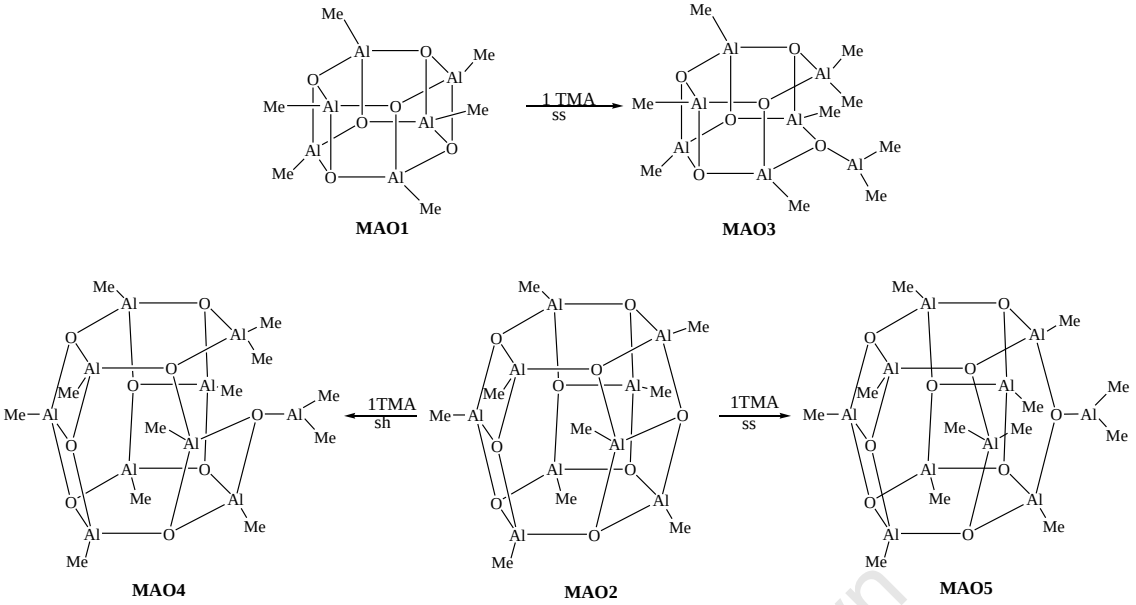

(a)

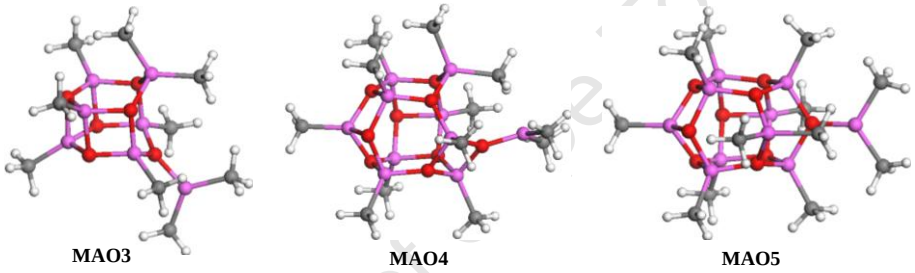

(b)

Scheme 2.8 MAO models used in the study.

2.3.2 Palladium complexes in the presence of MAO models

2.3.2.1 $(AlOMe)_6$-TMA model

Despite the fact that very little $(AlOMe)_6$ (~ 0.01%) is present at room temperature in a typical MAO solution, this is the smallest feasible model that may be used to represent MAO. In the past related theoretical studies, a $(AlOMe)_6$-TMA cage was used by Ziegler[41(c)] and considered as a "strip-down" model by Janse van Rensburg.[33] The idea to use this small model is to facilitate relatively fast initial calculations, which can be used in turn for expansion to more realistic MAO models discussed later. The interaction of neutral $(AlOMe)_6$-TMA, i.e., **MAO3**, with a neutral palladium methyl complex was modelled by coordination of the unsaturated three-coordinate Al atom in **MAO3** with the methyl group of the palladium complex. The optimized geometries of these interaction models and their relative energy (ΔE_{0K}) data are illustrated in Figure 2.6.

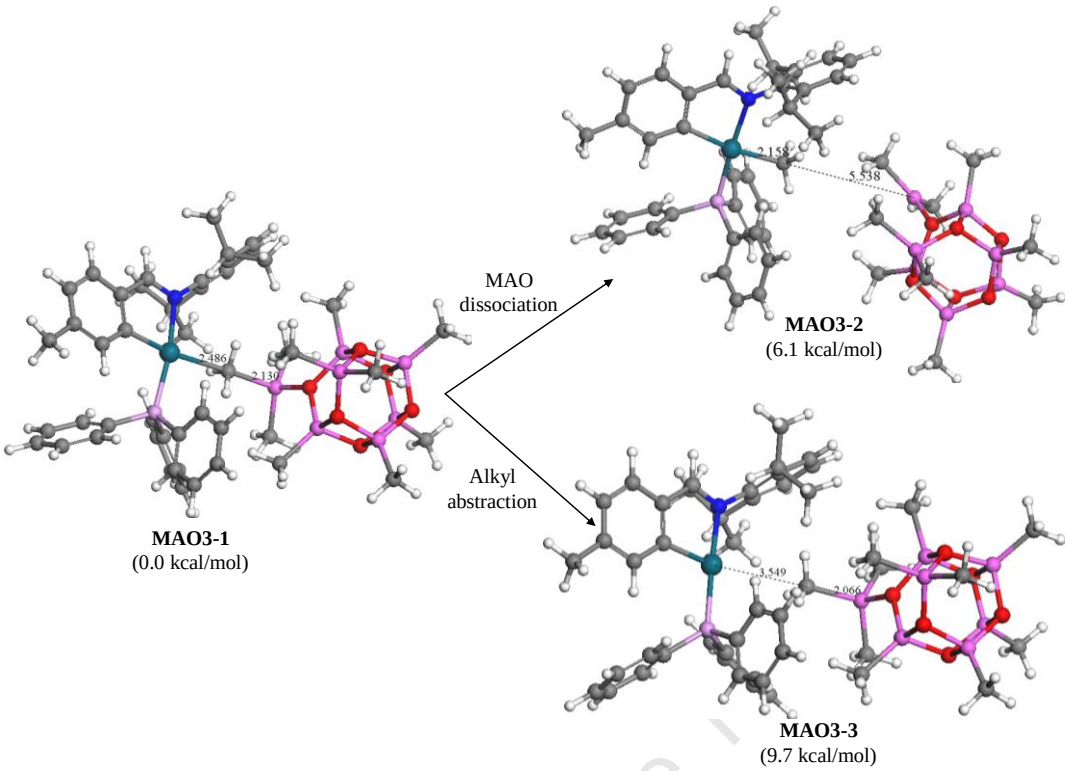

Figure 2.6 DMol^3/PW91-optimized geometries for interaction of $(AlOMe)_6$-TMA (**MAO3**) with palladium complex. Bond length in Å and ΔE_{0K} energies at 0K in kcal/mol relative to **MAO3-1**.

Formal coordination of the $(AlOMe)_6$-TMA (**MAO3**) fragment in **MAO3-1** is evident from the relatively short calculated Pd-Me and Me-Al bond distances of 2.486 Å and 2.130 Å. The interaction of the Me group with Al is evident from the elongation of the Pd-Me distance from 2.136 Å, when $(AlOMe)_6$-TMA (**MAO3**) is not present (see Figure 2.5, structure **III**), to 2.486 Å in **MAO3-1**. An attempt has been made to compare the energy difference between the two roles of MAO, i.e., alkylation and alkyl-abstraction, on palladium complexes. The MAO-dissociated structure in which a neutral $(AlOMe)_6$-TMA fragment is dissociated from the corresponding formally coordinated Pd-MAO complex was optimized, yielding **MAO3-2**. The neutral dissociated structure is found to be higher in energy compared to the low-energy counterpart **MAO3-1** by 6.1 kcal/mol. The same phenomenon was observed in the interaction of $(AlOMe)_6$-TMA with chromacycloheptanes and it was suggested that saturation of Al in the MAO fragment favourably overcomes the steric congestion experienced by tightly coordinated structures.[33]

Formal abstraction of the methyl group from palladium leads to the optimization of the "dissociated" ion-pair **MAO3-3**, exhibiting a Pd-Me distance of 3.54 Å. Formation of

MAO3-3 is energetically unfavourable compared to the MAO-dissociated structure (**MAO3-2**) by 3.6 kcal/mol.

2.3.2.2 $(AlOMe)_9$-TMA models

In an attempt to ensure a more comprehensive and realistic account of the interaction between MAO and palladium pre-catalysts, an expansion of the MAO model is presented in this section. For this purpose the "stripped-down" MAO model, $(AlOMe)_6$-TMA, is replaced by the more appropriate $(AlOMe)_9$ cage structure, activated by a single TMA unit. Due to the underlying uncertainty and complexity of active MAO structures during catalysis, two TMA-expanded MAO models as indicated in Scheme 2.8 (Section 2.3.1), i.e., $(AlOMe)_9$-TMA-*sh* (**MAO4**) and $(AlOMe)_9$-TMA-*ss* (**MAO5**), are incorporated into the current study. This effectively covers a more comprehensive range of structures and represents a more inclusive account of actual catalyst/MAO interactions. In the discussion to follow, the DFT results obtained focus on the neutral $(AlOMe)_9$-TMA models **MAO4** and **MAO5** interacting with the palladium complex. An example of the optimized geometry of one of these TMA-expanded MAO-palladium structures is illustrated in Figure 2.7, in which $(AlOMe)_9$-TMA-*sh* (**MAO4**) is bridged via a methyl group to the palladium complex (this structure corresponds to **MAO4-1** in Figure 2.8). Figure 2.8 illustrates the optimized geometries for interaction of both $(AlOMe)_9$-TMA-*sh* (**MAO4**) and $(AlOMe)_9$-TMA-*ss* (**MAO5**) with the palladium complex, along with the relative ΔE_{0K} energies. All data pertaining to $(AlOMe)_9$-TMA-*ss* (**MAO5**) in Figure 2.8 are denoted by square brackets to distinguish the geometrical and energy data for interactions of **MAO4** and **MAO5**. For all the structures, the interaction of $(AlOMe)_9$-TMA with the palladium complex involves bridging of the three-coordinate Al unit in **MAO4** and **MAO5** with the methyl functionality on Pd.

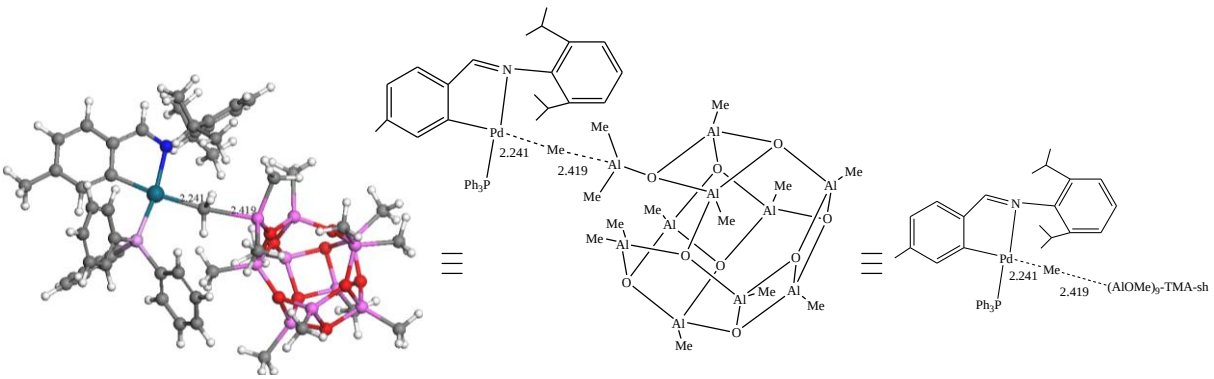

Figure 2.7 Example of an optimized geometry for $(AlOMe)_9$-TMA-*sh* (**MAO4**) interaction with palladium complex to yield **MAO4-1**.

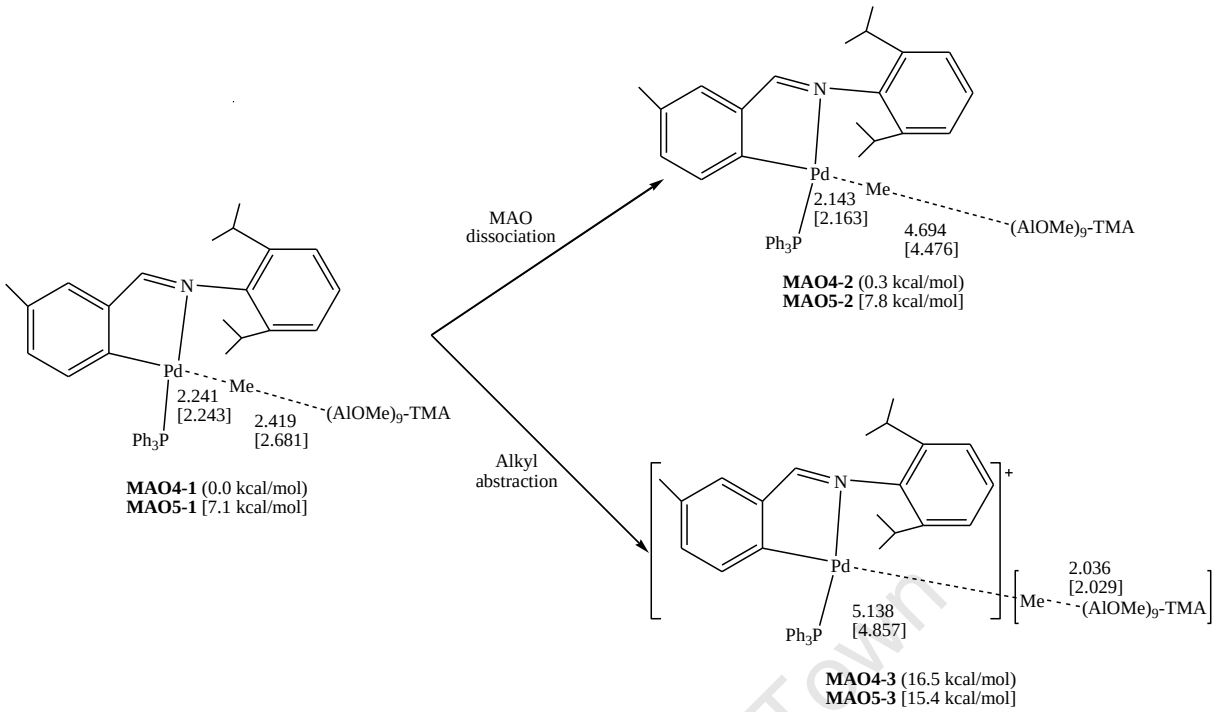

Figure 2.8 DMol^3/PW91/DNP-optimized geometries for interaction of $(AlOMe)_9$-TMA-*sh* (**MAO4**) and $(AlOMe)_9$-TMA-*ss* (**MAO5**) with palladium complex.[a] Bond lengths in Å and ΔE_{0K} energies at 0 K in kcal/mol relative to **MAO4-1**.

In the formal coordinated structures **MAO4-1** and **MAO5-1**, relatively tight coordination of **MAO4** and **MAO5** to the Pd complex is evident from the relatively short Pd-Me and Me-Al distances, and the Pd-Me distances in both structures were found to be elongated as a result of the coordination of MAO (2.241 Å and 2.419 Å for **MAO4-1** and 2.243 Å and 2.681 Å for **MAO5-1**). This is in good agreement with the structural parameters that were obtained from the "stripped-down" model **MAO3-1**.

The MAO-dissociated structures, i.e., neutral $(AlOMe)_9$-TMA-*sh* (**MAO4**) and $(AlOMe)_9$-TMA-*ss* (**MAO5**), which are dissociated from the corresponding formal coordinated structures, were optimized, yielding **MAO4-2** and **MAO5-2**. Compared to their corresponding formally coordinated structures, the Pd-Me bond distance in the neutral dissociated structures were shortened to a length similar to the Pd-Me complex **III** (see Figure 2.5) in the absence of MAO. They were found to be higher in energy by 0.3 – 0.5 kcal/mol compared to **MAO4-1** and **MAO5-1**.

[a] All data pertaining to $(AlOMe)_9$-TMA-*ss* (**MAO5**) are denoted in square bracket to distinguish it from the data for $(AlOMe)_9$-TMA-*sh* (**MAO4**).

The dissociated ion-pair complexes in which the methyl group is formally abstracted from palladium by MAO, i.e., structures in which the Pd-Me distances are *ca.* 5 Å, were successfully optimized, forming **MAO4-3** and **MAO5-3**. Formation of the Me-abstracted structures are, however, energetically unfavourable. They were found to be higher in energy compared to the relatively lower-energy counterparts (**MAO4-1** and **MAO5-1**) by 16.5 and 8.3 kcal/mol, respectively. The disfavouring of the formation of **MAO4-3** and **MAO5-3** compared to the formation of **MAO4-2** and **MAO5-2** could be attributed to either the unfavourable methyl abstraction or the unfavourable formal charge separation for $(Me\text{-}MAO)^-$ dissociation in the gas phase.[33]

2.3.2.3 Discussion on Pd-MAO interactions

The first important role of MAO is the alkylation of the catalyst precursor.[47] It was therefore deemed appropriate to use a palladium methyl structure (**III**) as a model palladium complex to study possible interactions with MAO models. Herein, three "TMA-expanded" MAO models, i.e., $(AlOMe)_6$-TMA (**MAO3**), $(AlOMe)_9$-TMA-*sh* (**MAO4**) and $(AlOMe)_9$-TMA-*ss* (**MAO5**), were chosen as representative MAO models. $(AlOMe)_6$-TMA (**MAO3**) is the smallest MAO cage structure containing both hexagonal and square faces and regarded as the smallest feasible structural model for MAO. Having larger cage sizes, $(AlOMe)_9$-TMA (**MAO4** and **MAO5**) are considered to be more "realistic" models. The use of the $(AlOMe)_9$ cage is justified by the predicted distribution of cage structures in which $(AlOMe)_9$ was found to be one of the most abundant cage structures containing a strained square-square (*ss*) Al-O bond (Figure 2.9).[41(d)]

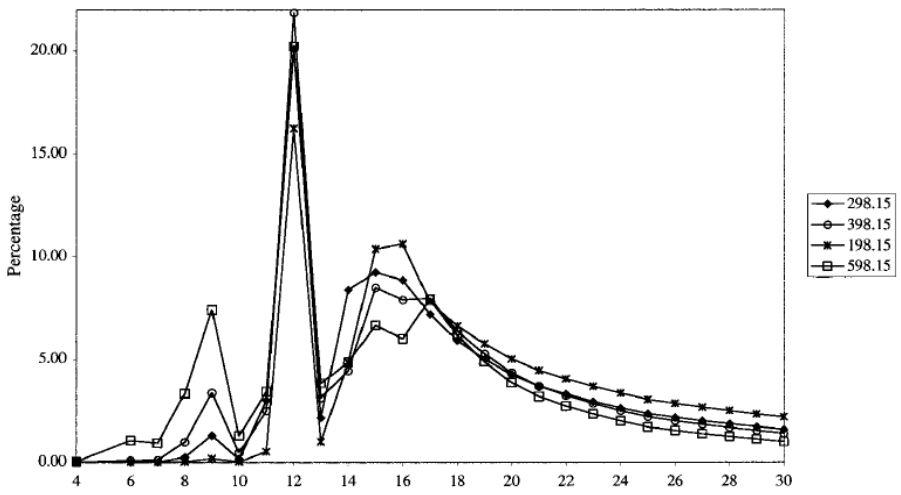

Figure 2.9 Composition of TMA free $(AlOMe)_n$ as a function of n within the temperature range of 198.15-598.15 K.[41(d)]

In our system, neutral MAO dissociation in the formal coordinated complexes, to yield MAO-dissociated structures with elongated Me-Al distances, was determined to proceed endothermically with low energies of 0.3 to 0.5 kcal/mol for $(AlOMe)_9$-TMA (**MAO4** and **MAO5**), 6.1 kcal/mol for $(AlOMe)_6$-TMA (**MAO3**). On the other hand, formal abstraction of the methyl group from palladium, to yield **MAO3-3**, **MAO4-3** and **MAO5-3**, was calculated to proceed endothermically with energies of 9.7, 16.5 and 8.3 kcal/mol compared to their low-energy counterparts **MAO3-1**, **MAO4-1** and **MAO5-1**, respectively. These values are in agreement with the calculated energies for similar transformations in chromium-MAO complexes, which were found to be 12.3 and 10.2 kcal/mol.[33] It was pointed out by Janse van Rensburg and co-workers that if abstraction of the bridging methyl group is found to proceed with relatively low energies in the gas-phase DFT analysis, methyl group abstraction in actual experiments is likely to be even more favourable where a solvent is formally introduced. Therefore they concluded that the formation of "dissociated" ion-pair structures is likely during catalysis.[33]

It is interesting to note that the energy difference between two possible Pd/MAO interactions using **MAO4**, which contains a cleaved *sh* Al-O bond, was relatively higher compared to those containing cleaved *ss* Al-O bond MAO models, i.e. **MAO3** and **MAO5**. Although the presence of **MAO4-1** should dominate in the $(AlOMe)_9$ cage distribution, **MAO5-1** should also be present. Due to the fact that a huge excess of MAO relative to Pd catalyst is used for actual catalysis, it will provide an opportunity for **MAO5-1** to take part in the catalysis. Thus some formal methyl abstraction to occur becomes feasible. Neutral MAO-dissociation without the formal methyl abstraction remains, however, the major Pd/MAO interaction that will take place as evident from all the MAO models be considered in the study.

Energetically speaking, it is likely that the neutral MAO-dissociation process will occur quickly during catalysis. Upon formation of this complex, ethylene will coordinate to palladium via ligand exchange with PPh_3, leading to a Cossee-type mechanism, which is the most common mechanism for Pd-catalysed ethylene oligomerization/polymerization reactions. On providing more energy to the catalysis reaction by, for example, increasing the reaction temperature, some formal abstraction of the methyl group from palladium will also occur. After the dissociation of PPh_3 from this cationic species, two molecules of ethylene will coordinate to palladium, and an oxidative coupling reaction takes place, thus leading to a

metallacycle mechanism. In the following sections, detailed DFT analyses on both mechanisms are reported and compared in terms of the energy.

2.4 Possible Mechanisms for Cyclometallated Palladium-Catalysed Ethylene Oligomerization

Some authors have mentioned that the role of the co-catalysts, counter ions, or solvents in ethylene oligomerization/polymerization catalytic process is very important to describe realistic active sites.[48] In recent years increasing availability of computational resources has made it possible to investigate the ethylene insertion mechanism proposed by Cossee and Arlman involving contact catalyst/co-catalyst ion-pairs.[41(a),49(b)] There are, however, only two studies using MAO as co-catalyst reported in the literature. Zurek *et al*.[41(a)] studied the mechanism of ethylene insertion into the Zr-C bonds of **Zr-1** and **Zr-2** (Figure 2.10) in olefin polymerization, whereas $(AlOMe)_6$ was used as a model for MAO.

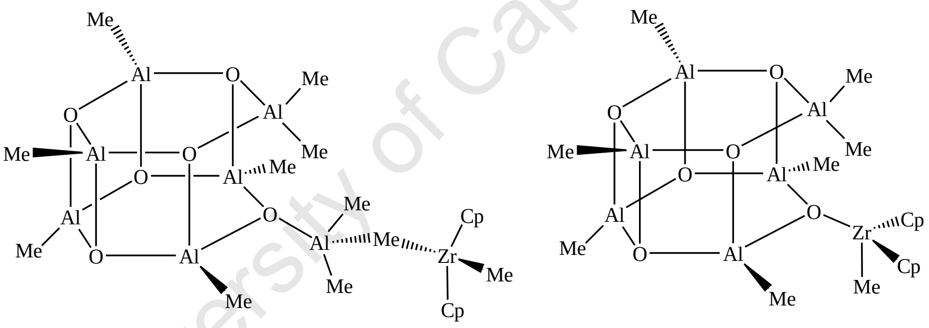

Zr-1 **Zr-2**

Figure 2.10

Fusco and co-workers[49(b)] studied the role of olefin separated ion pairs (OSIP) in the ethylene polymerization mechanism using the system $[Cp_2(Ti/Zr)CH_3]^+[Cl_2Al[O(AlMe_3)AlHMe]_2]^-$, where $[Cl_2Al[O(AlMe_3)AlHMe]_2]$ was used to model MAO.

These studies suggest that total dissociation between cation (a cationic metal fragment $[LnM^+]$) and anion (an anionic co-catalyst fragment $[RX^-]$) does not occur. However, these kinds of studies are still quite limited, because they would be exceptionally computationally demanding due to the large size of the ion pair systems. In theoretical work reported in the literature of the polymerization/oligomerization mechanisms, the most used model for the

active site was the isolated cation with different alkyl ligands, without counterion, to reduce the computational cost.

Therefore, in the following mechanistic studies, the neutral palladium methyl complex formed from the dissociation of MAO, **III**, and the isolated cation **IV** were used as models (see Scheme 2.9) for the active species in the catalytic process. Density functional theory (GGA/PW91/DNP) was employed. As a calculation model, the cyclometallated palladium complex **III** was simplified as **III-s** with removal of the methyl group on the cyclometallated aryl ring (Scheme 2.9), and **IV** was simplified as **IV-s**.

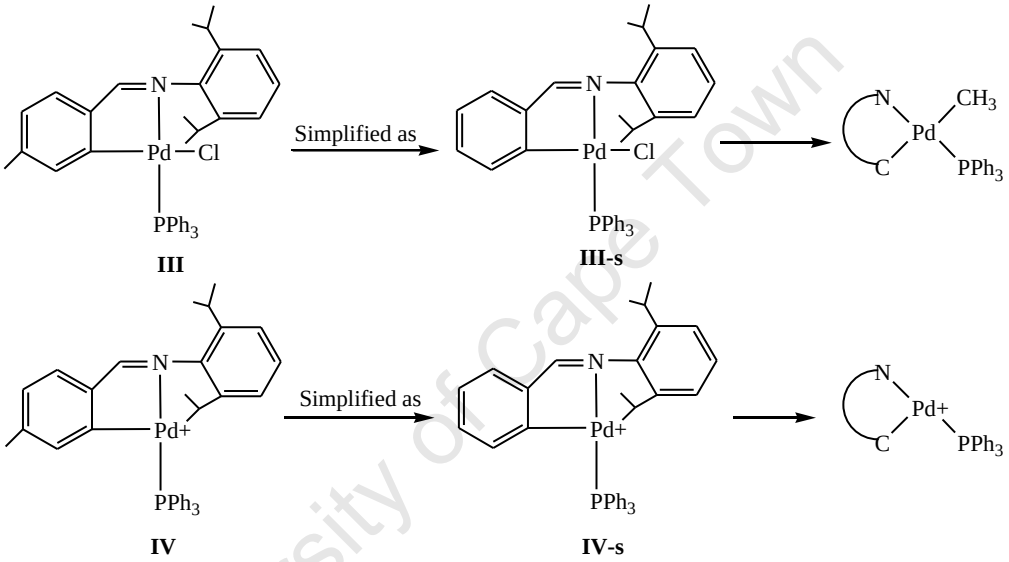

Scheme 2.9 Simplified structures of cyclometallated palladium complexes.

2.4.1 Mechanism A: Cossee-type pathway

Due to the asymmetrical character of the *N*-benzylidenebenzylamine ligand, *cis/trans* isomerization should be considered for the four-coordinate methyl complex **III-s** and similar complexes during catalysis. As will be discussed later (Chapter 4), methylation reactions were carried out to assess the possibility of *cis/trans* isomerization occurring on *N*-benzylidenebenzylamine metal complexes during the formation of a metal methyl complex. A platinum analogue was used as a model due to the poor stability of palladium complexes when reacting with LiMe. As expected, *cis* (methyl group *cis* to the cyclometallated carbon atom) and *trans* (methyl group *trans* to the cyclometallated carbon atom) Pt-Me complexes were formed in a ratio of 9:1 (Eq. 2.2, experimental details are discussed in Chapter 4), in which the *cis* isomer was confirmed by crystal structure. This preference can be attributed to

the large *transphobia* of a pair of C-donor/C-donor ligands in palladium and platinum complexes.[50] It is clear from Eq. 2.2 that the *cis/trans* isomerization is feasible for *N*-benzylidenebenzylamine metal complexes during the methylation and should be taken into account in any cyclometallated palladium-catalysed ethylene oligomerization process. Therefore, both *cis* and *trans* methylpalladium species **III'-s** and **III-s** could be generated in the MAO alkylation process (see Eq. 2.3) in an actual catalysis reaction.

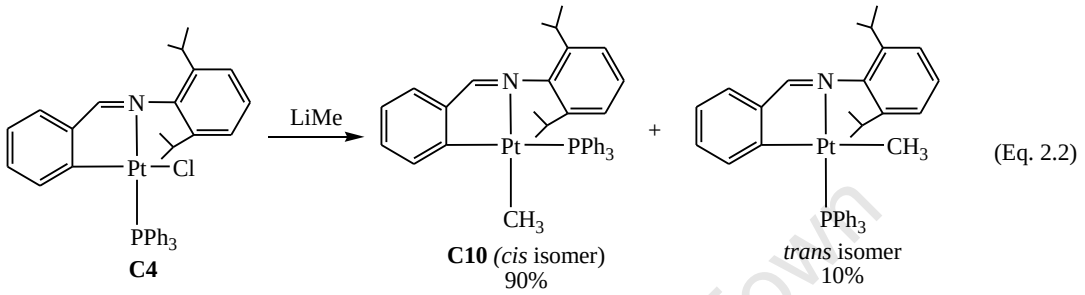

C4 **C10** (*cis* isomer) 90% *trans* isomer 10%

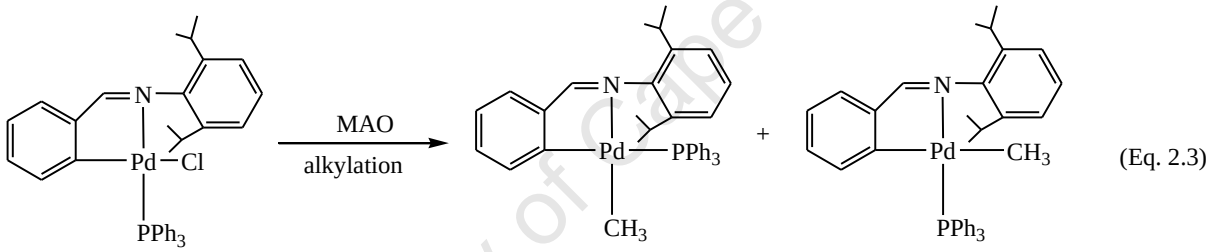

Ia-s **III'-s** (*cis* isomer) **III-s** (*trans* isomer)

2.4.1.1 Chain growth initiation

In the Cossee-Arlman mechanism, the chain growth intiation proceeds via coordination of an olefin at the open site of the square-planar metal center and is followed by direct insertion of the coordinated olefin into the Pd-alkyl bond without the formation of any intermediate.[16] Herein, we propose a chain growth intiation process starting from either **III-s** or **III'-s** as shown in Scheme 2.10. The geometry optimization of **III-s** and **III'-s** without any constraints was successful, and the structures are shown in Figure 2.11. The *cis* isomer **III'-s** was calculated to be energetically more favourable than its *trans* isomer by 2.5 kcal/mol. This is consistent with the observation that during the methylation reaction of the platinum analogue, the *cis* isomer was formed predominantly. The *cis/trans* isomers, **III-s** and **III'-s** will lead to the *cis*/*trans* Pd-ethylene π complexes, i.e. **A2** and **A2'**. These types of complexes have been observed by other researchers as the catalyst resting states using NMR spectroscopy.[51]

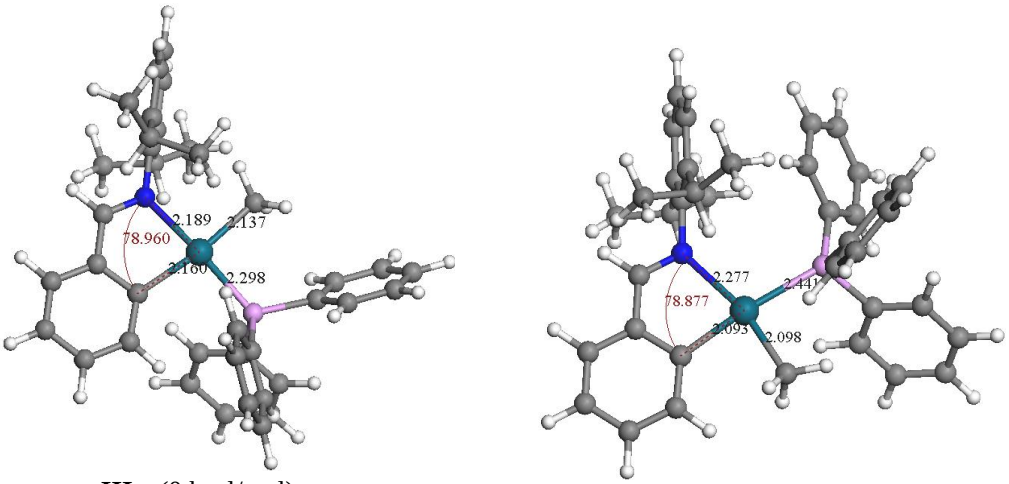

III-s (0 kcal/mol) **III'-s** (-2.5kcal/mol)

Figure 2.11 Optimized structures of *trans/cis* Pd-Me complexes, **III-s** and **III'-s**. Gibbs free energy is relative to **III-s**

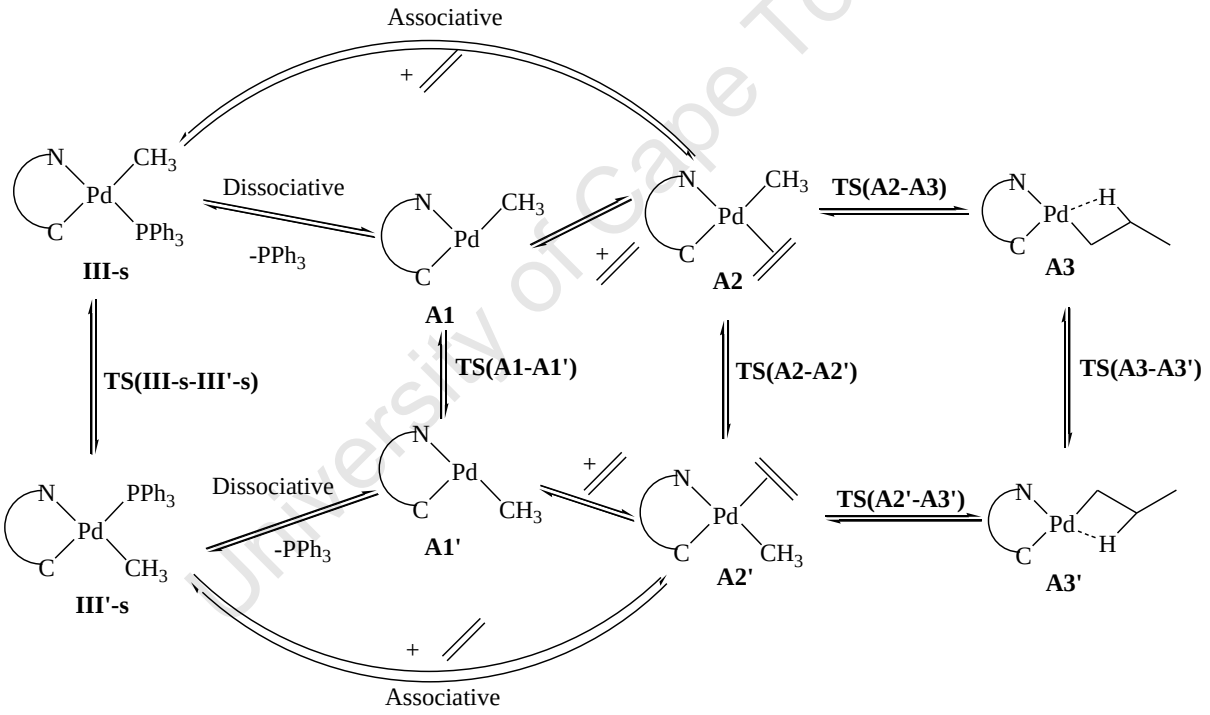

Scheme 2.10 Proposed chain growth initiation process for either **III-s** or **III'-s**.

Orbital interactions in ethylene-substitution reactions

Ethylene oligomerization/polymerization is considered to be a nucleophilic reaction.[52] The incoming ethylene reacts as a donor of electron density (nucleophile) and will attack the catalyst species at the most favourable site for electron addition, whereas the metal centre reacts as an electron acceptor (electrophile). This applies to both associative and dissociative mechanisms for ethylene coordination. Taking consideration of frontier molecular orbital

(FMO) theory, the lowest unoccupied molecular orbital (LUMO) corresponds to the molecular regions where the addition of electronic density is energetically more favourable. Thus, ethylene-substitution reactions are initiated by the interaction between the highest occupied molecular orbital (HOMO) on the ethylene and the LUMO on the catalyst (Figure 2.12).[53] Orbital interactions in ethylene-substitution reactions on the open site of square-planar palladium complexes were studied, where **A1** and **A1'** were used as the model complexes to indicate the possible positions of the open site.

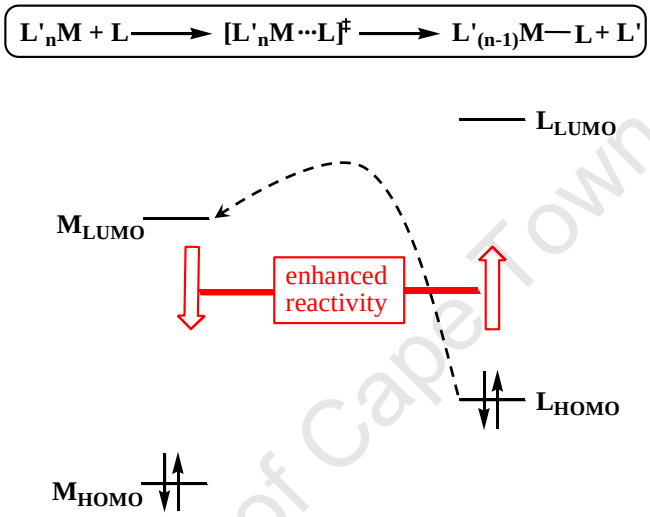

Figure 2.12 Simplified molecular-orbital analysis of an associative ligand-substitution reaction at a transition-metal centre.[a]

The HOMO and LUMO energy for the three-coordinate, *cis/trans* (N^C)Pd(CH_3) complexes, **A1** and **A1'**, and ethylene were estimated based on DFT calculations and are shown in Figure 2.13. The HOMO-LUMO gap estimated for the *trans* isomer **A1** was 0.78 eV, while for the *cis* **A1'**, it was 1.02 eV (Figure 2.13). When the HOMO-LUMO gap is large (other things being equal), one expects high stability and low reactivity. When it is small, one expects low stability and high reactivity. This is consistent with calculations showing the *cis* isomer more stable than the *trans* isomer.

The most reasonable acceptor orbital on palladium in our system is a p_x-orbital (LUMO).[53] In the case of **A1**, the LUMO was largely located on the Pd atom with energy of -3.32 eV. The HOMO is a Cσ-Pd($d_{x^2-y^2}$)-Cσ antibonding combination, largely centred on both Pd-CH_3 and

[a] The primary orbital overlap occurs between a ligand-based HOMO and a metal-based LUMO, and improved overlap will lead to higher reaction rates (where L = ethylene).[52]

Pd-$C_{metallated}$ moieties. In contrast, the LUMO in **A1'** was localized on the imine fragment, which is thought to be the common LUMO in the transition metal complexes of N^C-cyclometallated ligands.[54] The energy level of the LUMO of **A1'** is more positive than that of **A1**, i.e., -2.80 eV. The HOMO of this fragment is a Pd-d_{z^2} type orbital, located on the Pd atom. This could cause the ethylene substitution first to occur on the imine fragment in **A1'**.

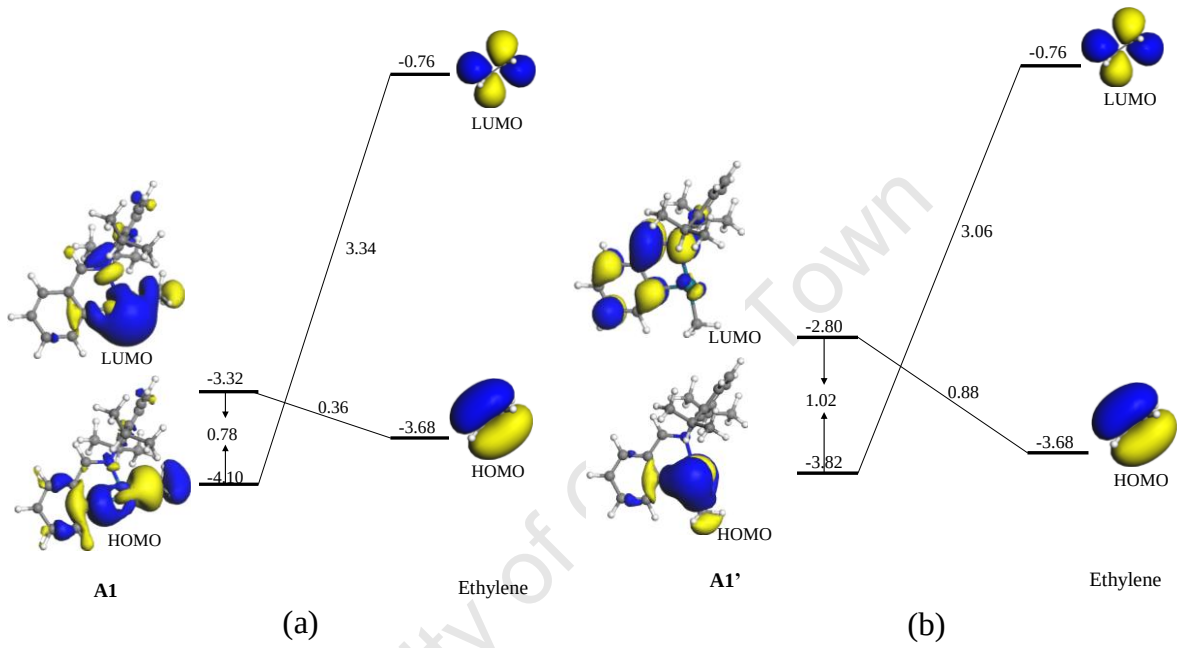

Figure 2.13 Kohn-Sham GGA/PW91/DNP frontier orbitals and energies (eV) for *trans*-(N^C)Pd(CH_3) (**A1**), *cis*-(N^C)Pd(CH_3) (**A1'**) and ethylene.

The FMO gap between $C_2H_{4\text{-HOMO}}$–**A1**$_{LUMO}$ is small (0.36 eV), while the **A1**$_{HOMO}$–$C_2H_{4\text{-LUMO}}$ is much larger (3.34 eV). This is in agreement with the principal orbital interaction in traditional ligand-substitution reactions shown in Figure 2.12, involving the HOMO on the ligand and LUMO on the metal (in our system, ligand = ethylene), i.e., the smaller the $C_2H_{4\text{-HOMO}}$–Pd_{LUMO} gap, the more enhanced the reactivity. On the other hand, the FMO gaps obtained between **A1'** and ethylene were 0.88 eV for $C_2H_{4\text{-HOMO}}$–**A1'**$_{LUMO}$ and 3.06 eV for **A1'**$_{HOMO}$–$C_2H_{4\text{-LUMO}}$.

In addition, we employed Fukui function analysis on the *cis/trans* isomers. The Fukui function is a chemical index of reactivity in the sense of "frontier orbital" theory. The HOMO and LUMO orbital densities are known to be decisive for determining chemical reactivity: high or low frontier density at a molecular site often confers high chemical reactivity to that

site. In essence, this is what the Fukui function is measuring.[55] The nucleophilic Fukui function (f(+)) in DMol^3 corresponds to reactivity with respect to nucleophilic attack. This can be mapped onto a molecular electron density isosurface to describe the electrophilic site of the molecule. Red-yellow indicates the electrophilic regions and green-blue the nucleophilic regions. As shown in Figure 2.14 the FMO densities and the Fukui function, f(+), both predict that nucleophilic attack occurs at the palladium centre on **A1**, while at the imine-carbon atom on **A1'**.

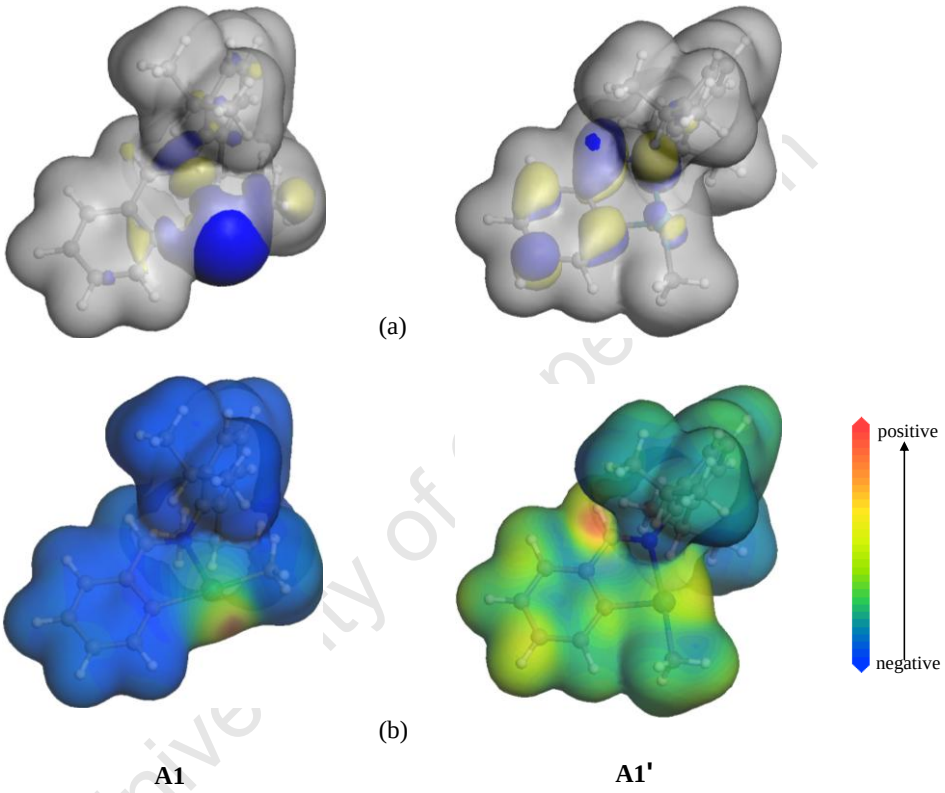

Figure 2.14 DFT estimated electrophilic site on *trans/cis* (N^C)Pd(CH_3) fragments **A1** and **A1'**. This can be deduced by plotting (a) total electron density over the LUMO density and (b) mapping the Fukui function, f(+), on the total electron density of the molecule.

Moreover, it was not possible to locate either a transition state or a five-coordinate intermediate for the associated mechanism from **III'-s** to form the Pd-ethylene π species **A2'**, indicating that ethylene is reluctant to coordinate to the palladium center when the PPh_3 ligand is *cis* to the nitrogen atom. Taken together, the incoming ethylene monomer will only coordinate on the open site, which is *trans* to the nitrogen atom as shown in the three-coordinate "*trans*-like" **A1**. The formation of the Pd-ethylene π complex **A2'**, in which the methyl group is *cis* to the metallated carbon atom is not likely according to DFT calculations.

This agrees with the experimental observation reported by Otto *et al.*[56] in their olefin substitution reaction of $[Pt(\mu\text{-}Cl)(2\text{-}Me_2NCH_2C_6H_4)]_2$. As shown in Eq. 2.4 the monomeric species with olefin coordinated *cis* to the metallated aryl group was the only isomer, and there was no evidence for an isomer with the olefin coordinated to platinum *trans* to the σ-bonded aryl.

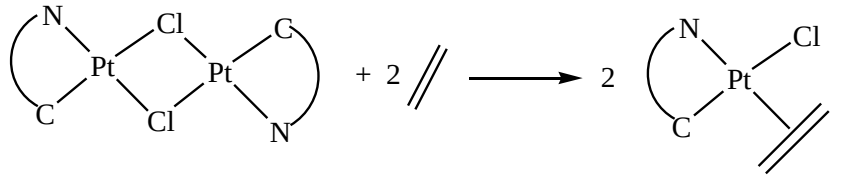

(Eq. 2.4)

The possible process for chain initiation could therefore take place from **III-s** directly, followed by ethylene-substitution reactions via either a dissocative or associative mechanism. On the other hand, the energy barrier for the dissociation of PPh_3 from the *cis* complex **III'-s** to form the three-coordiante "*cis*-like" species **A1'** is fairly low [see Figure 2.15 (A)], so *cis/trans* isomerism could occur on the four-coordiante **III'-s**, or on the three-cooridnate **A1'** if **A1'** exists (Scheme 2.11).

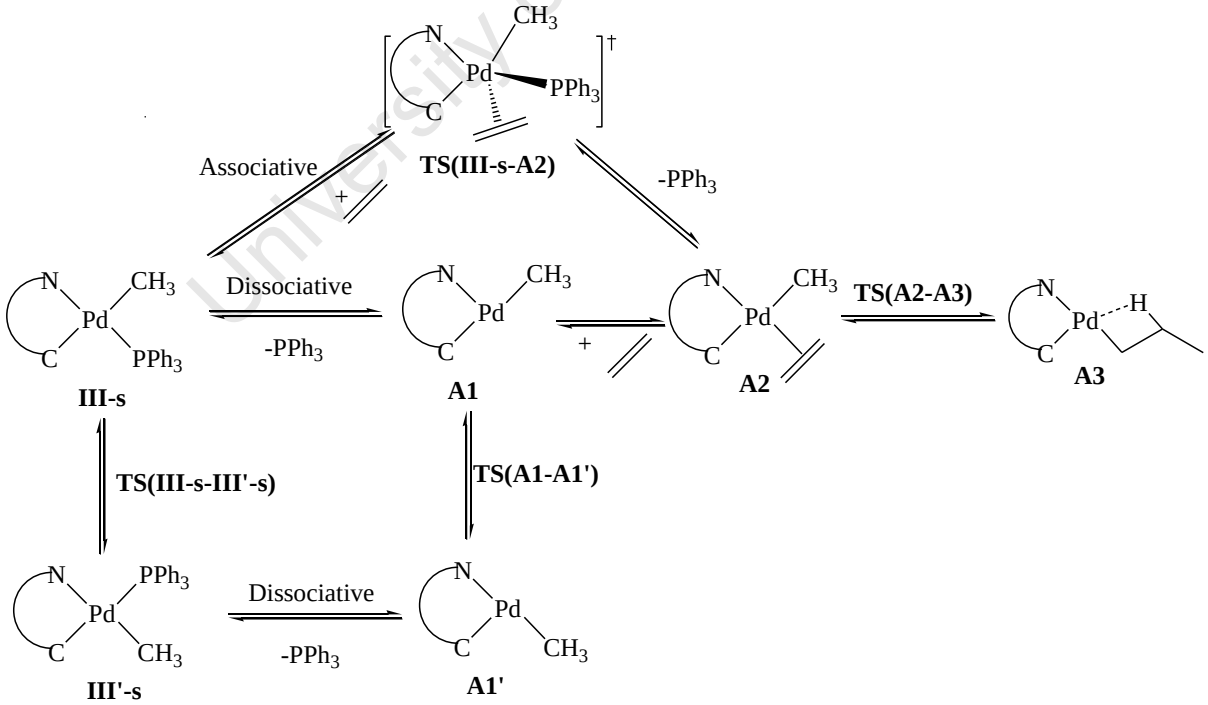

Scheme 2.11 Possible path for the generation of the Pd-ethylene π species **A2**.

Cis-trans isomerization and ethylene-substitution reactions

Based on the observation of the methylation reaction of platinum with LiMe giving *cis/trans* Pt-Me complexes in a ratio of ~ 9:1 (Eq. 2.2), we assume that the formation of *cis*-Pd-Me complex **III'-s** via the methylation by MAO could be predominant. This is also due to the fact that a pair of C-donor/C-donor ligands has the largest phobia of being mutually *trans* in palladium(II) complexes.[50] Therefore, the isomerization of **III'-s** to **III-s** and of **A1'** to **A1** is crucial in the chain initiation process. The energy profile for the isomerization is given in Figure 2.15 (A). Relative energies are calculated with respect to the energy of the *trans*-[(N^C)Pd(CH_3)(PPh_3)] complex indicated as **III-s**. Figure 2.15 (B) shows the fully optimized geometrical structures of minima and TS along with the most relevant calculated geometrical parameters. The isomerization process comprises (i) direct conversion of *cis*-[(N^C)Pd(CH_3)(PPh_3)] **III'-s** to the *trans* isomer **III-s** [black line in Figure 2.15 (A)] and (ii) conversion of a three-coordinate intermediate from a "*cis*-like" to a "*trans*-like" geometry after the dissociation of PPh_3 ligand [red line in Figure 2.15 (A)].

As mentioned above, the formation of the *cis* Pd-ethylene π complex **A2'** from **III'-s** is not likely. Here, we compare both associative and dissociative mechanisms for ethylene-substitution reactions on **III-s** to generate the *trans* Pd-ethylene π complex **A2** [blue line in Figure 2.15 (A)]. For the associative ethylene-substitution reaction, the transition state **TS(III-s-A2)** was found with a relative energy of 14.2 kcal/mol [blue solid line Figure 2.15 (A)]. Dissociation of PPh_3 from **III-s** requires at least a relative energy of 25 kcal/mol to give the three-coordinate intermediate **A1-d** (blue dotted line). Thus, the associative route is more favourable for the formation of **A2**.

The *cis/trans* isomerization mechanisms of square-planar palladium complexes are well studied,[57] a simple geometry change via a tetrahedral four-coordinate species has been reported. For *cis/trans* isomerization between the palladium methyl complexes **III'-s** and **III-s**, the tetrahedral transition state [**TS(III'-s-III-s)**] was located, and is 32.7 kcal/mol above complex **III'-s**. On the other hand, conversion from three-coordinate "*cis*-like" to "*trans*-like" T-shaped configuration occurs via a TS that possesses a Y-shaped configuration.[58] As shown in Figure 2.15 (B), Jahn-Teller instability[59] favours a T-shaped configuration for both "*cis*-like" three-coordinate species **A1'** and "*trans*-like" **A1**, which mutually converge passing through a Y-shaped transition state, **TS(A1'-A1)** with energy higher than that of complex **A1'** by 30.5 kcal/mol.

In our case, both isomerization processes (i and ii) require very high activation energies. Therefore, the transformation from **III's** to **III-s** is unlikely to take place, and consequently the chain initiation process will only take place in the case of the *trans* Pd-Me complex **III-s**, which starts from the associative ethylene-substitution on **III-s**.

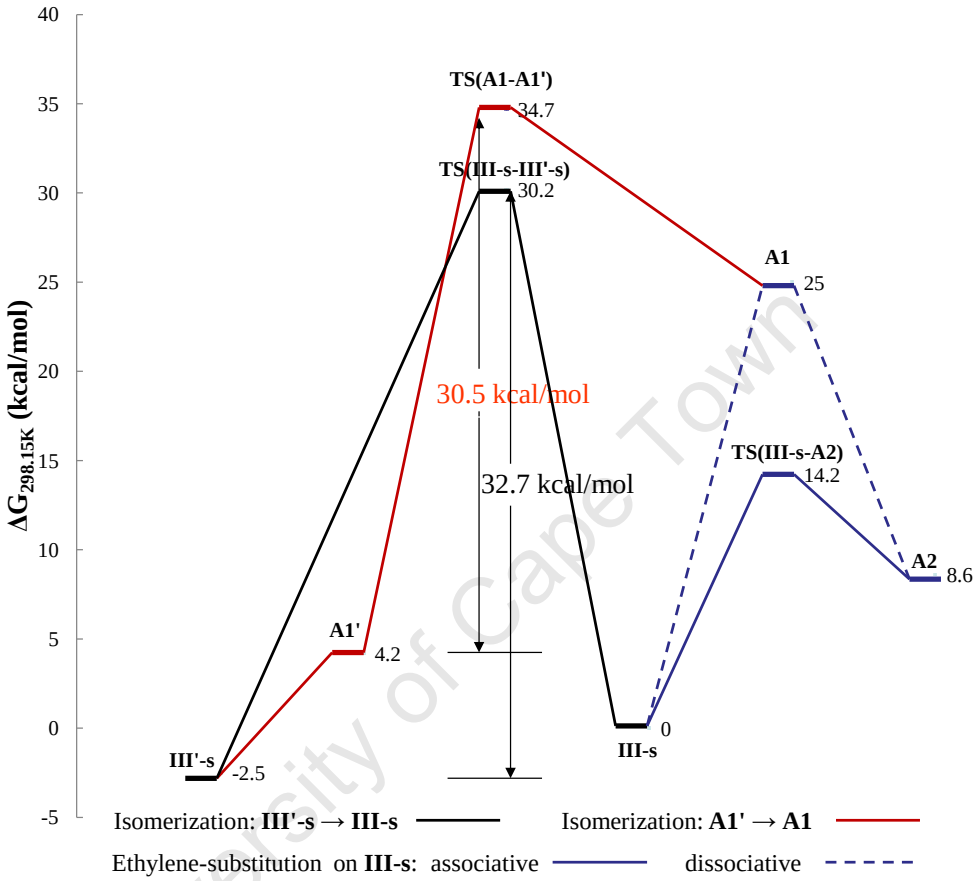

(A)

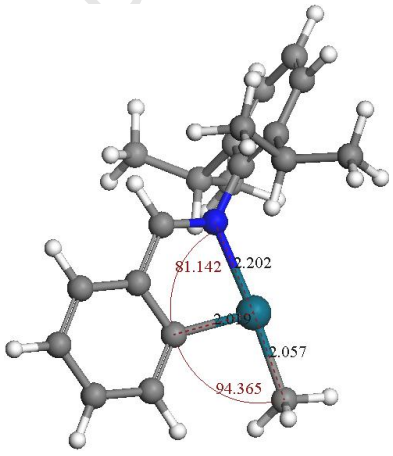

A1'

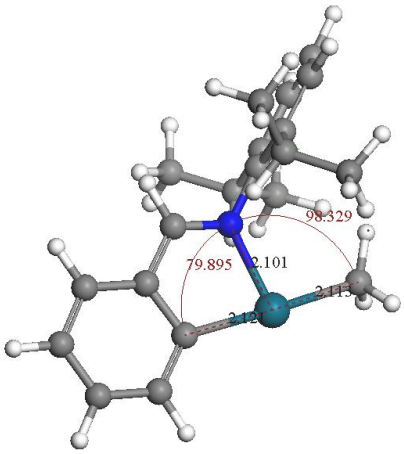

A1

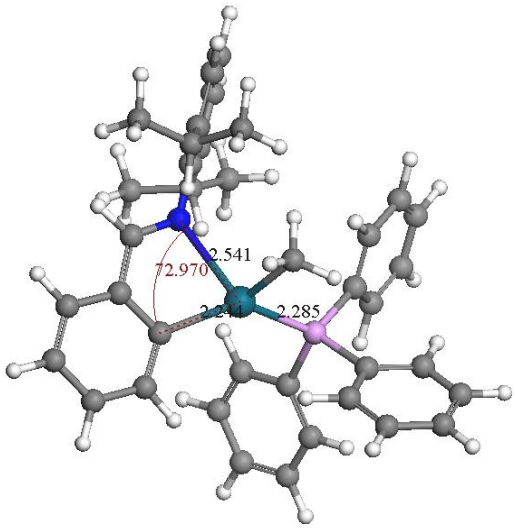

TS(III'-s-III-s)

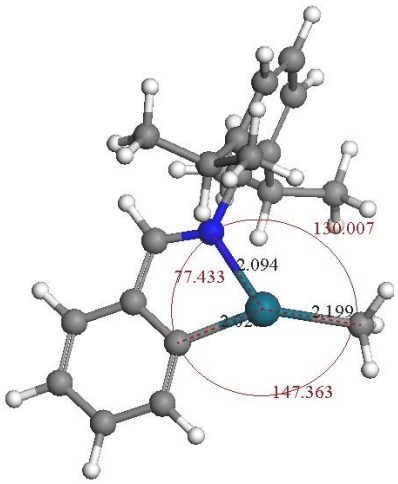

TS(A1'-A1)

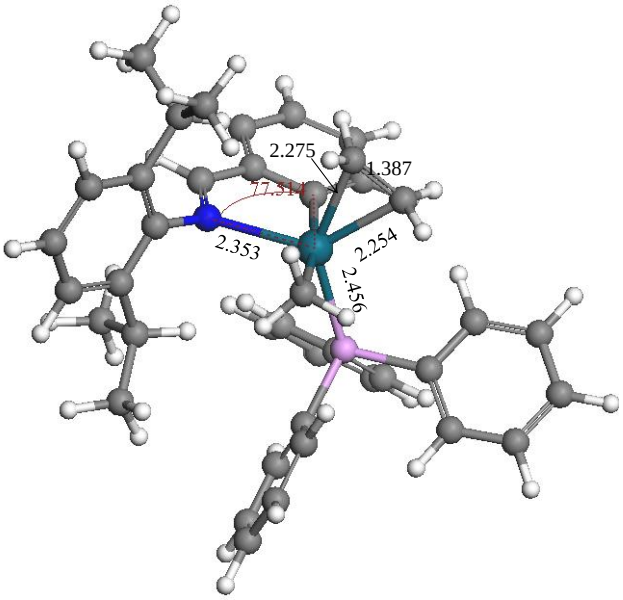

TS(III-s-A2)

(B)

Figure 2.15 (A) Energy profile for the isomerization of *cis*-[(N^C)Pd(CH_3)(PPh_3)] (**III'-s**) and *cis*-[(N^C)Pd(CH_3)] (**A1'**), and the ethylene-substitution reaction on **III-s** via both associative and dissociative mechanisms. Calculated Gibbs free energies ($\Delta G_{298.15K}$) at 298.15 K and 1 atm in kcal/mol relative to **III-s** are given. (B) Optimized structures of involved key species.

First ethylene insertion

The initiation reaction for olefin oligomerization/polymerization includes olefin coordination and insertion.[60] Barriers to the first insertion of ethylene in palladium ethylene π-species have been addressed both experimentally (see Table 1.3 on p. 37) and theoretically (see Table 1.4 on p. 40).

In our system, the ethylene π-complex **A2** was formed via an ethylene-substitution reaction on **III-s**, in which the ethylene is rotated out of the molecular plane to reduce steric repulsion (Figure 2.16). Starting from **A2**, insertion of ethylene into the Pd-methyl bond proceeds via rotation of the ethylene moiety into the molecular plane. The transition state **TS(A2-A2a)** associated with the rotation of the ethylene lies 5.3 kcal/mol above **A2**. The product of this rotation is the stable in-plane π-complex **A2a**, which lies 2.9 kal/mol above **A2**. The geometry of complex **A2a** is different from **A2**, with significant differences seen in the Pd-olefin bonds: in **A2** the Pd-C_2 and Pd-C_3 bonds are almost equal, 2.213 and 2.215 Å, while in **A2a** the Pd-C_2 bond is 0.05 Å longer than Pd-C_3 bond. A decrease of the methyl-ethylene distance in **A2a** brings about the four-membered ring transition state **TS(A2a-A3γ)**. The energy barrier associated with ethylene insertion is 9.6 kcal/mol.

Relaxation of **TS(A2a-A3γ)** to the product side yields the kinetic insertion product **A3γ**, which exhibits γ-agostic bonding via the terminal methyl hydrogen. During this olefin insertion process, the Pd-C_1 and Pd-C_2 bonds are broken and Pd-C_3 and C_1-C_2 bonds are formed. Structure **A3γ** is a real agostic complex with a Pd-$H_{agostic}$ bond distance of 2.288 Å and C-$H_{agostic}$ bond distance of 1.113 Å (vs. 1.089 Å in the free C_2H_4 molecule), where the Pd-N bond is longer by 0.046 Å while the Pd-$C_{metallated}$ is shorter by 0.112 Å compared with those in the reactant **A2**. These changes can easily be explained in terms of the *trans* influence.

The direct product of the insertion reaction, γ-agostic complex **A3γ**, is calculated to be 17.3 kcal/mol lower in energy than **A2**. Furthermore, complex **A3γ** can easily be converted into the final β-agostic thermodynamic product **A3β** by twisting the C_1-C_2 bond. The reorganized transition state **TS(A3γ-A3β)** lies 2.2 kcal/mol above **A3γ**. Thus, the entire initiation reaction from **III-s** is calculated to be exothermic by 9.6 kcal/mol, and the rate-determining step after ethylene coordination is the insertion of the olefin into the Pd-alkyl bond, which takes place with a barrier of 9.6 kcal/mol. This value is much smaller than those in the diimine Ni and Pd systems.[21,22]

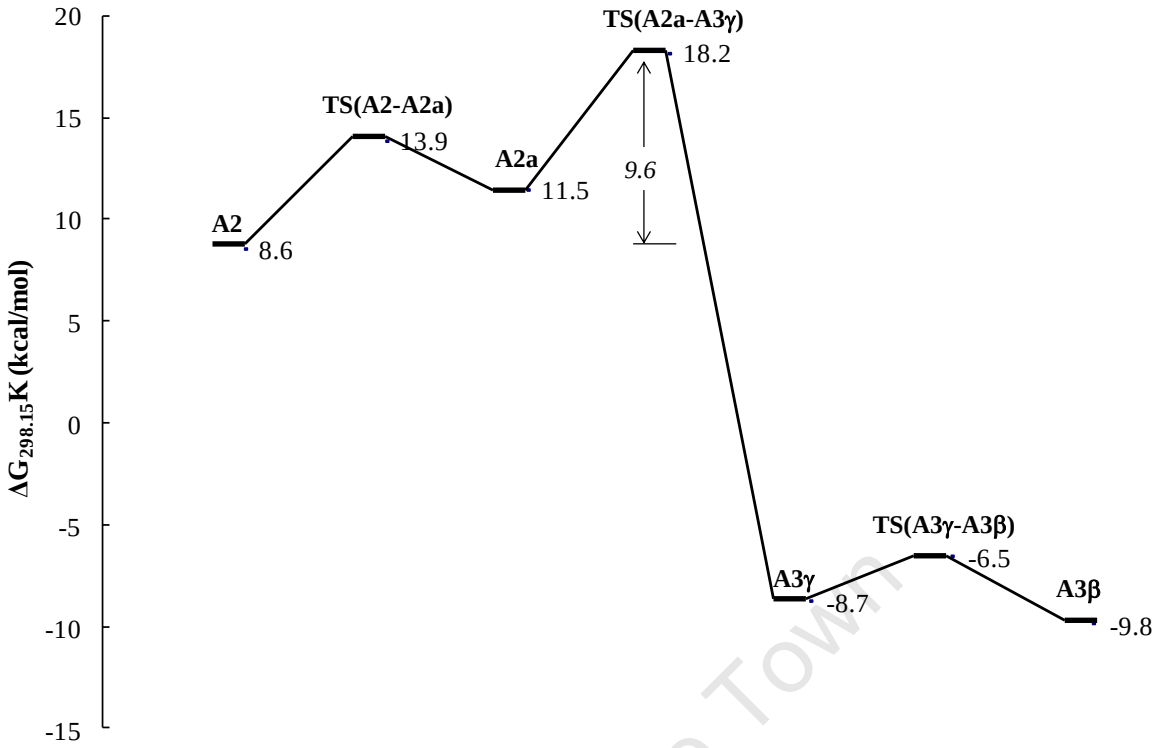

(A)

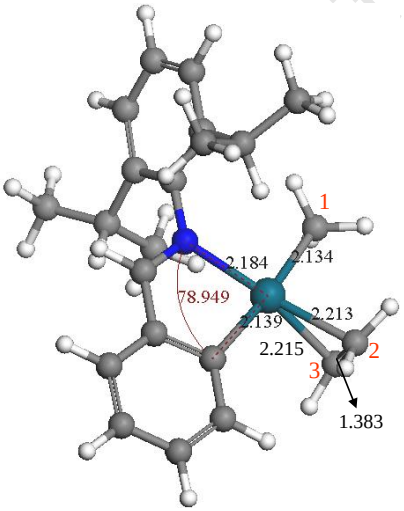

A2

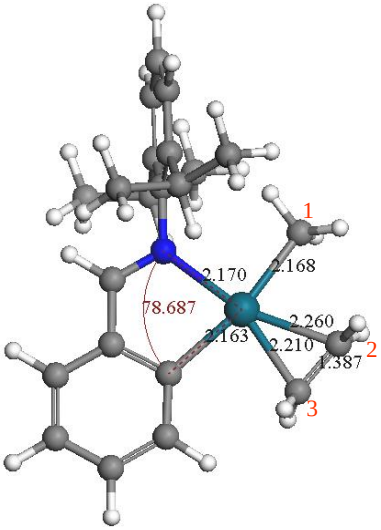

A2a

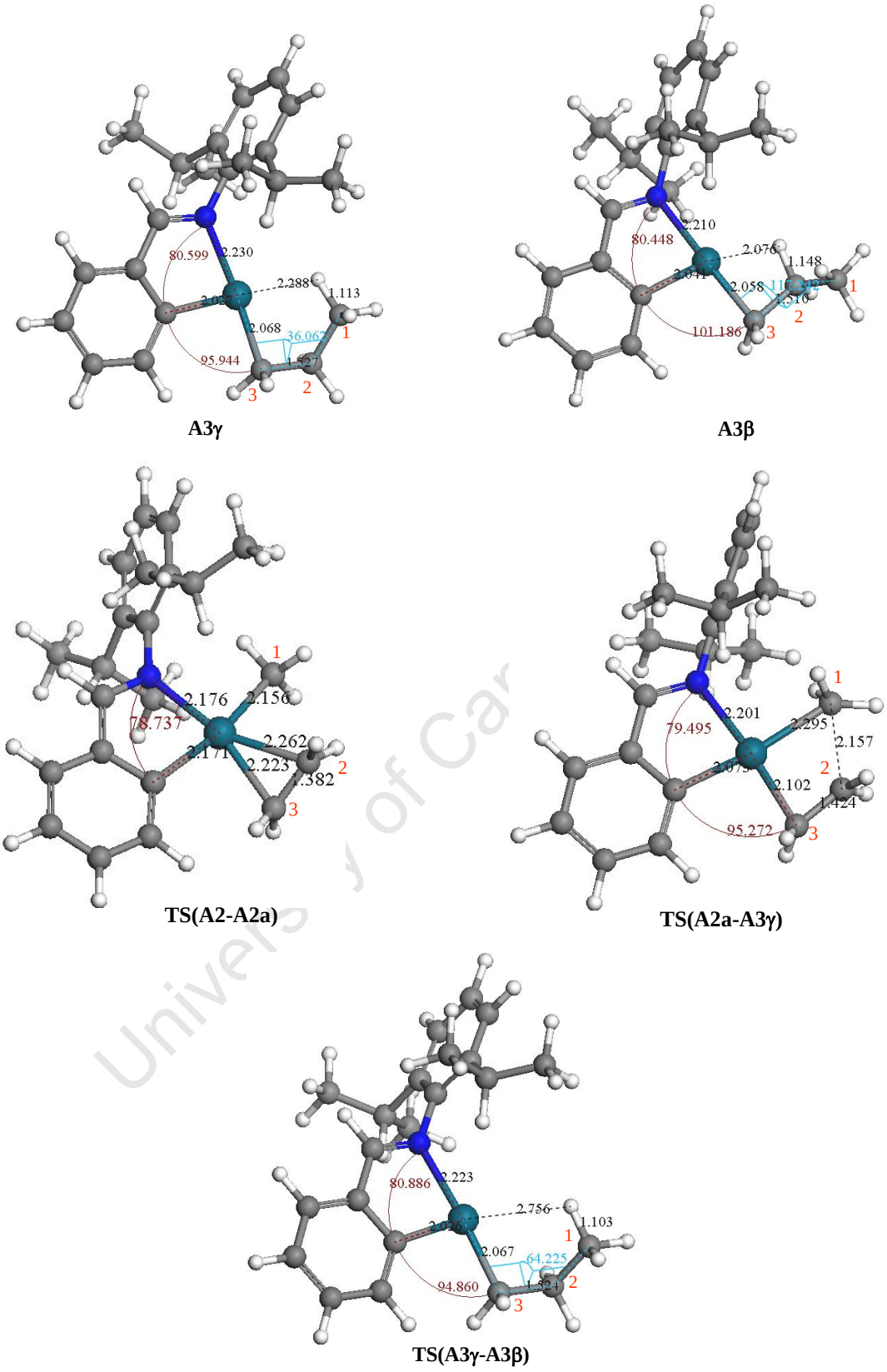

(B)

Figure 2.16 (A) Energy profile for the fisrt ethylene insertion process. Calculated Gibbs free energies ($\Delta G_{298.15K}$) at 298.15 K and 1 atm in kcal/mol relative to **III-s** are given. (B) Optimized structures of involved key species.

2.4.1.2 Chain transfer processes

β-Hydride transfer and dissociation. The β-agostic *cis*-alkyl complex **A3β** undergoes β-hydride elimination to give the olefin hydride complex **A4** via transition state **TS(A3β-A4)**. **TS(A3β-A4)** is a late transition state with a product-like structure and differs from **A4** by the slightly shorter C^{β}-H^{β} (2.025 Å) bond and slightly longer C^{α}=C^{β} bond (1.428 Å) [cf. Figure 2.17 (B)]. The relative energy for **TS(A3β-A4)** from **III-s** is 9.8 kcal/mol, compared to the barrier of 19.6 kcal/mol when considered from **A3β**. The C=C bond of the coordinated olefin in the complex **A4** is rotated into the square-planar plane. Dissociation [Path (i) in Scheme 2.12] of propylene from **A4** requires energy of 24.9 kcal/mol relative to **III-s** to give the three-coordinate Pd-H complex **A5-d**, which is very close to the energy requirement for forming **A1**. This value is much smaller than the calculated energy for the elimination of propylene from β-agostic diimine-palladium-propyl complexes, which is calculated to be endothermic by 43.9 kcal/mol.[22]

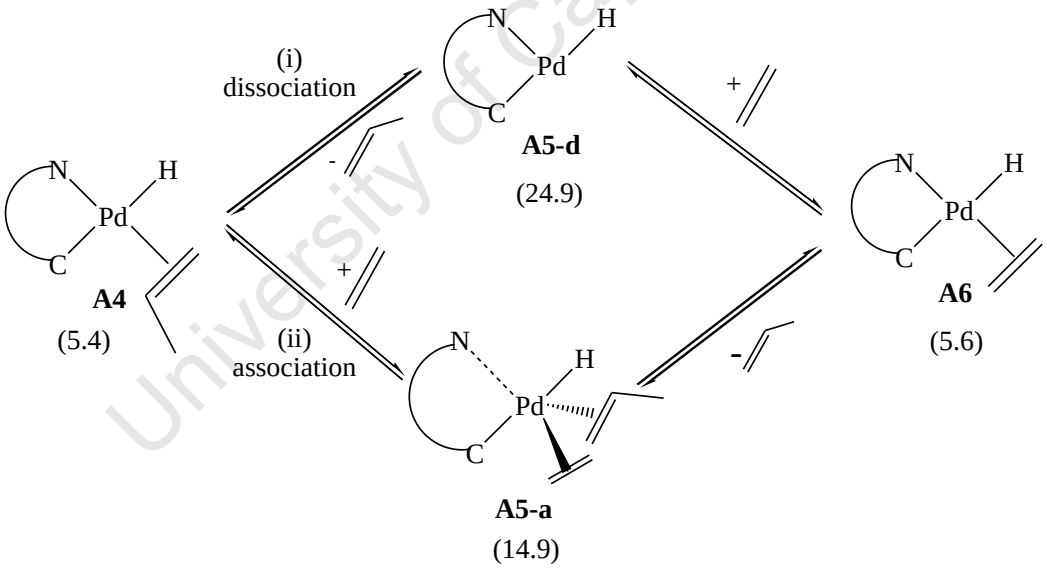

Scheme 2.12 Dissociative and associative olefin displacement as possible chain transfer processes. Calculated Gibbs free energies ($\Delta G_{298.15K}$) at 298.15 K and 1 atm in kcal/mol relative to **III-s** are given in parentheses.

β-Hydride transfer and associative displacement. According to Brookhart *et al*.[60] and Musaev *et al*.,[22] the coordinating olefin rapidly exchanges with ethylene in solution via an associative mechanism [Path (ii) in Scheme 2.12]. This suggests the existence of a stable five-coordinate bis(olefin) complex or the presence of a low-lying five-coordinate olefin exchange transition

state. For the associative olefin displacement from **A4** to **A6**, the transition state **TS(A4-A6)** could not be located. However a five-coordinate intermediate[22, 61] **A5-a** (see Figure 2.17) was found with a relative energy of 14.9 kcal/mol. The inability to locate the transition state for coordination of the second olefin [**TS(A4-A6)**], suggests that the second olefin coordination takes place without a barrier. Such observations, *i.e.*, the inability to locate a transition state have also been made for other Pd(II) systems, notably Pd(II) diimine[22] and Pd(II)(S^O)[61] systems. Complex **A5-a** has a pseudo-square-pyramidal structure with one ethylene and one propylene, as well as Pd-H and Pd-$C_{metallated}$ bonds in the plane, while the P-N bond sits on the top of the plane, which is contrary to a trigonal-bipyramidal structure reported for Pd(II)diimine complex.[22] The elongated Pd-N bond distance (2.848 Å) reveals the hemilability of the N^C ligand. The binding energy of the second ethylene is calculated to be only 9.5 kcal/mol compared to **A4**. This 18e species is electronically saturated and sterically crowded but still has a small positive binding energy.

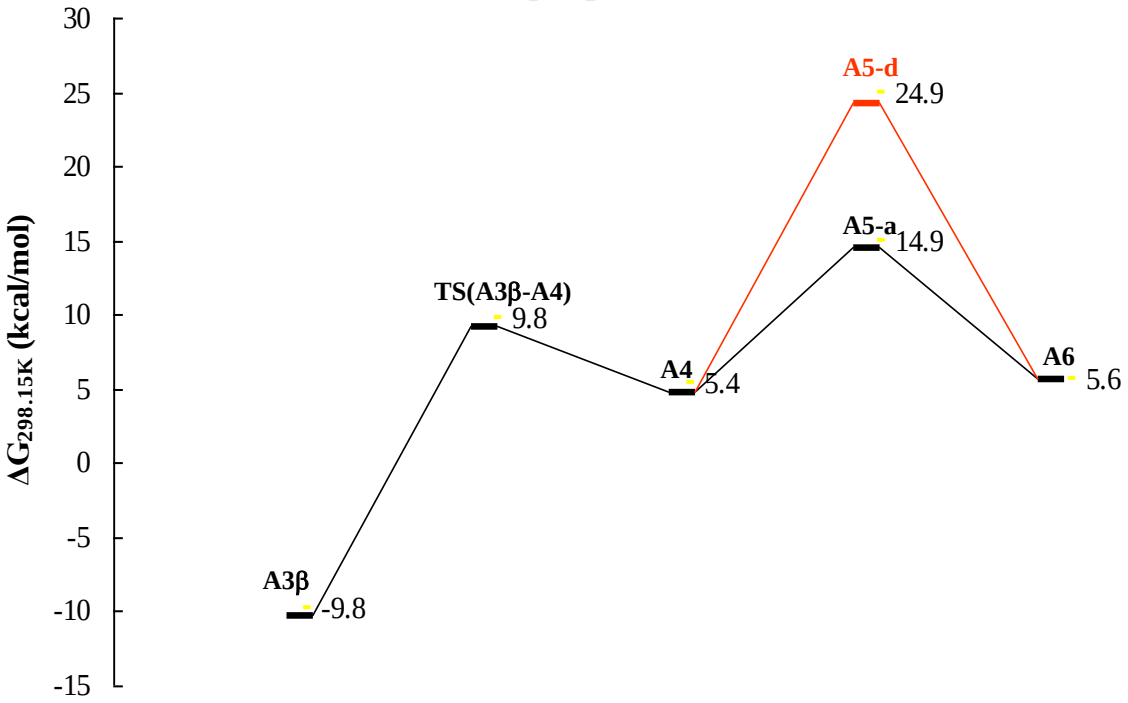

(A)

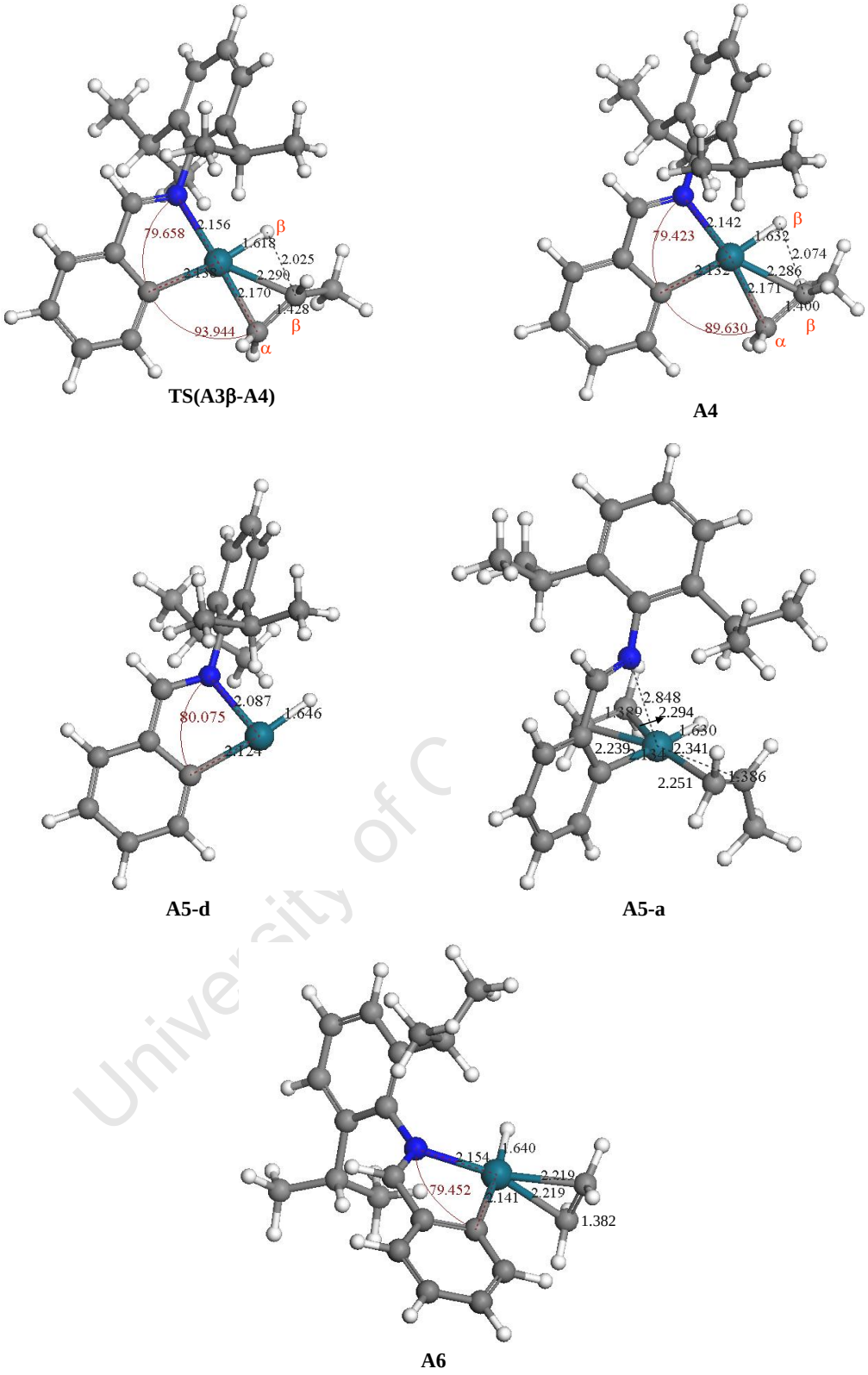

(B)

Figure 2.17 (A) Energy profile for the chain transfer and β-hydride elimination steps. Calculated Gibbs free energies ($\Delta G_{298.15K}$) at 298.15 K and 1atm in kcal/mol relative to **III-s** are given. (B) Optimized structures of involved key species.

2.4.1.3 Chain propagation: ethylene dimerization and trimerization

The chain propagation processes of the Cossee-type catalytic cycle we studied include a dimerization and a trimerization reaction. Isomerization via β-hydride elimination and re-insertion reactions was excluded in the study. Possible intermediates and transition states for dimerization and trimerization starting from the active species **A6** are depicted in Scheme 2.13. The energy profile and optimized structures are shown in Figure 2.19 (see p. 93).

Chain propagation proceeds via the Cossee-type mechanism, including olefin insertion into the palladium-hydride or palladium-carbon bonds. Analogy with the initiation step, in which **A2** and **A2a** were found, suggests that there may exist structures like **A6a**, **A8a** and **A11a** with an in-plane olefin. Since their roles in the reaction mechanism are not important, we have not searched for such structures.

After the ethylene migratory insertion step, new metal-alkyl complexes will be formed, i.e. **A9'** and **A12'**. In general, for the metal-alkyl complex several structures with α-, β-, γ-agostic hydrogen etc. may exist. As concluded in the previous studies, the most stable conformation of the polymer chain contains a β-agostic interaction, and the other agostic structures are expected to rearrange easily to the more stable β-agostic one.[62] Therefore, only β-agostic palladium-alkyl complexes have been searched for in the reaction mechanism.

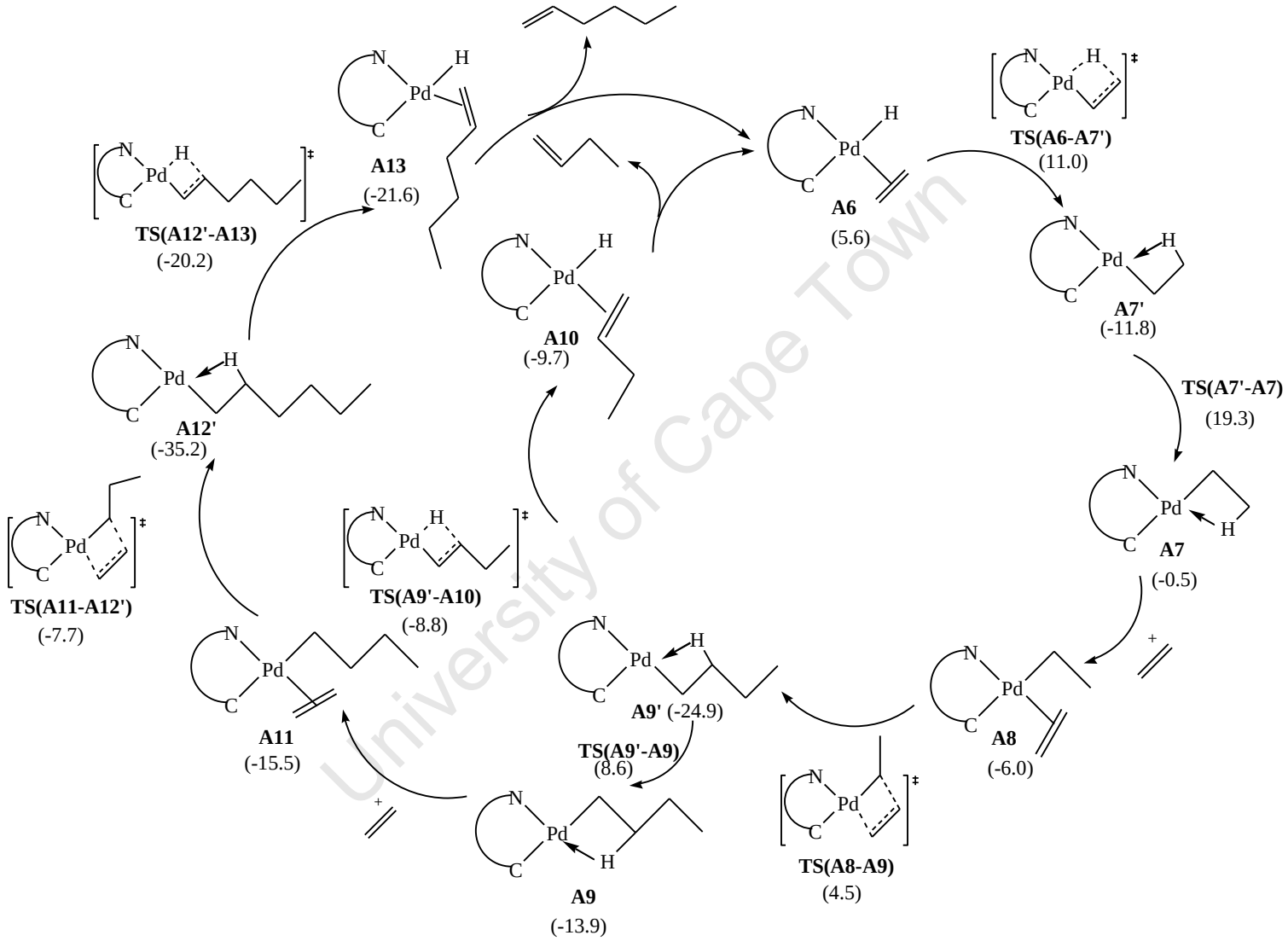

Scheme 2.13 Chain propagation process for the Cossee-type mechanism: ethylene dimerization and trimerization. Calculated Gibbs free energies ($\Delta G_{298.15K}$) at 298.15 K and 1 atm in kcal/mol relative to **III-s** are given in parentheses.

Chain propagation reactions to form a dimer and trimer

The β-agostic *cis*-ethyl palladium complex **A7'** was formed from **A6** via the four-membered ring transition state **TS(A6-A7')** with an insertion barrier of 5.4 kcal/mol. As suggested by its analogous Pd-Me complex **A1'**, the LUMO for **A7'** was estimated after breaking its β-agostic Pd-H bond. It is the same as **A1'**, the LUMO is not located on Pd atom (Figure 2.18). As a consequence, it requires isomerization of the more stable **A7'** to the less stable but more reactive *trans* mode **A7** prior to uptake of ethylene monomer. Conversion of the agostic *cis* form **A7'** to its trans form **A7** via a Y-shaped transition state **TS(A7'-A7)** requires 31.1 kcal/mol energy. As expected, the DFT-estimated LUMO is found to be largely concentrated on Pd after breaking the β-agostic Pd-H bond in **A7** (Figure 2.18).

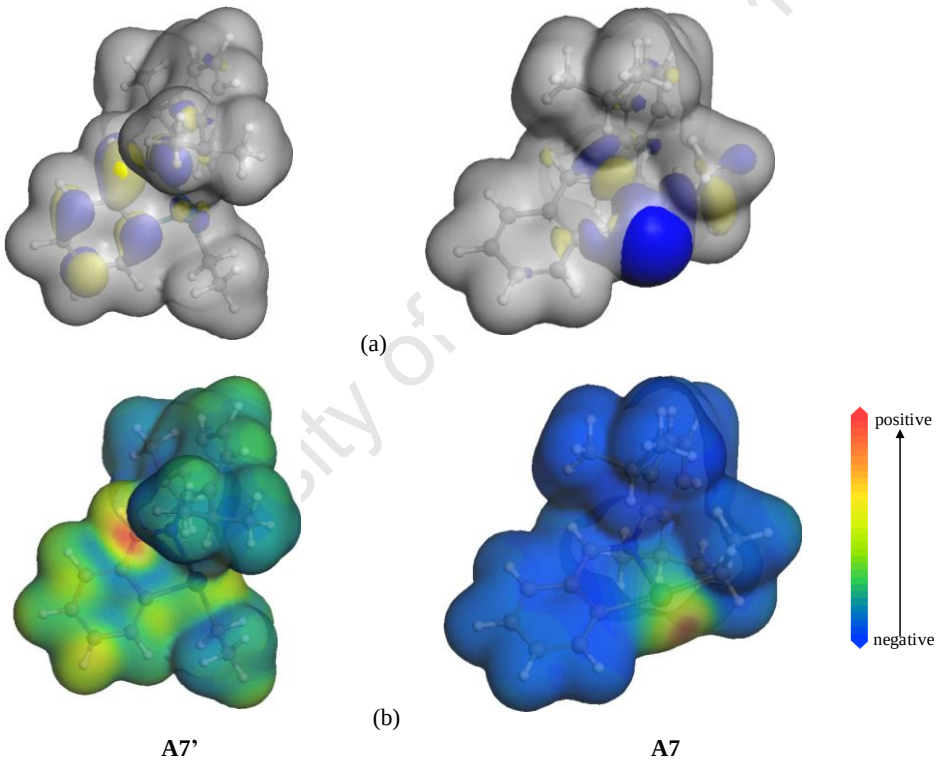

Figure 2.18 DFT estimated electrophilic site on *trans/cis* (N^C)Pd(CH_2CH_3) fragments **A7** and **A7'**. This was deduced by plotting (a) total electron density over the LUMO density and (b) mapping the Fukui function, f(+), on the total electron density of the molecule.

Propagation of the chain commences with uptake of an ethylene unit by **A7**. The new alkyl olefin complex **A8** is calculated to be 5.5 kcal/mol exothermic relative to the complexation energy of **A7** + C_2H_4. As shown in Figure 2.19 (B), the coordination of the olefin to **A7** distorts the geometry of the reactant, *i.e.* its β-agostic feature disappears in **A8**. The next step is the migratory insertion of the olefin into the Pd-CH_2CH_3 bond via the transition state

TS(A8-A9') to give a new metal-alkyl complex **A9'**. As seen in Figures 2.19(B) and 2.16(B), the structures of the transition states **TS(A8-A9')** and **TS(A2a-A3γ)**, which are for olefin insertion into the Pd-CH_2CH_3 and Pd-CH_3 bonds, respectively, are very similar. **TS(A8-A9')** is an early transition state with its geometry close to that of the reactant **A8**, and the barrier height calculated relative to complex **A8** is 10.5 kcal/mol. After the transition state is crossed, the β-agostic *cis*-butyl product complex **A9'** is obtained and calculated to be energetically lower than the reactant **A8** by 18.9 kcal/mol.

It has been known for a long time that late-transition metal catalysts can dimerize or oligomerize olefins due to competing β-hydrogen elimination.[63] Thus, the *cis*-butyl palladium complex **A9**, which is a key intermediate in the catalytic cycle, could undergo either β-hydride elimination to complete a dimerization cycle (isomerization is not considered) or ethylene insertion to form a longer chain oligomer. The butyl group in **A9'** undergoes isomerization to form **A9** with the alkyl group *trans* to the N atom via the transition state, **TS(A9'-A9)**. The addition of a new ethylene molecule to the complex **A9** leads to ethylene trimerization.

β-Hydride elimination reactions

For the dimerization process, the β-agostic *cis*-butyl complex **A9'** undergoes β-hydride elimination to give olefin hydride complex **A10** via transition state **TS(A9'-A10)**. For the β-agostic complex **A9'**, the C-$H_{agostic}$ bond length (1.151 Å) is calculated to be 0.05 Å longer than a non-agostic C-H bond (1.099 Å). Activation of the C-$H_{agostic}$ takes place with a 16.1 kcal/mol barrier relative to the β-agostic complex **A9'**. The transition state corresponding to this process, **TS(A9'-A10)**, is a late transition state, as shown in Figure 2.18. The resulting complex, **A10**, is an asymmetric olefin π-complex, which can easily rearrange both to the β-agostic complex **A9'** due to the small barrier for the reverse reaction **A10→A9'** (0.9 kcal/mol), and to the more symmetrical olefin π-complex **A10a** (structure optimized without symmetry constraint). The barrier height from **A10** to **A9'** is quite similar to the reported value for Pd(II) diimine analogues, which was calculated to be 0.2 kcal/mol.[22] The barriers separating **A10** from **A10a** corresponding to the rotation of the butyl fragment around the Pd-X axis, X being the centre of the CH_2=$CHCH_2CH_3$ double bond. The transition state was not located. Probably the barrier is similar to that of the **A2→A2a** rearrangement.

The β-hydride elimination reaction for the trimerization process is very similar to that for the dimerization. Firstly, the optimized structure of the β-agostic *cis*-hexyl complex **A12'** is very similar to **A9'** with the same Pd-$H_{agostic}$ and C-$H_{agostic}$ bond lengths. Secondly, the relative energy for **TS(A12'-A13)** from **A12'** is 15 kcal/mol and the barrier for the reverse reaction **A13→A12'** is calculated to be 1.4 kcal/mol. Finally, the resulting complex **A13** is a symmetrical olefin π-complex similar to **A10a**.

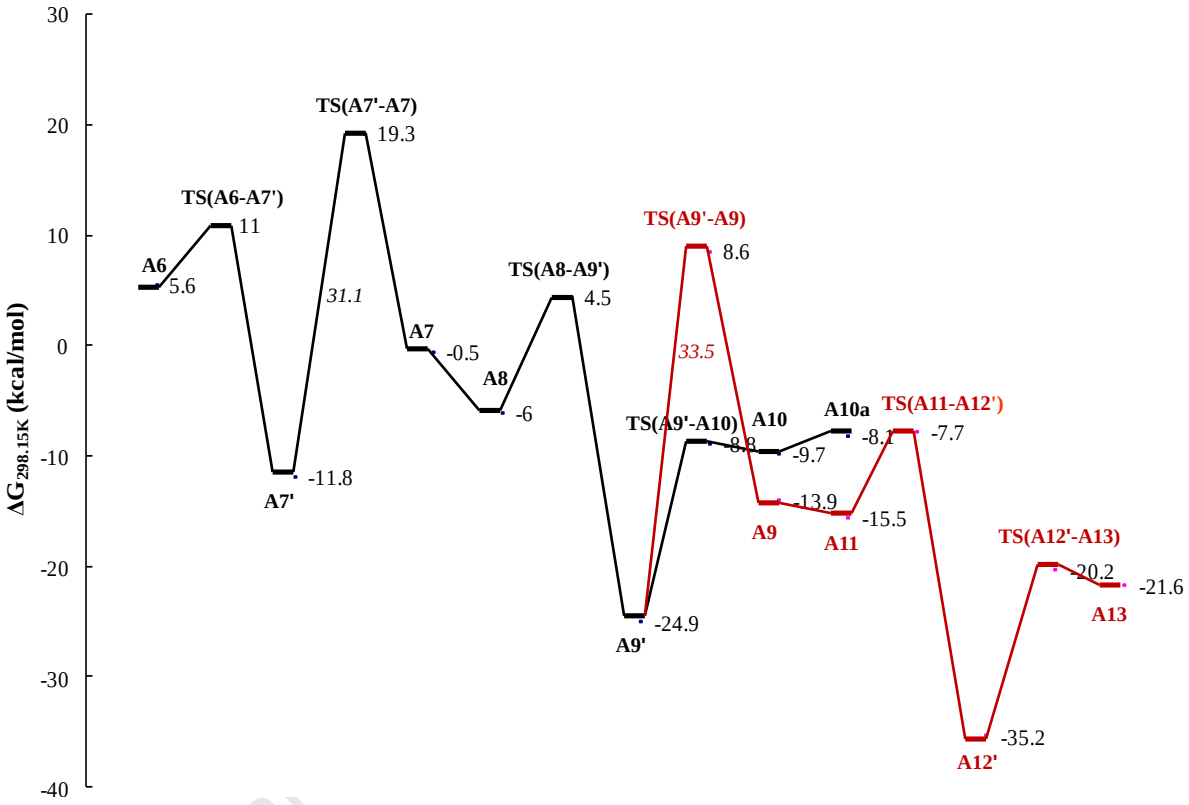

(A)

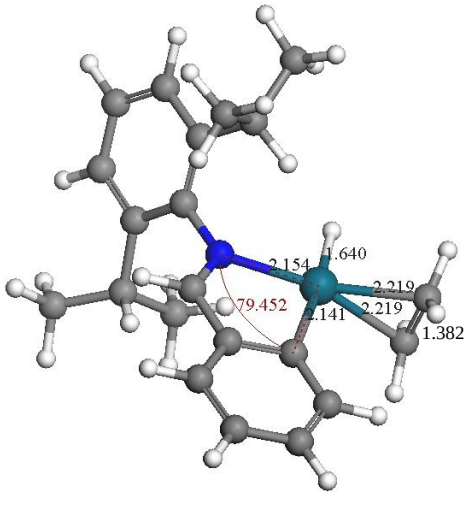

A6

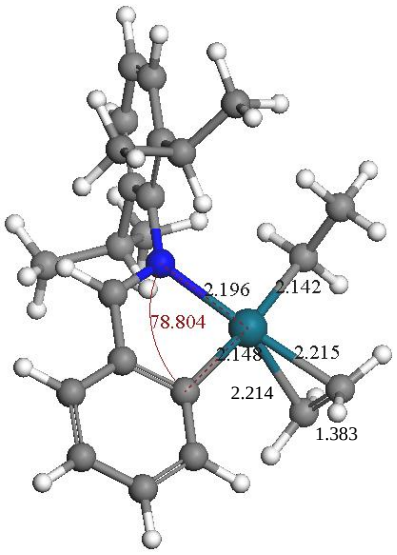

A8

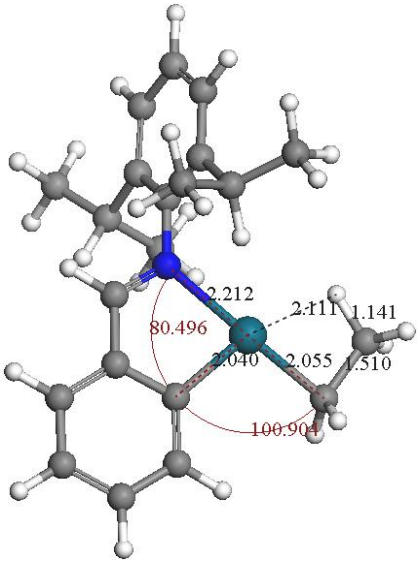

A7'

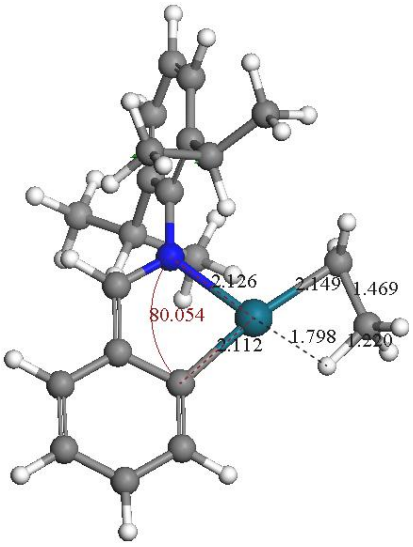

A7

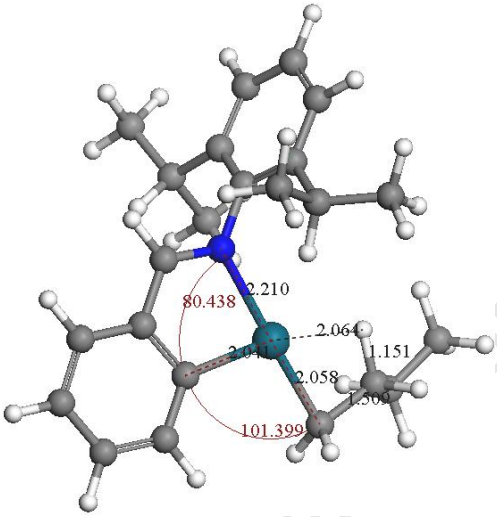

A9'

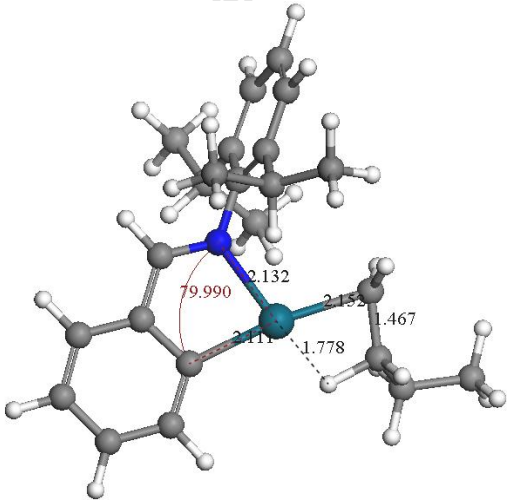

A9

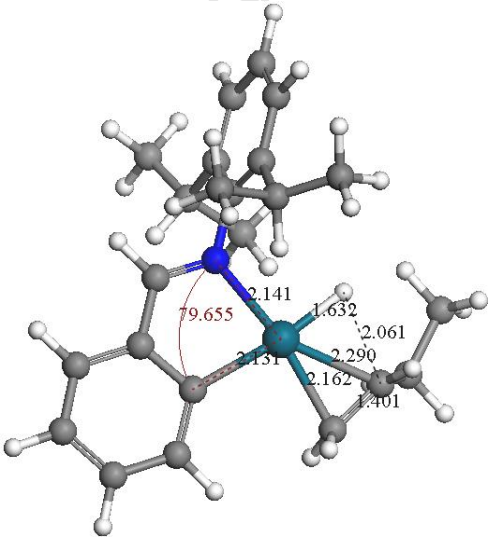

A10

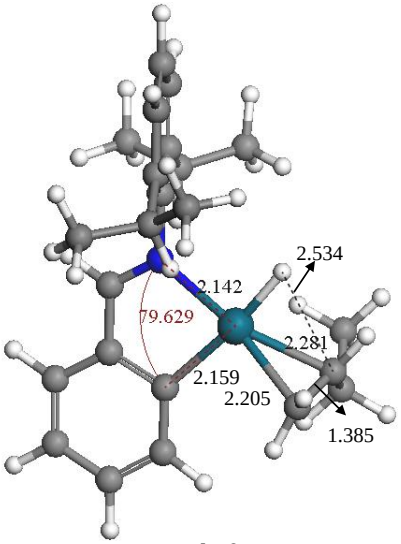

A10a

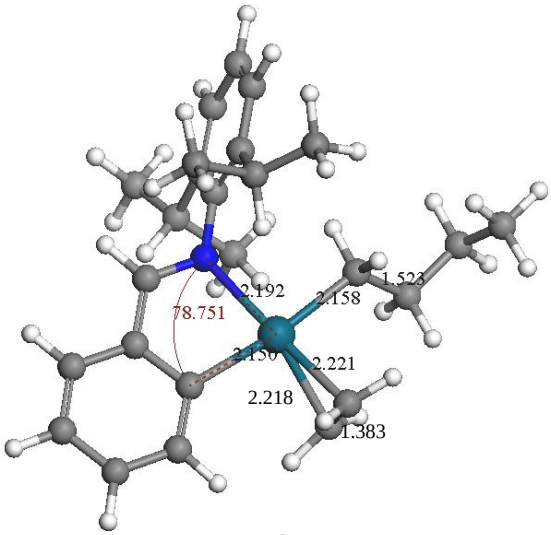

A11

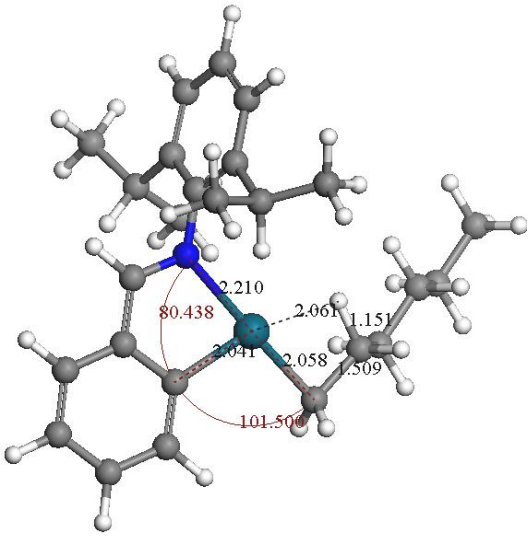

A12'

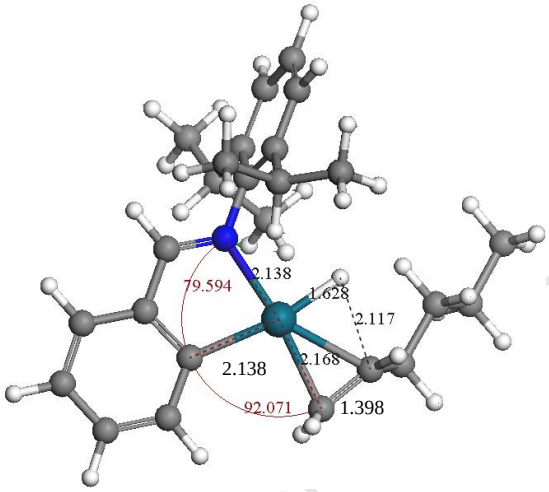

A13

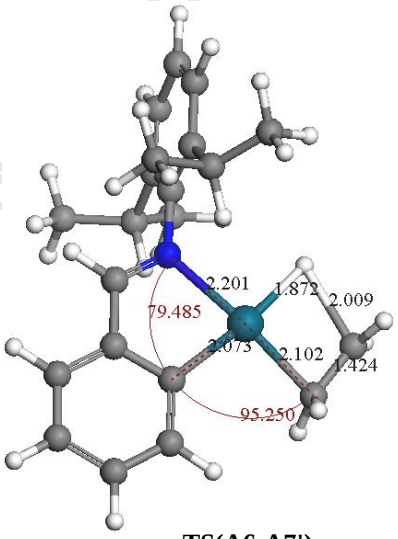

TS(A6-A7')

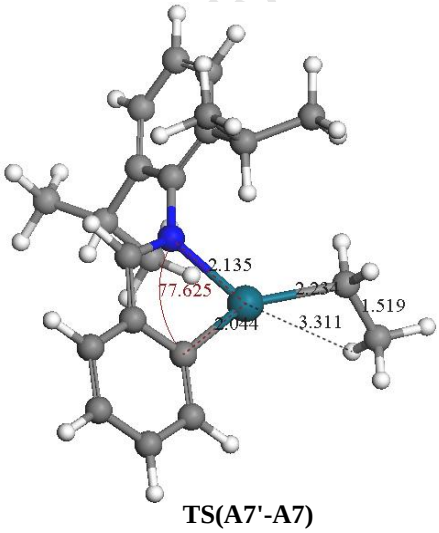

TS(A7'-A7)

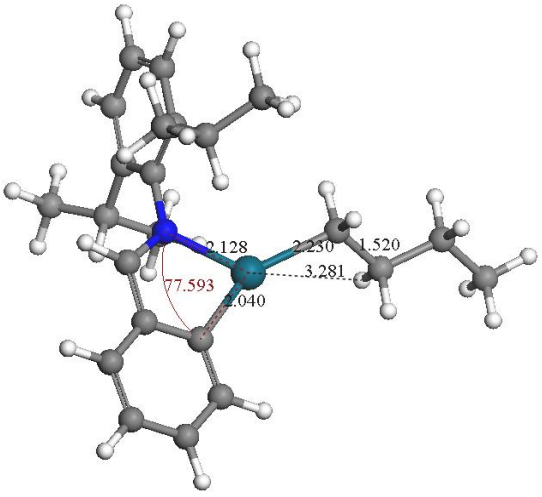

TS(A9'-A9)

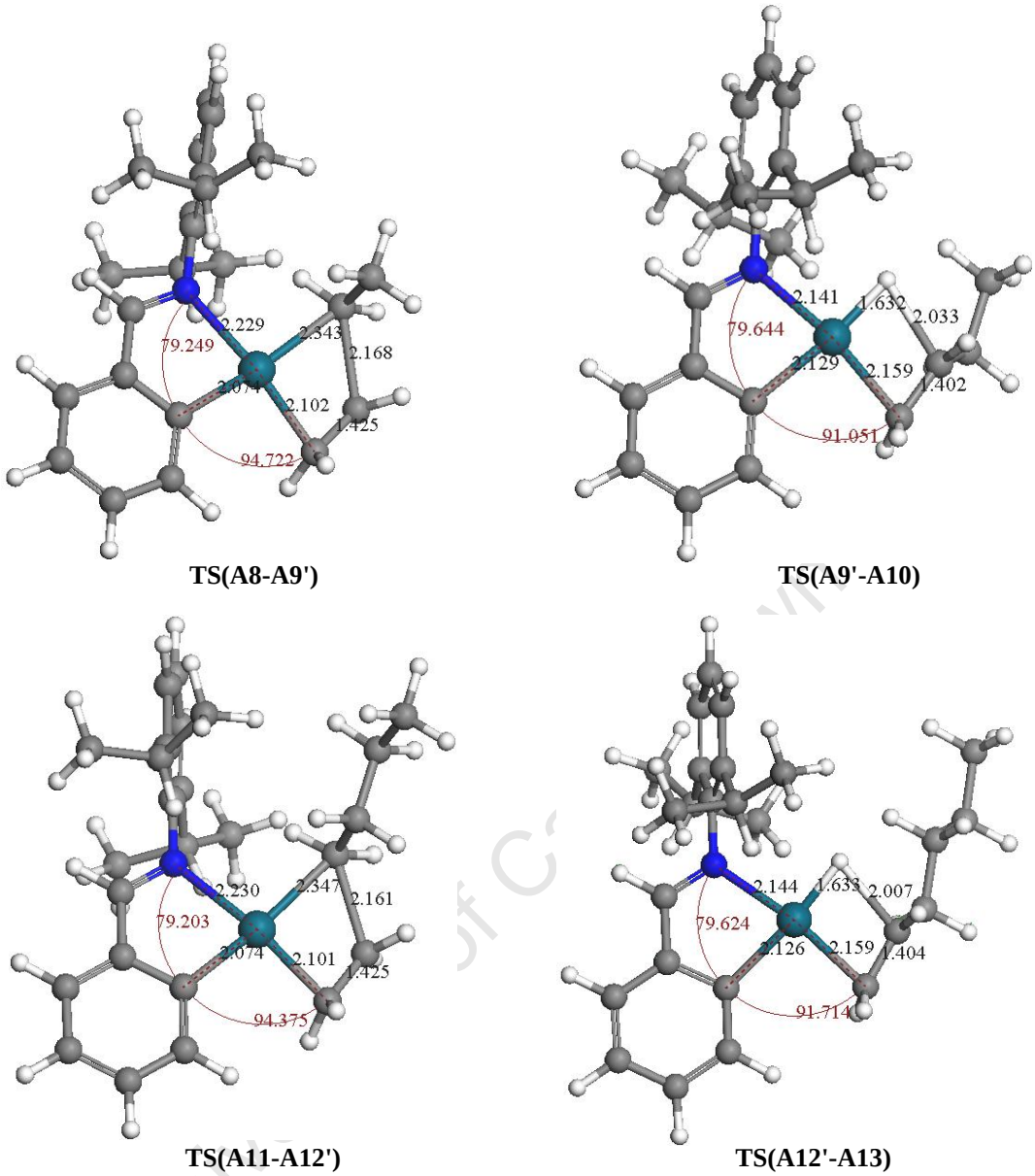

TS(A8-A9') **TS(A9'-A10)**

TS(A11-A12') **TS(A12'-A13)**

(B)

Figure 2.19 (A) Energy profile for chain propagation process to form the dimer and the trimer. Calculated Gibbs free energies ($\Delta G_{298.15K}$) at 298.15 K and 1 atm in kcal/mol relative to **III-s** are given. Black: ethylene dimerization, Red: ethylene trimerization. (B) Calculated bond distances (in Å) and angles (in deg) of the transition states and intermediates of Cossee-type mechanism.

2.4.2 Mechanism B: metallacycle pathway

Although the polyethylene and ethylene oligomers produced by palladium catalysts are likely the result of a polymerization/oligomerization reaction that has followed a Cossee-type mechanistic pathway according to the literature, a metallacyclic pathway should not be excluded. There are many palladacycloalkanes that have been synthesized and studied as models for intermediates in olefin dimerization and oligomerization reactions.[64] The key step in a metallacyclic pathway is the oxidative coupling of two coordinated ethylene units. In principle the oxidative coupling reaction can take place on M(0) or M(II) centres, to give, respectively, a M(II) or M(IV) metallacycle. As shown in Scheme 2.14, palladium is formally in a 2+ oxidation state in the starting complex **IV-s**, and stays the same oxidation state in the bis-olefin complex **B3**. The oxidation state of the metal ion is formally 4+ throughout for the rest of the structures except **B6** and **B9**. If the oxidative coupling could occur on the Pd(II) centre of **B3** to form the Pd(IV) metallacycle **B4**, then the catalytic reaction could follow a metallacyclic pathway.

In this section, we explore the dimerization and trimerization reactions of ethylene via a metallacyclic mechanism by applying GGA/PW91/DNP functional to Scheme 2.14, to compare with the Cossee-type mechanism discussed above in terms of the reaction energetics.

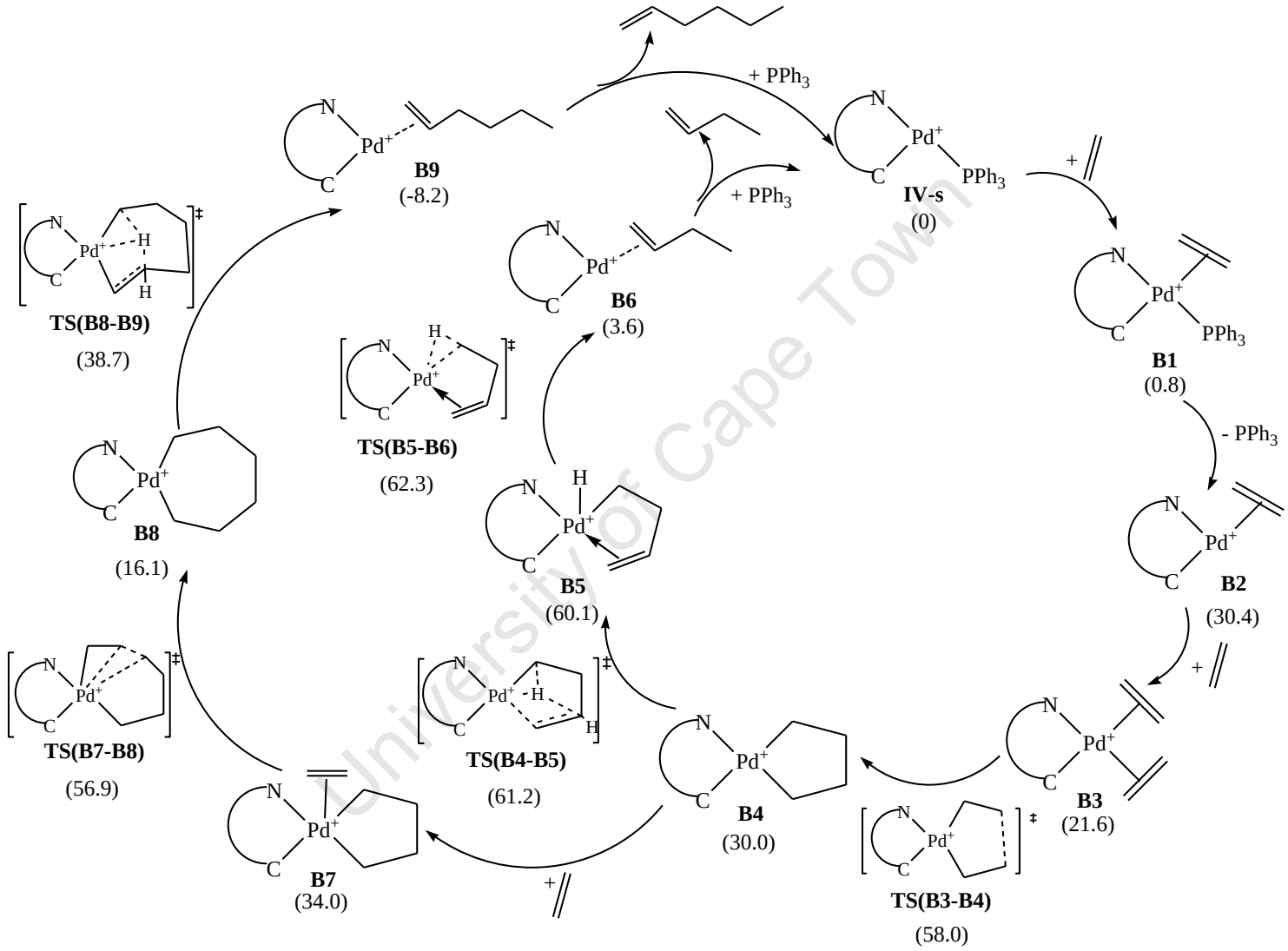

Scheme 2.14 Metallcycle mechanism for ethylene dimerization and trimerization. Calculated Gibbs free energies ($\Delta G_{298.15K}$) at 298.15 K and 1 atm in kcal/mol relative to **IV-s** are given in parentheses.

2.4.2.1 Exploration of crucial elementary steps in the mechanism

Oxidative coupling to generate the pallada(IV)cyclopentane

First, the LUMO for the three-coordinate complexes **IV-s** and **B2** were estimated in order to assess the possibility of olefin coordination to the palladium centre. In both cases, the LUMOs were largely located on the Pd atom, i.e., the nucleophilic attack by ethylene occurs at the palladium centre on **IV-s** and **B2**. This is also confirmed by the Fukui function [f(+)] analysis (Figure 2.20). The complex **IV-s** will therefore accept the coordination of two ethylene molecules stepwise. The two coordinated ethylene moieties undergo oxidative coupling, leading to the formation of the pallada(IV)cyclopentane **B4**. The key species for this step together with reaction and activation free energies are shown in Figure 2.22 (see p. 103).

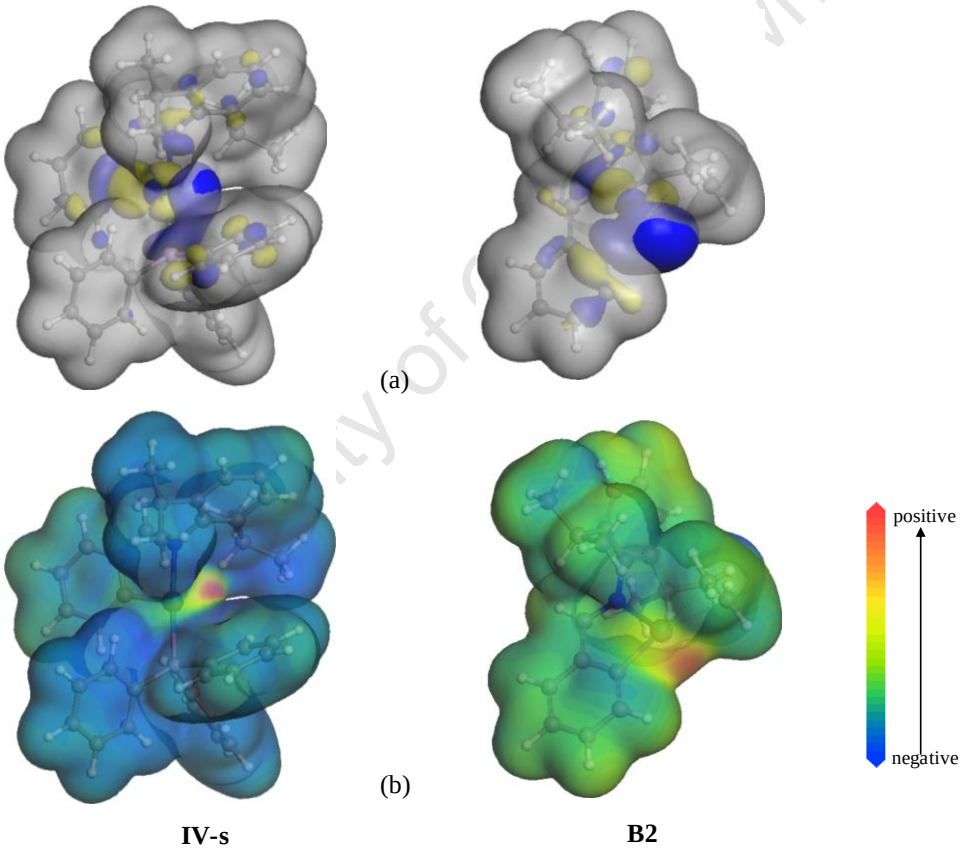

Figure 2.20 DFT-estimated electrophilic site on three-coordinate complexes **IV-s** and **B2**. This was deduced by plotting (a) total electron density over the LUMO density and (b) mapping the Fukui function, f(+), on the total electron density of the molecule.

In structure **IV-s**, the negatively charged N^C bidentate ligand and the PPh_3 ligand are both firmly bound to the Pd^+ ion, and the Pd-N, Pd-$C_{metallated}$ and Pd-P bond distances are 2.135, 2.039 and 2.326 Å, respectively. One of the phenyl groups in the PPh_3 ligand has a weak

agostic interaction between one hydrogen atom and the palladium ion (3.104 Å), forming a distorted square-planar geometry with N-Pd-$C_{metallated}$ and P-Pd-$C_{metallated}$ angles of 80.9^o and 102.1^o, respectively. This may stabilize the coordinatively unsaturated structure. **IV-s** is a formal 14-electron species and lacks two electrons to fulfil the 16-valence electron count of palladium. This species is therefore able to accept the coordination of electron-donating ligands, such as an ethylene molecule. Upon the addition of one ethylene molecule the binding modes of the N^C ligand and PPh_3 ligand clearly make the ligands in the coordination sphere less tightly bound to the Pd centre, i.e., the Pd-N, Pd-$C_{metallated}$ and Pd-P bond distances all increases by *ca*. 0.06 Å, and the N-Pd-P angle decreases from 183.1^o to 172.4^o (N-Pd-$C_{metallated}$ and P-Pd-$C_{metallated}$ angles of 79.6^o and 92.8^o, respectively). In addition, the weak Pd-H_{phenyl} agostic interaction no longer exists in **B1**. Consequently, there is more space for the coordination of the ethylene unit. The ethylene molecule (ethylene 1) is weakly coordinated to Pd via a π-bonding interaction and is perpendicular to the square plane, as can be seen from the Pd-C distances of 2.397 and 2.411 Å. The relatively weak nature of the π-bonding is reflected in the relatively short C-C bond distance of 1.360 Å, which is only 0.027 Å longer than the calculated C=C bond distance in free ethylene.

The dissociation of the PPh_3 group from **B1** leads to the three-coordinate complex **B2**, in which the Pd-C distances for the ethylene fragment are symmetrical with lengths of 2.433 Å. The N^C ligand is more tightly coordinated to Pd compared to **B1**, i.e. the Pd-N and Pd-$C_{metallated}$ bond distances are 2.118 and 2.018 Å, respectively. The 14-electron species accepts the coordination of the second ethylene molecule to form the bis-olefin complex, **B3**. Two ethylene molecules are coordinated in such a way that they are perpendicular with respect to each other. The new coordinated ethylene molecule (ethylene 2) has a strong interaction with the Pd, as can be seen from the Pd-C distances of 2.282 and 2.285 Å. The elongated C-C bond distance in ethylene 2 (1.375 Å vs. 1.333 Å non-coordinated) clearly indicates that there is a substantial amount of electron back-donation from the filled d orbital of Pd into the empty π* orbital of the ethylene.[10] In addition, the coordination of ethylene 2 makes the interaction between ethylene 1 and Pd relatively weaker, which is suggested by the slightly increased Pd-C bond distances for the ethylene 1 fragment (2.487 and 2.496 Å) and slightly decreased C-C bond distance (1.355 Å) compared to **B2**. The carbon atom in ethylene 2 exhibiting the longer Pd-C bond distance is designated for coupling with the other ethylene fragment as suggested for the Cr system.[8]

The coordination of the first ethylene seems to take place readily with a very small barrier of 0.8 kcal/mol relative to **IV-s**. The dissociation of the PPh_3 group makes the complex **B2** coordinatively unsaturated. Unlike **IV-s**, **B2** is energetically unstable due to the lack of a Pd-H agostic interaction and lies 30.4 kcal/mol above **IV-s**. The coordination of the second ethylene unit stabilizes the complex slightly. The energy barrier for ethylene coordination could be due to the relatively weak interaction between the ethylene moieties and the Pd atom compared to the other systems,[8,17(b)] as well as the coordination mode of two ethylene units. In the Ti system studied by de Bruin *et al.*,[10] two binding modes of the titanium bis-olefin were observed. The one with two ethylene molecules perpendicular to each other was found to have a higher energy.

In view of this, we attempted to optimize a bis-olefin structure similar to the reported Ti and Cr bis-olefin complexes, in which two ethylene molecules almost form a flat plane with the metal centre.[8,17(b)] We were, however, unable to optimize such a geometry; every attempt led to the formation of **B3**. This may be due to the position and shape of the LUMO orbitals in **IV-s** and **B2**, which prefer the coordination of the ethylene unit in a perpendicular position.

Formation of the five-membered metallacycle Pd(IV) species **B4** is obtained by oxidative coupling of the two ethylene fragments via the transition state **TS(B3-B4)**. In **TS(B3-B4)** the coupling C-C bond distance is decreased from 3.280 Å in **B3** to 1.766 Å, and the two new Pd-C σ-bond lengths are 2.119 and 2.102 Å. The geometry of **TS(B3-B4)** is still a distorted square-planar arrangement. Once the metallacycle reaction is complete to form **B4**, these latter distances relax to 2.103 and 2.100 Å, respectively; the C-C bond distance becomes 1.524 Å. The hemilabile character of the N^C ligand is shown by the elongation of the Pd-N distances from 2.167 Å→2.182 Å→2.212 Å in the sequence **B3**→**TS(B3-B4)**→**B4**, while the Pd-$C_{metallated}$ bond distance does not vary a lot. The DFT-optimized structure of **B4** displays two agostic interactions between Pd and H atoms, i.e., H_a in the five-membered ring and H_b in the isopropyl group, with Pd···H agostic interactions of 2.575 and 2.388 Å, respectively. The two Pd···H agostic interactions make the configuration into a pseudo-octahedral geometry [Figure 2.21(A)]. This is consistent with general Pd(IV) complexes which normally have an octahedral geometry surrounding the Pd centre [Figure 2.21(B)]. The species **B4** shows a *cis*-orientation between two $H_{agostic}$ atoms, and two metallacycles are perpendicular with respect to each other. Molecular structures of N^C metallacyclic Pd(IV) complexes have been reported and show the similar conformation of the two metallacycles.[65]

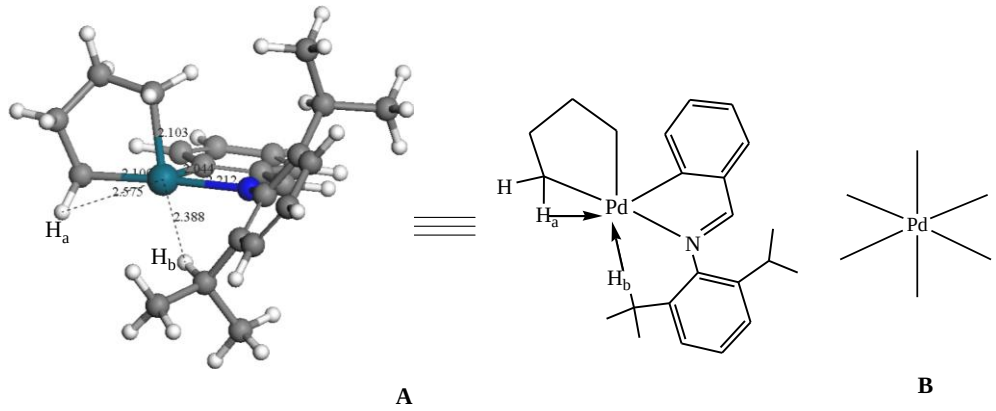

Figure 2.21 (A) DFT-optimized structure of the Pd(IV) metallacycle complex **B4**. (B) A general octahedral geometry of Pd(IV).

Commencing from the perpendicular arrangement of the two reactive ethylene moieties in **B3**, further reorientation is required along the favourable pathway for oxidative coupling. As a consequence, the oxidative coupling is seen to be highly unfavourable kinetically and accompanied by a free-energy barrier of 36.4 kcal/mol [**B3→TS(B3-B4)**]. The transformation of the active species **B3** into **B4** is endothermic by 8.4 kcal/mol. These energies indicate that the formation of the pallada(IV)cyclopentane **B4** is kinetically and thermodynamically unfavourable. It might be that **B4** is an unstable species due to its pseudo-octahedral geometry, in which the two Pd-$H_{agostic}$ bonds are not sufficient to stabilize the complex. In addition, Pd(IV) complexes are generally not very stable.

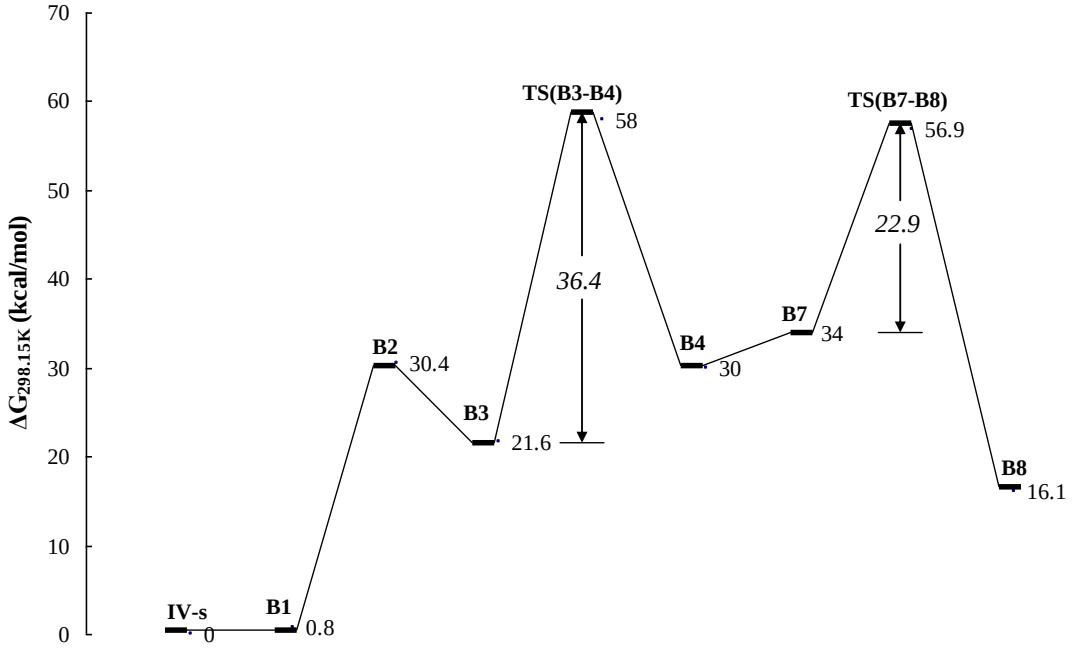

(A)

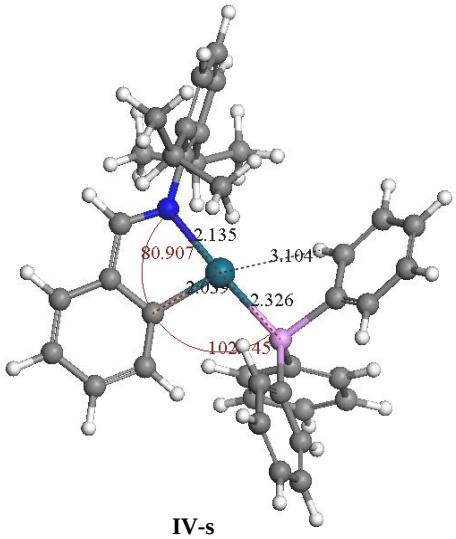

IV-s

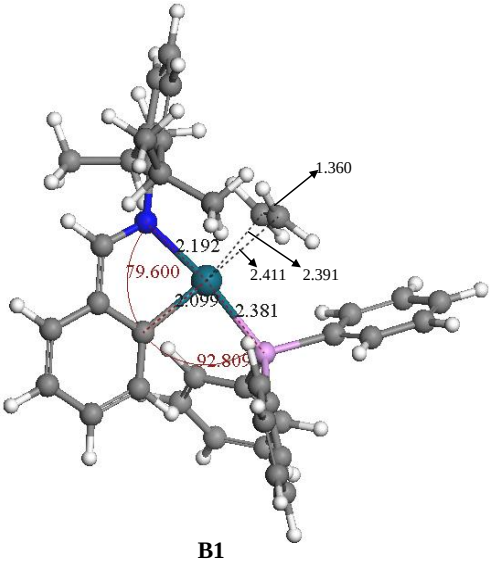

B1

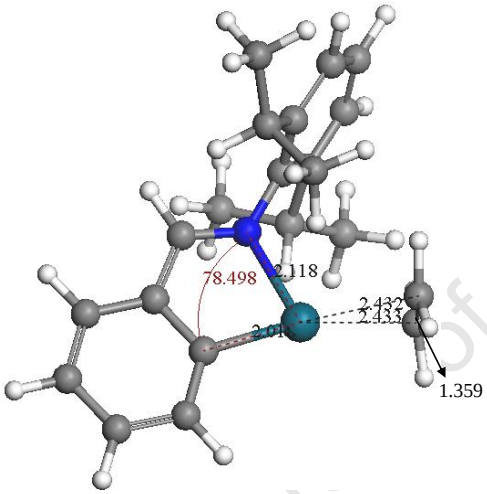

B2

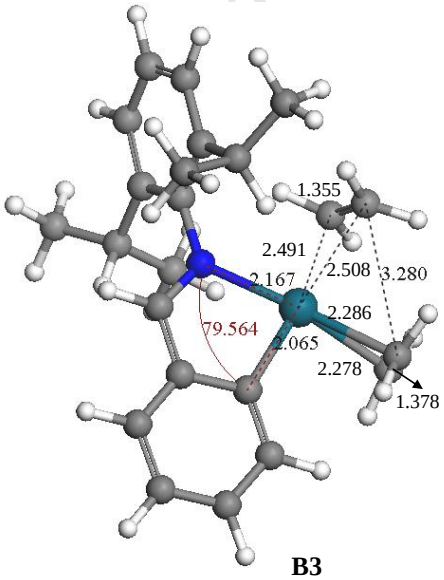

B3

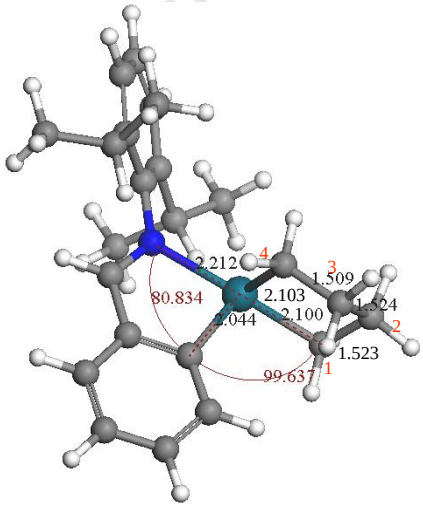

B4

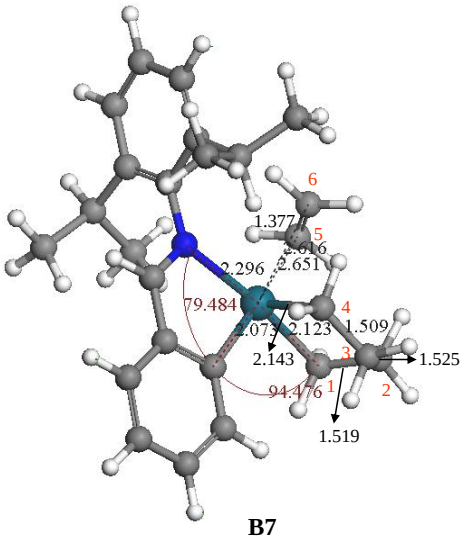

B7

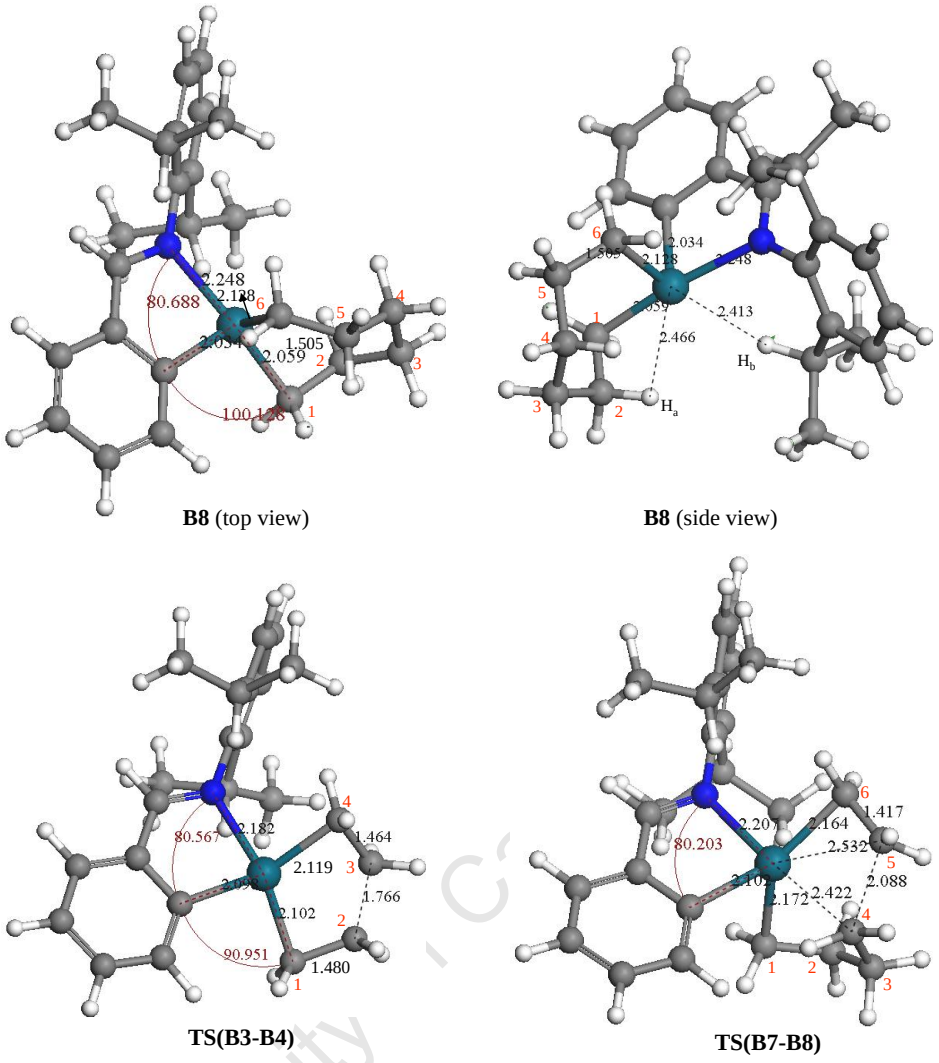

(B)

Figure 2.22 (A) Energy profile for the reaction cascade for generation of pallada(IV)cycle intermediates. Calculated Gibbs free energies ($\Delta G_{298.15K}$) at 298.15 K and 1 atm in kcal/mol are given relative to **IV-s** corrected in terms of respective number of ethylenes. (B) Optimized structures of key species involved.

Increase of the size of the pallada(IV)cycle

Starting from the pallada(IV)cyclopentane **B4**, the generation of larger metallacycle intermediates occurs via a repeated sequence of consecutive elementary steps of ethylene uptake and insertion into the Pd^{IV}-C bond of the last generated pallada(IV)cycle, with the Pd^{IV} formal oxidation state being preserved throughout the overall process. The free-energy profile of the reaction cascade for the metallacycle growth is shown in Figure 2.22, together with a pictorial representation of important key species.

The coordination of an additional (third) ethylene molecule could occur at two positions on **B4**, i.e. (a) side position of the square plane, or (b) top position of the plane, which is shown in Figure 2.23.

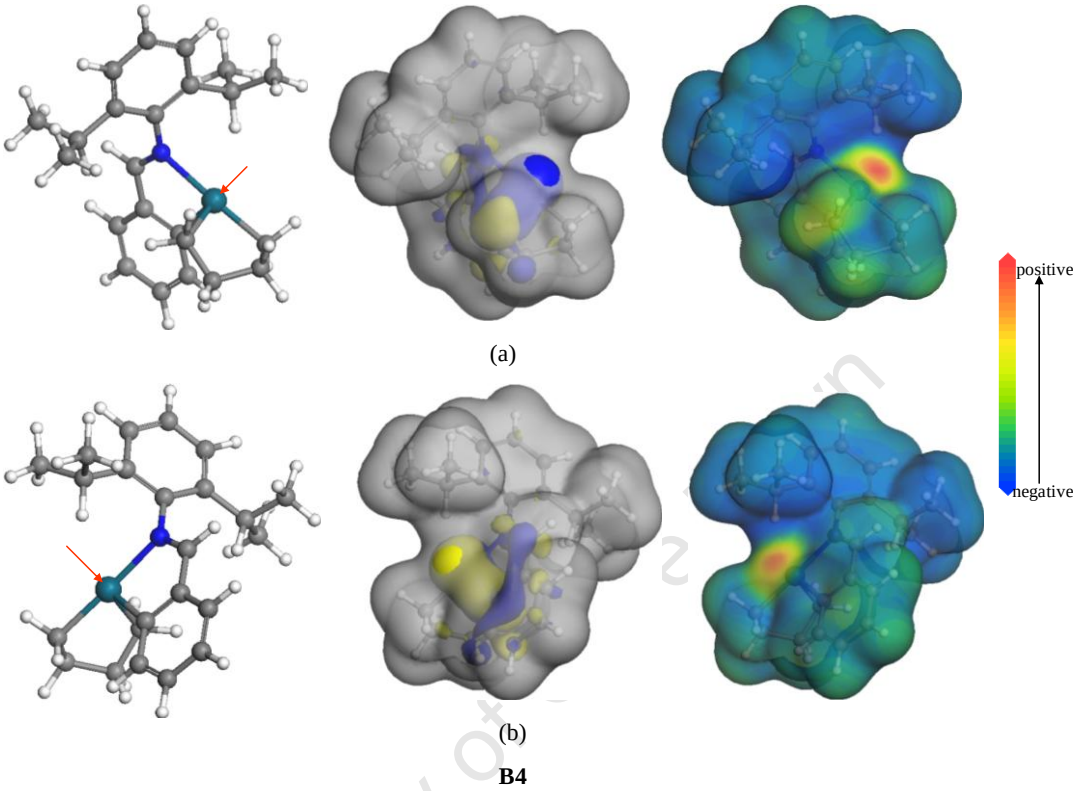

Figure 2.23 DFT-estimated electrophilic site on pallada(IV)cyclopentane **B4**. (a) Side position of the square plane and (b) top position of the plane.

As evident from Figure 2.22, ethylene uptake goes along with an elongation of the Pd···H agostic interactions (2.615 Å for Pd-H_a distance and 2.618 for Pd-H_b distance), to accommodate the incoming ethylene in the side position in **B7**. The ethylene preferably approaches perpendicular with respect to the square plane. Interaction of ethylene with the five-membered metallacycle **B4** affords **B7**, in which the ethylene fragment is weakly coordinated via a long-range π-interaction. This is evident from the elongated Pd-C distances (2.616 and 2.651 Å) between the Pd centre and the third ethylene in **B7**, as well as the relatively short C=C distance of 1.377 Å for the coordinated ethylene fragment. The elongation of the Pd-N and Pd-$C_{metallated}$ bonds is also observed compared to **B4**, which are 2.296 and 2.073 Å, respectively. Insertion of the coordinated ethylene fragment by the C atom with longer Pd-C distance (2.651 Å) into the Pd-C_4 bond, and not the Pd-C_1 bond, of pallada(IV)cycle **B7** is suggested based on the elongated nature of Pd-C_4 bond (2.143 Å)

compared to Pd-C_1 bond (2.123 Å). After crossing the transition state **TS(B7-B8)**, a seven-membered metallacycle, **B8** is formed. In **TS(B7-B8)** formation of the Pd-C_6 (2.164 Å) and C_4-C_5 (2.088 Å) bonds and the rupture of the Pd-C_4 (2.422 Å) and C_5-C_6 (1.417 Å) π-bond proceed in a concerted fashion. In **B8** the new C_4-C_5 bond is 1.505 Å, and the new σ-Pd-C_6 bond is 2.128 Å. Since **B8** is the "higher" homologue of **B4**, again, it has a pseudo-octahedral geometry with two Pd-$H_{agostic}$ bonds, in which the H_a atom changes from a α-position in **B4** to a β-position in **B8**, while H_b remains in place.

The general trends analyzed so far on the basis of the structural characteristics of the involved key species are reflected in the energy profile (cf. Figure 2.22). Ethylene uptake in **B4** is accompanied by an activation free energy of 4 kcal/mol relative to **B4**. The insertion reaction of the third ethylene has a relatively moderate activation energy of 22.9 kcal/mol [**B4→TS(B6-B7)**] compared to the similar insertion reaction (**B3→B4** of 36 kcal/mol), and the reaction itself is exothermic (-17.9 kcal/mol), as a result of the relatively strongly coordinated N-atom (2.248 Å, Pd-N bond distance) in the product obtained, **B7**.

Decomposition of pallada(IV)cycle intermediates under $Pd^{IV} \rightarrow Pd^{II}$ reduction affording α-olefin

According to the literature,[4] this reaction step can proceed in two different ways. For the pallada(IV)cyclopentane **B4**, the first (stepwise) pathway involves a β-hydrogen transfer to the Pd centre, while the oxidation state of Pd remains unchanged (**B5**), and 1-butene is coordinated to Pd at the 4-position involving a σ-bond; this reaction step is subsequently followed by a reductive elimination reaction to finally yield **B6** (Path i in Scheme 2.15). This reductive elimination has been proposed for Cr and Pt systems.[66] The second (concerted) pathway is the concerted reductive elimination from **B4** via an agostic hydrogen transfer to form the π-bonded Pd-butene complex (**B6**) (Path ii in Scheme 2.15). As the "higher" homologue of **B4**, the decomposition of pallada(IV)cycloheptane **B8** can take place via these two mechanisms as well.

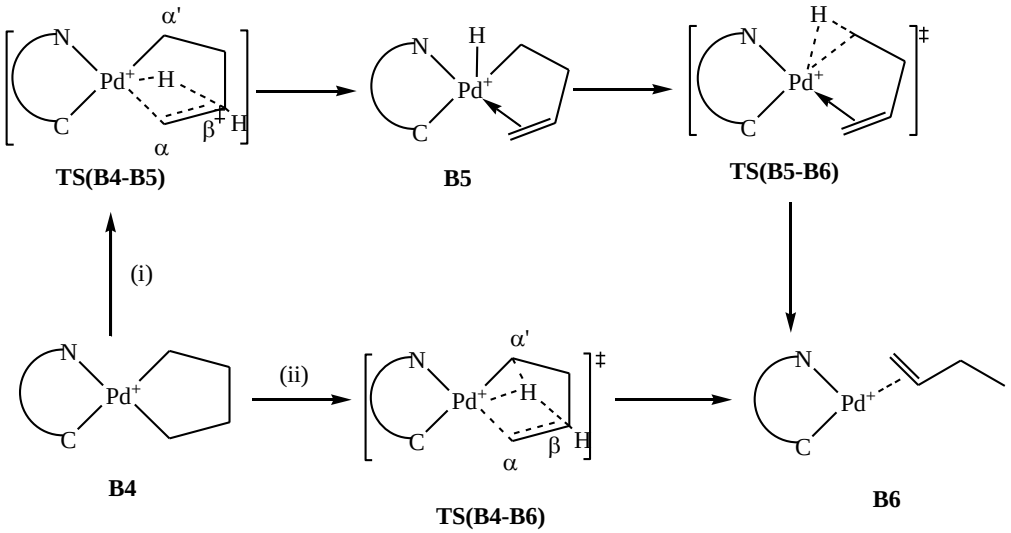

Scheme 2.15 Stepwise (Path i) and concerted (Path ii) reaction paths for the decomposition of pallada(IV)cycle intermediates affording α-olefins, exemplified for the five-membered cycle.

Our calculations show that, for a relatively small metallacycle such as **B4**, the decomposition step seems to occur exclusively via the stepwise pathway involving the Pd-H species, since **TS(B4-B6)** could not be located on the potential energy surface (PES). By contrast, this step for the relative large metallacycle **B8**, primarily takes place via the concerted pathway, i.e. a direct hydrogen transfer in the hydrocarbon cycle, assisted by the Pd metal centre [**TS(B8-B9)**]. No stationary point on the PES could be located for the analogue of **TS(B4-B5)**. This is also evident from unsuccessful efforts to optimize geometry similar to **B5** for the hydride intermediate; each attempt leads to the spontaneous formation of **B9**. This behaviour has also been observed by Yu *et al*. for a Ta system[12] and de Bruin *et al*. for a Ti system,[10] in which a stepwise decomposition mechanism was calculated for the five-membered ring, while a concerted mechanism was operative for the seven-membered ring. The key species for this step together with the reaction and activation free energies are presented in Figure 2.24.

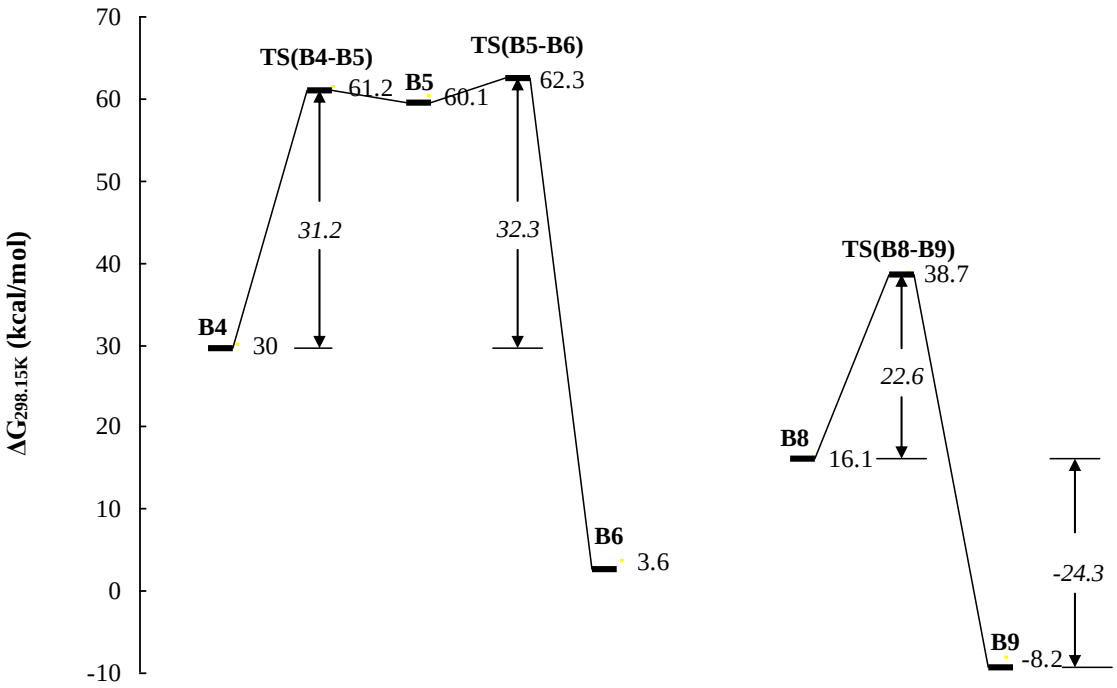

(A)

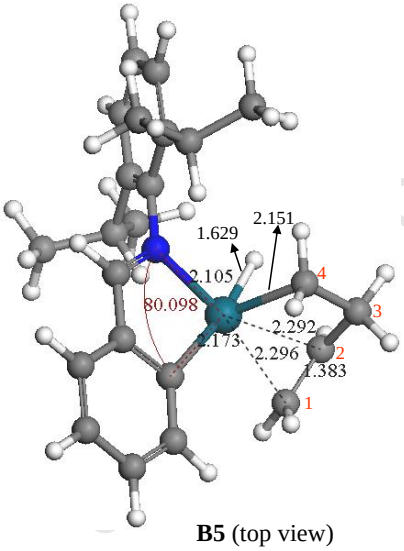

B5 (top view)

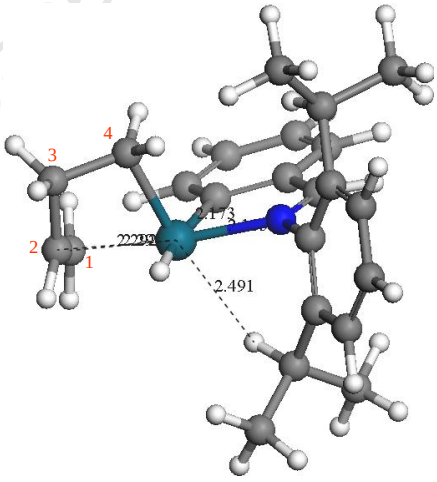

B5 (side view)

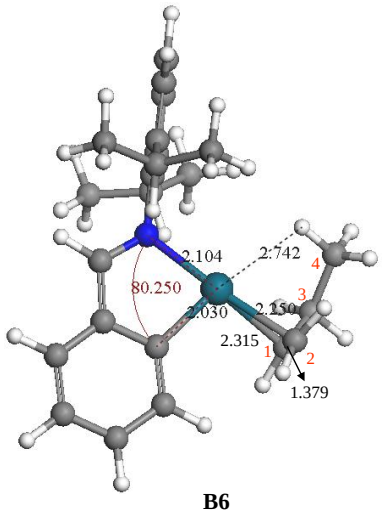

B6

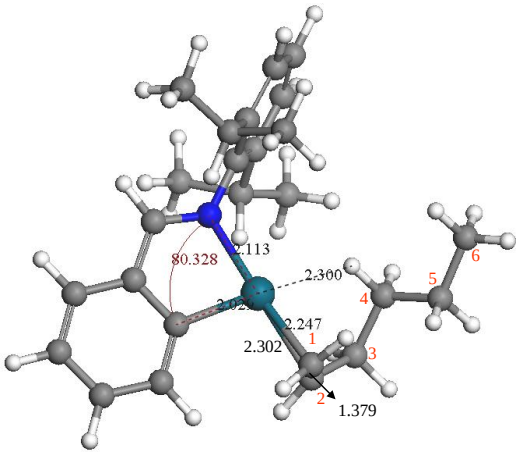

B9

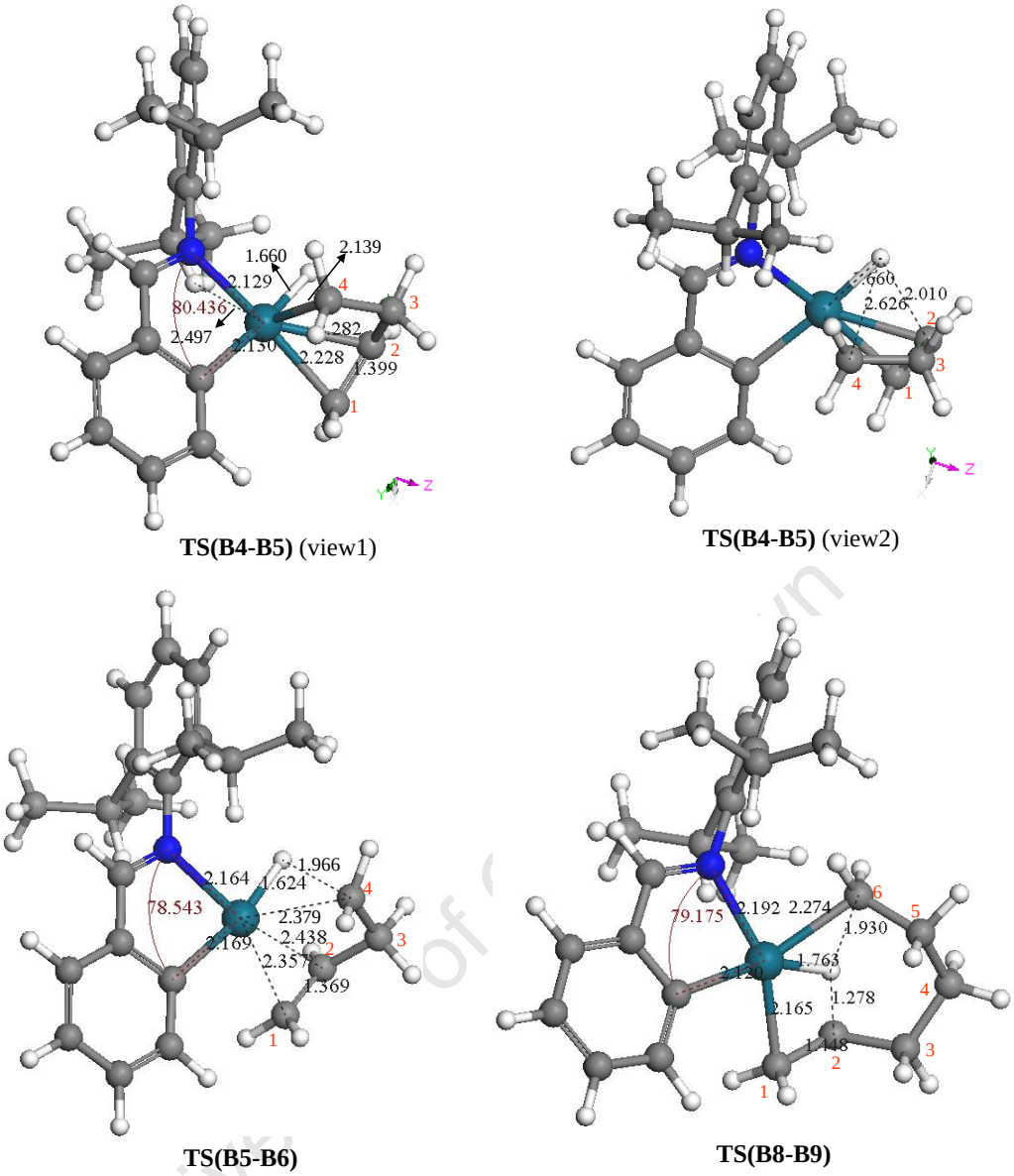

(B)

Figure 2.24 (A) Energy profile for the generation of a-olefins through decomposition of Pallada(IV)cycle intermediates. Calculated Gibbs free energies ($\Delta G_{298.15K}$) at 298.15 K and 1atm in kcal/mol are given relative to **IV-s** corrected in terms of respective number of ethylenes. (B) Optimized structures of involved key species.

Starting with the stepwise pathway for pallada(IV)cyclopentane **B4**, the transition state for β-hydrogen abstraction, **TS(B4-B5)**, exhibits a hydrido-palladium bond that seems to be almost fully established already, together with an emerging olefinic subunit that is moving out of the coordination sphere of Pd^{IV}. In this case, the hydrogen undergoing the transfer lies "above" the plane formed by Pd and two carbon atoms, making a kind of tetrahedral configuration (Figure 2.24). The Pd-H bond distance in **TS(B4-B5)** is 1.660 Å, while the C-H bond

distances are relatively longer, 2.010 and 2.626 Å, respectively. Similar features were also observed in an analogous Ti complex.[10] **TS(B4-B5)** is a later transition state, appearing with product-like geometry. It decays into a stable Pd^{IV}-alkenyl-hydride intermediate **B5**. In **B5** the alkenyl moiety is η1-coordinated to Pd^{IV} by its alkyl terminus (2.319 Å), and the C=C bond has a strong π-interaction with Pd^{IV}, as can be seen from the Pd-C bond distances of 2.296 and 2.292 Å, as well as the relatively long C=C bond distance of 1.399 Å. For the subsequent reductive elimination, **B5** then proceeds to the Pd-π-olefin complex, **B6**, via the transition state **TS(B5-B6)**. This transition state is reached at a distance of 1.966 Å of the emerging CH bond with a relative weak π-interaction between C=C bond and Pd^{IV}.

The predicted free-energy for the decomposition of pallada(IV)cyclopentane **B4** exhibits a double-valley curve, where almost identical activation barriers have to be overcome for the β-hydrogen abstraction [31.2 kcal/mol for **TS(B4-B5)** – **B4**] and for reductive CH elimination [32.3 kcal/mol for **TS(B5-B6)** – **B4**]. The intervening Pd^{IV}-alkenyl-hydride species, **B5**, is separated by free energy barriers of only 1.1 and 2.2 kcal/mol from the adduct and product sides. The overall stepwise process, **B4→B5→B6**, is calculated to be highly exothermic (-26.4 kcal/mol), again, due to the instability of the Pd^{IV} intermediates.

In the case of pallada(IV)cycloheptane, **B8**, 1-hexene is formed by the decomposition occurring through a concerted β-hydrogen transfer ($C^{\beta}\rightarrow C^{\alpha'}$ hydrogen transfer), without a stable hydride intermediate involved. As revealed for **TS(B8-B9)**, the hydrogen, the palladium, and the two carbon atoms that are involved in the hydrogen transfer (C_2 and C_6) all lie practically in the same plane (Figure 2.24). Such geometry is not possible in **TS(B4-B5)**, due to the small ring size of the metallacycle. Moreover, the C-H bond distances are significantly shorter than in **TS(B4-B5)**, i.e., 1.278 Å for the C_2-H bond and 1.930 for the C_6-H bond. It is noteworthy to mention that the distance from the transferring hydrogen atom to C_6 is significantly longer than that to C_2, i.e. 1.930 Å and 1.278 Å, respectively, unlike the quasi-equal distances in Ti and Cr systems.[8,10,11] Since the coordination geometry of Pd^{IV} is octahedral, the Pd-C_6 bond is trying to sit on the square plane to maintain the pseudo-octahedral geometry; as a result, C_6-H bond has to be elongated. On the other hand, the Pd-H distance in **TS(B4-B5)** is slightly smaller than in **TS(B8-B9)**: 1.660 and 1.760 Å, respectively. The synchronous β-hydrogen is completed after crossing **TS(B8-B9)** with the formation of the Pd^{II}-1-hexene product complex, where the 1-hexene is η2-coordinated with

its double bond to Pd^{II}. This elementary step is accompanied by a decrease in the coordination sphere around the palladium presenting a square-planar arrangement with a Pd-$H_{agostic}$ distance (2.300 Å), as well as a reduction of the formal oxidation state of palladium by two ($Pd^{IV} \rightarrow Pd^{II}$).

In the decomposition step of the palladacycloheptane **B8**, the energy barrier for the transformation of **B8→B9** is 22.6 kcal/mol, which is significant, and higher than those for similar transformations in the Cr and Ti systems by 14.5 and 10.2 kcal/mol, respectively.[8,11] On the other hand, the reaction step **B8→B9** is significantly exothermic by -24.3 kcal/mol, similar to the stepwise process, **B4→B5→B6**.

2.4.3 Discussions on the theoretical studies of a possible mechanism

2.4.3.1 The entire catalytic reaction course: comparison between Cossee-type and metallacyclic mechanisms

On the basis of careful theoretical exploration of crucial elementary steps of the two mechanisms, we are now able to present the free-energy profiles of the two catalytic cycles. Figure 2.25 depicts the most feasible pathways for each of the crucial elementary steps for the linear dimerization and trimerization of ethylene via both Cossee-type and metallacyclic mechanisms.

In the Cossee-type mechanism, the step for rotation of the olefin fragment in palladium complex, **A2→A2a**, and formation of β-agostic alkyl complex from its γ-agostic precursor, **A3γ→A3β**, was not presented in the entire energy profile, since their role in the mechanism is not important. In addition, the dissociative olefin displacement was used as the chain transfer process to generate a Pd-H species.

In the metallacycle mechanism, the starting structure **IV-s** is generated from the formal methyl-abstraction by MAO. In the Pd/MAO interaction studies, **IV-s** was found to be higher in energy than **III-s**, ranging between 3.6 and 16.2 kcal/mol (ΔE_{0K}) (cf. Section 2.3.2). There are spurious imaginary vibrational modes due to methyl rotations that could not successfully be eliminated; therefore, full frequency analysis was not applied to the Pd-MAO complexes. In an attempt to put the neutral MAO-dissociated (**III-s**) and the formal methyl-abstracted

(**IV-s**) species on the same diagram, we assumed an average energy of 10 kcal/mol in Gibbs free energy ($\Delta G_{298.15K}$), which should represent a viable difference between **III-s** and **IV-s**. We can therefore plot the entire profile of the metallacyclic pathway together with the Cossee pathway. The Gibbs free energies ($\Delta G_{298.15K}$) of the key intermediates and transition states in the metallacycle pathway are related by (**IV-s** + 10 kcal/mol).

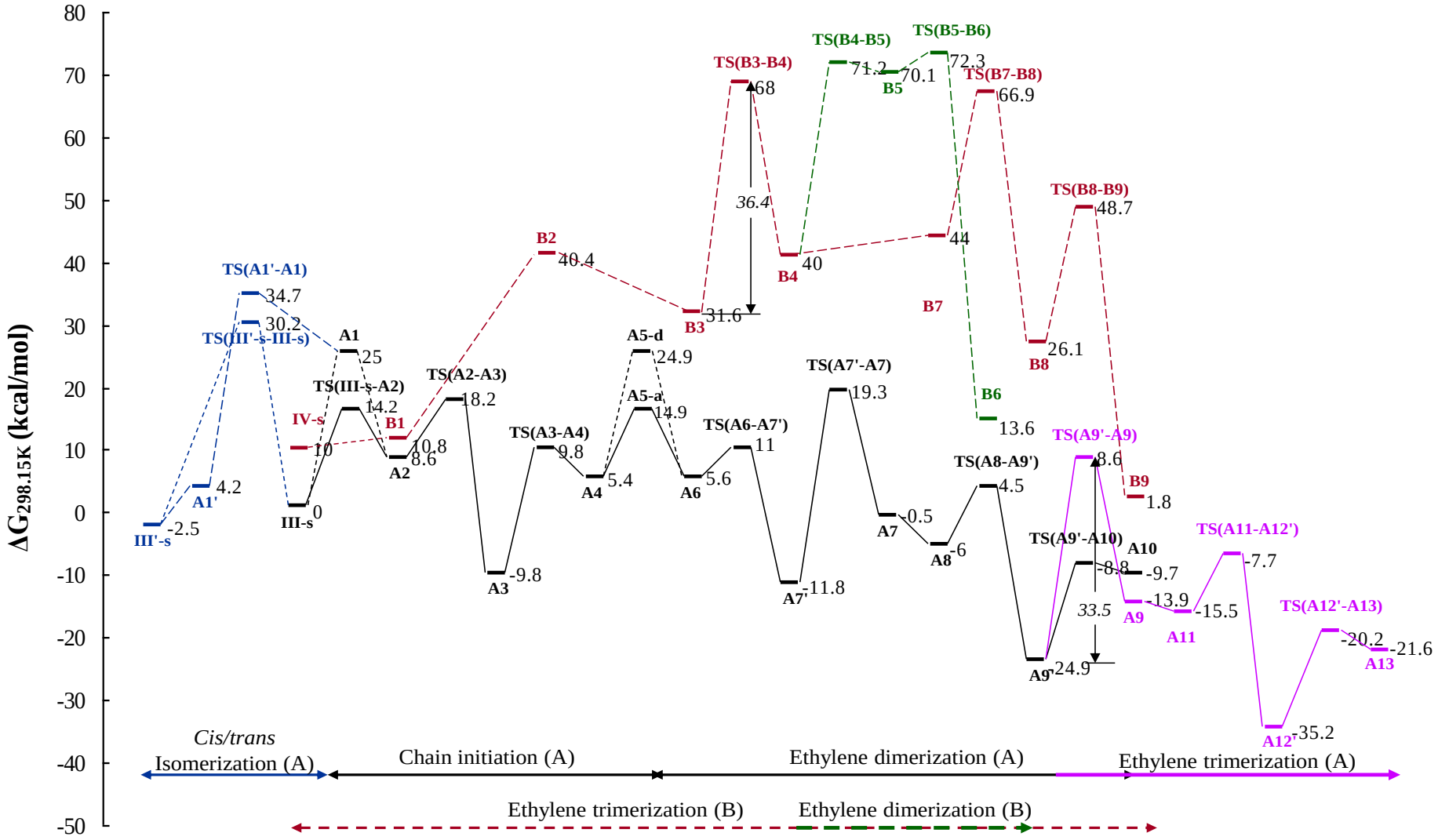

Figure 2.25 The energy profiles for the entire catalytic course via the Cossee-type mechanism (A) (black and purple solid lines) and the metallacycle mechanism (B) (red and green dotted lines). The most likely pathway is plotted as solid line. Calculated Gibbs free energies ($\Delta G_{298.15K}$) at 298.15 K and 1 atm in kcal/mol relative to **III-s** are given.

Kinetic effects

As can been seen in Figure 2.25, the overall barrier for the metallacycle mechanism, from **III-s** to **TS(B5-B6),** is 72.3 kcal/mol, while that for the Cossee-type mechanism, from **III-s** to **TS(A7'-A7)**, is more than three times lower, i.e. 19.3 kcal/mol. Therefore, the metallacycle mechanism is kinetically disfavoured due to the higher overall barrier. This kinetic effect is, however, not mainly caused by differences in individual elementary step barriers between the two mechanisms due to the fact that barriers for elementary reaction steps between the two mechanisms are similar. For example, from the Pd(II)-bis-olefin complex **B3**, the oxidative coupling reaction requires 36.4 kcal/mol to produce the pallada(IV)cyclopentane **B4**, which reflects the largest single barrier for the metallacycle mechanism (**B3**→**B4**). On the other hand, the largest single barrier for the Cossee-type mechanism is 33.5 kcal/mol, for the isomerization of *cis*-alkyl species **A9'** to its *trans* form **A9** (**A9'**→**A9**).

This indicates that the Cossee-type mechanism being kinetically favoured over the metallacycle mechanism is not caused by significant differences in individual elementary step barriers or a single rate determining step in either of the two mechanisms. Ultimately we conclude that it is differences in thermodynamics that causes the differences in overall barriers of the two mechanisms. This is best seen by the following thermodynamic comparison.

Thermodynamic effects

As shown in Table 2.2, the thermodynamic energy difference between the two catalyst precursors, **III-s** and **IV-s**, is 10 kcal/mol. By taking up the first ethylene unit to form **A6** and **B2**, respectively, the thermodynamic difference increases dramatically to 34.8 kcal/mol. This difference further increases after the second and third ethylene uptake, where a 37.6 kcal/mol energy difference is noted between **A8** and **B3**, which becomes much more significant between **A11** and **B7**, i.e. 59.5 kcal/mol. Therefore, the thermodynamic energy difference between the two mechanisms increases with each uptake of ethylene:

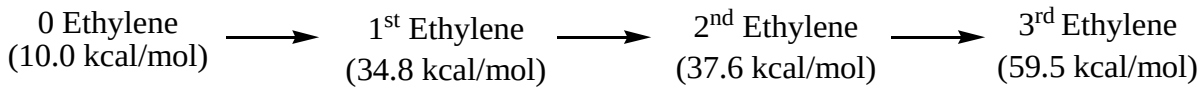

Table 2.2 Comparative data for thermodynamic energy differences between the Cossee-type and metallacycle mechanisms

	Catalytic step	Cossee-type		Metallacycle		Thermodynamic energy difference (kcal/mol)
		Species	$\Delta G_{298.15K}$* (kcal/mol)	Species	$\Delta G_{298.15K}$* (kcal/mol)	
A	Catalyst precursors	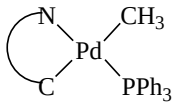 **III-s**	0.0	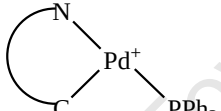 **IV-s**	10.0	10.0
B	1st Ethylene uptake	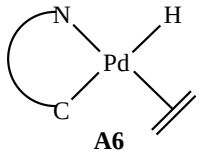 **A6**	5.6	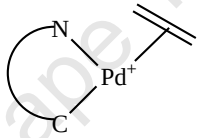 **B2**	40.4	34.8
C	2nd Ethylene uptake	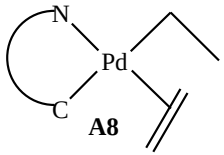 **A8**	-6.0	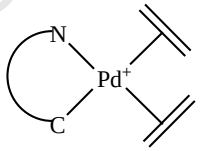 **B3**	31.6	37.6
D	3rd Ethylene uptake	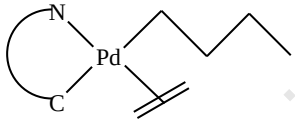 **A11**	-15.5	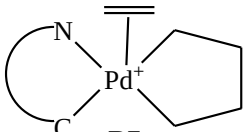 **B7**	44.0	59.5

* Calculated Gibbs free energies ($\Delta G_{298.15K}$) at 298.15 K and 1 atm in kcal/mol are given relative to **III-s** corrected in terms of respective number of ethylenes.

It can therefore be concluded that the Cossee-type mechanism is thermodynamically favoured with each uptake of ethylene, and the overall kinetic favouring of the Cossee-type mechanism is dictated by the thermodynamic differences of individual elementary steps.

In our cyclometallated palladium catalyst system, the possibility of ethylene oligomerization reaction through a metallacyclic pathway can therefore be excluded. This is in good agreement with literature reported experimental and DFT results in favour of the Cossee-type mechanism for palladium-catalysed olefin oligomerization or polymerization.[67]

2.4.3.2 Discussion on Cossee-type mechanism

The Cossee-type mechanism in the current study includes a chain-initiation process, which we studied starting from the model complex **III-s**, and the chain-growth and chain-transfer mechanisms for ethylene dimerization and trimerization.

As is evident from the alkylation reaction of the Pt analogue, the Pt-CH_3 complex in which the methyl group is *cis* to the metallated carbon atom was predominantly produced (Eq. 2.1 in Section 2.4.1). The formation of the Pd analogue **III'-s**, therefore, is considered likely to be formed from the alkylation reaction by MAO. If both Pd-CH_3 complexes **III'-s** and **III-s** could be generated, two Pd-H active species would consequently be generated. The Fukui function [f(+)] of the three-coordinate complexes **A1** and **A1'**, corresponding to reactivity with respect to nucleophilic attack, shows there is only one structure, viz. **A1**, which has an electrophilic site on Pd which will allow an ethylene molecule to attack at the Pd centre. This is similar for the rest of the three-coordinate Pd-H and Pd-alkyl complexes. We believe that this is one of the most characteristic features of a benzylidenebenzylamine ligand which differentiates it from other anionic bidentate ligands. For example, the electrophilic site of both three-coordinate palladium analogues with the N^O ligand is largely located on the Pd atom (Figure 2.26).

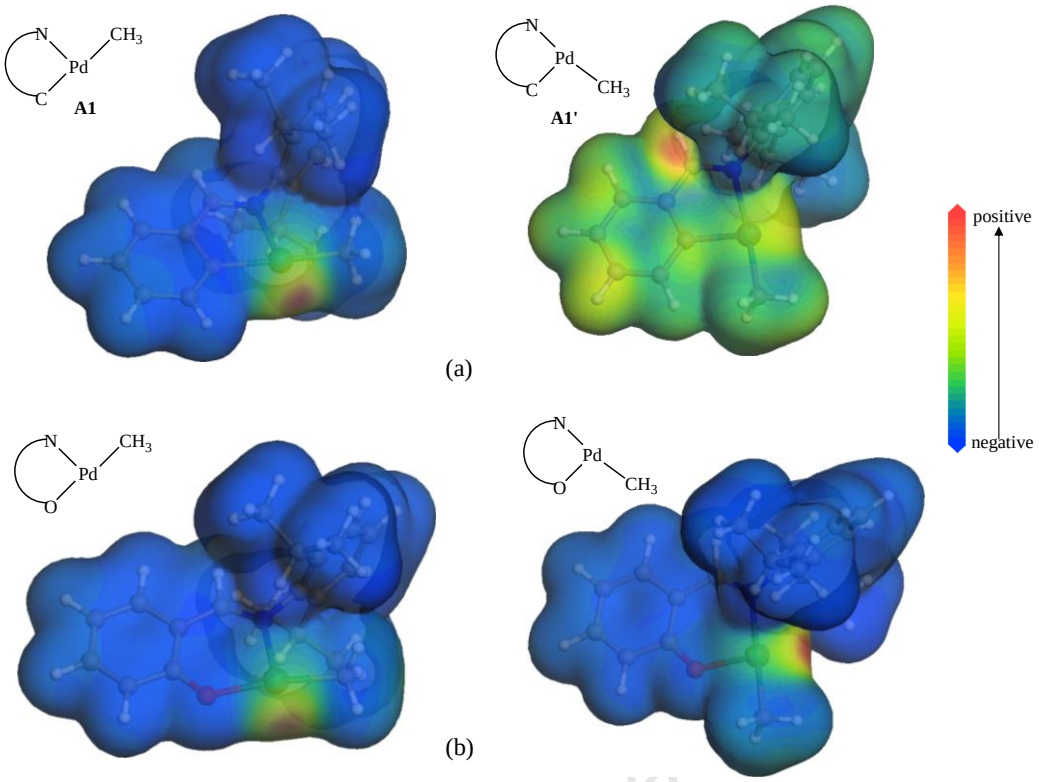

Figure 2.26 DFT-estimated electrophilic site on three-coordinate Pd-methyl complexes: (a) with N^C ligand, (b) with N^O ligand.

However, such a characteristic feature makes the mechanism a bit more complicated. To start chain initiation from **III'-s**, a *cis/trans* isomerization process needs to occur either from **III'-s** to **III-s** or from the three-coordinate **A1'** to **A1** if **A1' exists**. Both routes have to overcome a barrier of *ca*. 30 kcal/mol to cross the transition states and might be impossible to proceed. Therefore, the Pd-H generation step is suggested to take place from **III-s**. The activity of the catalyst could be dependent on the extent of the formation of **III-s** from the alkylation step by MAO. If **III-s** is formed as major product, the activity should be high, and vice versa.

Consequently, the most interesting feature in the chain propagation is the isomerization of the *cis*-Pd-alkyl complexes to their *trans* forms, i.e., **A7'→A7** and **A9'→A9**, which allows the nucleophilic attack by ethylene to occur on the Pd centre. The energy barrier for each isomerization step is consistently *ca*. 32 kcal/mol, which is kinetically unfavourable. Energy in the form of heat would be necessary in the actual catalytic process to facilitate the isomerization process to initiate the overall reaction. For all pairs of *cis/trans* isomers in the intermediates (**III'-s**/**III-s**, **A1'**/**A1**, **A7'**/**A7** and **A9'**/**A9**), the alkyl group or hydrogen atom located *trans* to nitrogen is the favoured isomer. This preference can be attributed to the

strong *transphobia* of the two C-donor groups which prefer not being *trans* to each other in palladium complexes.[49]

Both the associative and dissocative mechanisms were studied for the ethylene-substitution reaction in the chain growth initation process, and for the ethylene-displacement reaction in the chain-transfer process. In each case, the associative mechanism was calculated to be energetically lower than the dissociative route by *ca.* 10 kcal/mol, and was more likely to occur in the catalytic cycle.

For β-hydride elimination from the β-agostic *cis*-butyl complex **A9'** to form Pd(H)(olefin) **A10**, an energy barrier of -8.8 kcal/mol for the transition state **TS(A9'-A10)** should be overcome, resulting in formation of 1-butene. In contrast, much higher barriers should be overcome in order to reach the β-agostic *trans*-butyl complex **A9** via **TS(A9'-A9)** (8.6 kcal/mol), and from **A9** a third ethylene molecule could be taken for a trimerization process. The difference between the two transition states is 17.4 kcal/mol, suggesting that a statistical distribution of α-olefins and/or polymers is not likely. Instead, dimers should be formed preferentially along with a minor proportion of trimers and oligomers.

2.5 Conclusions

In this study we have presented a detailed theoretical investigation into the interactions of MAO models with a cyclometallated palladium precatalyst and into the crucial elementary steps of the linear dimerization and trimerization of ethylene to 1-butene and 1-hexene, respectively, by the Cossee-type and metallacycle mechanisms.

The Pd/MAO interactions showed that the energy difference between a neutral MAO-dissociation process and a formal methyl-abstraction process is relatively small, i.e. 3.6 kcal/mol using a $(AlOMe)_6$-TMA cage, or 7.6 and 16.2 kcal/mol using $(AlOMe)_9$-TMA cages. This suggested that the Cossee-type mechanism takes place in the main, but that metallacycle mechanisms could also be feasible when additional energy was employed.

On the basis of DFT calculations on the crucial elementary steps of the two mechanisms, it was found that the metallacycle mechanism is disfavoured kinetically due to the higher

overall barrier. As barriers for elementary reaction steps between the two mechanisms were found to be similar, the kinetic favouring of the Cossee-type mechanism over the metallacycle one is not caused by barrier differences of individual elementary steps or a single rate determining step in either of the two mechanisms. On the contrary, the overall kinetic favouring of the Cossee-type mechanism is dictated by thermodynamic differences for comparable elementary steps in the two mechanisms, i.e., the Cossee-type mechanism is thermodynamically favoured with each uptake of ethylene.

For the current Cossee-type mechanism, the isomerization of β-agostic *cis*-alkyl complexes to their *trans* form for the uptake of an ethylene molecule was found to be an unusual feature. The activity of the catalysis reaction is possibly dependent on the extent of the formation of the *cis*-methyl complex **III-s**. The selectivity of the olefin formation depends on the barriers for chain propagation and β-hydride elimination from β-agostic *cis*-alkyl complexes. These barriers from **A9'** were found not to be similar, with an energy difference of 17.4 kcal/mol. Thus, without extra introduced energy, β-hydride elimination dominates over the olefin propagation, leading to the production of butenes as major product. Therefore, one could expect low activity and production of mainly butenes with this catalytic system, in agreement with observations of actual catalytic reactions.[36]

The variation of the substituents on the cyclometallated phenyl ring could play a vital role in the catalytic reactions by tuning the electronic and steric environments of the Pd centre. This may lead to similar orbital features to the Pd(N^O) complexes as shown in Figure 2.26, i.e., both *cis* and *trans* isomers could be reactive with the ethylene molecule, which could overcome any difficulties in *cis/trans* isomerization and make the catalyst more active. This could be the subject for further investigations.

2.6 References

1. (a) E.Y.-X. Chen and T. J. Marks, *Chem. Rev*., 2000, **100**, 1391; (b) G. W. Coates, *J. Chem. Soc., Dalton Trans*., 2002, **4**, 467; (c) K. Angermund, G. Fink, V. R. Jensen and R. Kleinschmidt, *Chem. Rev*., 2000, **100**, 1457; (d) G. W. Coates, *Chem. Rev*., 2000, **100**, 1223.
2. (a) P. J. Flory, *J. Am. Chem. Soc*., 1940, **62**, 1561; (b) G. V. Z. Schulz, *Phys. Chem. B*, 1939, **43**, 25.
3. (a) P. J. Cossee, *J. Catal*., 1964, **3**, 80; (b) E. J. Arlman and P. J. Cossee, *J. Catal*., 1964, **3**, 99.
4. F. Zheng, A. Sivaramakrishna and J.R. Moss, *Coord. Chem. Rev.*, 2007, **251**, 2056.
5. (a) J. T. Dixon, M. J.Green, F. M. Hess and D. H. Morgan, *J. Organomet. Chem*., 2004, **689**, 3641; (b) A. Bollmann, K. Blann, J. T. Dixon, F. M. Hess, E. Killian, H. Maumela, D. S. McGuinness, D. H. Morgan, A. Neveling, S. Otto, M. J.Overett, A. M. Z. Slawin, P. Wasserscheid and S. Kuhlmann, *J. Am. Chem. Soc*., 2004, **126**, 14712; (c) M. J. Overett, K. Blann, A. Bollmann, J. T. Dixon, F. M. Hess, E. Killian, H. Maumela, D. H. Morgan, A. Neveling and S. Otto, *Chem. Commun*., 2005, 622.
6. D. S. McGuinness, *Chem. Rev*., 2011, **111**, 2321 and references therein.
7. (a) S. Tobisch and T. Ziegler, *Organometallics*, 2004, **23**, 4077; (b) S. Tobisch and T. Ziegler, *Organometallics* 2005, **24**, 256.
8. W. Janse van Rensburg, C. Grové, J. P. Steynberg, K. B. Stark, J. J. Huyser and P. J. Steynberg, *Organometallics*, 2004, **23**, 1207.
9. A. N. J. Blok, P. H. M. Budzelaar and A. W. Gal, *Organometallics*, 2003, **22**, 2564.
10. T. J. M. de Bruin, L. Magna, P. Raybaud and H. Toulhoat, *Organometallics*, 2003, **22**, 3404.
11. S. Tobisch and T. Ziegler, *Organometallics*, 2003, **22**, 5392; (e) S. Tobisch and T. Ziegler, *J. Am. Chem. Soc*., 2004, **126**, 9059.
12. Z.-X. Yu and K. N. Houk, *Angew. Chem., Int. Ed*., 2003, **42**, 808.
13. A. K. Tomov, J. J. Chirinos, D. J. Jones, R. J. Long and V. C. Gibson, *J. Am. Chem. Soc.*, 2005, **127**, 10166.
14. D. S. McGuinness, J. A. Suttil, M. G. Gardiner and N. W. Davies, *Organometallics*, 2008, **27**, 4238.
15. (a) P. Zielinski and I. G. Dalla Lana, *J. Catal*., 1992, **137**, 368; (b) V. J. Ruddick and J. P. S. Badyal, *J. Phys. Chem. B* ,1998, **102**, 2991; (c) Ø. Espelid and K. J. Børve, *J. Catal*.,

2002, **206**, 331.

16. S. Bhaduri and D. Mukesh, *Homogeneous Catalysis: Mechanisms and Industrial Applications*. Wiley-Interscience: New York, 2000, pp. 138-147.
17. (a) P. J. W. Deckers, B. Hessen and J. H. Teuben, *Organometallics*, 2002, **21**, 5122. (b) P. J. W. Deckers, B. Hessen and J. H. Teuben, *Angew. Chem., Int. Ed.*, 2001, **40**, 2516.
18. (a) C. Andes, S. B. Harkins, S. Murtuza, K. Oyler and A. Sen, *J. Am. Chem. Soc*., 2001, **123**, 7423; (b) A. Carter, S. A. Cohen, N. A. Cooley, A. Murphy, J. Scutt and D. F. Wass, *Chem. Commun*., 2002, 858; (c) D. S. McGuinness, P. Wasserscheid, W. Keim, C. Hu, U. Englert, J. T. Dixon and C. Grove, *Chem. Commun*., 2003, 334; (d) D. S. McGuinness, P. Wasserscheid, W. Keim, D. H. Morgan, J. T. Dixon, A. Bollmann, H. Maumela, F. Hess and U. Englert, *J. Am. Chem. Soc*., 2003, **125**, 5272; (e) D. H. Morgan, S. L. Schwikkard, J. T. Dixon, J. J. Nair and R. Hunter, *Adv. Synth. Catal*., 2003, **345**, 1; (f) R. D.Köhn, D. Smith, M. F. Mahon, M. Prinz, S. Mihan and G. Kociok-Köhn, *J. Organomet. Chem*., 2003, **683**, 200; (g) T. Wu, Y. Qian and J. Huang, *J. Mol. Catal. A*, 2004, **214**, 227; (h) M. E. Bluhm, O. Walter and M. Döring, *J. Organomet. Chem.*, 2005,**690**, 713; (i) D. de Wet-Roos and J. T. Dixon, *Macromolecules*, 2004, **37**, 93414; (j) K. Blann, A. Bollmann, J. T. Dixon, F. Hess, E. Killian, H. Maumela, D. H. Morgan, A. Neveling, S. Otto and M. Overett, *Chem. Commun*., 2005, 620.
19. (a) M. J. Overett, K. Blann, A. Bollmann, J. T. Dixon, D. Haasbroek, E. Killian, H. Maumela, D. S. McGuinness and D. H. Morgan, *J. Am. Chem. Soc*., 2005, **127**, 10723; (b) R. Walsh, D. H. Morgan, A. Bollmann and J. T. Dixon, *App. Catal. A*, 2006, **306**, 184; (c) S. Kuhlmann, J. T. Dixon, M. Haumann, D. H. Morgan, J. Ofili, O. Spuhl, N. Taccardi and P. Wasserscheid, *Adv. Synth. Catal*., 2006, **348**, 1200; (d) P. R. Elowe, C. McCann, P. G. Pringle, S. K. Spitzmesser and J. E. Bercaw, *Organometallics*, 2006, **25**, 5255; (e) A. Jabri, P. Crewdson, S. Gambarotta, I. Korobkov and R. Duchateau, *Organometallics*, 2006, **25**, 715; (f) D. S. McGuinness, M. Overett, R. P. Tooze, K. Blann, J. T. Dixon and A. M. Z. Slawin, *Organometallics*, 2007, **26**, 1108; (g) A. J. Rucklidge, D. S. McGuinness, R. P. Tooze, A. M. Z. Slawin, J. D. A. Pelletier, M. J. Hanton and P. B. Webb, *Organometallics*, 2007, **26**, 2782; (h) D. S. McGuinness, A. J. Rucklidge, R. P. Tooze and A. M. Z. Slawin, *Organometallics*, 2007, **26**, 2561; (i) S. Kuhlmann, K. Blann, A. Bollmann, J. T. Dixon, E. Killian, M. C. Maumela, H. Maumela, D. H. Morgan, M. Prétorius, N. Taccardi and P. J. Wasserscheid, *Catal.*, 2007, **245**, 279.
20. (a) T. Agapie, S. L. Schofer, J. A. Labinger and J. E. Bercaw, *J. Am. Chem. Soc*., 2004, **126**, 1304; (b) T. Agapie, J. A. Labinger and J. E. Bercaw, *J. Am. Chem. Soc*., 2007, **129**,

14281.

21. L. Deng, P. Margl and T. Ziegler, *J. Am. Chem. Soc.*, 1997, **119**, 1094.
22. D. G. Musaev, M. Svensson, K. Morokuma, S. Stromberg, K. Zetterberg and P. E. M. Siegbahn, *Organometallics*, 1997, **16**, 1933.
23. (a) L. Deng, T. K. Woo, L. Cavallo, P. M. Margl and T. Ziegler, *J. Am. Chem. Soc.*, 1997, **119**, 177; (b) A. Michalak and T. Ziegler, *Organometallics*, 1999, **18**, 3998; (c) T. K. Woo and T. Ziegler, *J. Organomet. Chem*., 1999, **591**, 204; (d) S. Stromberg, K. Zetterberg and P. E. M. Siegbahn, *J. Chem. Soc., Dalton Trans*., 1997, 4147; (e) R. D. J. Froese, D. G. Musaev and K. Morokuma, *J. Am. Chem. Soc*.,1998, **120**, 1581.
24. (a) R. H. Grubbs and A. Miyashita, *J. Am. Chem. Soc.*, 1978, **100**, 7416; (b) P. Binger, A. Brinkmann and P. Wademann, *Chem. Ber*., 1983, **116**, 2920.
25. S. Bhaduri, S. Mukhopadhyay and S. A. Kulkarni, *J. Organomet. Chem.*, 2009, **694**, 1297.
26. (a) N. W. Mungwe, M.Sc. thesis, *The synthesis of the cyclometallated palladium complexes and their applications in olefin oligomerization and in phenylacetylene oligomerization/polymerization*, University of Western Cape, 2008. (b) A. J. Swarts, M.Sc. thesis, *Mononuclear and multinuclear palladacycles as catalyst precursors*, Stellenbosch University, 2010.
27. (a) K. Matos and J.A. Soderquist, *J. Org. Chem*., 1998, **63**, 461; (b) F. Alonso, I.P. Beletskaya and M. Yus, *Tetrahedron*, 2008, **64**, 3047.
28. Pasynkiewicz, S. *Polyhedron*, 1990, **9**, 429.
29. (a) W. Kaminsky, R. Engehausen, K. Zoumis, W. Spaleck and J. Rohrmann, *Makromol. Chem*., 1992, **193**, 1643; (b) I. Kim and G. N. Hwang, *J. Mass Spectrom. Pure Appl. Chem. A*, 1998, **35**, 1987.
30. G. P. J. Britovsek, V. C. Gibson and D. F. Wass, *Angew. Chem. Int. Ed*., 1999, **38**, 428.
31. (a) A. Macchioni, *Chem. Rev*., 2005, **105**, 2039. (b) W. Keim, *Angew. Chem. Int. Ed. Engl*., 1990, **29**, 235. (c) W. Keim, B. Hoffmann, R. Lodewick, M. Peuckert, G. Schmidt, J. Fleischhauer and U. Meier, *J. Mol. Catal.*, 1979, **6**, 79.
32. E. Zurek and T, Ziegler, *Organometallics*, 2002, **21**, 83.
33. W. Janse van Rensburg, J.-A. van den Berg and P. J. Steynberg, *Organometallics*, 2007, **26**, 1000.
34. W. Kaminsky and R. Steiger, *Polyhedron*, 1988, **7**, 2375.
35. (a) G. Lanza, I. L. Fragal à and T. Marks, J. *Organometallics*, 2002, **21**, 5594; (b) Z. Xu, K. Vanka, T. Firman, A. Michalak, E. Zurek, C. Zhu and T. Ziegler, *Organometallics*, 2002, **21**, 2444.

36. (a) M. Bühl and H. Kabrede, *J. Chem. Theor. Comput*., 2006, **2**, 1282. (b) P. Rydberg and L. Olsen, *J. Phys. Chem. A*, 2009, **113**, 11949.

37. (a) B. Delley, *J. Chem. Phys*. 1992, **92**, 508. (b) B. Delley, *J. Phys. Chem*. 1996, **100**, 6107. (c) B. Delley, *J. Chem. Phys*. 2000, **113**, 7756.

38. J. Hurtadoy, M. Portaluppiy, R. Quijadazx, R. Rojasyx and M. Valderrama, *J. Coord. Chem*., 2009, **62**, 2772.

39. Y. Minenkov, G. Occhipinti and V. R. Jensen, *J. Phys. Chem. A*, 2009, **113**, 11833.

40. W. H. Meyer, T. Brull, H. G. Raubenheimer, C. Thompson and J. Kruger, *J. Organomet. Chem.*, 1998, **553**, 83.

41. (a) E. Zurek and T. Zieger, *Faraday Discuss*., 2003, **124**, 93. (b) E. Zurek and T. Ziegler, *Prog. Polym. Sci*., 2004, **29**, 107. (c) E. Zurek, T. K. Woo, T. K. Firman and T. Ziegler, *Inorg. Chem*., 2001, **40**, 361. (d) E. Zurek and T. Ziegler, *Inorg. Chem*., 2001, **40**, 3279.

42. (a) M. R. Mason, J. M. Smith, S. G. Bott and A. R. Barron, *J. Am. Chem. Soc*., 1993, **115**, 4971; (b) C. J. Harlan, M. R. Mason and A. R. Barron, *Organometallics*, 1994, **13**, 2957.

43. I. I. Zakharov and V. A. Zakharov, *Macromol. Theory Simul*., 2001, **10**, 108.

44. M. Ystenes, J. L. Eilertsen, J. Liu, M. Ott, E. Rytter and J. A. Støvneng, *J. Polym. Sci., Part A: Polym. Chem*., 2000, **123**, 3106 and references therein.

45. (a) I. I. Zakharov, V. A. Zakharov, A. G. Potapov and G. M. Zhidomirov, *Macromol. Theory Simul*., 1999, **8**, 272; (b) V. N. Panchenko, V. A. Zakharov, I. G. Danilova, E. A. Paukshtis, I. I. Zakharov, V. G. Goncharov and A. P. Suknev, *J. Mol. Catal. A*, 2001, **174**, 107; (c) E. Rytter, J. A. Støvneng, J. A. Eilertsen and M. Ystenes, *Organometallics*, 2001, **20**, 4466.

46. (a) D. W. Imhoff, L. S. Simeral, S. A. Sangokoya and J. H. Peel, *Organometallics*, 1998, **17**, 1941; (b) T. Sugano, K. Matsubara, T. Fujita and T. Takahashi, *J. Mol. Catal*., 1993, **82**, 93; (c) A. R. Siedle, W. M. Lamanna, R. A. Newmark, J. Stevens, D. E. Richardson and M. Ryan, *Macromol. Symp*., 1993, **66**, 215; (d) A. R. Siedle, R. A. Newmark, W. M. Lamanna and J. N. Schroepfer, *Polyhedron*, 1990, **9**, 301.

47. P. G. Belelli, M. M. Branda and N. J. Castellani, *J. Mol. Cat., A: Chem*., 2002, **3740**, 1.

48. T. K. Woo, L. Fan, T. Ziegler, in: G. Fink, R. Mülhaupt and H. H. Brintzinger (Eds.), *Ziegler Catalysts*, Springer, Berlin, 1995, p. 292.

49. (a) G. Lanza, I. L. Fragalá and T. J. Marks, *J. Am. Chem. Soc*., 1998, **20**, 8257; (b) R. Fusco, L. Longo, F. Masi and F. Garbassi, *Macromol. Rapid Commun*., 1998, **19**, 257; (c) F. Bernardi and G. P. Miscione, *Organometallics*, 1998, **17**, 16; (d) M. S. W. Chan, K. Vanka, C. C. Pye and T. Ziegler, *Organometallics*, 1999, **18**, 4624; (e) M. S. W. Chan and

T. Ziegler, *Organometallics*, 2000, **19**, 5182; (f) I. E. Nifantew, L. Y. Ustynyuk and D. N. Laikov, *Organometallics*, 2001, **20**, 5375; (g) F. Schaper, A. Geyer and H. H. Brintzinger, *Organometallics*, 2001, **21**, 473.

50. J. Vicente, J-A. Abad and E. Martínez-Viviente, *Organometallics*, 2002, **21**, 4454.
51. (a) S. A. Svejda, L. K. Johnson and M. Brookhart, *J. Am. Chem. Soc.*, 1999, **121**, 10634; (b) M. Brookhart, M. L. H. Green and L.-L. Wong, *Inorg. Chem*., 1988, **36**, 1; (c) D. J. Tempel and M. Brookhart, *Organometallics*, 1998, **117**, 2290; (d) F. M. Conroy-Lewis, L. Mole, A. D. Redhouse, S. A. Litster and J. L. Spencer, *J. Chem. Soc., Chem. Coummun.*, 1991, 1601.
52. V. L. Cruz, J. Ramos, S. Martinez, A. Muñoz-Escalona and J. Martinez-Salazar, *Organometallics*, 2005, **24**, 5095.
53. B. V. Popp, J. L. Thorman, C. M. Morales, C. R. Landis and S. S. Stahl, *J. Am. Chem. Soc*., 2004, **126**, 14832.
54. J. Forniés, V. Sicilia, C. Larraz, J. A. Camerano, A. Martín, J. M. Casas and A. C. Tsipis, *Organometallics* 2010, **29**, 1396.
55. W. Kohn, A. D. Becke and R. G. Parr, *J. Phys. Chem*., 1996, **100**, 12974.
56. S. Otto, P. V. Samuleev, V. A. Polyakov, A. D. Ryabov and L. I. Elding, *Dalton Trans*., 2004, 3662.
57. (a) G. K. Anderson and R. Cross, *J. Chem. Soc. Rev*., 1980, **9**, 185; (b) D. V. Deubel, T. Ziegler, *Organometallics*, 2002, **21**, 4432; (c) K. E. Frankcombe, K. J. Cavell, B. F. Yates and R. B. Knott, *Organometallics*, 1997, **16**, 3199; (d) J. A. Casares and P. Espinet, *Inorg. Chem*., 1997, **36**, 5428; (e) J. A. Casares and P. Espinet, *Inorg. Chem*., 1998, **37**, 2096.
58. (a) D. L. Thorn and R. Hoffmann, *J. Am. Chem. Soc*., 1978, **100**, 2079; (b) T. J. McCarthy, R. G. Nuzzo and G. M. Whitesides, *J. Am. Chem. Soc*., 1981, **103**, 3396; (c) K. Tatsumi, R. Hoffmann, A. Yamamoto and J. K. Stille, *Bull. Chem. Soc. Jpn*., 1981, **54**, 1857.
59. E. Guido, G. D'Amico, N. Russo, E. Sicilia, S. Rizzato, A. Albinati, A. Romeo, M. R. Plutino and R. Romeo, *Inorg. Chem*., 2011, **50**, 2224.
60. D. E. James, *Encyclopaedia of Polymer Science and Engineering*; H. F. Mark, N. M. Bikales, C. G. Overberger and G. Menges, Eds.; Wiley-Interscience: New York, 1985; Vol. 6, pp. 429-454.
61. S. Noda, A. Nakamura, T. Kochi, L. W. Chung, K. Morokuma and K. Nozaki, *J. Am. Chem. Soc*., 2009, **131**, 14088.
62. (a) T. K. Woo, L. Fan and T. Ziegler, *Organometallics*, 1994, **13**, 2252. (b) L. Fan, D.

Harrison, T. K. Woo and T. Ziegler, *Organometallics*, 1995, **14**, 2018; (c) N. G. Alameddin, M. F. Ryan, J. R. Eyler, A. R. Siedle and D. E. Richardson, *Organometallics*, 1995, **14**, 5005 and references therein; (d) H. Weiss, M. Ehrig and R. Ahlrichs, *J. Am. Chem. Soc*., 1994, **116**, 4919; (e) L. Fan, D. Harrison, L. Deng, T. K. Woo, D. Swerhone and T. Ziegler, *Can. J. Chem*., 1995, **73**, 989.

63. M. Lamberti, M. Mazzeo, D. Pappalardo and C. Pellecchia, *Coord. Chem. Rev*., 2009, **253**, 2082.
64. (a) P. Diversi, G. Ingrosso, and A. Lucherini, *J. Chem. Soc. Chem. Comm*., 1978, 735; (b) A. J. Canty, J. L. Hoare, N. W. Davies and P. R. Traill, *Organometallics*, 1998, **17**, 2046; (c) P. Diversi, G. Ingrosso, A. Lucherini, T. Lumini, F. Marchetti, V. Adovasio and M. Nardelli, *J. Chem. Soc. Dalton Trans*., 1988, 133; (d) P. W. Jennings and L. L. Johnson, *Chem. Rev*., 1994, **94**, 2241; (e) T. Mahamo, F. Zheng, A. Sivaramakrishna, J. R. Moss and G. Smith, *J. Organomet. Chem*., 2008, **693**, 103.
65. (a) A. R. Dick, J. W. Kampf and M. S. Sanford, *J. Am. Chem. Soc*., 2005, **127**, 12790; (b) A. Bayler, A. J. Canty, P. G. Edwards, B. W. Skelton and A. H. White, *J. Chem. Soc., Dalton Trans*., 2000, 3325; (c) S. R. Whitfield and M. S. Sanford, *J. Am. Chem. Soc*., 2007, **129**, 15142.
66. J. X. McDermott, J. F. White and G. M. Whitesides, *J. Am. Chem. Soc*., 1973, **95**, 4451.
67. e.g. (a) D. J. Tempel, L. K. Johnson, R. L. Huff, P. S. White and M. Brookhart, *J. Am. Chem. Soc*., 2000, **122**, 6686; (b) R. D. J. Froese, D. G. Musaev and K. Morokuma, *J. Am. Chem. Soc*., 1998, **120**, 1581.

Chapter 3

Dimethylsulfoxide Platinum(II) Complexes of *N*-benzylidenebenzylamine and *N*-salicylidenebenzylamines: Spectroscopic and Structural Investigations of the Influence of Chelate Ligands

3.1 Introduction

It has been demonstrated in Chapter 1 that there is much interest in the use of Pd-based catalyst systems for ethylene oligomerization. In general these catalysts have a less sterically bulky environment and a combination of hetero-donor bidentate coordination like N^N, P^N, P^O chelates, among which, complexes containing hetero nitrogen donor ligands are the most widely reported in literature.

Recently, Mungwe and Swarts, working in Mapolie's group at Stellenbosch University, synthesized new palladium complexes bearing *N*-benzylidenebenzylamines (**I**) through a cyclometallation method.[1] These complexes were prepared as candidates for ethylene oligomerization; however, low or no activity was observed. They were also tested for phenylacetylene polymerization, and in this case, reasonable catalytic activity was observed.[2]

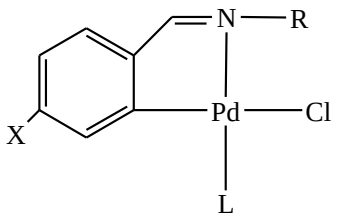

X = H, Cl, Br, Me
R = 2,6-di-^{i}Pr, Ph, Pr
L = PPh_3, PMe_3

I

The poor activity of the complexes towards ethylene oligomerization could be due to various factors, including non-activation of the palladium pre-catalyst by the co-catalyst or inactivity of the palladium catalyst itself toward ethylene oligomerization. A third possibility is that the palladium catalyst dimerizes ethylene and the volatile butenes formed are lost during the workup. Given this, it is necessary to investigate the reasons for such low activity.

Density functional theory (DFT) is an important tool for computational investigations on Group 10 complexes today, as demonstrated by Dedieu.[3] Keeping the above possible factors in mind, we have predicted (i) the possible interactions between the cyclometallated palladium complex and three TMA-expanded MAO models, and (ii) possible mechanism for ethylene oligomerization, reported in Chapter 2. By means of DFT we have been able to conclude that the ethylene oligomerization reactions catalysed by cyclometallated palladium complexes have low activity and produce mainly ethylene dimers, and we could rationalize the observations made during actual catalytic reactions.

The role played by the ligands in ethylene oligomerization, as in almost all kinds of catalytic reactions, is particularly important. It is of interest to consider a nitrogen containing ligand system having similar features to *N*-benzylidenebenzylamines (N^C), which could be utilized in olefin oligomerization/polymerization as well as in Suzuki and Heck reactions. Therefore it would be interesting to compare the chemistry of its transition metal complex with the (N^O) analogue to investigate the ligand effects on properties of the transition metal complexes and their subsequent effects in ethylene oligomerization.

Salicylaldimines are (N^O) chelates, and there has been much focus on the use of transition-metal-complexes bearing salicylaldimines as polymerization catalysts.[4] Palladium complexes have been investigated as catalysts for polymerization of methyl acrylate, acrylonitrile, and norbornene.[4(b),5] Palladium complexes bearing N^O chelating ligands have also been reported to catalyze ethylene oligomerization, as shown in Chapter 1 (**33** and **34** in Table 1.2). The phenoxyimine palladium complex **Pd-A** was synthesized and tested for ethylene oligomerization by Mogorosi, and was found to produce up to 99% of butenes in the presence of the co-catalyst $EtAlCl_2$.[6] Complexes of this metal have proven to be versatile and flexible; for example, palladium (N^O) complexes were also found to be effective catalysts for the Suzuki and Heck cross-coupling reactions.[7]

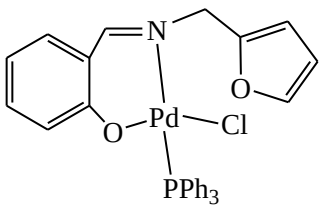

Pd-A

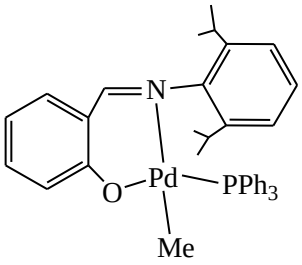

Pd-B

As previously mentioned, we consider (salicylidene)(2,6-diisopropylphenyl)amine (N^O, **L_B**) as an analogue of the currently studied ligand (benzylidene)(2,6-diisopropylphenyl)amine (N^C, **L_A**). These two ligands have similar nature, i.e. both are mono-anionic heteroditopic ligands, and their palladium complexes are known to catalyze C-C cross-coupling reactions. On the other hand, the Pd-Me complex **Pd-B** with (salicylidene)(2,6-diisopropylphenyl)amine (**L_B**) showed activity for copolymerization of an olefin with a polar monomer.[8] (Salicylidene)(phenyl)amine (**L_C**) has also been considered in this study, where it can be used to study the steric effect of the ligands by comparison with **L_B**

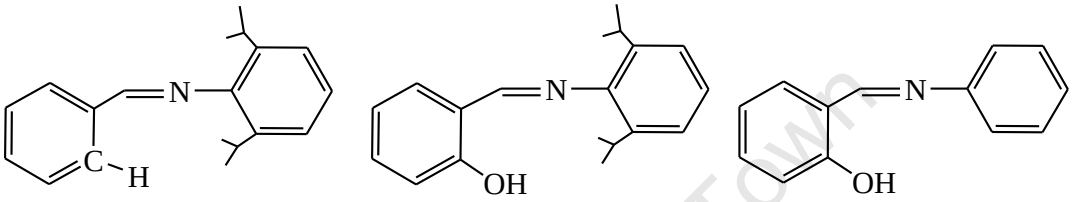

L_A **L_B** **L_C**

Platinum is a member of the Group 10 metals and lies below palladium in the periodic table. It has a very similar chemistry to that of palladium. The most stable oxidation states for both metals are the +2 and +4 states. In their most common oxidation state (+2) both metals have a d^8 configuration and constantly form square-planar diamagnetic complexes with various ligands and where the metal is dsp^2 hybridized. Both metals are characterized as soft acids. Pt(II) complexes are generally more stable than Pd(II), both thermodynamically and kinetically.[9] Furthermore, cyclometallated platinum group metal complexes containing nitrogen ligands have been extensively studied,[10] and the synthetic routes are well established. In view of this, platinum complexes bearing both (N^O) and (N^C) ligands have been chosen as model complexes for the palladium catalysts for comparative studies.

This chapter describes the synthesis and characterization of a dmso-ligated cyclometallated platinum complex bearing (benzylidene)(2,6-diisopropylphenyl)amine (**L_A**) and its analogues containing (salicylidene)(2,6-diisopropylphenyl)amine (**L_B**) or (salicylidene)(phenyl)amine (**L_C**). These compounds have been characterized using a range of analytical and spectroscopic techniques, including ^{1}H-NMR, 2D-COSY NMR, 2D-HSQC-NMR, ^{13}C-NMR, ^{31}P-NMR, FTIR spectroscopy, mass spectrometry and elemental analysis. Single crystal X-ray structure determinations of selected complexes were also conducted. The effect introduced by the

chelating ligands bonded to the Pt atom has been compared both by looking at spectroscopic features and crystal structure properties.

3.2 Results and Discussion

3.2.1 Synthesis and characterization of dmso platinum(II) complexes

3.2.1.1 Cyclometallated platinum(II) complex of (benzylidene)(2,6-diisopropylphenyl)amine

(Benzylidene)(2,6-diisopropylphenyl)amine, ligand $\mathbf{L_A}$ was prepared by a condensation reaction of the amine with the corresponding aldehyde.[1] Complex **C1** was obtained via the cyclometallation reaction of the ligand with *cis*-[$PtCl_2(dmso)_2$]. Initially, the reaction was carried out according to the most widely reported conditions,[11,12] using *cis*-[$PtCl_2(dmso)_2$], the imine and Na(CH_3CO_2) in a 1:1:1 ratio and heating the obtained mixture in refluxing methanol for 48 h. The formation of metallic platinum was however observed. Workup of the reaction mixture included filtration of metallic platinum and other insoluble residues, followed by crystallization of the desired compound **C1** from dichloromethane (DCM) and methanol (MeOH), to yield bright yellow microcrystals. However, the yield was extremely low, *ca.* 7%. It was thought the low yield was due to the decomposition of the *cis*-[$PtCl_2(dmso)_2$] precursor, as resulting from reduction of the Pt(II) by the methanol solvent.

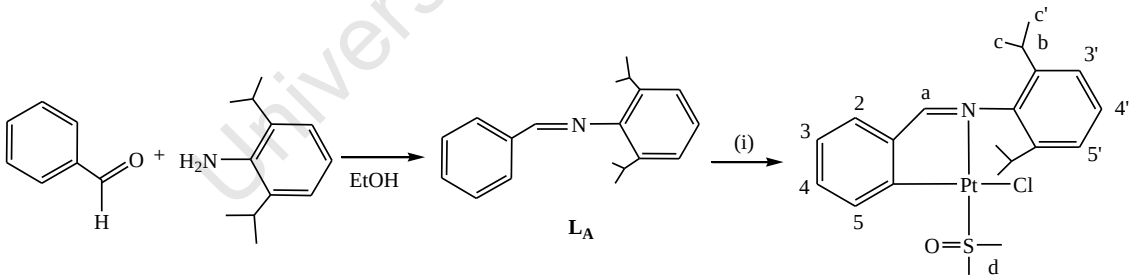

(Eq. 3.1)

(i), *cis*-[$PtCl_2(dmso)_2$], dry MeOH, in presence of sodium acetate

C1 (*trans*)

Slight modifications were introduced in order to obtain a higher yield. Following a method reported in the literature,[12] the reaction was carried out under nitrogen using dry toluene and heated at 90 ^oC for 48 h. It was reported that smaller amounts of metallic platinum are formed under these conditions.[13] In this case, however, there was no noticeable reduction of metallic platinum formation and the crystallization of compound **C1** from the resultant dark reaction mixture was not successful. Since it was assumed that a higher concentration of the base could favour the cyclometallation process,[13] another modification introduced was the use of a

molar ratio [Pt]:[$\mathbf{L_A}$]:[acetate] = 1:1:2. The reaction was carried out under nitrogen in dry methanol and heated at 65 ^{o}C for 48 h. Under these conditions, an improved yield at *ca.* 25% was obtained. The low yields are possibly caused by the decomposition of the platinum complexes and the hydrolysis of the imines, along with formation of metallic platinum and the corresponding aldehyde.[13]

3.2.1.2 Platinum(II) complexes of salicylidenebenzylamines

In order to achieve the successful syntheses of the analogous salicylidenebenzylamine complexes, the reactions of imines $\mathbf{L_B}$ and $\mathbf{L_C}$ were tested under different conditions. Following the method for the synthesis of compound **C1**, the reaction of ligand $\mathbf{L_B}$ with *cis*-[$PtCl_2(dmso)_2$] in the presence of Na(CH_3CO_2) in a 1:1:1 ratio was carried out in refluxing methanol. Two isomeric products were obtained (Eq. 3.2). The use of column chromatography (silica, ethyl acetate:hexane = 15:85) allowed the separation of these two products. Both compounds are thermally stable, with the *trans* complex **C2b** (when L is *trans* to the N atom, L = dmso) being slightly more stable than its *cis* analogue **C2a** (when L is *cis* to the N atom, L = dmso).

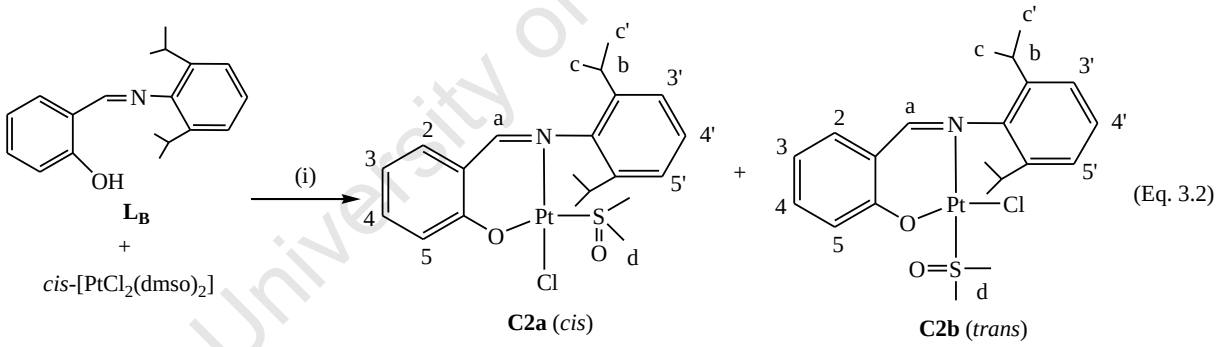

(Eq. 3.2)

(i), Dry MeOH, in presence of sodium acetate

Table 3.1 summarizes the different experimental conditions studied and the relevant ratios of **C2a**:**C2b** obtained. When $\mathbf{L_B}$ was treated with an equimolar amount of *cis*-[$PtCl_2(dmso)_2$] in the presence of NaOAc in refluxing methanol for either 30 min (the minimum period required for complete dissolvation), or 2 h, the ratio of **C2a**:**C2b** is around 5:1. A similar ratio was obtained when the reaction was carried out at room temperature with stirring overnight. When the reaction time was increased in the refluxing methanol (Table 3.1 entry IV), the ratio of the two isomers was observed to decrease to 1:1. It indicates that **C2a** converts to **C2b** during the heating process. In this reaction, some decomposition of the platinum complexes was also observed.

Table 3.1 Summary of the experimental conditions [reagents, temperature (T) and reaction time (t)] used to prepare platinum(II) complexes **C2a** + **C2b**

	Reagent (molar ratio)	T	t	Final products
I	$\mathbf{L_B}$ + *cis*-[$PtCl_2(dmso)_2$] + NaOAc (1:1:1)	298 K	16 h	**C2a**:**C2b** = ~ 5:1
II	$\mathbf{L_B}$ + *cis*-[$PtCl_2(dmso)_2$] + NaOAc (1:1:1)	reflux	30 min	**C2a**:**C2b** = ~ 5:1
III	$\mathbf{L_B}$ + *cis*-[$PtCl_2(dmso)_2$] + NaOAc (1:1:1)	reflux/298K	2 h/16h	**C2a**:**C2b** = ~ 5:1
IV	$\mathbf{L_B}$ + *cis*-[$PtCl_2(dmso)_2$] + NaOAc (1:1:1)	reflux	16 h	**C2a**:**C2b** = ~ 1:1
V*	$\mathbf{L_B}$ + *cis*-[$PtCl_2(dmso)_2$] + NaOAc (1:1:1)	Reflux/298K	2 h / 48 h	**C2a**:**C2b** = ~ 1:3

* *cis*-[$PtCl_2(dmso)_2$] was suspended in methanol and the mixture refluxed until complete dissolution. The hot and yellow solution was filtered, and the filtrate was added to a solution containing $\mathbf{L_B}$. The resulting mixture was stirred at room temperature for 48 hrs until some Pt black formed. All reactions were carried out in MeOH.

The initial steps in the proposed mechanism of cycloplatination of the ligand by *cis*-[$PtCl_2(dmso)_2$] are shown in Eq. 3.3.[14] It is suggested that one dmso ligand dissociates from *cis*-[$PtCl_2(dmso)_2$] in methanol and is replaced by a methanol molecule, after which there is a conversion to the *trans* geometry. The aim of refluxing *cis*-[$PtCl_2(dmso)_2$] in methanol (Table 3.1 entry V) until its complete dissolution was to obtain an intermediate complex with two Cl^- ligands *trans* to each other before reaction with $\mathbf{L_B}$. From the final products obtained, the ratio of the two isomers obtained from the reaction increased to 1:3 (**C2a**:**C2b**).

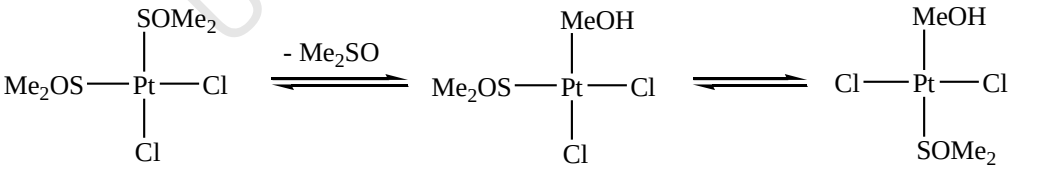

(Eq. 3.3)

In order to determine any steric effects of the ligand, platinum complex **C3** was synthesized by the reaction of the ligand $\mathbf{L_C}$ with *cis*-[$PtCl_2(dmso)_2$] under the reaction conditions outlined in entry I in Table 3.1. In this case, complex **C3** precipitated out of the solution as a single isomer, in which the dmso group is *cis* to the N atom in the chelating ligand (Eq. 3.4).

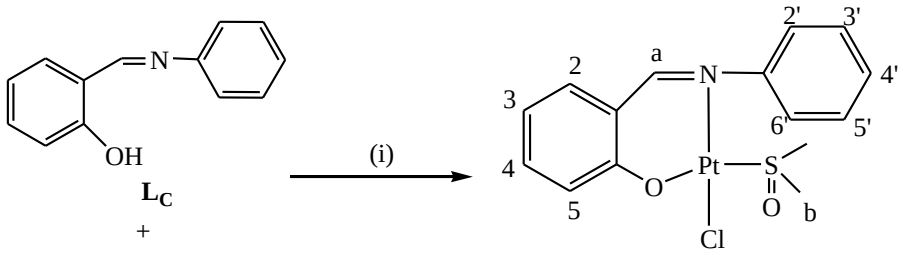

$\mathbf{L_C}$ + *cis*-[$PtCl_2(dmso)_2$] → **C3** (*cis*) (Eq. 3.4)

(i) Dry MeOH, in presence of sodium acetate

All the dmso platinum(II) complexes **C1** – **C3** were obtained as bright yellow crystalline solids after recrystalization from DCM/MeOH or DCM/n-hexane. They were found to be highly thermally stable and air stable in the solid state. These complexes were characterized by elemental analysis, mass spectrometry, IR and NMR spectroscopy and were also characterized crystallographically.

3.2.1.3 IR spectroscopy and mass spectrometry

IR spectroscopy was used to confirm the presence of functional groups indicative of a successful reaction. Coordination of the imine nitrogen to the platinum metal centre was confirmed by a bathochromic (red) shift (38 cm^{-1} for **C1**, 18 cm^{-1} for **C2** and 6 cm^{-1} for **C3**) of the imine stretching vibration bands in the region $\upsilon_{C=N}$ 1601 – 1607 cm^{-1} with respect to the free ligands (Table 3.2). Furthermore, the IR spectroscopic data of the *trans* complexes revealed a bathochromic shift of around 12 cm^{-1}, with $\upsilon_{S=O}$ stretching vibration bands appearing at 1139 and 1140 cm^{-1} for **C1** and **C2b**, respectively. In contrast, a hypsochromic (blue) shift around 4 cm^{-1} was observed for the *cis* complexes with $\upsilon_{S=O}$ stretching vibration bands at 1154 and 1155 cm^{-1} for **C2a** and **C3**, respectively. For complexes with (N^O) ligands, **C2a**, **C2b** and **C3**, the disappearance of the band at 2884 cm^{-1} (due to the OH) confirmed the deprotonation of hydroxyl group and formation of a σ-bond to the metal centre (Table 3.2).

Table 3.2 Selected spectroscopic data (IR, MS, ^{1}H, and ^{13}C NMR) for the dmso complexes **C1** – **C3**

Complex	Formula	[ii] IR / cm^{-1}		$[M]^+$ / *m/z*	^{1}H-NMR					^{13}C-NMR		
		$\upsilon_{S=O}$	$\upsilon_{C=N}$	(calc.)	H^a	H^b	H$^{c/c'}$	H^d	H^5	C^a	C^d	C^5
C1	$C_{21}H_{28}ClNOPtS$	1139	1601	[iii] 500.2 (500.03)	7.95 (s, J_{Pt-H} = 114.3 Hz)	3.29 (sept, 6.84 Hz)	1.30 (d, 7.77 Hz) 1.12 (d, 6.87 Hz)	3.52 (s, J_{Pt-H} = 40.1 Hz)	8.31 (d, 7.83 Hz, J_{Pt-H} = 40.1 Hz)	181.0	46.8	133.9
C2a[i]	$C_{21}H_{28}ClNO_2PtS$	1154	1606	[v] 474.12 (474.13)	7.81(s, J_{Pt-H} = 93.3 Hz)	3.59 (sept, 6.82 Hz)	1.35 (d, 6.88 Hz) 1.10 (d, 6.79 Hz)	3.40 (s J_{Pt-H} = 18.7 Hz)	6.71 (ddd, 7.33, 1.06 Hz)	163.2 (d)	47.3 (d)	117.3
C2b	$C_{21}H_{28}ClNO_2PtS$	1140	1606	[iv] 474.12 (474.13)	7.81 (s, J_{Pt-H} = 63.3 Hz)	3.36(sept, 6.84 Hz)	1.35 (d, 7.77 Hz) 1.11 (d, 6.87 Hz)	3.39 (s, J_{Pt-H} = 13.9 Hz)	6.73 (ddd, 7.83 Hz)	161.3 (d)	42.3 (d)	117.3 (d)
C3[i]	$C_{15}H_{16}ClNOPtS$	1155	1607	[v] 469.05 (469.05)	7.83 (s, J_{Pt-H} = 86.3 Hz)			3.24 (s, J_{Pt-H} = 16.5 Hz)	6.64 (d, 7.42 Hz)	162.7	46.4	117.6
L_A			1638		8.21 (s)	2.99 (sept, 6.82 Hz)	1.18 (d, 6.87 Hz)		7.53 (d, 1.74 Hz)	161.4		128.6
L_B			1624		8.33 (s)	3.03 (sept, 6.90 Hz)	1.21 (d, 6.90 Hz)		6.99 (t, 7.50 Hz)	162.1		117.0
L_C			1613		8.64 (s)				6.97 (td, 7.4, 0.1 Hz)	162.6		116.8
cis-$[PtCl_2(dmso)_2]$		1151						3.52 (s, J_{Pt-H} = 40.1 Hz)				

[i] L is *cis* to N atom (L = dmso, PPh_3)
[ii] Recorded as KBr pellets.
Represents *m/z* for the highest molecular weight fragment: [iii] $[M\text{-iPr-2Me}]^+$; [iv] $[M\text{-Cl-dmso}]^+$; [v] $[M\text{-Cl}]^+$.

Excellent microanalytical data and positive ion mass spectra were consistent with the proposed structures for the dmso complexes **C1** – **C3**. Different abundances for the fragmentation pathways were observed in the mass spectra of these complexes. The proposed fragmentation patterns of complexes **C1** and **C2b** are shown in Scheme 3.1 and the actual spectra are illustrated Figure 3.1. The (N^C) complex **C1** generated an ion cluster at *m/z* 540.2 – 545.5. The isotope distribution pattern and *m/z* values allow assignment of this ion to the fragment [**C1** - 2Me]$^+$. The most abundant cluster is found at *m/z* 498.2 – 503.2, corresponding to the further loss of an isopropyl group from [**C1** - 2Me]$^+$. The fragment at *m/z* 457.1 can be assigned as [Pt(N^C)]$^+$, resulting from the loss of the chloride and dmso groups from **C1**.

The mass spectra of the (N^O)-containing complexes **C2a** and **C2b** were similar; the *cis* and *trans* geometries did not affect the fragmentation pattern observed. As shown in Scheme 3.1, similar fragmentation pathways to that of **C1** (A) were obtained for complex **C2b** (B). The most abundant peak is due to the loss of the chloride and dmso groups from **C2b**. The two minor fragment ions at *m/z* 612.1 and 639.3 in Figure 3.1 (B) are attributed to the sodium adducts, [**C2b** + Na]$^+$ and [**C2b** + 2Na]$^+$. There are also two peaks corresponding to sequential loss of a chloride and a dmso group from the [**C2b** + Na]$^+$ adduct, to yield [**C2b** + Na - Cl]$^+$ (*m/z* 575.1) and [**C2b** + Na – Cl - dmso]$^+$ (*m/z* 497.1). Similarly, the fragment at *m/z* 557.2 can be assigned as [**C2b** + 2Na - dmso]$^+$, due to the loss of dmso from the [**C2b** + 2Na]$^+$ ion. The higher *m/z* range of the spectra for **C2b** (*m/z* 650-780) contain two relatively significant clusters. These could be due to the chelation of a dissociated (N^O) ligand (**L_B**) to the [Pt(N^O)]$^+$ ion to generate a [Pt(N^O)$_2$]$^+$ fragment (where N^O = **L_B**). The peak at *m/z* 719.3 can be attributed to [Pt(N^O)$_2$ + Na - ^{i}Pr - Me - H]$^+$, and the relatively strong peak at *m/z* 682.3 corresponds to the further loss of an isopropyl group from [Pt(N^O)$_2$ - 2Me - ^{i}Pr]$^+$.

The mass spectrum of complex **C3**, containing a less bulky (N^O) ligand, is relatively simple compared to those of **C1** and **C2a, b**. The parent ion was observed at *m/z* 506.0, and the most abundant cluster at 469.05 *m/z* is due to the loss of chloride from the parent ion, i.e. [**C3** - Cl]$^+$. The peak at *m/z* 391.0 can be assigned to the fragment ion [**C3** – Cl - dmso]$^+$. The fragment due to the sodium adduct of the parent ion [**C3** + Na]$^+$ is found at *m/z* 528.0. In addition, minor peaks at higher *m/z* ranges were assigned as [Pt(N^O)$_2$ +2 Na]$^+$ ion (*m/z* 635.2) (where N^O = **L_C**) and the sodium adduct of the dimer ion [(**C3**)$_2$ + Na]$^+$ (*m/z* 1003.0).

It has been reported for palladium complexes that the formation of dimeric ions in ESI mass spectrometry studies is common.[15]

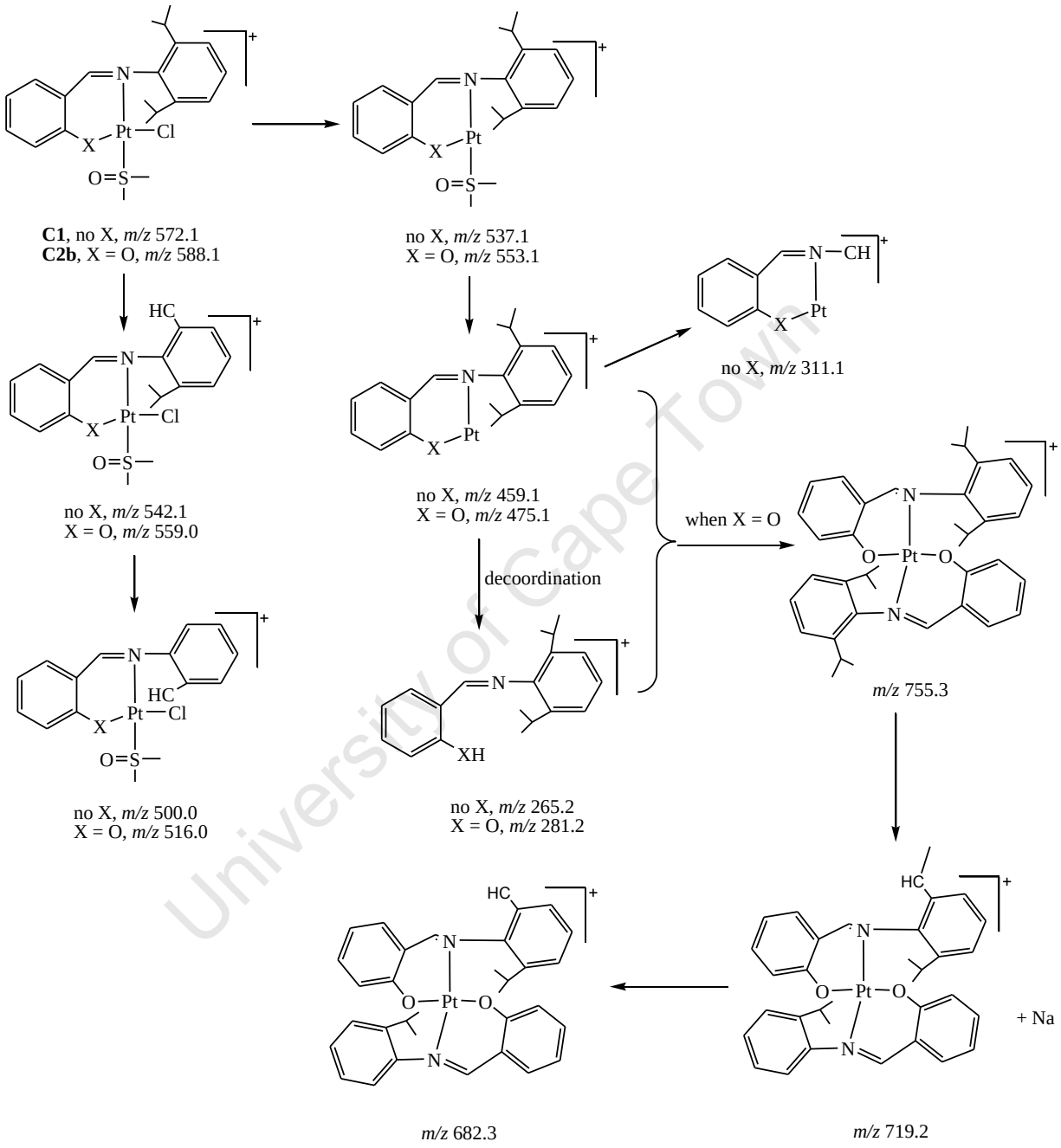

Scheme 3.1 Possible fragmentation pathways of platinum(II) complexes **C1** and **C2b**.

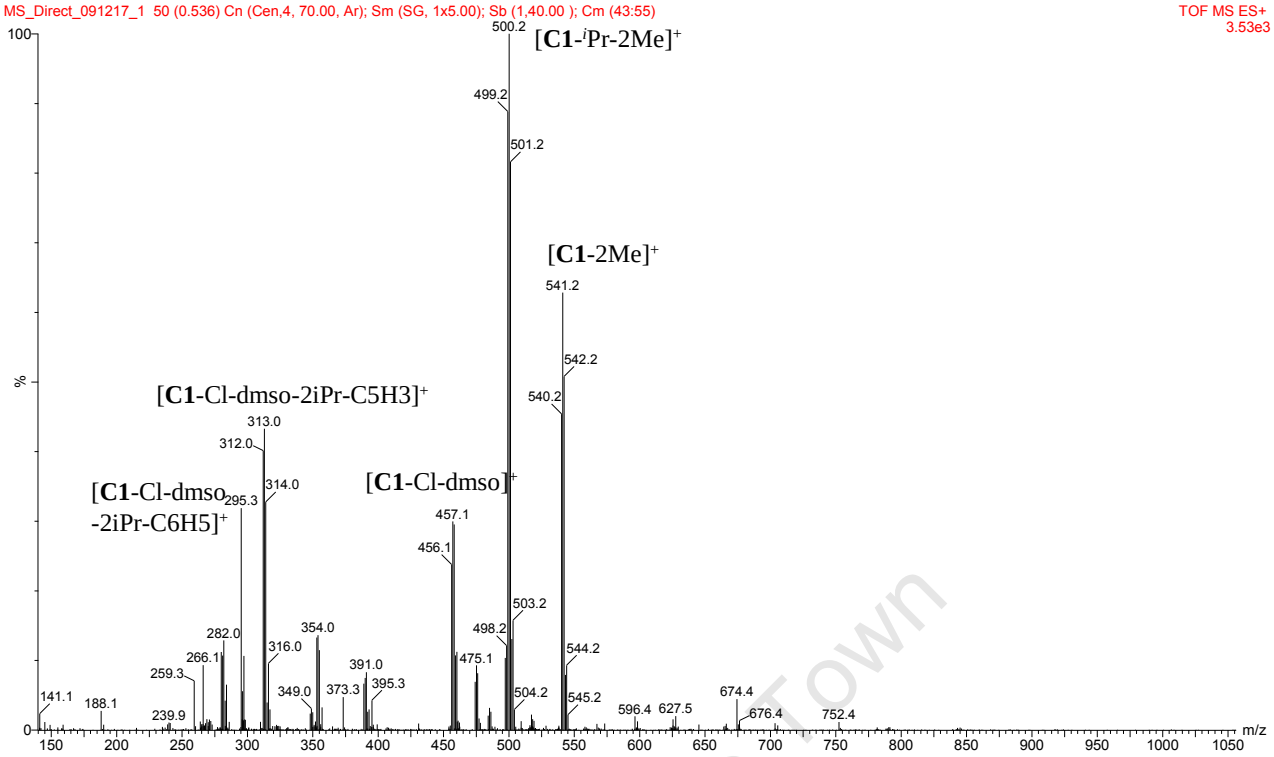

(A)

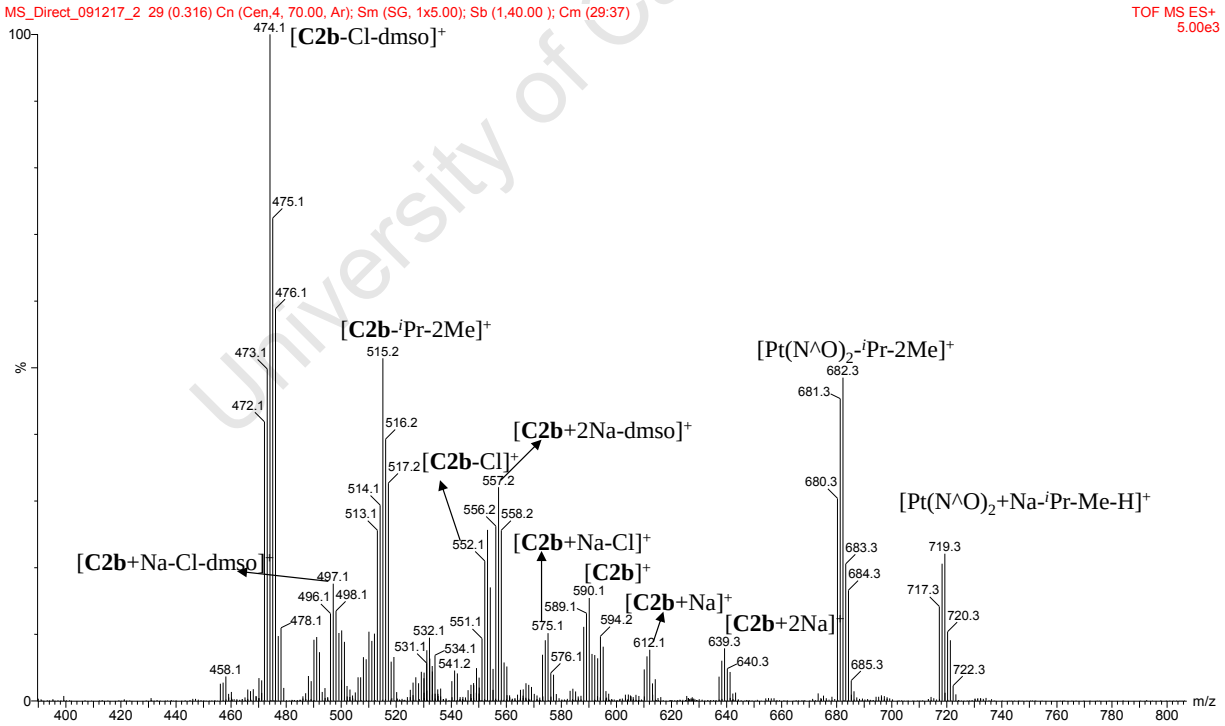

(B)

Figure 3.1 ESI mass spectra of **C1** (A), and **C2b** (B).

3.2.1.4 NMR spectroscopy

Selected ^{1}H NMR chemical shifts of the free ligands $\mathbf{L_A}$ - $\mathbf{L_C}$ and their corresponding dmso platinum(II) complexes are shown in Table 3.2. The assignments of the observed resonances were further confirmed by 2D-COSY spectra.

The ^{1}H NMR spectra of complexes **C1** – **C3** showed imine protons (H^a) appearing in the region δ 7.73 – 7.95 ppm which coupled to platinum. The observed upfield shift of δ 0.26 – 0.81 ppm with respect to the free ligands could be attributed to π-back-bonding from platinum to the imine bond, and confirmed coordination of the imino nitrogen to the metal centre. The ^{1}H NMR data for the cyclometallated complex **C1** agrees with the data reported for similar complexes.[16] Both the imine proton (H^a) and the aromatic proton adjacent to the metallated position (H^5) are coupled to platinum with coupling constants of J = 114.3 and J = 40.1 Hz, respectively, which confirms the formation of a bidentate [C,N] chelate system. The presence of seven cross-peaks in the aromatic region of the {^{1}H-^{13}C}-hetero-correlation spectra can also be taken as evidence of cyclometallation. In the ^{1}H-NMR spectra of (N^O) complexes **C2a**, **C2b** and **C3**, the disappearance of the phenolic proton around δ 13.5 ppm suggested successful deprotonation and formation of a phenoxy σ-bond with the metal centre. For the *cis* complexes **C2a** and **C3**, the imine protons display large $J_{Pt\text{-}H}$ values of 93.3 and 86.3 Hz, respectively, consistent with the presence of a chloride ligand in a *trans* position to the nitrogen atom. Conversely, for the *trans* complex **C2b**, the $J_{Pt\text{-}H}$ for the imine hydrogen is reduced (63.3 Hz) compared to the *cis* isomer, which is consistent with the presence of a dimethylsulfoxide ligand in a position *trans* to the nitrogen atom. A similar phenomenon has been observed for other platinum coordination compounds.[13]

For complexes **C1**, **C2a** and **C2b**, signals corresponding to the methyl protons of the isopropyl moieties ($H^{c/c'}$) on the ligands were split into two doublets, indicating that rotations between the nitrogen and the *ipso* carbon of these complexes are restricted. A downfield shift of δ 0.23 – 0.48 ppm was also observed for the methylene protons of the isopropyl moieties (H^b), presumably due to the coordination of the imine nitrogen and consequent deshielding of these protons. Both methyl groups of the dimethylsulfoxide (H^d) are equivalent and coupled to platinum in (N^C) complex **C1**, and the chemical shift does not change with respect to *cis*-[$PtCl_2(dmso)_2$]. However, this is not observed in the complexes with (N^O) chelate systems. For the (N^O) complexes **C2a**, **C2b** and **C3**, an upfield shift of *ca*. 0.12 ppm for the dmso

protons is observed upon coordination and the J_{Pt-H} value is reduced to 13 – 18 Hz. On the other hand, the chemical shift of the aromatic proton H^2 in (N^C) complex **C1** showed an upfield shift of 0.52 ppm, while there is no change in the (N^O) complexes. Compared to their related free bidentate ligands, there are significant downfield shifts (0.78 – 1.32 ppm) of the aromatic proton H^5 in the *trans* complexes **C1** and **C2b** (the dmso group is *trans* the nitrogen atom). On the contrary, the chemical shifts of H^5 in the *cis* complexes **C2a** and **C3** showed little change upon coordination. This suggests that when the dmso group is *trans* to the nitrogen atom and close to the aromatic proton H^5, the latter is more deshielded by dmso.

Although cyclometallated platinum complexes of the type described in this chapter are known, it appears that their ^{13}C-NMR spectra have not been reported anywhere in the literature. Examples of platinum complexes with N^O chelates are particularly rare. In this section, the ^{13}C NMR spectra of the dmso ligated platinum complexes are described. The selected chemical shifts are shown in Table 3.2.

The carbon NMR spectra for all dmso ligated complexes show the expected number of peaks. The assignments of the observed resonances were confirmed by ^{1}H-^{13}C HSQC spectroscopy. Coordination of the imine nitrogen was confirmed by the downfield shifts of the imine signal (C^a) in the ^{13}C NMR spectra of **C1** – **C3**. Similar trends have been noted in the literature for related palladium complexes.[17] The change in chemical shift of C^a for the (N^C) complex **C1** was more significant (19.65 ppm) than those for (N^O) complexes (0.1 – 1.8 ppm), probably due to the coordination of the aromatic carbon (C^6) to the platinum centre and consequent deshielding of C^a in complex **C1**. Furthermore, the imine carbon for the *cis* isomer **C2a** appears more upfield than that for the *trans* isomer **C2b**. The signal for the dmso carbons (C^d) occurs as a doublet at approximately 47 ppm for all complexes except **C2b**. The peak of C^d in **C2b** appears more upfield (42.31 ppm) than its *cis* isomer **C2a**, presumably due to a lesser degree of deshielding by the oxygen atom. For the *trans* complexes **C1** and **C2b**, the peaks representing the methyl carbons ($C^{c/c'}$) of the isopropyl moieties on the ligands are especially recognizable as two doublets at around 22 and 24 ppm, which is consistent with their corresponding ^{1}H resonances. For the *cis* isomer, two singlets are observed for the isopropyl carbons. Another point of interest is that the signal for methine (CH) carbon (C^b) appears as a doublet in the spectrum of *cis* isomer **C2a** while it is a singlet for the *trans* isomer **C2b**. There seems to be no clear explanation for this observation.

3.2.1.5 Crystal structures

Suitable single crystals of dmso complexes **C1** – **C3** were grown from dichloromethane-methanol at low temperature (*ca.* 4 ^{o}C). The molecular structures of **C1** – **C3** have been successfully determined by single crystal X-ray diffraction. The structure of **C2b** consists of discrete monomeric molecules with two different geometries [**C2b**(A) and **C2b**(B)]. These geometries are not significantly different in structural parameters such as bond lengths or angles. This phenomenon is common in the literature for related platinum and palladium complexes.[13,17(b)] The atomic labels of these complexes are given in the ORTEP pictures in Figures 3.2 – 3.4 and selected molecular dimensions are listed in Table 3.3. These confirm the geometries predicted from spectroscopic data. A full list of bond lengths and angles as well as the X-ray data collection parameters (data sets 1 – 4) and CIF files can be found in supporting information.

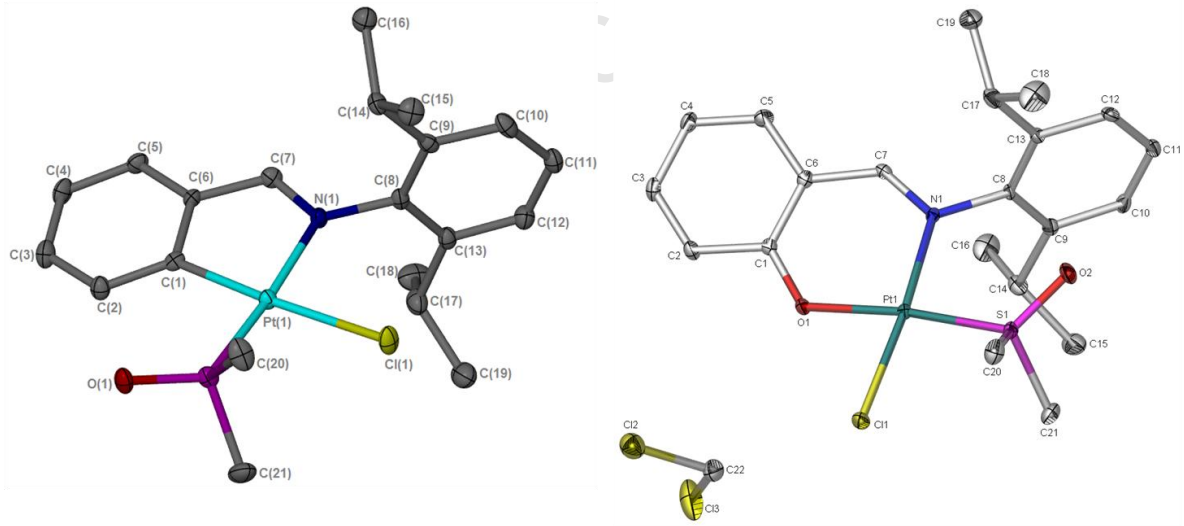

C1 **C2a**

Figure 3.2 Molecular structures of **C1** and **C2a** showing the atomic numbering scheme. All H atoms are omitted for clarity. All non-hydrogen atoms are presented as an ellipsoidal model with probability level 30%.

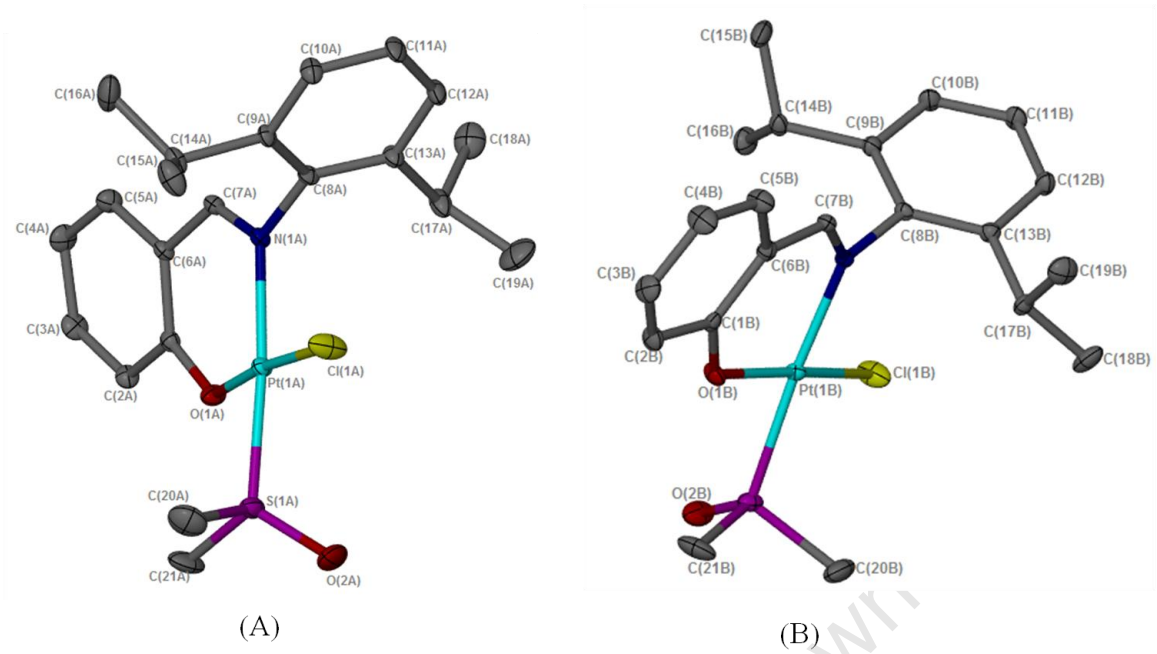

Figure 3.3 Molecular structure of **C2b** is shown with the atomic labelling scheme. The two crystallographically independent molecules are labelled with suffix 'A' and 'B'. All H atoms are omitted for clarity. All non-hydrogen atoms are presented as an ellipsoidal model with probability level 30%.

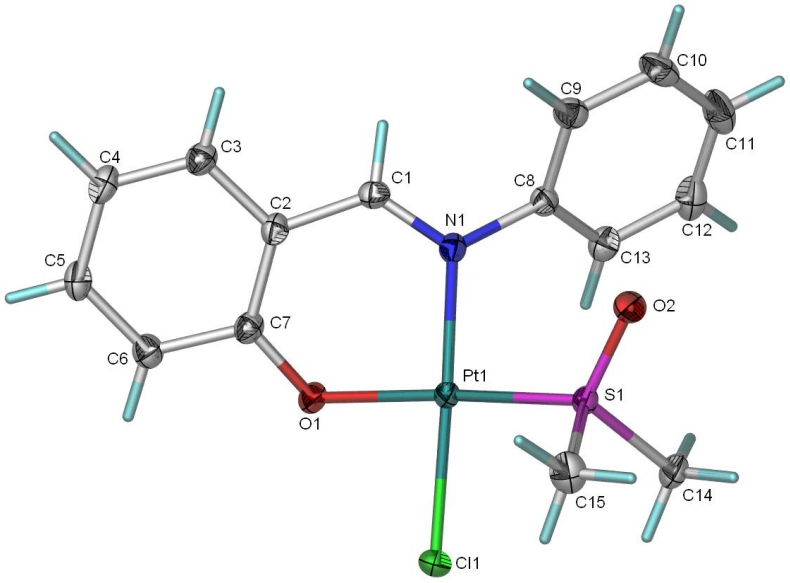

Figure 3.4 Molecular structure of **C3** showing the atomic labelling scheme. All non-hydrogen atoms are presented as an ellipsoidal model with probability level 50%.

Table 3.3 Selected bond lengths (Å), bond angles (°) and torsion angles (°) for the dmso ligated complexes **C1** – **C3**

C1		**C2a**[i]		**C2b**		**C3**[i]	
					(B) [ii]		
Pt(1)–C(1)	2.011(5)	Pt(1)–O(1)	2.015(2)	Pt(1)–O(1)	1.992(2)	Pt(1)–O(1)	2.019(18)
Pt(1)–N(1)	2.054(5)	Pt(1)–N(1)	2.040(3)	Pt(1)–N(1)	2.029(3)	Pt(1)–N(1)	2.029(2)
Pt(1)–S(1)	2.2133(12)	Pt(1)–S(1)	2.2181(8)	Pt(1)–S(1)	2.2304(8)	Pt(1)–S(1)	2.2062(6)
Pt(1)–Cl(1)	2.3769(1)	Pt(1)–Cl(1)	2.3118(8)	Pt(1)–Cl(1)	2.2961(9)	Pt(1)–Cl(1)	2.2981(16)
N(1)–C(7)	1.292(5)	N(1)–C(7)	1.300(4)	N(1)–C(7)	1.292(4)	N(1)–C(1)	1.297(3)
Cl(1)···H(7) [iii]	2.593			O(2)···H(2) [iii]	2.224		
C(1)-Pt(1)-N(1)	80.89(7)	O(1)-Pt(1)-N(1)	90.26(10)	O(1)-Pt(1)-N(1)	92.17(9)	O(1)-Pt(1)-N(1)	89.01(8)
C(1)-Pt(1)-S(1)	97.78(14)	O(1)-Pt(1)-S(1)	172.36(7)	O(1)-Pt(1)-S(1)	87.52(7)	O(1)-Pt(1)-S(1)	172.56(6)
N(1)-Pt(1)-Cl(1)	91.57(10)	N(1)-Pt(1)-Cl(1)	174.13(8)	N(1)-Pt(1)-Cl(1)	92.98(7)	N(1)-Pt(1)-Cl(1)	173.87(6)
S(1)-Pt(1)-Cl(1)	90.21(4)	S(1)-Pt(1)-Cl(1)	88.46(3)	S(1)-Pt(1)-Cl(1)	87.85(3)	S(1)-Pt(1)-Cl(1)	89.39(2)
N(1)-Pt(1)-S(1)	173.85(11)	N(1)-Pt(1)-S(1)	97.35(7)	N(1)-Pt(1)-S(1)	174.58(7)	N(1)-Pt(1)-S(1)	95.19(6)
C(1)-Pt(1)-Cl(1)	171.13(13)	O(1)-Pt(1)-Cl(1)	83.94(7)	O(1)-Pt(1)-Cl(1)	172.70(7)	C(1)-Pt(1)-Cl(1)	86.87(6)
Total 1[iv]	360.45	Total 1[iv]	360.01	Total 1[iv]	360.52	Total 1[iv]	360.46
C(1)-Pt(1)-N(1)	80.89(7)	O(1)-Pt(1)-N(1)	90.26(10)	O(1)-Pt(1)-N(1)	92.17(9)	O(1)-Pt(1)-N(1)	89.01(8)
C(7)-N(1)-Pt(1)	114.3(3)	C(7)-N(1)-Pt(1)	121.8(3)	C(7)-N(1)-Pt(1)	123.3(2)	C(11)-N(1)-Pt(1)	121.41(18)
C(6)-C(1)-Pt(1)	111.9(3)	C(1)-O(1)-Pt(1)	126.1(2)	C(1)-O(1)-Pt(1)	126.8(2)	C(7)-O(1)-Pt(1)	119.21(16)
C(1)-C(6)-C(7)	115.0(4)	O(1)-C(1)-C(6)	124.1(3)	O(1)-C(1)-C(6)	124.6(3)	O(1)-C(7)-C(2)	124.2(2)
N(1)-C(7)-C(6)	117.6(4)	C(1)-C(6)-C(7)	122.5(3)	C(1)-C(6)-C(7)	124.2(3)	C(7)-C(2)-C(1)	122.2(2)
		N(1)-C(7)-C(6)	129.8(3)	N(1)-C(7)-C(6)	128.0(3)	N(1)-C(1)-C(2)	126.4(2)
Total 2[v]	539.69	Total 2[v]	714.59	Total 2[v]	719.07	Total 2[v]	702.508
N(1)-Pt(1)-C(1)-C(2)	171.2(5)	N(1)-Pt(1)-C(1)-C(6)	-25.0(3)	N(1)-Pt(1)-C(1)-C(6)	-8.2(3)	N(1)-Pt(1)-C(1)-C(6)	-43.1(2)
Pt(1)-N(1)-C(8)-C(13)	90.8(4)	Pt(1)-N(1)-C(8)-C(13)	-104.7(3)	Pt(1)-N(1)-C(8)-C(13)	-82.8(3)	Pt(1)-N(1)-C(8)-C(13)	46.9(3)

[i] L is *cis* to N atom (L = dmso)
[ii] Molecule B
[iii] Intermolecular interactions
[iv] Sum of angles in the coordination environment of the platinum atom.
[v] Sum of internal angles of the metal-containing ring.

For complexes **C1** – **C3**, the coordination sphere of platinum is square-planar with κ^2-N^C - (for $\mathbf{L_A}$) or κ^2-N^O- bound bidentate ligands (for $\mathbf{L_B}$ and $\mathbf{L_C}$), the S-bound dimethylsulfoxide and the chloride ligand completing the coordination sphere. The molecular structures provide decisive evidence of the fact that in **C1** and **C2b** the dmso ligand occupies the position *trans* to the imine nitrogen, while in **C2a** and **C3** it lies in the *cis* position. In all cases, the imine bond is included in the metal-containing ring leading to an endo-cycle[16] (e.g. Figure 3.5). Figure 3.2 clearly shows that the (N^C) complex **C1** consists of a fused [5,6]-bicyclical system containing a five-membered metal-containing ring and the phenyl group, while the (N^O) complexes **C2a**, **C2b** and **C3** have fused [6,6]-bicyclical systems in the same manner. As shown in Table 3.3, bond lengths and angles are well within the range of values obtained for analogous compounds (for **C1**[11,16]; **C2 - C3**[18]).

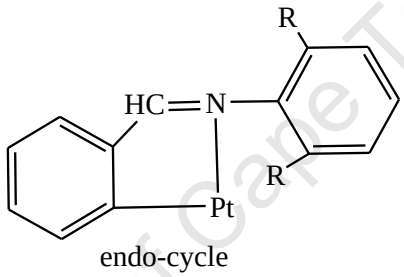

Figure 3.5

In all cases, the angles between adjacent atoms in the coordination sphere are close to the expected value of 90°. The most noticeable distortion corresponds to the angle C(1)-Pt(1)-N(1) of 80.89(17)° in **C1** (a consequence of chelation) and angle O(1)-Pt(1)-Cl(1) of 83.94(7)° in **C2a**. For complex **C1**, the smallest bite angle is presumably due to the strain imposed by the five-membered chelate ring C(1)-C(6)-C(7)-N(1)-Pt(1). However, this reduction is compensated for by an increase in the C(1)-Pt(1)-S(1) angle of 97.78(14)° . In the cases of complexes with a six-membered metal-containing ring, the bite angles are in the range of 89.01(8) – 92.17(9)°. The smallest angle, in **C2a**, is probably caused by the two relatively bulky groups, i.e., dmso and isopropyl phenyl groups, *cis* to each other, forming an angle N(1)-Pt(1)-S(1) of 97.35(7)° and consequently a reduced angle O(1)-Pt(1)-Cl(1). This is not observed either in **C2b**, which has dmso in the position *trans* to the isopropyl phenyl moiety, or in **C3** when the steric bulk of the phenyl group attached to the nitrogen atom is reduced. The sum of angles around platinum for all complexes is around 360°.

In the *trans* complexes **C1** and **C2b**, the atoms of the metal-containing ring adopt a practically planar arrangement, as shown by the sum of their internal bond angles of 539.7° [a] and 719.1° [b], respectively. Similar arrangements have been reported for related cyclometallated complexes.[11(c),16,19] The metal-containing ring (plane 1) in **C1** and **C2b** is nearly coplanar with the coordination plane (plane 2), and the torsion angle between plane 1 and plane 2 is 171.2(5)° for **C1** and -8.2(3)° for **C2b**. In contrast, different degrees of strain of the metal-containing ring are observed for the *cis* complexes **C2a** and **C3** with a sum of internal angles of 714.59° and 702.508°, respectively. Furthermore, the non-coplanarity of the plane 1 and plane 2 is indicated by the torsion angle of values of -25.0(3)° for **C2a** and -43.1(2)° for **C3**.

The steric effect on molecular structure is significant. As mentioned above, the less sterically bulky ligand $\mathbf{L_C}$ in complex **C3** enhances the strain of the metal-containing chelate ring (plane 1) and consequently enhances the non-coplanarity of plane 1 and plane 2 when compared to **C2a**. In addition, a nearly facial (perpendicular) orientation[20] of the 2,6-diisopropyl phenyl ring (plane 3) to the mean plane of the chelate ring (plane 1) is observed in complexes **C1**, **C2a** and **C2b**, as indicated by the torsion angle between the two planes around 90° (90.8(4)° for **C1**, -104.7(3)° for **C2a** and -82.8(3)° for **C2b**). With reduction of the steric bulk in **C3**, this angle is observed to decrease to 46.9(3)°. The alternative edge (parallel) and facial arrangement[20] does not exist in this case.

The Pt-Cl bond lengths for complex **C1** – **C3** are found to decrease in the sequence: Pt-Cl(1)$_{trans\text{-}C}$ [2.3769(1) Å] in **C1** > Pt-Cl(1)$_{trans\text{-}N}$ [2.3118(2) Å] in **C2a** > Pt-Cl(1)$_{trans\text{-}N}$ [2.2981(16) Å] in **C3** > Pt-Cl(1)$_{trans\text{-}O}$ [2.2961(9) Å] in **C2b**. This reflects the decrease in *trans* influence of the different donor atoms of the organic ligands, the order being the aryl carbon atom > the imine nitrogen atom > the phenoxy oxygen atom.[21] In addition, the longer Pt-S(1)$_{trans\text{-}N}$ [2.2304(8) Å] in **C2b** than the Pt-S(1)$_{trans\text{-}O}$ in the *cis* analogues **C2a** and **C3** [2.2181(8) Å and 2.2062(6) Å, respectively] also reveal the higher *trans* influence of the imine nitrogen as compared to the oxygen atom of the N^O ligands. As expected from the high *trans* influence of dmso,[22] the Pt-O(1)$_{trans\text{-}S}$ bond lengths in **C2a** and **C3** are slightly longer [2.015(2) Å and 2.019(18) Å, respectively] than that *trans* to a chloride ligand, i.e. Pt-O(1)$_{trans\text{-}Cl}$ in **C2b** [1.991(2) Å] .

[a] The sum of the internal angles of planar five-membered ring is 540°.
[b] The sum of the internal angles of planar six-membered ring is 720°.

The C=N bond length in complex **C1** [1.292 (5) Å] is observed to be greater than the uncoordinated C=N bond lengths in related palladium[1] and platinum[a] complexes [1.265(3) Å and 1.271(4) Å, respectively]. This is presumably due to a certain degree of aromaticity in the endo-cycle involving the imine bond, one C=C bond of the phenyl ring and a filled d orbital of the platinum as previously suggested for five-membered metallacycles.[16,23] The imine C=N bond lengths for (N^O) complexes lie in the usual range compared to their related palladium complexes.[17(b),19]

In the *trans* complexes **C1** and **C2b** intermolecular interactions are observed (Figure 3.6). The intermolecular distance between the imine proton and the chloride ligand N=CH···Cl in complex **C1** was measured to be *d*(H(7A)···Cl(1B)) = 2.59(3) Å, while the imino hydrogen in **C2b** is involved in an interaction with the oxygen atom in the dmso ligand, N=CH···O (*d*(H(7A)···O(1B)) = 2.24(4) Å). These interactions increase the stability of complexes **C1** and **C2b** as previously suggested for analogous compounds.[11(c)] No intermolecular interactions are found for the *cis* complexes.

[a] Complex **C7** in Chapter 4.

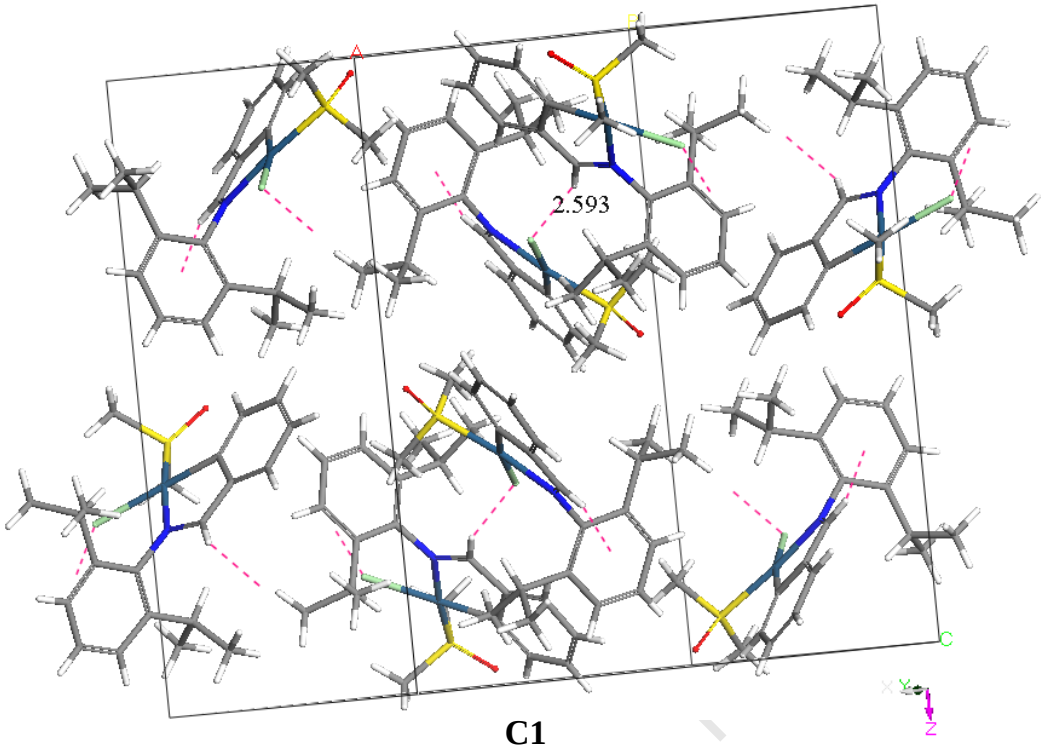

C1

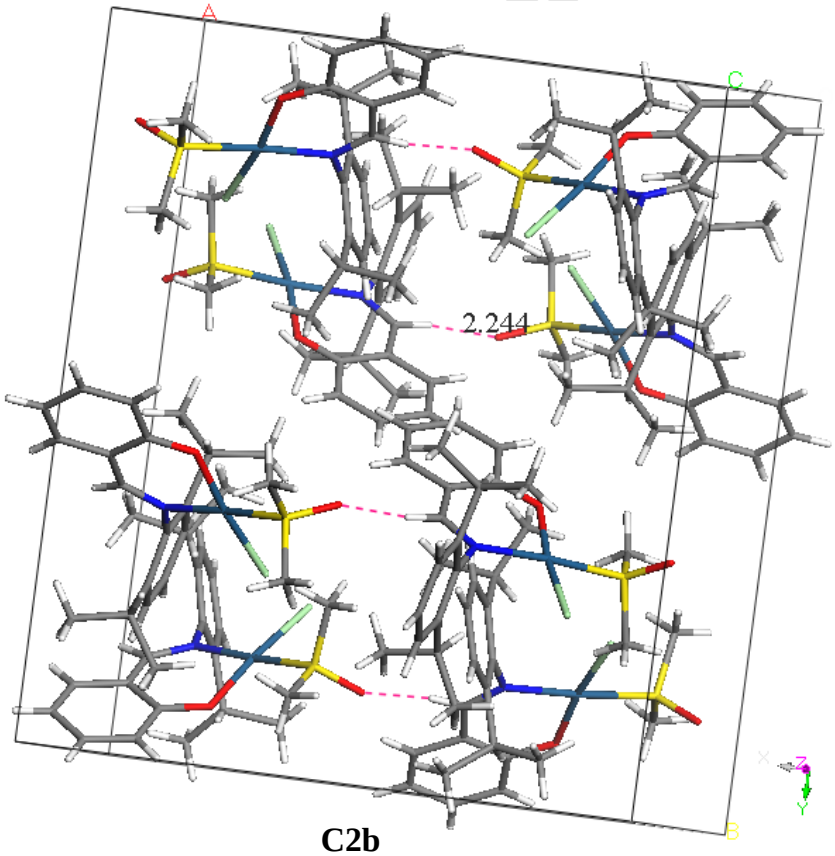

C2b

Figure 3.6 Projection viewed along [010] for **C1** and **C2b**.

3.2.1.6 Thermal analysis

Thermal analytical methods are often applied to measure the changes in physical properties of a compound as a function of temperature. In this section, thermogravimetric analysis (TGA) and differential scanning calorimetry (DSC) were used in combination to investigate the loss of the coordinated dmso group and/or chloride from complexes **C1** – **C3**. The further mass losses of these complexes are not of interest and are therefore not discussed here. The TGA and DSC traces for complexes **C1** – **C3** are shown in Figure 3.7.

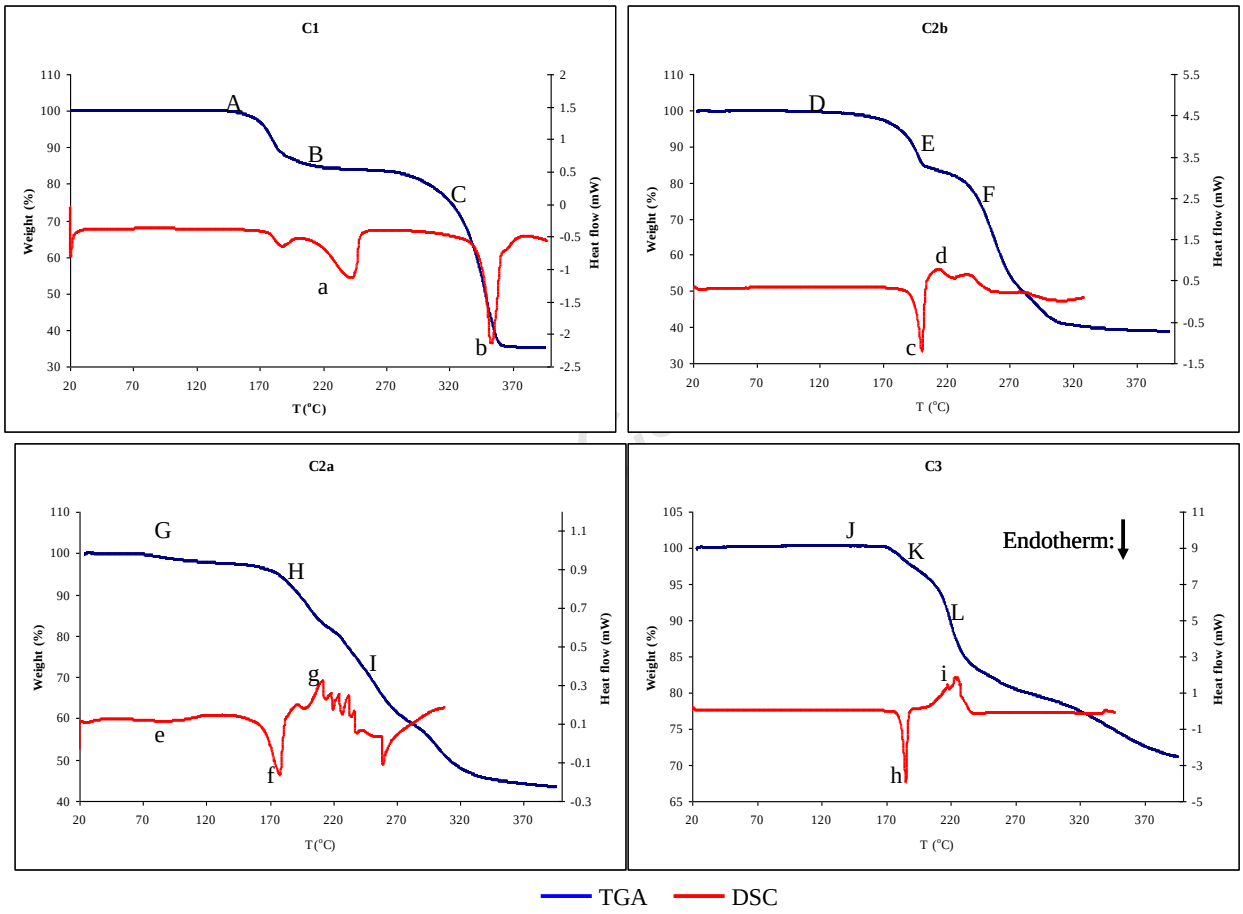

Figure 3.7 TGA and DSC traces for dmso ligated complexes **C1** – **C3**.

The N^C complex **C1** started to show mass loss at 140 °C, represented by (A) in Figure 3.8. Based on its first derivative curve (not shown), **C1** showed a multiple-step mass loss indicating the dmso group and chloride were lost simultaneously during the heating process (given as B in Figure 3.7). Point C indicates the decomposition of **C1** with an onset temperature of 300 °C. The calculated mass loss is comparable to the experimental mass loss for **C1** in the temperature range of 140 °C to 300 °C; these losses are 19.8% and 19.6%, respectively. The DSC trace of **C1** exhibited one broad endotherm (a) in the temperature

range of 190 – 244 ^{o}C, comprising two overlapping peaks. This corresponds to the compound melting and is consistent with the multiple-step mass loss B in the TGA. A large endotherm (b) at 354 ^{o}C was observed, indicating decomposition. Among the four complexes presented, the N^C complex **C1** is the most thermally stable. The melting point obtained from hot stage determination (194 – 196 ^{o}C) is in agreement with the DSC result; however, we were not able to observe the decomposition on the hot stage due to the very high temperature (> 350 ^{o}C).

Similarly to **C1**, the N^O complex with *trans* geometry **C2b** exhibited an instantaneous loss above 120 ^{o}C (shown as D in Figure 3.7). This appears to be a multiple-step mass loss, as it does not correspond convincingly to loss of only dmso or chloride from the complex. This provides proof that **C2b** loses the dmso and chloride groups concurrently during the heating process (represented by E in Figure 3.7). The experimental mass loss for **C2b** is 19.8% in the temperature range of 120 ^{o}C to 233 ^{o}C, and this is consistent with the calculated value of 19.3% for the loss of these two ligands. A sharp endotherm (c) represents the melting of complex **C2b** at ~ 201 ^{o}C followed by decomposition at ~ 216 ^{o}C. The findings from DSC indicated that the mass loss of dmso and chloride occurred during the melting and initial stage of decomposition. Afterwards, a further decomposition indicated by point F was observed.

The TGA curve of the *cis* isomer **C2a** showed a steeper slope compared to that of **C2b**. The first step G is attributed to the release of a water molecule, occurring over a temperature range 66 ^{o}C to 145 ^{o}C with a mass loss of 2.7%. The calculated mass loss is 3.0% and agrees well with the experimental mass loss. The second step H is due to a multiple-step mass loss between the temperatures 150 ^{o}C and 230 ^{o}C, and is similar to that observed for **C2b**, indicating the loss of both dmso and chloride ligands. The experimental mass loss of this step is found to be 18.8% and correlates well with the calculated mass loss of 19.3%. In the DSC trace for **C2a**, a small broad endotherm (e) was due to the loss of water at 95 ^{o}C and consistent with the TGA observation. The relatively sharper endotherm (f) indicates the melting of **C2a** at ~179 ^{o}C, showing that the *cis* isomer is slightly less thermally stable compared to **C2b**. Similarly to **C2b**, the mass loss of dmso and chloride occurred during the melting and initial stage of decomposition. Afterwards, a further decomposition, indicated by point I, was observed. The loss of both dmso and chloride is also observed in mass spectra of **C2a** and **C2b**, in which the fragment ion $[M - dmso - Cl]^{+}$ was found as the most abundant peak for both complexes (see Section 3.2.1.3).

A different behaviour was observed in the TGA trace for **C3**, the complex with a less sterically bulky N^O chelate. Event J represented an instant mass loss above 170 ^{o}C and corresponded to the loss of chloride ligand during the heating process (given as K in Figure 3.7). This is in agreement with the observation of its mass spectrum in which the $[M - Cl]^{+}$ ion is the most abundant fragment. Point L indicates the decomposition of **C3** with an onset temperature of ~215 ^{o}C. The calculated mass loss is comparable to the experimental mass loss in the temperature range of 170 ^{o}C to 212 ^{o}C; these losses are 7.0% and 6.6%, respectively. The DSC trace for **C3** showed two independent thermal events, h and i. A sharper endotherm (h) was attributed to the melting of **C3** at ~185 ^{o}C. The exothermic peak (i) represents the decomposition.

3.3 Conclusions

The dimethylsulfoxide (dmso) cyclometallated platinum(II) complex bearing (benzylidene)(2,6-diisopropylphenyl)amine (**L_A**) and its analogues containing (salicylidene)(2,6-diisopropylphenyl)amine (**L_B**) and (salicylidene)(phenyl)amine (**L_C**) were synthesized and characterized by standard techniques. When using the bulky (N^O) chelate **L_B**, a pair of *cis*/*trans* isomers was obtained. The influence of the chelate ligands, i.e. the N^C and N^O ligands, on the corresponding platinum complexes was investigated by spectroscopic methods and X-ray crystallography.

The mass spectra of the N^O complexes showed the fragments of bis(salicylaldiminato) platinum(II) species (with **L_B**) or dimeric species (with **L_C**) which are formed during the MS analysis, while for the N^C complex, these were not observed.

The NMR spectral data revealed the occurrence of cyclometallation for the N^C complex **C1**, and the *cis/trans* geometries for N^O complexes **C2a** and **C2b**. The coupling constants (J_{Pt-H}) for the imine protons in **C2a** and **C2b** were found to be similar to those of the related *cis/trans* isomeric complexes.[16] These *J* values are consistent with their *cis/trans* geometries. For complex **C1**, the J_{Pt-H} value for the imine proton is much greater compared to the N^O analogue **C2b**.

With regard to structural properties, there was no significant difference between the N^C complex **C1** and the N^O analogue **C2b**. Intermolecular interactions were only observed in the two complexes in which the dmso group is *trans* to the imine nitrogen.

Thermal analysis studies using TGA and DSC were performed on the dmso-ligated complexes, and showed the loss of both dmso and chloride ligands during the heating process for the complexes with bulky chelates, i.e. **C1**, **C2a** and **C2b**, while the loss of only chloride was observed for **C3**.

This chapter has shown that the dmso-ligated platinum(II) complexes with both N^C and N^O ligands were successfully synthesized. These precursor complexes will be used to synthesize platinum model complexes of the palladium pre-catalysts, as described in the following chapter.

3.4 References

1. (a) N. W. Mungwe, M.Sc. thesis, *The synthesis of the cyclometallated palladium complexes and their applications in olefin oligomerization and in phenylacetylene oligomerization/polymerization*, University of Western Cape, 2008; (b) A. J. Swarts, MSc thesis, *Mononuclear and multinuclear palladacycles as catalyst precursors*, Stellenbosch University, 2010.
2. N. Mungwe, A. Swarts, S. F. Mapolie and G. Westman, *J. Organomet. Chem*., 2011, **696**, 3527.
3. A. Dedieu, *Chem. Rev*., 2000, **100**, 543.
4. (a) H. Makio and T. Fujita, *Acc. Chem. Res*., 2009, **42**, 1532; (b) H. Makio, N. Kashiwa and T. Fujita, *Adv. Synth. Catal*., 2002, **344**, 477; (c) V. C. Gibson and S. K. Spitzmesser, *Chem. Rev*., 2003, **103**, 283; (d) T. Matsugi and T. Fujita, *Chem. Soc. Rev*., 2008, **37**, 1264; (e) D. A. Bansleben, S. K. Freiedrich, T. R. Younkin, R. H. Grubbs, C. Wang and R. T. Li, WO98/03165, 1998; (f) C. Wang, S. Friedrich, T. R. Younkin, R. T. Li, R. H. Grubbs, D. A. Bansleben and M. W. Day, *Organometallics*, 1998, **17**, 3150; (g) T. R. Younkin, E. F. Connor, J. I. Henderson, S. K. Friedrich, R. H. Grubbs and D. A. Bansleben, *Science*, 2000, **287**, 460; (h) E. F. Connor, T. R. Younkin, J. I. Henderson, A. W. Waltman and R. H. Grubbs, *Chem. Commun*., 2003, 2272; (i) W. H. Sun, H. Yang, Z. Li and Y. Li, *Organometallics*, 2003, **22**, 3678; (j) C. Carlini, A. Macinai, F. Masi, A. M. R. Galletti, R. Santi, G. Sbrana and A. Sommazzi, *J. Polym. Sci. A*, 2004, **42**, 2534; (k) C. Carlini, M. Martinelli, A. M. R. Galletti and G. Sbrana, *J. Polym. Sci. A*, 2006, **44**, 1514; (l) Q. Chen, J. Yu and J. Huang, *Organometallics*, 2007, **26**, 617; (m) M. Delferro, J. P. McInnis and T. J. Marks, *Organometallics*, 2010, **29**, 5040; (n) D. J. Darensbourg, C. G. Ortiz and J. C. Yarbrough, *Inorg. Chem*., 2003, **42**, 6915; (o) H. Liang, J. Liu, X. Li and Y. Li, *Polyhedron*, 2004, **23**, 1619.
5. (a) Y. Chen, S. Mandal and A. Sen, *Organometallics*, 2010, **29**, 3160; (b) M. Kang and A. Sen, *Organometallics*, 2005, **24**, 3508; (c) L. F. Groux, T. Weiss, D. N. Reddy, P. A. Chase, W. E. Piers, T. Ziegler, M. Parvez and J. Benet-Buchholz, *J. Am. Chem. Soc*., 2005, **127**, 1854; (d) T. Hu, Y. G. Li, Y. S. Li and N. H. Hu, *J. Mol. Catal. A: Chem*., 2006, **253**, 155; (e) K. Ishizaki, S. Washimi and K. Kimura, JP200172654, 1999.
6. M. M. Mogorosi, PhD thesis, *Synthesis and Characterization of Nickel, Palladium and Chromium Complexes as Olefin Oligomerization Catalysts*, University of Cape Town, 2009.

7. (a) J. Cui, M. Zhang and Y. Zhang, *Inorg. Chem. Commun*., 2010, **13** 81; (b) Y. Liu, M. G. B. Drew and Y. Liu, *J. Mol. Struct.: THEOCHEM*, 2007, **809**, 37.
8. I. Kenichi, W. Akira and K. Kaoru, *Jpn. Kokai Tokyo Koho*, JP 2001072654 (A), 2001.
9. (a) F. R. Hartley, *The Chemistry of Platinum and Palladium*, Applied Science Publishers Ltd, London, 1973, pp. 331 – 334; (b) A. Garoufis, S. K. Hadjikakou and N. Hadjiliadis, *Metallotherapeutic Drugs and Metal-based Diagnostic Agents*; M. Gielen, E. R. T. Tiekink, Eds; John Wiley & Sons Ltd, England, 2005, pp. 339 – 415.
10. (a) A. D. Ryabov, *Synthesis*, 1985, 233; (b) V. V. Dunina, O. A. Zalevskaya and V. M. Potapov, *Russ. Chem. Rev. (Engl. Transl.)*, 1988, **57**, 434; (c) A. D. Ryabov, *Chem. Rev*., 1990, **90**, 403; (d) P. Espinet, M. A. Esteruelas, L. A. Oro, J. L. Serrano and E. Sola, *Coord. Chem. Rev*., 1992, **117**, 215; (e) C. Navarro-Ranninger, I. López-Solera, J. M. Pérez, J. R. Masaguer and C. Alonso, *Appl. Organomet. Chem*., 1993, **7**, 57; (f) M. Albrecht, M. Lutz, A. L. Spek and G. van Koten, *Nature*, 2000, **406**, 970; (g) M. Albrecht and G. van Koten, *Angew. Chem., Int. Ed*., 2001, **40**, 3750; (h) J. Dupont, M. Pfeffer and J. Spencer, *Eur. J. Inorg. Chem*., 2001, 1917; (i) I. Omae, *Coord. Chem. Rev*., 2004, **248**, 995; (j) J. Dupont, C. S. Consorti and J. Spencer, *Chem. Rev*., 2005, **105**, 2527.
11. (a) S. Prez, C. López, A. Caubet, X. Solans and M. Font-Bardía, *New J. Chem*., 2003, **27**, 975; (b) M. Crespo, M. Font-Bardía, J. Granell, M. Martínez and X. Solans, *Dalton Trans*., 2003, 3763; (c) A. Capapé, M. Crespo, J. Granell, M. Font- Bardía and X. Solans, *J. Organomet. Chem*., 2005, **690**, 4309.
12. (a) L. Ding, D. P. Zou and Y. J. Wu, *Polyhedron*, 1998, **17**, 2511; (b) C. López, A. Caubet, S. Pérez, X. Solans and M. Font-Bardía, *Chem. Commun*., 2004, 540; (c) Y. J. Wu, L. Ding, H. X. Wang, Y. H. Liu, H. Z. Yuan and X. A. Mao, *J. Organomet. Chem*., 1997, **535**, 49.
13. M. Crespo, R. Martin, T. Calvet, M. Font-Bardia and X. Solans, *Polyhedron*, 2008, **27** 2603.
14. (a) A. D. Ryabov, S. Otto, P. V. Samuleev, V. A. Polyakov, L. Alexandrova, G. M. Kazankov, S. Shova, M. Revenco, J. Lipkowski and M. H. Johansson, *Inorg. Chem*., 2002, **41**, 1633; b) S. Otto, A. Chanda, P. V. Samuleev and A. D. Ryabov, *Eur. J. Inorg. Chem*., 2006, 2561.
15. W. Zawartka, A .Gniewek, A .Trzeciak, J. Ziolkowski and J. Pernak, *J. Mol. Catal .A:*, 2009, **304**, 8.
16. A. Capapé, M. Crespo, J. Granell, M. Font-Bardía and X. Solans, *Dalton Trans*., 2007, 2030.

17. (a) S. Budagumpi, Y. Liu, H. Suh and I. Kim, *J. Organomet. Chem*., 2011, **696**, 1887; (b) Y. Murata, H. Ohgi, T. Fujihara, J. Terao, Y. Tsuji, *Inorg. Chim. Acta*, 2011, **368**, 237.
18. (a) O. M. N íDhubhghaill, J. Lennona and M. G. B. Drew, *Dalton Trans*., 2005, 3213; (b) P. Bhattacharyya, J. Parr and A. M. Z. Slawin, *J. Chem. Soc., Dalton Trans*., 1998, 3609; (c) A. Lombardi, O. Maglio, V. Pavone, B. Di Blasio, M. Saviano, F. Nastri, C. Pedone and E. Benedetti, *Inorg. Chim. Acta*., 1993, **204**, 87; (d) C. Schmidt, K. Polborn and W. Beck, *Chem. Ber*., 1992, **125**, 61.
19. H.-F. Klein, S. Camadanli, R. Beck, D. Leukel, and U. Fl örke, *Angew. Chem. Int. Ed.* 2005, **44**, 975.
20. (a) R. Munzenberg, P. Rademacher and R. Boese, *J. Mol. Struct*., 1998, **444**, 77; (b) W. S. Knowles, B. D. Vineyard, M. J. Sabacky, G. L. Bachmann and D. J. Weinkauff, *J. Am. Chem. Soc*., 1977, **99**, 5946.
21. (a) S. S. Zumdahl and R. S. Drago, *J. Am. Chem. Soc*., 1968, **90**, 6669 (b) W. L. Steffen and G. J. Palenik, *Inorg. Chem*., 1976, **15**, 2432.
22. R. Mart ín, M. Crespo, M. Font-Bardia and T. Calvet, *Polyhedron*, 2009, **28**, 1369.
23. (a) A. Crispini and M. Ghedini, *J. Chem. Soc., Dalton Trans*., 1997, 75; (b) C. Navarro-Ranninger, I. L ópez-Solera, A. Alvarez-Vald és, J. Rodriguez-Ramos, J. R. Masaguer, J. L. Garc á-Ruano and X. Solans, *Organometallics*, 1993, **12**, 4104.

Chapter 4

Phosphine Platinum(II) Complexes: Spectroscopic, Structural, Reactivity and Electrochemical Investigations of the Influence of Chelate Ligands

4.1 Introduction

For the cyclometallated palladium and platinum complexes, the tendency to break the metal-nitrogen bond upon reaction with phosphines has been taken as a metallacycle stability criterion.[1] It has been proposed for the cyclometallated platinum systems that coordination of a monodentate phosphine should displace the more labile dimethylsulfoxide (dmso) ligand, while the reaction with an excess of a monodentate phosphine or with bidentate phosphines may produce either cleavage of the metallacycle leading to monodentate [C] systems or extrusion of the chloride ligand giving an ionic derivative.[2] This can also be applied to the salicylaldiminato platinum complexes to determine the stability of the metal-containing ring. Therefore, a comparative analysis of the stability of metal-containing cycles of the analogous N^C and N^O complexes containing platinum was carried out.

On the other hand, bidentate phosphines can adopt various modes of coordination by using different molar ratios of phosphine to transition metal complexes. Among these diphosphine ligands, 1,1'-bis(diphenylphosphino)ferrocene (dppf) has been used extensively in many chelating, binuclear, and cluster complexes of transition metals.[3] In the present work, we have also studied the reactions of the dmso-ligated complexes **C1** – **C3** with 0.5 equiv of dppf.

This chapter describes the reactions of various phosphines with the dmso-ligated platinum complex bearing (benzylidene)(2,6-diisopropylphenyl)amine (**C1**) and its salicylaldiminato analogues (**C2** and **C3**). The phosphine-ligated complexes were characterized using a range of analytical and spectroscopic techniques, including ^{1}H-NMR, ^{2}D-COSY NMR, ^{2}D-HSQC-NMR, ^{13}C-NMR, ^{31}P-NMR, FTIR spectroscopy, mass spectrometry and elemental analysis. Single crystal X-ray structure determinations of selected complexes were also conducted. The influence of the (N^C) and (N^O) chelate ligands on these phosphorus derivatives has been compared in terms of both spectroscopy aspects and reactivity properties, including isomerization reactions, methylation reactions as well as cyclic voltammetry (CV) studies.

4.2 Results and Discussion

4.2.1 Reactions with phosphines

The reactions of triphenylphosphine with N^C and N^O complexes were studied and the resulting complexes are depicted in Scheme 4.1. When the (N^C) complex **C1** was reacted with triphenylphosphine in a 1:1 ratio in acetone at room temperature, its PPh_3 derivative **C4** was obtained. The *trans* arrangement of the PPh_3 and the imine is expected according to the *transphobia* effect [Scheme 4.1(A)].[2,4]

Under the same reaction conditions, two isomers **C5a** and **C5b**, with the PPh_3 ligand in a *cis* or *trans* arrangement, were isolated from (N^O) complex **C2a** or **C2b** reacting with PPh_3 [Scheme 4.1(B)]. **C5a** and **C5b** were isolated by chromatographic separation, and it is interesting to note that **C5b** is less polar than **C5a**, while their parent complexes **C2a** and **C2b** show opposite behaviour [Scheme 4.1(B)].

A different behaviour was observed in the case of the complex bearing the less sterically bulky N^O ligand, **C3**, as its reaction with PPh_3 (1:1) in acetone only gave the product **C6** with a *trans* arrangement of the PPh_3 and the imine [Scheme 4.1(C)]. In this case, the most stable compound is formed selectively. As revealed by the molecular structure of **C3**, the lack of the isopropyl substituents on the phenyl group attached to the nitrogen atom leads to the phenyl ring and the coordination plane being somewhat coplanarly distorted, *i.e.*, the angle between these two planes is $46.9(3)^{o}$ (see Section 3.2.1.5).

Complexes **C4** – **C6** did not react further with excess triphenylphosphine.

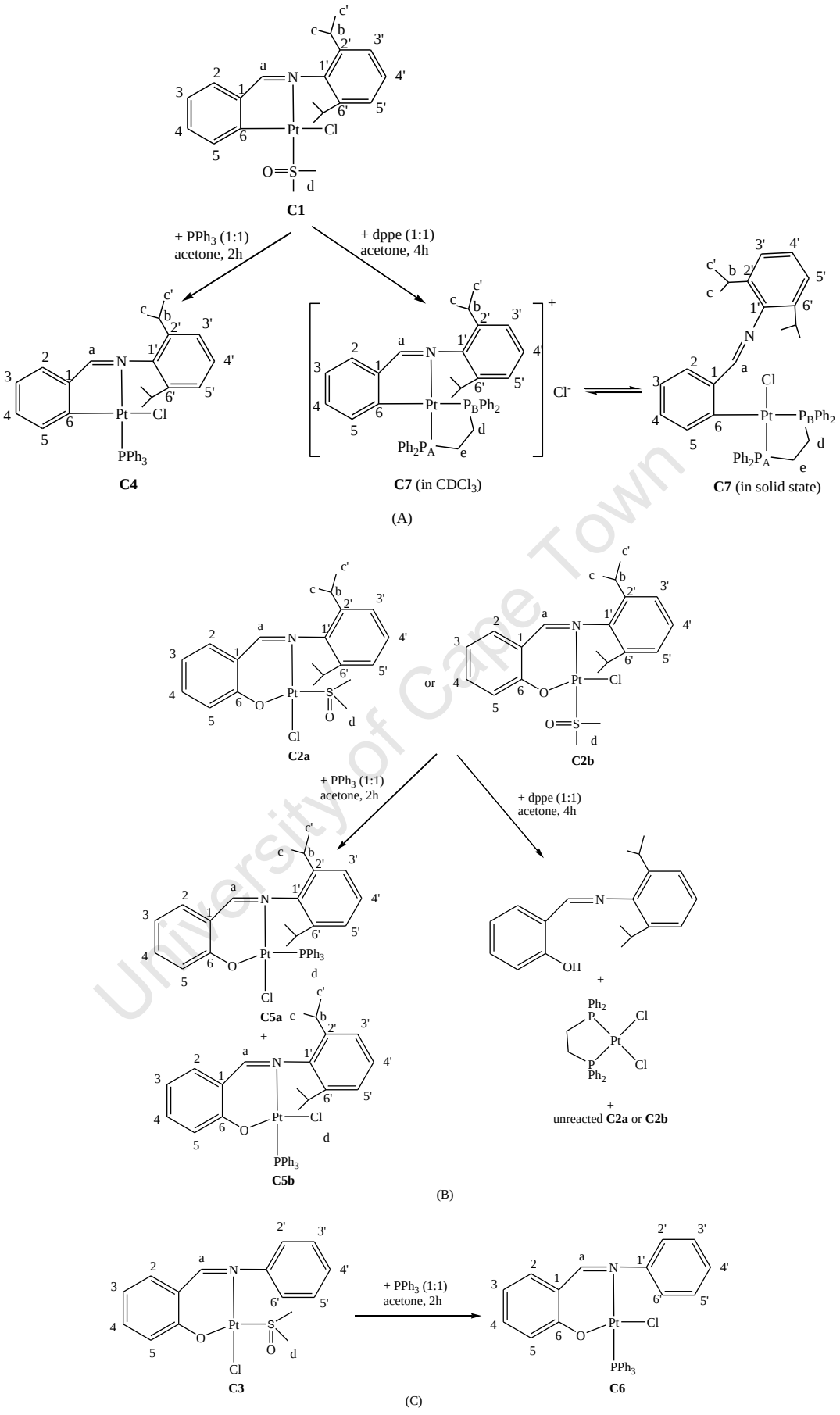

Scheme 4.1 Reactions of phosphines with the dmso ligated complexes **C1** – **C3**.

To study further the stability of metal-containing rings, the reactions of complexes **C1**, **C2a** and **C2b** with the bidentate ligand 1,2-bis(diphenylphosphino)ethane (dppe) were carried out (Scheme 4.1). Similar studies on cyclometallated platinum complexes with endo-cycles were previously reported, resulting in rather unstable ionic products in which both the imine and the diphosphine behave as bidentate ligands.[2,5] Work-up of the mother liquor from the reaction of **C1** and dppe (1:1) after 4 h rendered an intractable mixture which then yielded an off-white crystalline solid, **C7**, after recrystallization from acetone. A prolonged reaction time (16 h) resulted in a large amount of a white precipitate without the formation of **C7**. It is interesting to note that the off-white crystalline solid **C7** changed to a light yellow solution in a polar solvent such as dichloromethane. The ^{1}H and ^{31}P NMR spectra for **C7** recorded in $CDCl_3$, as well as the IR spectrum recorded in DCM, indicated the presence of the ionic species in solution. On the contrary, the IR spectrum recorded as a KBr pellet and the X-ray crystal structure of **C7** confirmed a neutral species in the solid state in which the imine nitrogen does not bond to the platinum centre [Scheme 4.1(A)].

Similar reactions of **C2a** or **C2b** yielded a large amount of a white precipitate which consisted of $[PtCl_2(dppe)]$, unreacted parent precursor and free (N^O) ligand as the only identifiable products in solution [Scheme 4.1 (B)]. A literature search showed that similar reactions on (N^O) platinum complexes have not been reported. The only related example was that reported by Capapé *et al.*[2] on the reactions of cyclometallated platinum complexes having exo-cycles with an excess of PPh_3. These authors reported that from this reaction, $[PtCl_2(PPh_3)_2]$ and free ligand were found to be the only identified products. The authors suggested that such a complete dissociation process of the nitrogen ligand could be due to the instability of the exo-platinacycle. This could be also applicable to our reactions. The dissociation of the nitrogen ligand of **C2a** and **C2b** upon the reaction with dppe points to a higher lability of the Pt-N bond in the metal-containing (N^O) ring compared to that for the (N^C) ring.

The reactions of the *trans* complexes **C1** and **C2b** with dppf (2:1) in dichloromethane at room temperature gave the diplatinum(II) complexes $[Pt_2Cl_2(N^C)_2(\mu\text{-dppf})]$ **C8** and $[Pt_2Cl_2(N^O)_2(\mu\text{-dppf})]$ **C9**, respectively, in good yields [Scheme 4.2(A)]. In **C8** and **C9** two individual organoplatinum(II) units were combined in one molecular system by a dppf spacer ligand. Single crystals of complex **C8** were obtained. To the best of our knowledge, diplatinum(II) complexes containing a bridging dppf unit are not common.[6,7] There is only

one X-ray structural determination of a related diplatinum complex having an "open bridge" dppf ligand in the literature,[6] although crystal structures of some other related transition metal complexes have been reported.[8]

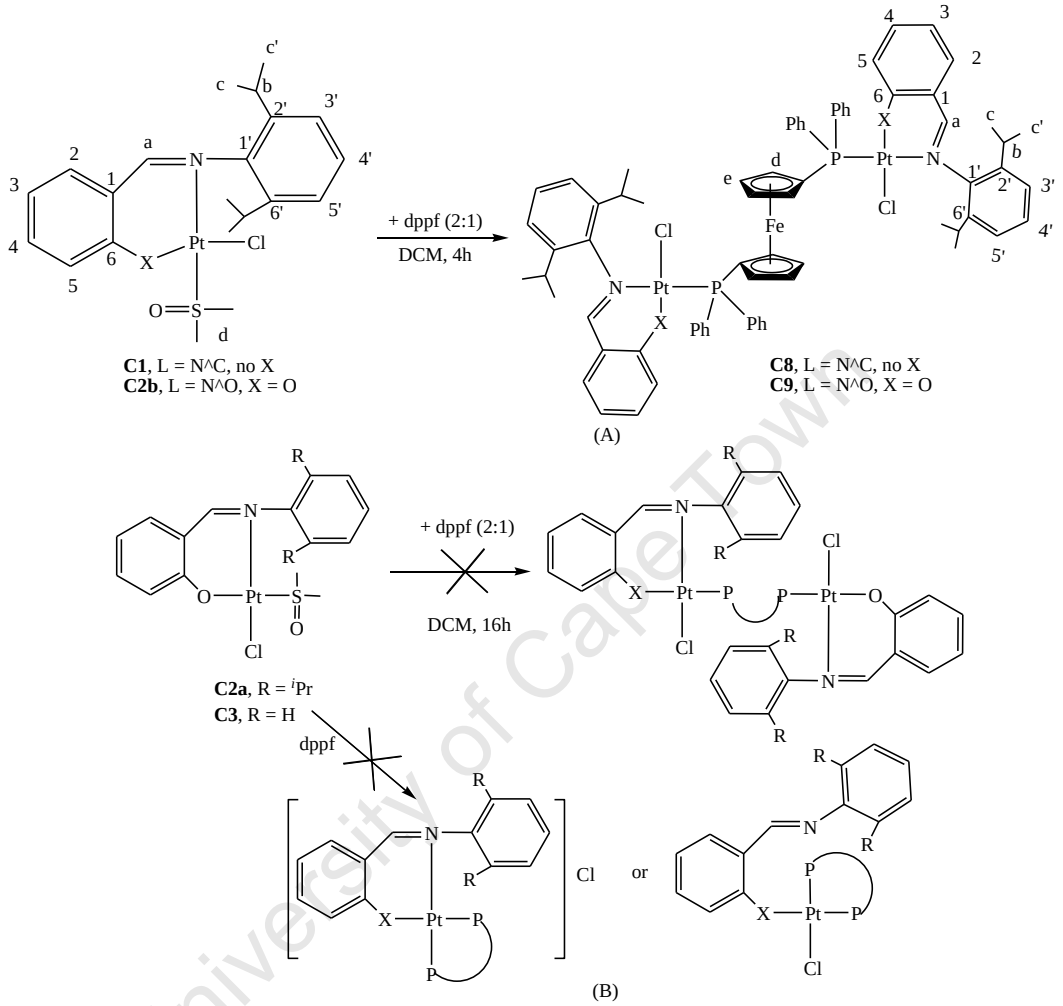

Scheme 4.2 Reactions of dppf with the dmso ligated complexes **C1** – **C3**.

Attempts to obtain similar complexes to the diplatinum(II) complex **C9** from the *cis* complexes **C2a** and **C3** under the same reaction conditions were not successful [Scheme 4.2(B)]. This could be due to the undesirable steric bulkiness dictated by the environment around the metal centre in the involved complexes, in which the dmso group is *cis* to the imine, and consequently prevents the dppf from behaving as a spacer ligand. Based on the cyclometallated platinum systems reported by Capapé *et al.*[2] and Jamali *et al.*,[7] one might expect that if the dppf did not behave as a spacer ligand, then it could be a bidentate ligand to produce either cleavage of the Pt-N bond leading to monodentate [O] systems or extrusion of the chloride ligand giving a mononuclear cationic complex. However, the formation of the

possible dppf chelating complexes was not observed. It is worth noting that the complete dissociation of the (N^O) ligand was also not observed even after prolonged reaction times. The starting complex and free dppf were the only two species which could be indentified in the reaction mixture.

The PPh_3 derivatives **C4** – **C6** are obtained as bright yellow crystalline solids after recrystallization from DCM/MeOH. The dppe-chelating complex **C7** is an off-white crystalline solid, while the diplatinum(II) complexes with a dppf spacer, **C8** and **C9**, are orange solids. It is shown in Table 4.1, that replacing the dmso group by phosphine ligands enhance the thermal stability of the platinum(II) complexes except in the case of the dppf derivative **C8**. The PPh_3 derivatives with *trans* geometry (where the PPh_3 group is *trans* to the imine) are more thermally stable than those with *cis* geometry, which is similar as their dmso precursors. All these complexes were characterized by microanalysis, mass spectrometry, IR and NMR spectroscopies. These complexes were also characterized crystallographically.

Table 4.1 Melting points (m.p.) of platinum(II) complexes containing N^C or N^O chelate ligands

Chelate	N^C (**L_A**)				N^O (**L_B**)				N^O (**L_C**)		
L	dmso	PPh_3	dppe	dppf	dmso		PPh_3		dppf	dmso	PPh_3
Complex	**C1**	**C4**	**C7**	**C8**	**C2a**	**C2b**	**C5a**	**C5b**	**C9**	**C3**	**C6**
M.p. (^oC)	194-196	302-304	320-323	184-187	164-167	193-196	210-214	236-239	281-285	170-172	210-212

4.2.1.1 IR spectroscopy and mass spectrometry

As shown in Table 4.2, the $\nu_{C=N}$ stretching vibration bands of the (N^C) complexes with phosphine ligands, **C4** and **C8**, are almost identical to their dmso precursor **C1**. Replacing the dmso group by phosphines was confirmed by the disappearance of the band at 1138 cm^{-1} (due to the $\nu_{S=O}$ stretching vibration of dmso) and the appearance of strong absorption bands at 1434 cm^{-1} (due to the C-P bond). Similar trends were observed in the IR spectrum of the N^O complexes.

Table 4.2 Selected spectroscopic data (^{1}H, ^{13}C, and ^{31}P NMR, IR, MS) for phosphine ligated complexes **C4** – **C9**

Complex	Formula	[ii] IR / cm^{-1}	$[M]^+$ / *m/z*	^{1}H-NMR		^{13}C-NMR		^{31}P-NMR
		$\upsilon_{C=N}$	(calc.)	H^{a}	H^{5}	C^{a}	C^{5}	
C4	$C_{37}H_{37}ClNPPt$	1599	[iii] 721.22 (721.75)	8.28 (d, $J_{P\text{-}H}$ = 9.3 Hz, $J_{Pt\text{-}H}$ = 90.5 Hz)	6.55 (dd, 7.65, 2.35 Hz, $J_{Pt\text{-}H}$ = 43.08 Hz)	179.98 (d, $J_{P\text{-}C}$ = 3.22 Hz, $J_{Pt\text{-}C}$ = 85.13 Hz)	136.97 (d, $J_{P\text{-}C}$ = 5.68 Hz, $J_{Pt\text{-}C}$ = 85.41 Hz)	21.79 ($J_{Pt\text{-}P}$ = 4271 Hz)
C5a[i]	$C_{37}H_{37}ClNOPPt$	1607	[iv]774.2 (774.21)	7.61 (s)	7.19 (d, 8.76Hz)	163.94 (s)	122.05 (s)	-2.14 ($J_{Pt\text{-}P}$ = 4064 Hz)
C5b	$C_{37}H_{37}ClNOPPt$	1610	[iv] 774.2 (774.21)	8.06 (d, $J_{P\text{-}H}$ = 13.9 Hz)	6.31 (dd, 8.57, 0.49 Hz)	160.48 (s)	121.10 (s)	8.87 ($J_{Pt\text{-}P}$ = 3819 Hz)
C6[i]	$C_{31}H_{25}ClNOPPt$	1608	[iv] 689.10 (689.04)	8.20 (d, $J_{P\text{-}H}$ =13.4 Hz)	6.16 (d, 8.62 Hz)	160.89 (s)	121.86 (s)	7.40 ($J_{Pt\text{-}P}$ = 3869 Hz)
C7	C45H46ClNP2Pt	KBr: 1631 DCM: 1602	[iii] 857.28 (857.28)	8.28 (d, $J_{P\text{-}H}$ = 8.1 Hz, $J_{Pt\text{-}H}$ = 83.8 Hz)	6.98 – 6.88 (m)	184.92 (s)	138.51 (d, $J_{P\text{-}C}$ = 3.19 Hz, $J_{Pt\text{-}C}$ = 90.59 Hz)	43.30 (P_B) (s, $J_{Pt\text{-}P}$ = 1901 Hz) 39.65 (P_A) (s, $J_{Pt\text{-}P}$ = 3711 Hz)
C8	$C_{72}H_{72}Cl_2FeN_2P_2Pt_2$	1604	[iii]1508.4 (1508.76)	8.17 (d, $J_{P\text{-}H}$ = 9.5 Hz, $J_{Pt\text{-}H}$ = 82.7 Hz)	6.45 (dd, 7.92, 2.31 Hz)	179.47 (d, $J_{P\text{-}C}$ = 3.07 Hz, $J_{Pt\text{-}C}$ = 79.31 Hz)	137.36 (d, $J_{P\text{-}C}$ = 4.36 Hz, $J_{Pt\text{-}C}$ = 92.23 Hz)	9.42 ($J_{Pt\text{-}P}$ = 4239 Hz)
C9	$C_{72}H_{72}Cl_2FeN_2O_2P_2Pt_2$	1610	[iii]1540.4 (1540.76)	8.03 (d, $J_{P\text{-}H}$ = 9.5 Hz)	6.14 (d, 8.60 Hz)	160.68	120.98	1.98 ($J_{Pt\text{-}P}$ = 3851 Hz)

[i] L is *cis* to N atom (L = PPh_3)
[ii] Recorded as KBr pellets.
Represents *m/z* for the highest molecular weight fragment: [iii] $[M\text{-}Cl]^+$; [iv] $[M+H]^+$.

It is notable that the $\nu_{C=N}$ stretching vibration band of the dppe complex **C7**, which appears at 1602 cm^{-1} in dichloromethane (DCM), is consistent with that observed for the PPh_3 analogue **C4**. This confirms the coordination of the imine nitrogen to the platinum centre. However, the IR spectrum recorded as a KBr pellet showed a higher frequency for the $\nu_{C=N}$ band at 1631 cm^{-1}. This is similar to that of the free ligand ($\mathbf{L_A}$) and indicates that the imine nitrogen is not coordinated to the metal centre (Figure 4.1).

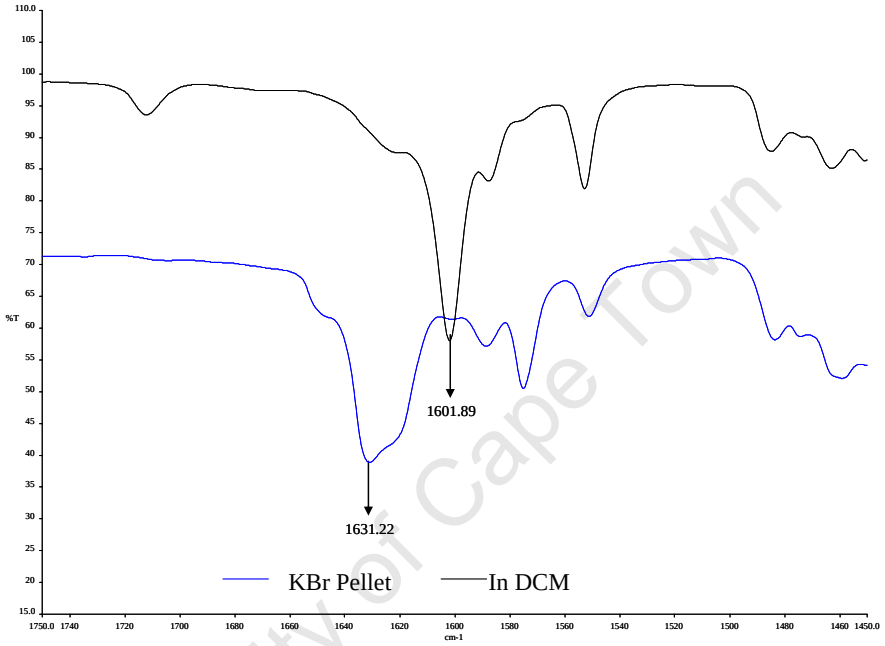

Figure 4.1 IR spectra for the (N^C) complex bearing the dppe ligand **7**.

Microanalysis and mass spectrometry confirmed the proposed structures for complexes **C4** – **C9**. The mass spectral data for complexes **C4** and **C6** – **C8** showed $[M - Cl]^+$ as the highest molecular weight fragment, while complexes **C5a** and **C5b** gave $[M]^+$ as the highest molecular weight fragment (Table 4.1). Both complexes show peaks which correspond to the sodium adduct of a dimeric species $[2M + Na]^+$. The sodium adduct of the parent ion was also observed for complex **C4** as $[M + 2Na]^+$ and for the dppf derivatives **C8** and **C9** as $[M + Na]^+$.

4.2.1.2 NMR spectroscopy

Selected ^1H NMR chemical shifts of the PPh_3-containing complexes **C4** – **C6**, the dppe derivative **C7** and the diplatinum(II) complexes with a dppf spacer ligand **C8** and **C9** are shown in Table 4.2. The assignments of the observed resonances were confirmed by 2D-COSY NMR.

By replacing the dmso group with PPh_3, all the imine protons (H^a) of the complexes with *trans* geometry (where PPh_3 is *trans* to the imine) were observed in the region δ 8.03 – 8.28 ppm. The increase of the covalency from S-donor to P-donor renders the platinum centre more electron rich. This increased electron density on the metal can then be transferred toward the N=C group and the phosphine ligand. The extent of this back bonding is dependent on the π-acceptor strength of the ligands. Since the N-donor centre has almost exclusive σ-donating properties whereas the P-donor centre can have both electron-donating and electron-accepting character,[9] back-bonding from platinum into low lying empty phosphorus-based orbitals is more pronounced. This reduces the back-bonding from platinum to the imine group and slightly elongates the Pt-N bonds (see Section 4.2.2.5), consequently causing the downfield shift of 0.08 – 0.37 ppm with respect to their dmso precursors. In the case of the phosphine derivatives with (N^C) ligand, **C4** and **C8**, the imine protons were coupled to platinum with lower values (82.7 - 90.5 Hz) than that of the parent compound **C1**. For the (N^O) analogues **C5a**, **C5b**, **C6** and **C9**, however, no coupling of the imine proton with the ^{195}Pt nuclei was observed. Similar observations have been reported in the literature for related platinum complexes.[10] In the ^1H-NMR spectrum of **C5a** the chemical shift of the imine proton moved to higher field and appeared as a singlet, while doublets were observed for the *trans* complexes **C5b** and **C6**, indicating a *cis* geometry of **C5a**.

For the *trans* complexes **C4**, **C5b**, **C6** and **C8** - **C9**, another salient feature observed in ^1H-NMR spectra was the chemical shift of the aromatic proton H^5, which moved up-field to the region 6.14 – 6.55 ppm compared to their dmso precursors, which were found in the range 6.64 – 8.31 ppm. This has been ascribed to the anisotropic shielding effect of the aromatic ring current that a phenyl group in PPh_3 has on the H^5 proton pointing toward it.[11] Similar behaviour was not observed for the *cis* complex **C5a**. In the N^C complexes **C4** and **C8**, the resonances of H^5 were obtained as a doublet of doublets (dd) with a $^4J_{Pcis\text{-}H}$ value of 2.3 Hz. In the case of the N^O complexes, however, no coupling of H^5 with the ^{31}P nucleus was observed.

The ^1H NMR spectrum for the dppe chelating complex **C7** [Figure 4.2(A)] was recorded in $CDCl_3$ and showed that the imine proton (H^a) appears as a doublet at 8.28 ppm with a $^4J_{P\text{-}H}$ of 8.1 Hz and Pt satellites ($^3J_{Pt\text{-}H}$ = 83.8 Hz). This is in very good agreement with what is found for the PPh_3 analogue, **C4**, and confirms the coordination of the imine nitrogen to the

platinum centre. This is also consistent with the $\nu_{C=N}$ stretching vibration recorded in DCM at 1601 cm^{-1} due to the coordination of N to the Pt centre. The ^1H resonances of the methyl protons of the isopropyl moieties ($H^{c/c'}$) exhibit two broad peaks (0.4 – 1.2 Hz) at room temperature [Figure 4.2(A)].

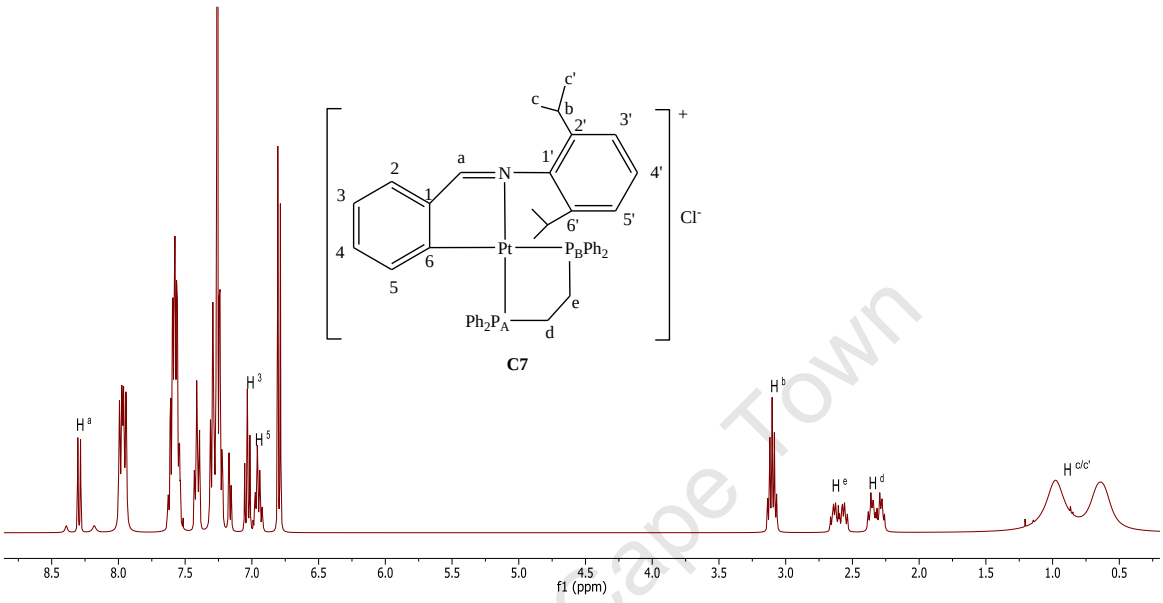

(A)

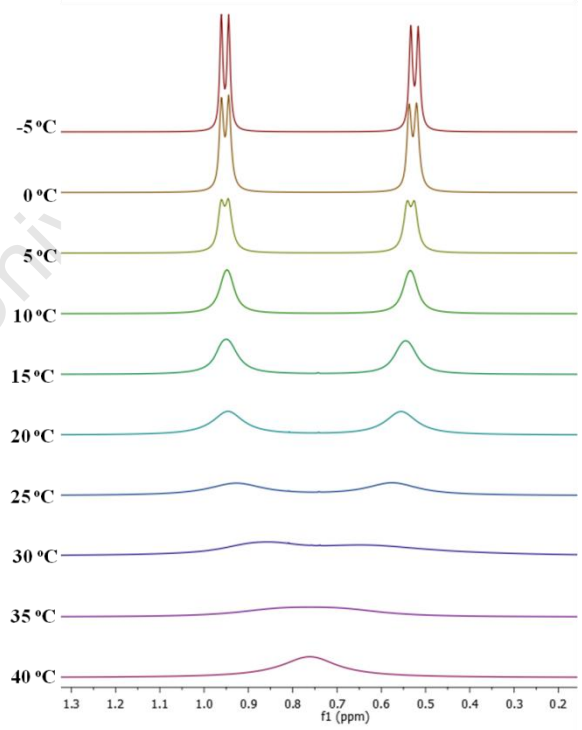

(B)

Figure 4.2 (A) The ^1H NMR spectrum for the dppe chelating complex **C7**. (B) The array of ^1H NMR spectrum of **C7** depicting the ^{i}Pr region ($H^{c/c'}$) in the temperature range from -5 to 40 ^oC.

We examined the fluxional behaviour of **C7** by conducting a dynamic ^{1}H NMR study at various temperatures. We screened the temperature range from -50 to 40 ^{o}C in $CDCl_3$ solution. The variable-temperature ^{1}H NMR spectrum of **C7** showed that the proton peaks assigned to the two methyl groups in each isopropyl moiety ($H^{c/c'}$) exhibit a typical two-site exchange dynamic behaviour as shown in Figure 4.2 (B). The dppe complex **C7** is fluxional in solution above 35 ^{o}C. The low-temperature spectrum (0 ^{o}C and lower) shows two doublets at 0.95 and 0.53 ppm. Warming the sample results in the broadening of the resonance peaks with coalescence at 35 ^{o}C. Above 40 ^{o}C a single resonance at the fast-exchange limit is observed at 0.76 ppm. The observed interchange of H^{c} and $H^{c'}$ indicates a free rotation of the isopropyl groups.

The ^{13}C-NMR spectra of **C4** – **C9** gave the expected number of signals and selected chemical shifts are shown in Table 4.2. In the ^{13}C-NMR spectra for the N^C complexes **C4** and **C8**, the imine carbon (C^{a}) and the aromatic carbon adjacent to the metallation site (C^{5}) appear as doublets and are coupled to platinum ($J_{Pt\text{-}C5}$ *ca.* 80 – 85 Hz and $J_{Pt\text{-}Ca}$ *ca*. 85 – 92 Hz, respectively). The aromatic carbon (C^{5}) for the dppe chelating complex **C7** also appears as a doublet at 138.51 ppm with a $J_{Pt\text{-}C}$ coupling constant of 90.6 Hz. This is consistent with the N^C analogues **C4** and **C8**. However, the resonance of its imine carbon exhibits an upfield singlet (184.92 ppm) compared to **C4** and **C8** (179.98 and 179.47 ppm, respectively).

Compared to their dmso precursors, no significant shifts in ^{13}C resonances were observed for the phosphine complexes bearing N^O ligands. The differences between the *cis*/*trans* isomers **C5a** and **C5b** in their ^{13}C spectra are consistent with the trends observed for their dmso precursors.

The ^{31}P NMR spectra show singlets for the platinum(II) complexes containing the PPh_3 group, **C4** – **C6**, with resolved coupling to ^{195}Pt. The phosphorus atom of the N^C complex **C4** reveals a much lower-field chemical shift ($\Delta\delta$ = 21.79 ppm) compared to the N^O analogues, presumably due to the deshielding effect caused by the O atom. With the N^O chelates $\mathbf{L_B}$, the *cis* isomer **C5a** shows an even higher-field shift ($\Delta\delta$ = -2.14 ppm) compared to its *trans* isomer **C5b** ($\Delta\delta$ = 8.87 ppm), suggesting that the *cis* arrangement of the oxygen atom and the imine nitrogen enhances the shielding effect.

Two sets of resonances with J_{Pt-P} values of 3711 and 1902 Hz were observed in the ^{31}P NMR spectrum for the complex with the dppe chelating ligand **C7**, due to two non-equivalent phosphorus atoms. The higher *J* value is assigned to the phosphorus atom *trans* to the imine and the lower to that *trans* to the metallated carbon, which is in agreement with the reported values for related complexes.[2,5,12] The J_{PA-PB} coupling was not observed in either complex **C7** or the reported analogous complexes, probably due to the ionic nature of the complex in polar solvents.

In the ^{31}P NMR spectra of the binuclear complexes $[Pt_2Cl_2(N\text{^}X)(\mu\text{-dppf})]$ (X = C, O), **C8** and **C9**, the observation of sharp singlets for each of the analogues at chemical shifts of 9.42 ppm and 1.98 ppm, respectively, was accompanied by Pt satellites. This confirms that the two PtCl(N^X) moieties, joined together by the dppf spacer ligand, are equivalent. The chemical shift of the P atoms in **C8** and **C9** appeared at higher field compared to the PPh_3-containing mononuclear complexes **C4** and **C5b**, due to the electron rich ferrocenyl moiety in the spacer ligand.

The coupling constant $^1J_{M-P}$ is a characteristic property of the metal phosphorus σ bond in phosphorus coordination compounds.[13] The platinum phosphine coupling constants, $^1J_{Pt-P}$, were measured in complexes **C4** – **C9**. For the N^C complexes, the $^1J_{Pt-P}$ values vary from 4270 Hz in **C1** to 4239 Hz in **C8**, consistent with a phosphine ligand positioned *trans* to nitrogen.[2,5,14,15] For the N^O analogues, the $^1J_{Pt-P}$ coupling constants were measured as 4062 Hz in the *cis* complex **C5a** and *ca.* 3850 Hz in the *trans* complexes **C5b**, **C6** and **C9** (see Table 4.2), which are of the order of magnitude expected for P *trans* to an O atom.[10,12,16] The magnitude of $^1J_{Pt-P}$ coupling constants is a measure of the strength of the Pt-P σ bonding.[13] Thus the lower values for the N^O complexes with *trans* geometry **C5b**, **C6** and **C9** are indicative of a weakening of the Pt-P σ bonding compared to the *cis* **C5a** and N^C analogues **C4** and **C8**. Interestingly, there is a *ca.* 6% increase in the ^1J for the *cis* isomer **C5a** over its *trans* isomer **C5b**, probably due to a higher *trans* influence of the imine nitrogen compared to that of the coordinated oxygen, which weakening the Pt-P σ bonding in **C5b** as a consequence. The differing $^1J_{Pt-P}$ values of 3711 and 1902 Hz in the dppe chelating complex **C7** are due to the *trans* influence of the metallated C atom being much greater than that of the imine nitrogen.

4.2.1.3 Crystal structures

Suitable crystals were grown from dichloromethane/methanol at low temperature (*ca.* 4 ^{o}C) (**C4**, **C5a** and **C5b**), or by slowly evaporating dichloromethane/n-hexane (**C8**) or acetone (**C7**) solutions of complexes. The labelling schemes for all the compounds are in Figures 4.3 – 4.6. All crystals consist of discrete molecules, separated by normal van der Waals distances. Selected interatomic distances and angles are listed in Tables 4.3 – 4.4. A full list of bond lengths and angles, as well as the X-ray data collection parameters (data sets 5 – 9) and CIF files can be found in supporting information.

All the molecular structures exhibit distortions from idealized square-planar geometry at the metal, due to the bulky phosphine group and the small bite angle of the chelating ligands. These structures fall into two distinct categories, the first group consisting of **C4**, **C8**, **C5a** and **C5b**, which contain a monodentate phosphine donor, while the second category, of which **C7** is an example, contains a bidentate phosphine donor set. As is apparent from Figures 4.3 – 4.5, in the first category with N^C or N^O chelating ligands, the four coordinate environment is completed by one P atom and one Cl atom. Complexes **C4**, **C5a** and **C5b** are mononuclear species, while complex **C8** has a crystallographic two-fold symmetry and sits astride a two-fold axis, making only one-half of the complex unique. Two planes containing a Pt atom are connected via the dppf ligand. The P atom occupies the *trans* position to the N atom in **C4**, **C8** and **C5b**, but a position *trans* to the O atom in **C5a**.

In the first category, the chelating N^C or N^O bite angles and other bond angles in the phosphine complexes **C4**, **C8**, **C5a** and **C5b** are very similar to those of their dmso precursors. In all cases, the sum of angles around platinum is *ca*. 360^{o}, and the metal-containing ring (plane 1) adopts practically a planar arrangement. Plane 1 is nearly coplanar with the mean coordination plane (plane 2). Again, a nearly facial orientation of the 2,6-diisopropylphenyl ring (plane 3) to plane 1 is observed in all first category complexes.

For the binuclear complex **C8**, the Cp(centroid)-Fe-Cp(centroid) twist angle of the dppf ligand is 143^{o} (the angle has been determined as the torsion angle C32-Cp(centroid)1-Cp(centroid)2-C32A), so the dppf is arranged in a nearly ideal "anticlinical eclipsed" conformation[h].[17] This is in agreement with related platinum[7] and palladium[18] complexes.

[h] The ideal torsion angle for the "anticlinal eclipsed" conformation is 144^{o}.

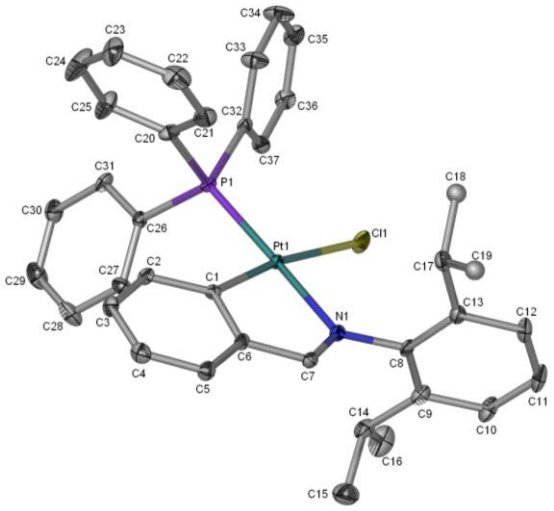

Figure 4.3 Molecular structure of **C4** showing the atomic labelling scheme. All H atoms are omitted for clarity. All non-hydrogen atoms, except C18 and C19, are presented as an ellipsoidal model with probability level 30%. The solvent molecules (methanol and ethanol) are excluded.

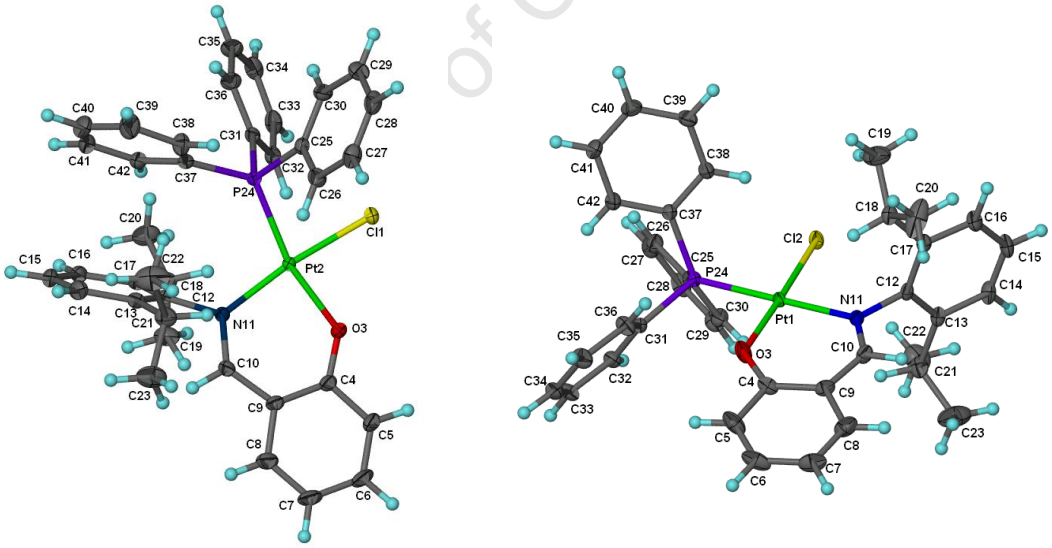

C5a **C5b**

Figure 4.4 Molecular structures of **C5a** and **C5b** showing the atomic numbering scheme. All non-hydrogen atoms are presented as an ellipsoidal model with a probability level of 40%. The solvent molecules have been omitted in this diagram.

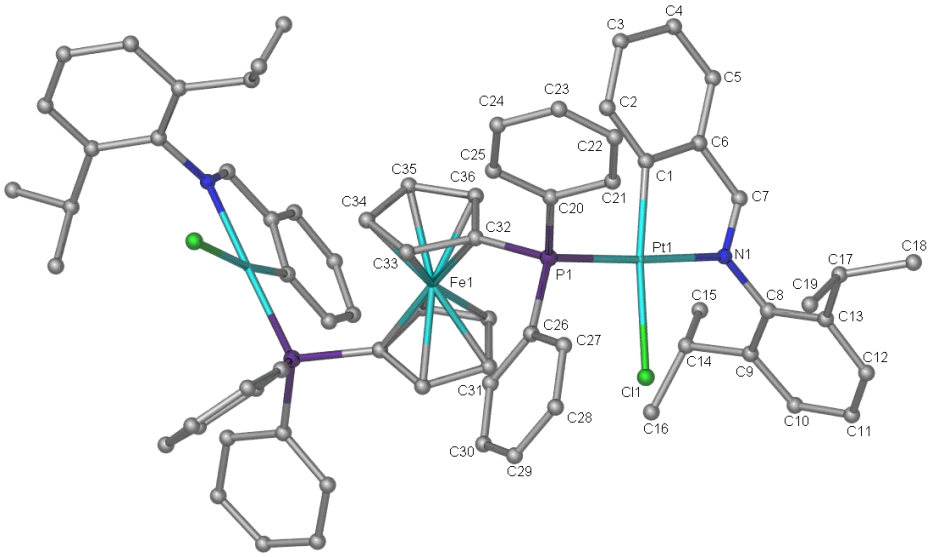

(A)

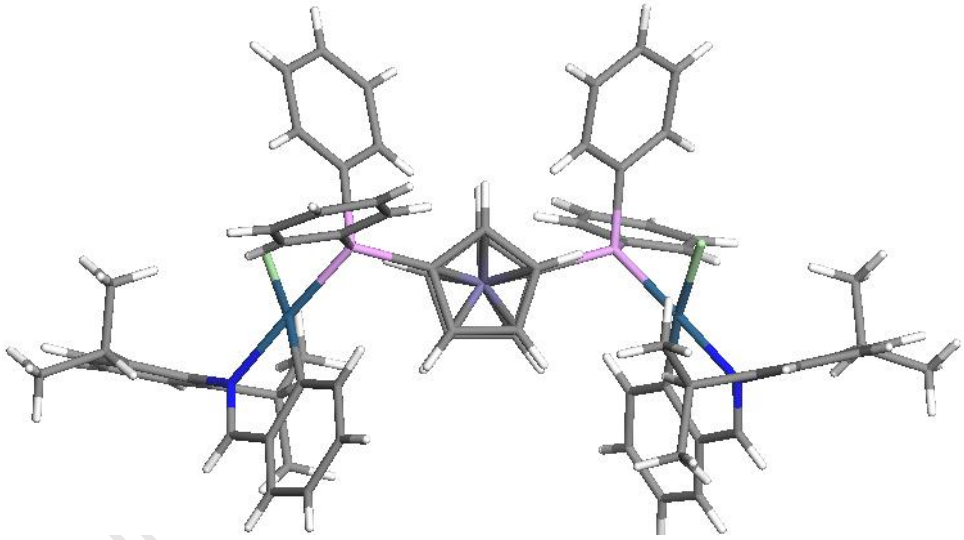

(B)

Figure 4.5 (A) Molecular structure of **C8** showing the atomic numbering scheme. All non-hydrogen atoms are presented as an ellipsoidal model with probability level 30%. The H atoms are omitted for clarity [symmetry operator for the unlabeled atoms: -x+1, y, -z+0.5]. (B) Conformation of the cyclopentadienyl rings of the ferrocene moiety in complex **C8**. The diagram highlights the relative dispositions of the five-membered rings as well as the relative orientations of the platinum atoms in the structure.

Table 4.3 Selected bond lengths (Å), bond angles (°) and torsion angles (°) for complexes **C4, C5a**, **C5b** and **C8**

C4		**C8**		**C5a**[i]		**C5b**	
Pt(1)–C(1)	2.013(6)	Pt(1)–C(1)	2.005(9)	Pt(2)–O(3)	2.042(3)	Pt(1)–O(3)	2.001(2)
Pt(1)–N(1)	2.098(5)	Pt(1)–N(1)	2.077(8)	Pt(2)–N(11)	2.021(3)	Pt(1)–N(11)	2.0707(19)
Pt(1)–P(1)	2.2334(15)	Pt(1)–P(1)	2.231(2)	Pt(2)–P(24)	2.2586(9)	Pt(1)–P(24)	2.2566(7)
Pt(1)–Cl(1)	2.3630(15)	Pt(1)–Cl(1)	2.364(2)	Pt(2)–Cl(1)	2.3174(9)	Pt(1)–Cl(2)	2.2993(8)
N(1)–C(7)	1.273(8)	N(1)–C(7)	1.287(13)	N(11)–C(10)	1.301(5)	N(11)–C(10)	1.297(3)
C(1)-Pt(1)-N(1)	80.4(2)	C(1)-Pt(1)-N(1)	80.3(3)	O(3)-Pt(2)-N(11)	90.57(12)	O(3)-Pt(1)-N(11)	91.75(8)
C(1)-Pt(1)-P(1)	95.94(18)	C(1)-Pt(1)-P(1)	97.2(3)	O(3)-Pt(2)-P(24)	165.90(9)	O(3)-Pt(1)-P(24)	87.73(6)
N(1)-Pt(1)-Cl(1)	90.62(15)	N(1)-Pt(1)-Cl(1)	90.7(2)	N(11)-Pt(2)-Cl(1)	172.38(9)	N(11)-Pt(1)-Cl(2)	91.10(7)
P(1)-Pt(1)-Cl(1)	93.12(6)	P(1)-Pt(1)-Cl(1)	91.87(8)	P(24)-Pt(2)-Cl(1)	85.95(3)	P(24)-Pt(1)-Cl(2)	89.45(2)
N(1)-Pt(1)-P(1)	175.77(15)	N(1)-Pt(1)-P(1)	177.4(2)	N(11)-Pt(2)-P(24)	103.50(9)	N(11)-Pt(1)-P(24)	178.90(5)
C(1)-Pt(1)-Cl(1)	170.171(18)	C(1)-Pt(1)-Cl(1)	170.8(3)	O(3)-Pt(2)-Cl(1)	82.01(9)	O(3)-Pt(1)-Cl(2)	176.92(6)
Total 1[ii]	360.1	Total 1[ii]	360.2	Total 1[ii]	360.0	Total 1[ii]	360.0
C(1)-Pt(1)-N(1)	80.4(2)	C(1)-Pt(1)-N(1)	80.3(3)	O(3)-Pt(2)-N(11)	90.57(12)	O(3)-Pt(1)-N(11)	91.75(8)
C(7)-N(1)-Pt(1)	113.7(4)	C(7)-N(1)-Pt(1)	114.4(6)	C(10)-N(11)-Pt(2)	122.5(3)	C(10)-N(11)-Pt(1)	122.5(2)
C(6)-C(1)-Pt(1)	112.6(4)	C(6)-C(1)-Pt(1)	113.3(6)	C(4)-O(3)-Pt(2)	127.3(3)	C(4)-O(3)-Pt(1)	127.2(2)
C(1)-C(6)-C(7)	114.6(6)	C(1)-C(6)-C(7)	114.0(9)	O(3)-C(4)-C(9)	123.6(4)	O(3)-C(4)-C(9)	125.2(3)
N(1)-C(7)-C(6)	118.7(6)	N(1)-C(7)-C(6)	118.0(9)	C(4)-C(9)-C(10)	123.0(3)	C(4)-C(9)-C(10)	124.5(2)
				N(11)-C(10)-C(9)	130.4(4)	N(11)-C(10)-C(9)	128.7(2)
Total 2[iii]	540.2	Total 2[iii]	540.3	Total 2[iii]	717.5	Total 2[ii]	720.0
N(1)-Pt(1)-C(1)-C(2)	-175.5(7)	N(1)-Pt(1)-C(1)-C(2)	-178.6(9)	Pt(2)-O(3)-C(4)-C(5)	-169.1(3)	Pt(2)-O(3)-C(4)-C(5)	-173.97(15)
Pt(1)-N(1)-C(8)-C(13)	92.3(6)	Pt(1)-N(1)-C(8)-C(13)	-95.4(10)	Pt(2)-N(11)-C(12)-C(13)	108.0(3)	Pt(1)-N(11)-C(12)-C(13)	-94.70(19)

[i] L is *cis* to N atom (L = PPh3)
[ii] Sum of angles in the coordination environment of the platinum atom.
[iii] Sum of internal angles of the metal-containing ring

As expected, there is slight lengthening of the Pt-N bonds in the range of 0.023 – 0.042 Å for the *trans* compounds **C4**, **C8** and **C5b** as compared to their dmso precursors **C1** and **C2b**, due to the higher *trans* effect of the P-donor ligand compared to the S-donor ligand.[19] The lengthening of the Pt-N distances agrees with the down-field shift of the imine proton in the ^{1}H NMR spectra for these complexes. The Pt-Cl bond lengths for complex **C4** – **C8** are found to decrease in the sequence: Pt-Cl(1)$_{trans\text{-}C}$ [2.3630(15) Å] in **C4** ≈ Pt-Cl(1)$_{trans\text{-}C}$ [2.364(2) Å] in **C8** > Pt-Cl(1)$_{trans\text{-}N}$ [2.3174(9) Å] in **C5a** > Pt-Cl(1)$_{trans\text{-}O}$ [2.2993(9) Å] in **C5b**. This again reflects the decrease in the *trans* influence in the order: aryl carbon atom > imine nitrogen atom > phenoxy oxygen atom,[20,21] consistent with the dmso precursors. The similar Pt-Cl distances in the N^C complexes **C4** and **C8** indicate that this parameter is not affected by the nature of the phosphorus ligands. The same observation was reported in other platinum complexes with phosphorus ligands.[13] Furthermore, it is noteworthy that a shortening of the N-C bond lengths is found in the N^C complexes **C4** and **C8** as compared to the parent complex **C1**. These N-C bond lengths are close to the uncoordinated N-C bond in complex **C7** as shown in Figure 4.6. Intermolecular interactions such as hydrogen bonding or π-stacking do not exist in these complexes.

The platinum atom in complex **C7** is surrounded by a chelating dppe, C and Cl atoms. This reveals that the strong chelating ability of dppe has forced the Pt-N bond of the cyclometallated ligand to cleave, forming the neutral complex with a monodentate η^1-C-bond to the platinum centre in the solid state. As shown in Table 4.4, in the structure of **C7** the angles around the platinum centre are rather close to the ideal angle of 90^o. The dppe chelate ring has P-Pt-P bond angle of 86.88(3)^o which is a result of the limited flexibility of the five-membered ring. Similar values were found in other platinum dppe complexes.[19] The metal-containing ring (plane 1) adopts a practically planar arrangement as the sum of the internal bond angles is found to be 540.3^o. The imine nitrogen atom is not coordinated to the platinum centre. The Pt-P(2) length of 2.3120(7) Å at the *trans*-position to a C atom is significantly longer than the Pt-P(1) distance of 2.2193(7) Å at the *trans* position to a Cl atom, indicating that the N-C-κ^1*C* ligand exerts a higher *trans* influence than the chloride ligand.[7] The Pt-C$_{trans\text{-}P}$ distance of 2.073(3) Å in **C7** is much longer than the Pt-C$_{trans\text{-}Cl}$ distances in the dmso precursor **C1** (2.011(5) Å) or the phosphine-containing N^C complexes **C4** (2.013(6) Å) and **C8** (2.005 Å), attributable to the strong *trans*-influence of a P atom in comparison with a Cl atom.[20]

In contrast, the NMR-predicted structure of **C7** in $CDCl_3$ suggests that both the imine and dppe behaved as bidentate ligands giving an ionic complex (see Section 4.2.2.3). In this case the polar solvent played an important role to initiate extrusion of the chloride ligand and to re-form the Pt-N bond. This explains the observation of different IR spectra obtained depending on whether the spectrum is recorded in solution or in the solid state. It was reported by Jamali *et al*.[7] that the reaction of $PtMe(SMe_2)(ppy)$ (ppy = deprotonated 2-phenylpyridyl) with 1 equiv of dppf produced cleavage of the metallacycle leading to the complex with monodentate η^1-C bonded to the Pt centre. In their system, however, the structure of the complex remained constant in both solution and the solid state. To the best of our knowledge, this is the first observation of an intramolecular geometry transformation from the solid state to solution for a single metallacyclic complex.

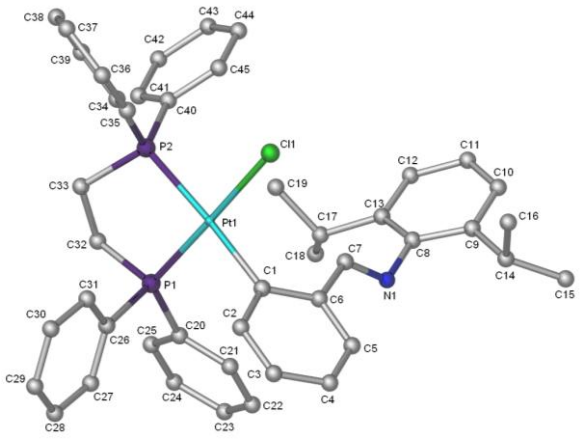

Figure 4.6 Molecular structure of **C7** showing the atomic numbering scheme. All H atoms are omitted for clarity. All non-hydrogen atoms are presented as an ellipsoidal model with a probability level of 30%. The solvent molecule (acetone) has been omitted in this diagram.

Table 4.4 Selected bond lengths (Å) and bond angles (°) for the dppe chelating complex **C7**

Bond length		**Bond angle**	
Pt(1)–C(1)	2.073(3)	C(1)-Pt(1)-Cl(1)	89.09(7)
Pt(1)–P(1)	2.2193(7)	C(1)-Pt(1)-P(1)	91.78(7)
Pt(1)–P(2)	2.3120(7)	P(2)-Pt(1)-Cl(1)	92.20(2)
Pt(1)–Cl(1)	2.3592(6)	P(1)-Pt(1)-P(2)	86.88(3)
N(1)–C(7)	1.271(4)	Total 1[i]	360.0
		P(1)-Pt(1)-P(2)	86.88(3)
		C(33)-P(2)-Pt(1)	105.32(10)
		C(32)-P(1)-Pt(1)	108.25(9)
		C(33)-C(32)-P(2)	110.16(19)
		C(33)-C(32)-P(2)	109.69(19)
		Total 2[ii]	520.3

[i] Sum of angles in the coordination environment of the platinum ato[ii] Sum of internal angles of the metal-containing ring.

4.2.2 Methylplatinum(II) complexes

As has been previously discussed, the *cis*/*trans* isomerization has been considered for four-coordinate palladium complex containing an asymmetrical *N*-benzylidenebenzylamine ligand in the oligomerization catalytic cycle via a Cossee-type pathway. The first *cis*/*trans* isomerization could occur in the methylation step by MAO on the palladium precatalyst to give an active Pd-Me species which starts the catalytic cycle (see Chapter 2). In this section, we aimed to assess the possibility of the occurrence of *cis*/*trans* isomerization on *N*-benzylidenebenzylamine metal complexes during methylation reactions.

Following the model Pd-Me complexes outlined in Chapter 2, the initial aim of the present work was to study a model methylation reaction on the real palladium precatalyst **Ia-s** (**I** where X = H, R = 2,6-di-^{i}Pr, L = PPh_3) using methyllithium (LiMe) (Eq. 4.1). The reaction was carried out using anhydrous tetrahydrofuran (THF) under nitrogen atmosphere at -50 ^{o}C for one hour using standard Schlenk line techniques. A prolonged reaction time caused the formation of a black decomposition product. After working up the reaction, a light yellow solution was formed. However, it turned to deep orange when removing the solvent even at room temperature. ^{1}H NMR indicated a complex mixture of products. ^{31}P NMR showed three peaks (Figure 4.7), the most downfield signal is due to the starting complex **Ia-s**, while the two singlets in the region 25 – 26 ppm could be attributed to the products. The deep orange residue obtained, however, was quite unstable in either polar or non-polar solvents such as $CDCl_3$ and C_6D_6. Formation of a black decomposition product was observed from the NMR sample during analysis. Attempts to isolate the pure product were not successful.

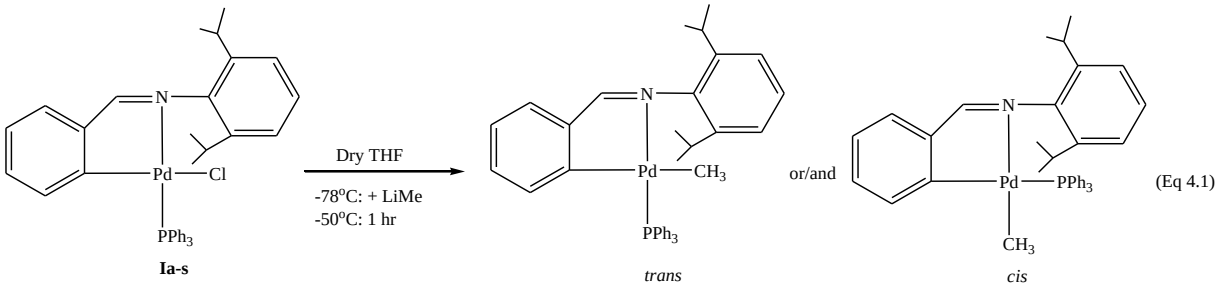

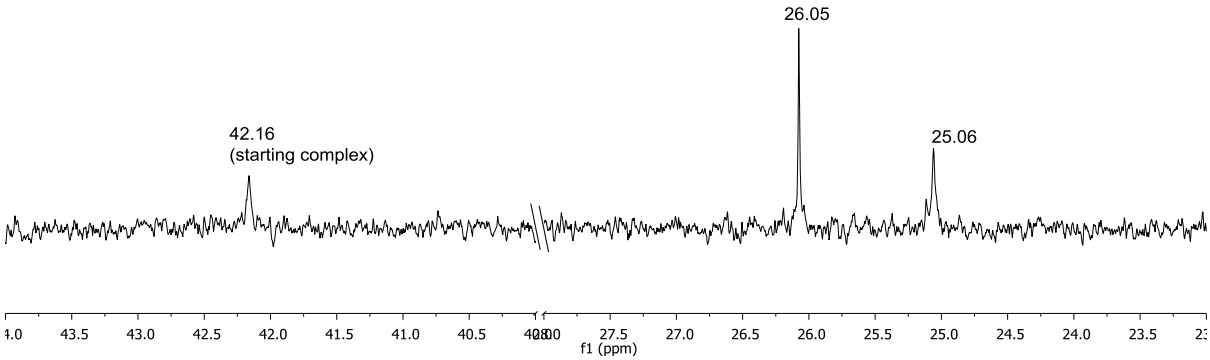

Figure 4.7 ^{31}P NMR spectrum of crude product obtained from the reaction of palladium precatalyst **Ia-s** with LiMe.

The initial aim, to synthesize a Pd-Me complex via the methylation reaction using LiMe, was consequently not achieved. However, as mentioned previously, platinum has a very similar chemistry to that of palladium, and Pt(II) complexes are generally more stable than Pd(II) both thermodynamically and kinetically.[22] Therefore, the methylation reaction was studied using the platinum model complex **C4**. The methylplatinum(II) complex bearing the analogue N^O chelate ligand (**L_B**) was synthesized for comparison with the N^C complex. In addition, the successful preparation of a methylpalladium(II) complex bearing the N^O ligand **L_B** also allowed us to compare its chemistry with that of the Pt(II) analogue using spectroscopic methods.

4.2.2.1 Methylplatinum(II) complex of N^C chelate ligand

The methylation reactions on platinum(II) complex **C4** using LiMe, which was considered as a model reaction representing the methylation step by MAO on the precatalyst in this study, were carried out using a similar procedure for making the Pd-Me complex. In this case the reaction mixture was kept stirring at room temperature for 16 h. Again, ^{31}P NMR showed three singlets (Figure 4.8) which correspond to the unreacted starting complex **C4** and two products (Eq. 4.2).

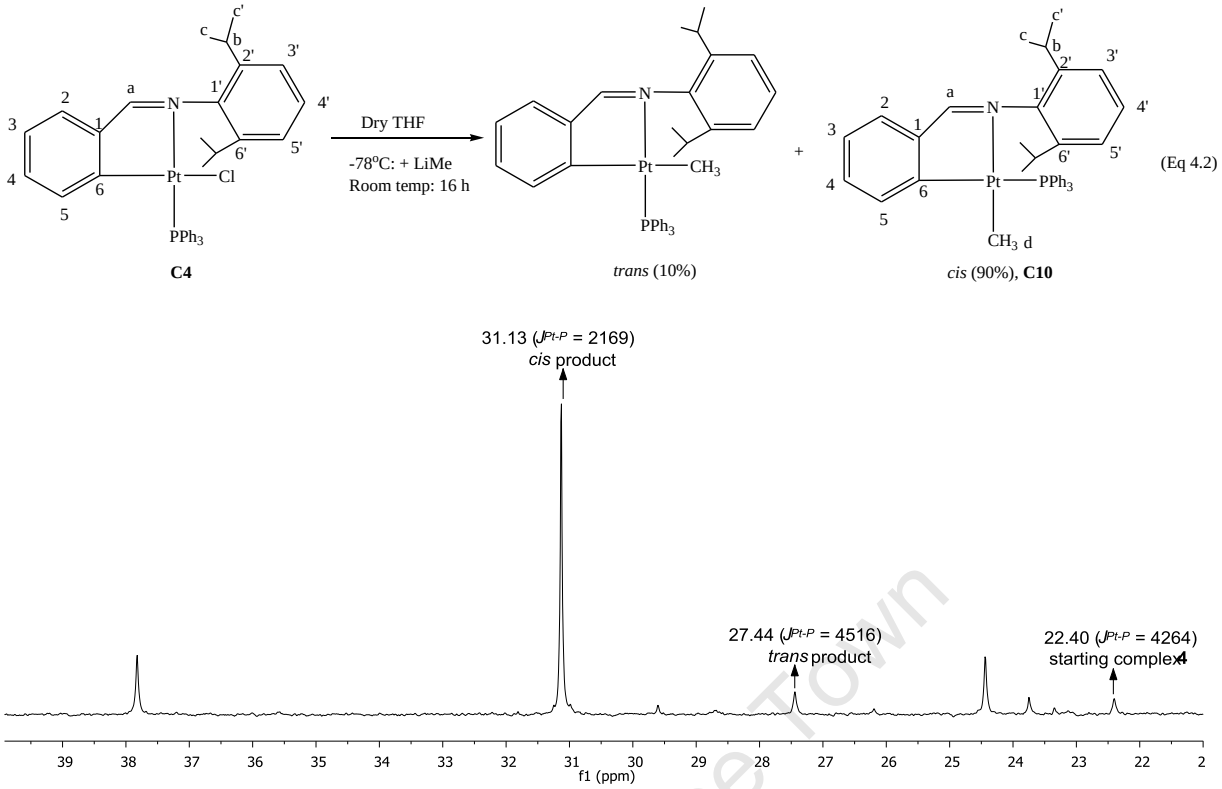

Figure 4.8 ^{31}P NMR spectrum of crude product obtained from the reaction of **C4** with LiMe.

The crude product was purified by passing it through a SiO_2 column and recrystallizing in benzene/methanol at 4 ^{o}C, to give an orange solid **C10** with X-ray quality crystals. The methylplatinum(II) complex **C10** was characterized using standard spectroscopic techniques and X-ray crystallography.

4.2.2.2 Methylplatinum(II) complex of N^O chelate ligand

Methylation reactions were also carried out on the N^O complex **C5b** using LiMe in a similar manner. The reaction mixture changed from golden yellow to very pale yellow during the course of the reaction. Quenching the reaction by the addition of saturated ammonium chloride solution, however, resulting in formation of a black decomposition product, which immediately precipitated from the reaction mixture. As will be discussed later, the methylplatinum(II) complex containing the N^O chelate ligand $\mathbf{L_B}$, which was obtained using an alternative route, is very stable. The methylation reaction attempted here could lead to other rather unstable complexes in which the N^O chelating ring could be possibly cleaved by LiMe reagent.

The salicylaldiminato methylplatinum(II) complex (**C11**) was then prepared from a reaction of the ligand $\mathbf{L_B}$ with [PtCl(Me)(COD)] as shown in Scheme 4.3 according to a similar

procedure reported by Mogorosi.[23] First, the reaction of the ligand precursor with 2 equiv. of sodium acetate afforded a deprotonated intermediate *in situ*. Then, addition of equimolar amounts of [PtCl(Me)(COD)] and PPh_3 to the reaction mixture gave an immediate yellow precipitate from the solution. After stirring the reaction for 14 h, the precipitate was collected as a mixture of **C11** and a small amount of the by-product *trans*-[PtCl(Me)$(PPh_3)_2$].[24] Column chromatography on SiO_2 was employed to purify the target complex. Elution with ethyl acetate/hexane (6:94) gave a band containing *trans*-[PtCl(Me)$(PPh_3)_2$] followed by a second band containing the product **C11**. The solvent was removed from the eluate and the resultant yellow solid was recrystallized from DCM/MeOH to give **C11** as a yellow crystalline solid in good yield (88 %). For comparison, a palladium analogue **C12** was also synthesized by the reaction of the salicylaldimine $\mathbf{L_B}$ with NaOAc followed by adding [PdClMe(COD)] and PPh_3. All complexes were fully characterized by spectroscopic methods (^{1}H-NMR, ^{13}C-NMR, ^{31}P-NMR spectroscopy, FTIR spectroscopy and mass spectroscopy) and microanalysis.

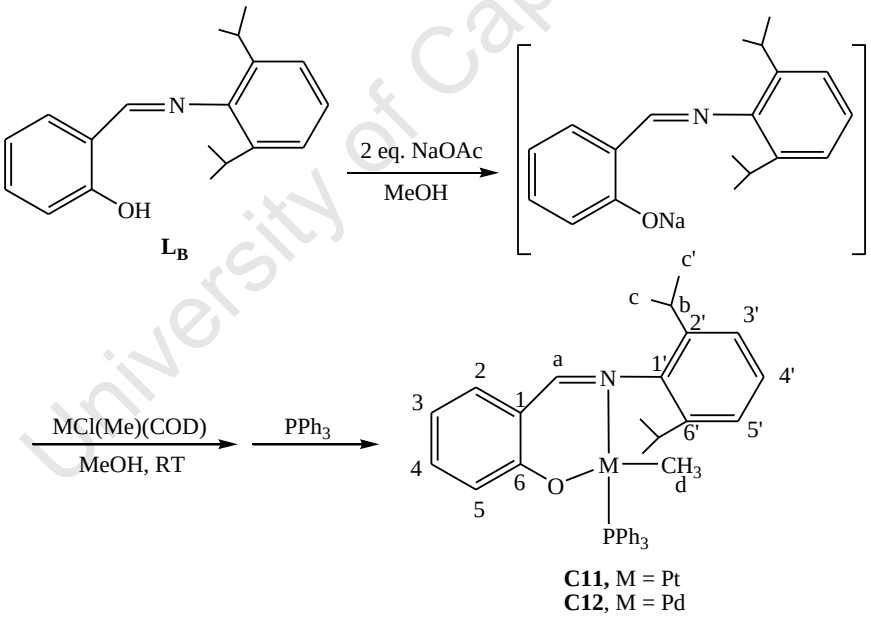

Scheme 4.3 Preparation of salicylaldiminato methylplatinum(II) and methylpalladium(II) complexes **C11** and **C12**.

4.2.2.3 IR, NMR spectroscopy and mass spectrometry

The methylation reaction on **C4** to form the methylplatinum (II) complex **C10** does not effect the $\upsilon_{C=N}$ stretching vibration band. In the IR spectrum for **C10**, it appears at the same frequency as that for **C4**, i.e., 1599 cm^{-1} (Table 4.5). A similar trend was observed for the

methylplatinum(II) complex bearing the N^O chelate ligand, **C11**, with its $\upsilon_{C=N}$ vibration band being identical to that of the palladium analogue **C12**, i.e., 1608 cm^{-1}.

The mass spectroscopic data of the two methylplatinum(II) complexes, **C10** and **C11**, gave $[M]^+$ as the highest fragments, with exception of the methylpalladium(II) complex **C12**. The most abundant peak for **C12** is assigned to the $[M\text{-}CH_3]^+$ fragment. The sodium adduct of the parent ion, $[M + Na]^+$, is observed for both **C10** and **C12**. In the mass spectrum of **C11**, a peak at 282.2 *m/z* with a relatively high abundance is attributed to the dissociation of the N^O ligand. No dimeric fragments were found in all spectra, unlike in the case for the chloride analogues discussed earlier (Section 4.2.2.1).

In the ^{1}H NMR spectrum of **C10**, the most significant changes with respect to the starting complex, **C4**, are i) The significant downfield shift of the aromatic proton adjacent to the metallation position (H^5). This is due to the absence of the anisotropic shielding effect of the phenyl group in PPh_3. ii) The reduced $^3J_{Pt\text{-}H}$ coupling constant (57.1 Hz) for the imine proton signal. The methyl protons (H^d) appear at 1.31 ppm and are coupled to ^{195}Pt and ^{31}P (Table 4.5). The downfield shift of the Pt-methyl resonance is in agreement with the analogous shift for methyl groups in related N^C-cyclometallated platinum complexes.[9,25,26] The magnitude of the $^2J_{Pt\text{-}H}$ (83.9 Hz) suggests it to be *trans* to nitrogen, since coordination *trans* to carbon would result in a smaller coupling. All these observations are consistent with the *cis* arrangement of the Pt-$C_{metallated}$ and Pt-CH_3 bonds in the molecular structure and can be seen in Figure 4.10.

In the ^{1}H NMR spectra of the N^O complexes **C11** and **C12**, signals corresponding to the imine proton (H^a) are displayed as doublets near 8.0 ppm with a phosphorus coupling ($^4J_{P\text{-}H}$) *ca.* 12 Hz (Table 4.5). In addition, the imine group of **C11** was also coupled to platinum with a $^3J_{Pt\text{-}H}$ coupling constant of 70.9 Hz, suggesting it to be *trans* to phosphorus. The aromatic proton adjacent to the oxygen atom, H^5, of methyl-Pt(II) and -Pd(II) complexes, appeared upfield at *ca.* 6.3 – 6.5 ppm, and is consistent with that of the *trans* platinum complex containing a chloride ligand, **C5b**. Resonances of the methyl group on the metal appeared as doublets at -0.29 ppm ($^3J_{P\text{-}H}$ = 3.2 Hz, $^2J_{Pt\text{-}H}$ = 73.3 Hz) for **C11** and -0.43 ppm ($^3J_{P\text{-}H}$ = 3.1 Hz) for **C12**, respectively. These resonances are similar to those of other methylpalladium(II) complexes bearing salicylaldiminato ligands and all of these complexes having the geometry with the methyl group *trans* to the oxygen atom.[27,28]

Table 4.5 Selected spectroscopic data (^{1}H, ^{13}C, and ^{31}P NMR, IR, MS) for complexes **C10** – **C11**

Complex	Formula	[ii] IR / cm^{-1}	[M]$^{+}$ / *m/z*	^{1}H-NMR			^{13}C-NMR			^{31}P-NMR
		$\upsilon_{C=N}$	(calc.)	H^{a}	H^{d}	H^{5}	C^{a}	C^{d}	C^{5}	
C10[i]	$C_{38}H_{40}NPPt$	1599	[iii] 737.3 (736.78)	8.21 (s, J_{Pt-H} = 57.1 Hz)	1.31 (d, J_{P-H} = 7.5 Hz, J_{Pt-H} = 83.9 Hz)	8.28 (d, J_{P-H} = 6.44 Hz, J_{Pt-H} = 48.1 Hz)	180.28 (d, J_{P-C} = 6.51 Hz, J_{Pt-C} = 64.94 Hz)	-9.51 (d, J_{P-C} = 5.97 Hz, J_{Pt-C} = 744.06 Hz)	131.94 (d, J_{P-C} = 6.52 Hz, J_{Pt-C} = 51.05 Hz)	31.11 (J_{Pt-P} = 2166 Hz)
C11	$C_{38}H_{40}NOPPt$	1608	[iii] 753.3 (752.78)	8.11 (d, J_{P-H} = 12.2 Hz, J_{Pt-H} = 70.9 Hz)	-0.29 (d, J_{P-H} = 3.2Hz, J_{Pt-H} = 73.3 Hz)	6.48 – 6.42 (m)	162.12 (s)	-18.93 (d, J_{P-C} = 8.97 Hz)	123.15 (s)	20.43 (J_{Pt-P} = 4400 Hz)
C12	$C_{38}H_{40}NOPPd$	1608	[iv] 649.11 (649.09)	7.95 (d, J_{P-H} = 11.5 Hz)	-0.43 (d, J_{P-H} = 3.1Hz)	6.44 – 6.38 (m)	165.41 (s)	-0.14 (d, J_{P-C} = 10.8 Hz)	122.95 (s)	39.43

[i] L is *cis* to N atom (L = PPh_3)
[ii] Recorded as KBr pellets.
Represents *m/z* for the highest molecular weight fragment: [iii] $[M]^{+}$; [iv] $[M\text{-}CH_3]^{+}$

In the ^{13}C NMR spectrum of **C10**, the imine carbon (C^a), the aromatic carbon adjacent to the metallation site (C^5) and the methyl carbon (C^d) are coupled to both platinum and phosphorus (Figure 4.9). The $^2J_{Pt\text{-}C}$ value for C^a (65 Hz) is smaller than that observed for **C4** (85 Hz), which is consistent with a *cis* arrangement of the imine group and PPh_3. The methyl group signal was observed at -9.51 ppm with a large $^1J_{Pt\text{-}C}$ coupling constant of 744 Hz, which is in agreement with that of the related methylplatinum(II) complexes.[24] For the Pt(II) and Pd(II) complexes with the N^O ligand, signals corresponding to the methyl group bonded to the metal centre are also displayed as doublets at -18.93 ppm ($^2J_{P\text{-}C}$ = 8.9 Hz) for **C11** and at -0.14 ppm ($^2J_{P\text{-}C}$ = 10.8 Hz) for **C12**. In the case of **C11**, the platinum satellites were too small to be observed.

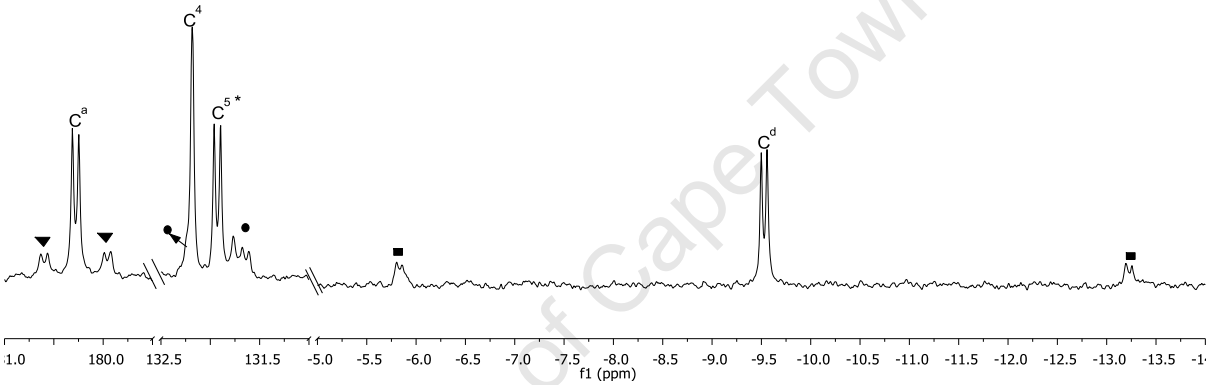

Figure 4.9 ^{13}C NMR spectrum of complex **C10** depicting the aromatic regions **(*** the satellite for C^5 on the left side is overlapped by the peak for C^4 as indicated by the shoulder peak).

The ^{31}P resonance of the N^C complex **C10** shifted to a lower field at 31.11 ppm with respect to the starting complex **C4** (21.79 ppm). The $J_{Pt\text{-}P}$ coupling constant (2166 Hz) is in the range expected for a *trans* arrangement of the phosphine and a phenyl group.[25,29,30] The ^{31}P NMR spectrum of the methylplatinum(II) complex bearing the N^O chelate ligand, **C11**, showed a downfield singlet at 20.43 ppm with expected platinum satellites as compared to the analogous chloride complex **C5b** (8.87 ppm). The value obtained for $J_{Pt\text{-}P}$ in **C11** (4400 Hz) is larger than that obtained for **C5b**, indicating that the more electron-donating group, CH_3, causes increased shielding of the platinum atom. This results in the increasing back-donation from the Pt centre to the P atom and strengthens the Pt-P σ bond. The ^{31}P resonance of the palladium complex **C12** is observed at 39.43 ppm, which is similar to that for related complexes.[27]

4.2.2.4 Crystal structure

Orange crystals suitable for X-ray diffraction were obtained by slow evaporation of a C_6D_6/n-hexane solution of **C10** at room temperature (Figure 4.10, Table 4.6). As can be seen, the platinum(II) centre exhibits a distorted square-planar environment due to the small bite angle of the cyclometallated ligand [79.17(8)^o]. A PPh_3 group and methyl ligand complete the coordination sphere of platinum(II). As expected from the spectroscopic characterization, the methyl ligand is *trans* to the nitrogen. Consequently, the P-Pt-N angle is significantly increased to 106.05(5) due to steric hindence caused by the *cis* arrangement of the PPh_3 group and the 2,6-diisopropylphenyl moiety. The metallacycle (plane 1) is approximately planar, i.e., the sum of its internal angles is 539.8^o; and it is nearly coplanar with the coordination plane (plane 2), as the dihedral angle being -178.1(2)^o. These angles and bond lengths are similar to those observed in other N^C-cyclometallated methylplatinum(II) complexes.[9,25,26]

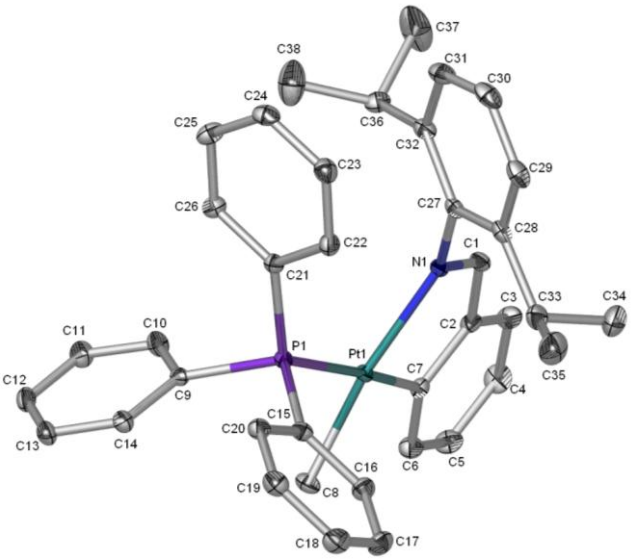

Figure 4.10 Molecular structure of **C10** showing the atomic labelling scheme. All H atoms are omitted for clarity. All non-hydrogen atoms were presented as an ellipsoidal model with probability level 30%.

Table 4.6 Selected bond lengths (Å), bond angles (°) and torsion angles (°) for **C10**

Bond length		**Bond angles and Torsion angles**	
Pt(1)–C(7)	2.044(2)	C(7)-Pt(1)-N(1)	79.17(8)
Pt(1)–N(1)	2.1451(17)	P(1)-Pt(1)-C(8)	85.71(7)
Pt(1)–P(1)	2.3015(5)	N(1)-Pt(1)-P(1)	106.05(5)
Pt(1)–C(8)	2.060(2)	C(7)-Pt(1)-C(8)	89.41(9)
N(1)–C(7)	1.286(3)	Total 1[i]	360.0
		C(7)-Pt(1)-N(1)	79.17(8)
		C(1)-N(1)-Pt(1)	112.99(15)
		C(2)-C(1)-Pt(1)	113.57(15)
		C(7)-C(2)-C(1)	115.05(19)
		N(1)-C(1)-C(2)	119.02(2)
		Total 2[ii]	539.8
		N(1)-Pt(1)-C(7)-C(6)	-178.1(2)
		Pt(1)-N(1)-C(27)-C(32)	75.0(3)

[i] Sum of angles in the coordination environment of the platinum atom.
[ii] Sum of internal angles of the metal-containing ring.

4.2.2.5 Discussion

During the preparation of methylplatinum(II) complexes containing both N^C and N^O chelate ligands, a spontaneous and rapid *cis*-to-*trans* isomerization must occur prior to the formation of the thermodynamically stable products (Scheme 4.4). Vicente and co-workers have shown that the following pairs of ligands have increasing phobia of being mutually *trans* to each other: N-donor/P-donor < C-donor/N-donor < C-donor/P-donor < C-donor/C-donor.[4] Therefore, in both methylplatinum(II) complexes **C10** and **C11**, the pair of ligands with less *transphobia*, i.e., N-donor/P-donor and C-donor/P-donor , respectively, prefer to be *trans* to each other. This is achieved via the occurrence of geometry isomerization, and also observed in the formation of the methylpalladium(II) complex **C12**.

It is interesting to note that the *cis* geometry, i.e., where the metallated carbon atom is *cis* to the methyl group (*cis* C, Me), have been observed in all N^C-cyclometallated methylplatinum (II) complexes.[9,25,26] This is compatible with the expected degree of *transphobia* (*T*) of pairs of trans ligands, *T*[C-donor/P-donor] < *T*[C-donor/C-donor].[4] In addition, *transphobia* is generally more marked for Pd(II) than for Pt(II).[4] One may expect that the formation of the N^C-methylpalladium(II) complex with *cis* geometry (*cis* C, Me) (Eq. 4.1) from the methylation step of the palladium precatalyst **I** with MAO could be predominant and is consistent with the DFT calculations (see Chapter 2).

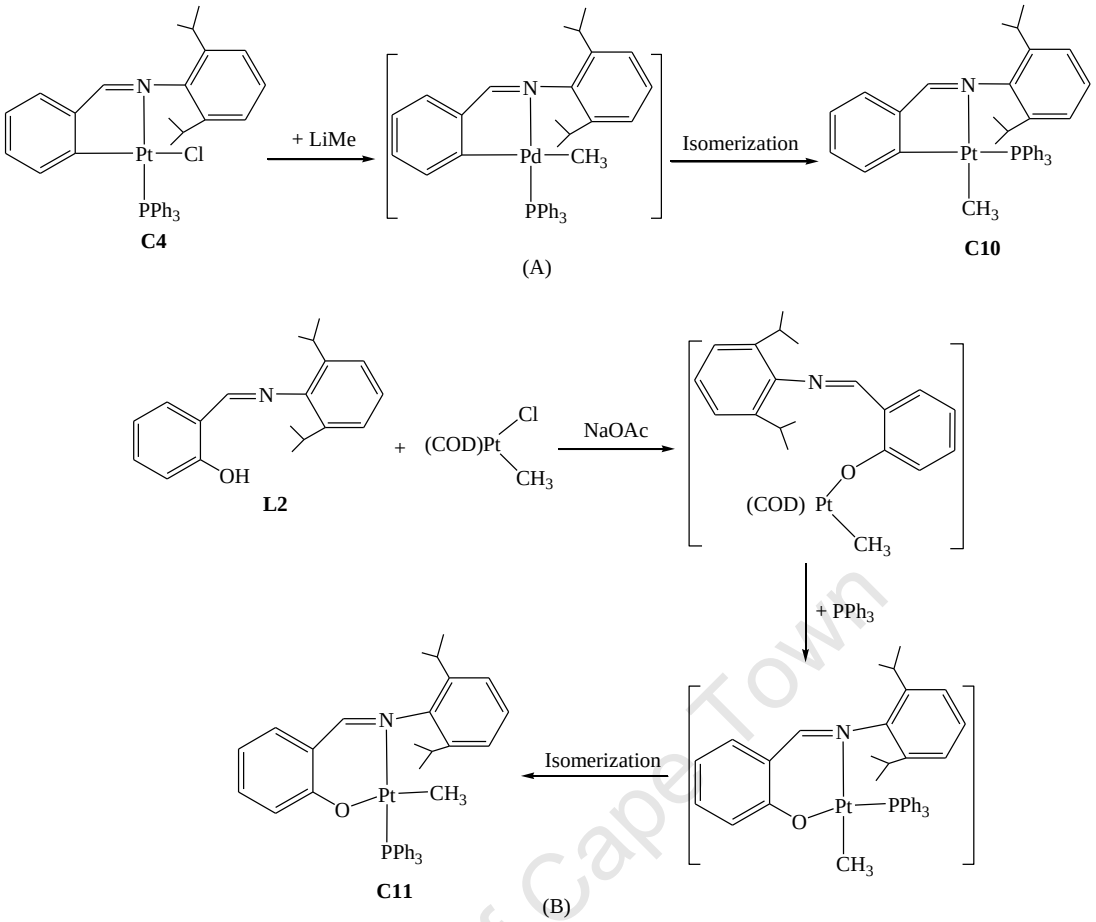

Scheme 4.4 The proposed pathway for the formation of methylplatinum(II) complexes.

The methylpalladium(II) complex **C12** is stable in $CDCl_3$ at room temperature, but only if protected from light through the use of amberized glassware or storage of the solution in the dark. Exposure of a $CDCl_3$ solution of **C12** to ambient room light, the solution slowly turned from yellow to orange after *ca*. 1 h, and the formation of triphenylphosphine oxide ($OPPh_3$) began to be observed. The peak at *ca.* 28 ppm is due to $OPPh_3$, which resonates at the same chemical shift in the ^{31}P NMR spectrum.[31] When the solution was allowed to stand in ambient light for longer periods, a decrease of the resonance due to **C12** was observed along with the increase of the $OPPh_3$ peak (Figure 4.11). In addition the solution changed from orange to brown. It indicates that degradative changes of **C12** took place. After exposure to room light for 7 days, complex **C12** completely decomposed, corresponding to the complete disappearance of the ^{31}P signal of **C12** in the NMR spectrum. A large amount of palladium black and some orange crystalline material, **C13** were formed after 7 days. **C13** was characterized by single crystal X-ray diffraction. A full list of bond lengths and angles, as well as the X-ray data collection parameters of **C13** (data sets 11) and the CIF file can be found in Supporting information.

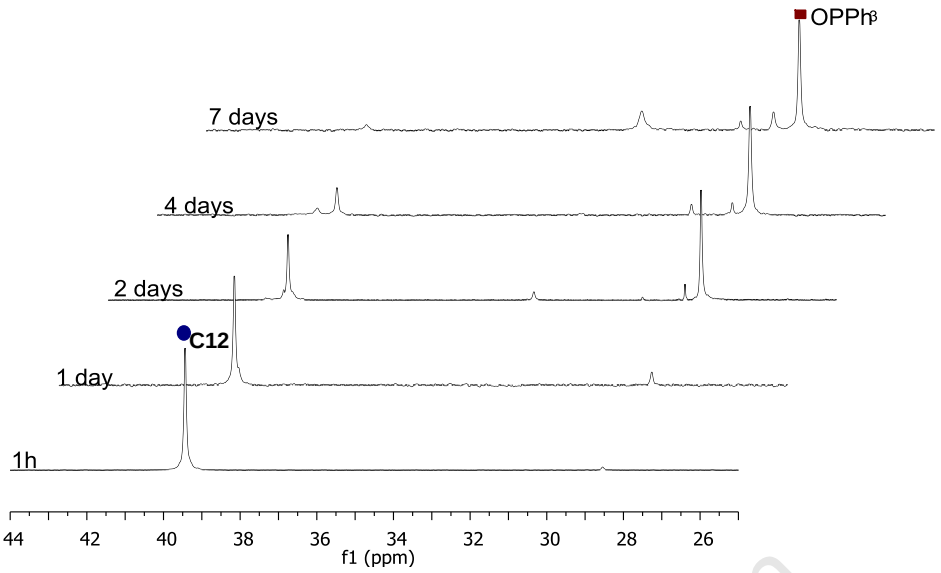

Figure 4.11 ^{31}P NMR spectral changes associated with the decomposition of **C12** in $CDCl_3$ with ambient room light.

A likely mechanism for the formation of the bis(salicylaldiminato)palladium complex **C13** is shown schematically in Scheme 4.5.[32] Photolytic cleavage of the Pd-Me bond generates a methyl radical and a [Pd(N^O)(PPh_3)] radical. The methyl radical abstracts a deuterium from $CDCl_3$ to form CH_3D. Upon exposure to air, the palladium radical rapidly converts to phosphine oxide producing a [Pd(N^O)] radical which further decomposes to give palladium black and a (N^O) radical. Finally the remaining [Pd(N^O)] radical couples with the resulting (N^O) radical to form [Pd(N^O)$_2$], **C13**.

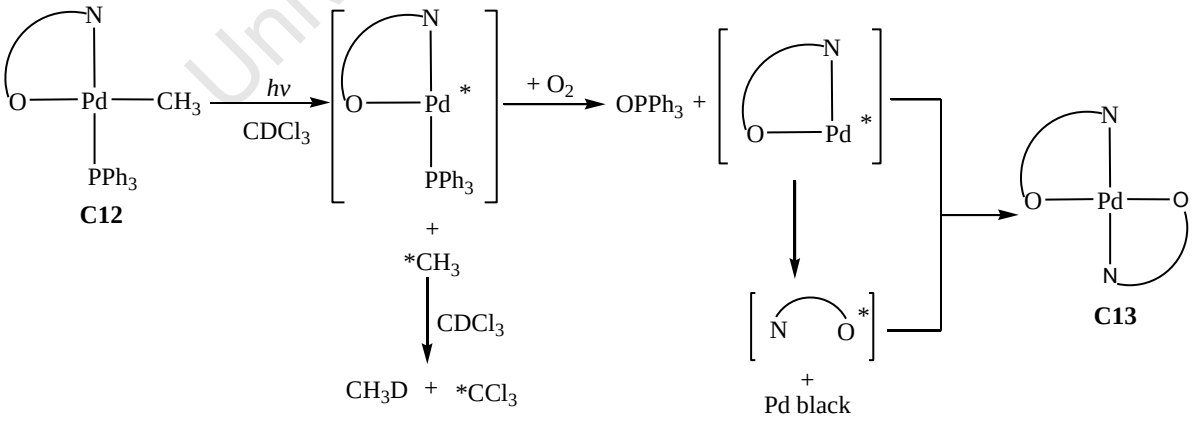

Scheme 4.5 Possible mechanism for the formation of the bis(salicylaldiminato)palladium complex **C13**.

As summarized in Table 4.7, significant geometry changes are observed in N^C complexes during the process of the interchange of ligands in the coordination sphere of platinum(II) (Eq. 4.3). An increase of the Pt-N bond length from C**1** to C**4** to C**10** was ascribed to the increasing *trans* influence of the ligand in the *trans* position to imine nitrogen, i.e., CH_3 > PPh_3 > dmso.[19]

Table 4.7 Selected bond lengths (Å), bond angles (°) and torsion angles (°) for the platinum(II) complexes containing N^C chelate (**L_A**)

Bond length and angle	C1	C4	C10
Pt-N	2.054(5)	2.098(5)	2.1451(7)
Pt-C	2.011(5)	2.013(6)	2.044(2)
N-C	1.292(5)	1.273(8)	1.286(3)
∠(N-Pt-C)	80.89(7)	80.4(2)	79.17(8)
∠(plane1-plane2)[a]	171.2(5)	-175.5(7)	-178.1(12)
∠(plane1-plane3)[a]	90.8(4)	92.3(6)	75.0(3)

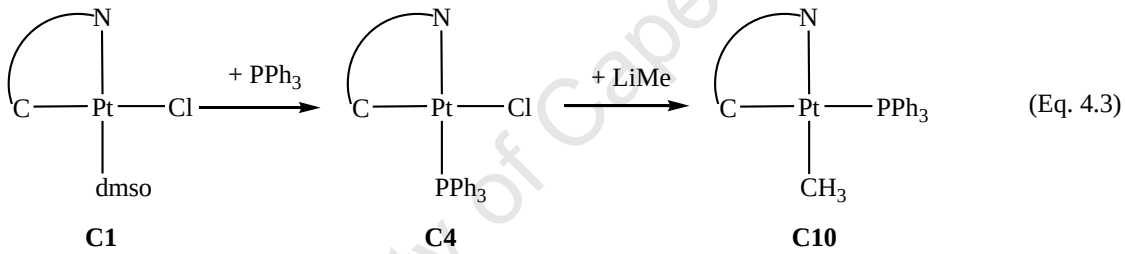

C1 **C4** **C10**

The steric bulk of the ligand and its position are found to affect the bite angle of the cyclometallated ligand as well as the torsion angles between three planes in the structures of **C1**, **C4** and **C10**. As can be seen, when the dmso group was replaced by the bulky PPh_3 group, the bite angle [∠(N-Pt-C)] was reduced from 80.89(7)° in **C1** to 80.4(2)° in **C4**, and a further reduction in **C10** [79.17(8)°] was observed when PPh_3 was positioned *cis* to the nitrogen atom. This is accompanied by the enhanced coplanarity between the metallacycle (plane 1) and the coordination plane (plane 2), as the torsion angle between the two planes [∠(plane1-plane2)] changed from [171.2(5)°] in **C1** to [-175.5(7)°] in **C4**, and to

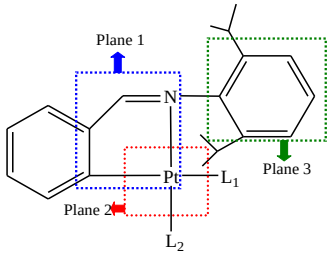

a

[-178.1(12)^{o}] in **C10**. When the dmso or PPh_3 ligand is *trans* to the imine group, a nearly facial (perpendicular) orientation[13,33] of the 2,6-diisopropylphenyl ring (plane 3) to the mean plane of the chelate ring (plane 1) is observed in complexes **C1** and **C4**, as the torsion angles between two planes [$\angle$(plane1-plane3)] are close to 90^{o}. However, the facial orientation is distorted [75.0(3)^{o}] by the *cis* arrangement of the PPh_3 and the imine group in **C10**.

4.2.3 Cyclic voltammetry studies of ferrocene containing complexes

The reactions of 1,1'-bis(diphenylphosphino)-ferrocene (dppf) with platinum dmso precursors in dichloromethane gave the ferrocene-containing complexes **C8** and **C9**, respectively. The complexes were characterized by NMR spectroscopy, and all the peaks were assigned using COSY and HSQC NMR spectra. For both complexes, the ^{1}H NMR spectra are similar to those of their PPh_3 analogues, while the singlets in ^{31}P NMR shift upfield due to the shielding effect of the ferrocene group. In order to elucidate the effect induced by the Schiff base ligands bound to the platinum(II) atom on the redox properties of the iron(II) atom in **C8** and **C9**, electrochemical studies were performed based on cyclic voltammetry (CV). In all cases, the cyclic voltammograms of freshly prepared solutions (1.5 mM) of dppf, **C8** and **C9** in dichloromethane were recorded. Cyclic voltammograms are presented in Figure 4.12. The ^{31}P NMR data of these complexes are collected in Table 4.8 along with the data obtained from CV measurements.

The platinum complexes show different redox behaviour in CH_2Cl_2 depending on the donor ability of N^O and N^C ligand (Figure 4.12). The N^C complex, **C8**, exhibits only one reversible redox peak at $E_{1/2}$ = 0.567 V (E_{pa} = 0.654 V, E_{pc} = 0.480 V), and it is the more cathodic potential in two complexes. On the other hand, the complex containing the N^O ligand, **C9**, gives one reversible redox peak at E_{pa} = 0.707 V (E_{pc} = 0.601 V) and one stepwise quasi-reversible peak at E_{pa} = 1.30 V (E_{pc} = 0.996 and 0.836 V). The first half-wave potential of N^O complex is observed at $E^{1}_{1/2}$ = 0.654 V, which can be attributed to the redox process of Fc/Fc^{+}. It suggests that $[dppf]^{+}$ formed during the first oxidation process is well stabilized by the [Pt(N^O)] moiety. Consequently, the quasi-reversible peak at E_{pa} = 1.30 V corresponds to the redox processes of $[Pt(N^O)]^{o}/[Pt(N^O)]^{+}/[Pt(N^O)]^{2+}$.

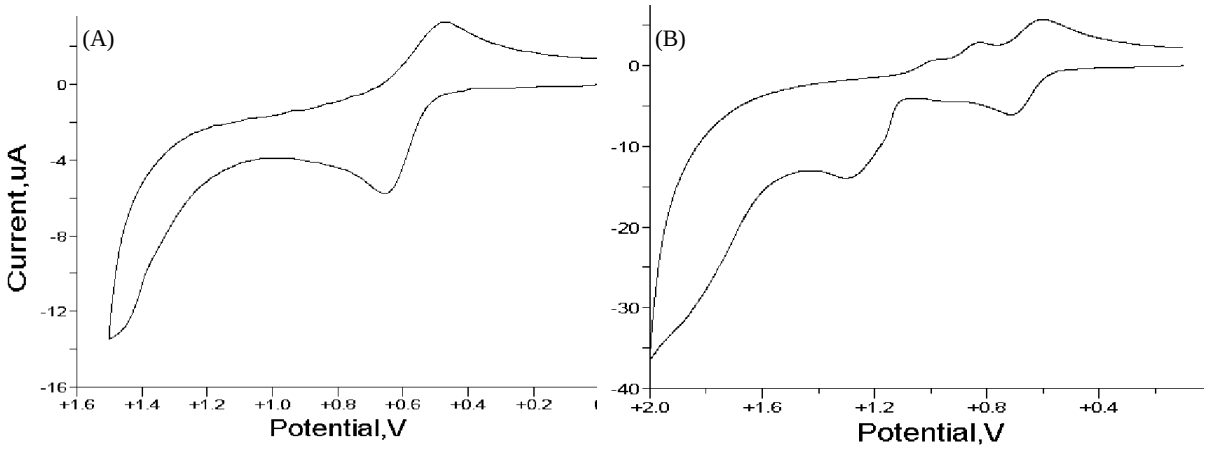

Figure 4.12 Cyclic voltammograms of complexes **C8** (A) and **C9** (B) in dichloromethane at 298 K and at a scan speed v = 100 mV/s

Table 4.8 ^{31}P NMR and CV parameters for (dppf)PtL complexes

	L	^{31}P NMR		cyclic voltemmatery (V)	
		δ (ppm)	J_{Pt-P} (Hz)	$E^1_{1/2}$	E^2_{pa}
C8	N^C	9.42	4239	0.567	
C9	N^O	1.98	3851	0.654	1.30

The free ligand, dppf exhibits a reversible oxidation wave at $E_{1/2}$ = 0.190 V (referenced to ferrocene) in dichloromethane solution containing 0.1M (Bu_4N)(PF_6) as supporting electrolyte. Both complexes show more anodic half-wave potentials compared to the uncoordinated dppf due to the electron-withdrawing property of the ligand and the Lewis acid character of the Pt(II) ion. Oxygen is more electronegative than carbon atom; therefore the electron-withdrawing ability is higher, causing the ferrocene moiety in **C9** to be oxidized with more difficulty than **C8**. This is supported by the higher $E_{1/2}$ potential of **C9** than that of **C8**, indicating N^C is a better donor than N^O ligand.

It has been previously mentioned that the more electron-donating group causes increased shielding of the platinum centre, and consequently increases the back-donation from the Pt centre to the P atom. Therefore, the Pt-P σ bond becomes stronger and gives a higher J_{Pt-P} coupling constant.[13] Judging from J_{Pt-P} and $E_{1/2}$ values, the order of the donor ability can be estimated: N^C > N^O.

According to the literature, reductive elimination can be faster from compounds with more electron-donating groups theoretically[34] and experimentally.[35] As N^C ligands are more electron-donating than N^O, one may expect that reductive elimination could proceed faster from their palladium-alkyl intermediates to form short chain oligomers compared to their N^O analogues during oligomerization reactions. Palladium complexes bearing N^O ligands (shown in Chapter 1) are catalysts for ethylene oligomerization. Thus it is quite possible for palladium complexes containing N^C ligands produce oligomers with even shorter chain length, viz, butenes. This is consistent with the results obtained from computational modelling in Chapter 2, i.e., the ethylene oligomerization reactions catalysed by cyclometallated palladium complex produce mainly ethylene dimers.

4.2.4 *Cis*-to-*trans* isomerization of Pt(N^O) complex

As previously mentioned, when triphenylphosphine is added to a solution of **C2a** or **C2b**, the kinetically controlled product **C5a** with phosphorus coordinating *cis* to the imine group is obtained. By heating, the kinetic product **C5a** undergoes a slow conversion to the thermodynamically more stable *trans* complex **C5b**, resulting in an increasing up-field resonance ascribed to the H^5 proton at 6.31 ppm as well as an alteration of both the Pt-P and Pt-H coupling constants. In particular, the Pt-P coupling constant changes from 4063 to 3818 in accord with the isomerization from the PPh_3 *cis* to the nitrogen atom to a *trans* position. This behaviour is similar to that observed by Fornié*s et al.*[11a] in their study of the isomerization of a [PtCl(N^C)PPh_3] complex.

Our interest in determining the possible mechanism for the *cis*-to-*trans* isomerization for the square-planar platinum(II) complex bearing N^O chelate ligand, and the comparison between kinetic and computational data led us to measure the kinetic conversion **C5a→C5b** (Eq. 4. 4) and to perform DFT calculations on this process.

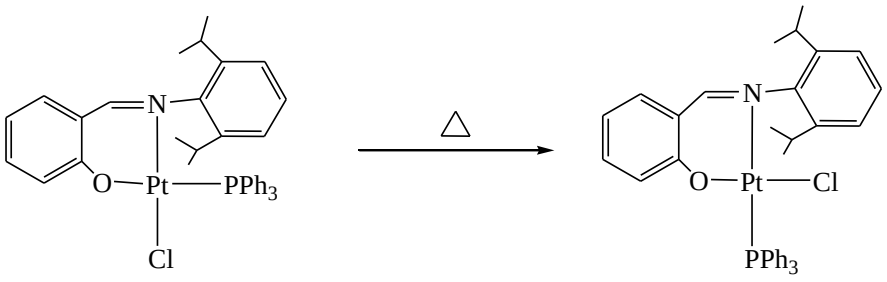

C5a (*cis*) **C5b** (*trans*) (Eq. 4.4)

4.2.4.1 Kinetic studies

In $CDCl_3$, the *cis*–to–*trans* geometrical conversion **C5a→C5b** was investigated quite easily in the temperature range 313 – 336 K by ^{31}P NMR measurements. In the temperature range, the conversion is *ca.* 95%, and gives the stable *trans* isomer and a small amount of the starting *cis* isomer presenting at the end of the reaction. The kinetics can be examined by using the time dependence of the reaction components. The pseudo-fist-order rate constants were calculated according to Eq.4.5, and given in Table 4.9.

$$\ln \frac{a_0}{a_t} = kt \qquad \text{(Eq. 4.5)}$$

Where $a_0 = \frac{[C5a]_0}{[C5a]_0 + [C5b]_0} = 1,\ a_t = \frac{[C5a]_t}{[C5a]_t + [C5b]_t}$

Table 4.9 Experimental pseudo-first-order rate constants for the isomerization of **C5a** to **C5b**

Entry	*T*/K	k_{obs} /$10^{-5}$$s^{-1}$
1	313	0.19±0.01
2	320	0.43±0.02
3	328	1.39±0.06
4	336	3.85±0.12

The progress of each reaction was monitored by following the decrease of the ^{31}P resonance at -2.14 ppm belonging to **C5a**. Figure 4.13 shows the spectral changes in the transformation **C5a→C5b** during the heating process at 338 K. The two clearly defined resonances at 8.67 and -2.37 ppm indicate that the isomerization is well-behaved and is free of kinetic complications. The relative intensity of the resonance belonging to **C5a** versus time plot, depicted in Figure 4.14(A), shows the least-squares fit of the NMR data to the decrease of **C5a** by a pseudo-first-order reaction.

The variable-temperature rate constants for compound **C5a** obtained in Table 4.5 were fitted to the Eyring equation (see Eq. 6.1 in Experimental Chapter) leading to $\Delta H^{\ddagger}$ = 26.9±1.1 kcal/mol, $\Delta S^{\ddagger}$ = 1.2±3.3 eu, $\Delta G^{\ddagger}_{298.15}$ =26.6±0.1 kcal/mol [Figure 4.14(B)]. The apparent

value of $\Delta H^{\ddagger}$ obtained is comparable to that of other similar systems,[36,37] while the value of $\Delta S^{\ddagger}$ always varies with different isomerization mechanisms.[38,39]

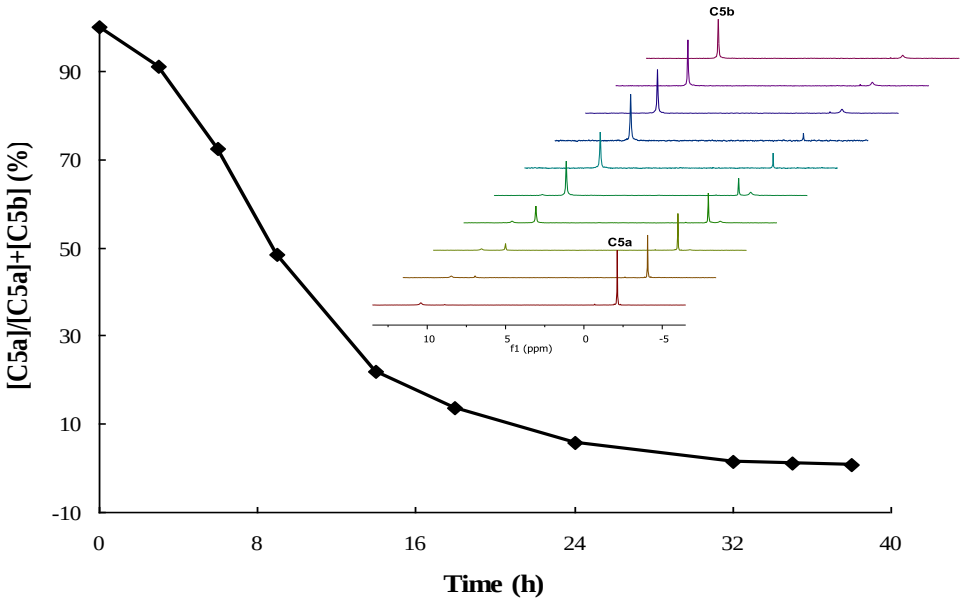

Figure 4.13 The relative intensity of the **C5b** resonance versus time plot for the experimental data at 338K (solid black line). Inside: ^{31}P NMR spectral changes associated with the geometrical isomerization of **C5a** to **C5b** in $CDCl_3$ at 338 K.

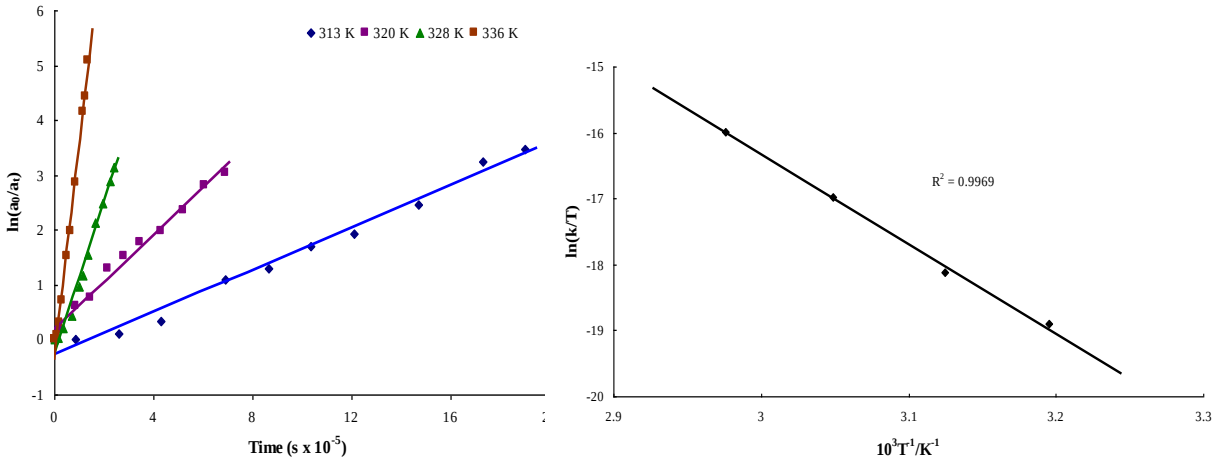

(A) (B)

Figure 4.14 (A) The pseudo-first-order plots for *cis*-to-*trans* isomerization of **C5a** at variable-temperature. (B) Eyring plot for the isomerization reaction of **C5a** constructed by the use of rate data obtained from ^{31}P NMR experiments.

4.2.4.2 DFT studies

The possible mechanisms for *cis*-to-*trans* isomerization depend on the nature of the solvent, the electronic nature of the ligands and the temperature.[40] Different mechanisms usually considered for *cis*-to-*trans* isomerization in square-planar complexes include the associative pathway [Scheme 4.6 (A)],[41] the Berry pseudo-rotation mechanism [Scheme 4.6 (A)],[42] the dissociative pathway [Scheme 4.6 (B)],[43] and direct geometry change via a tetrahedral four-coordinate species [Scheme 4.6 (C)].[34,44]

As can be seen from Scheme 4.6 (A), both associative and Berry's pseudo-rotation mechanisms need the coordination of a fifth ligand such as an extra PR_3 ligand, an ethylene or a solvent molecule.[42a,45] In our system, solvent is the only possible source as the fifth ligand. However, since $CDCl_3$ is a poor coordinating solvent, we could therefore rule out these two pathways *via* five-coordinate intermediates. Therefore, both dissociative and direct geometry change pathways could be possible mechanisms for the isomerization process from **C5a** to **C5b**. In addition, two dissociative pathways, which were previously mentioned in Chapter 2 (Section 2.2), could be possible: the dissociation of PPh_3 and the dissociation of the N-atom of the hemilabile imine ligand. We decided to use the results of electronic structure calculations to determine which of the above mechanisms is favoured in the rearrangement of **C5a**. As a test of our computational prediction of the preferred mechanism, we had to assess how well the computed results could reproduce the experimental activation parameters.

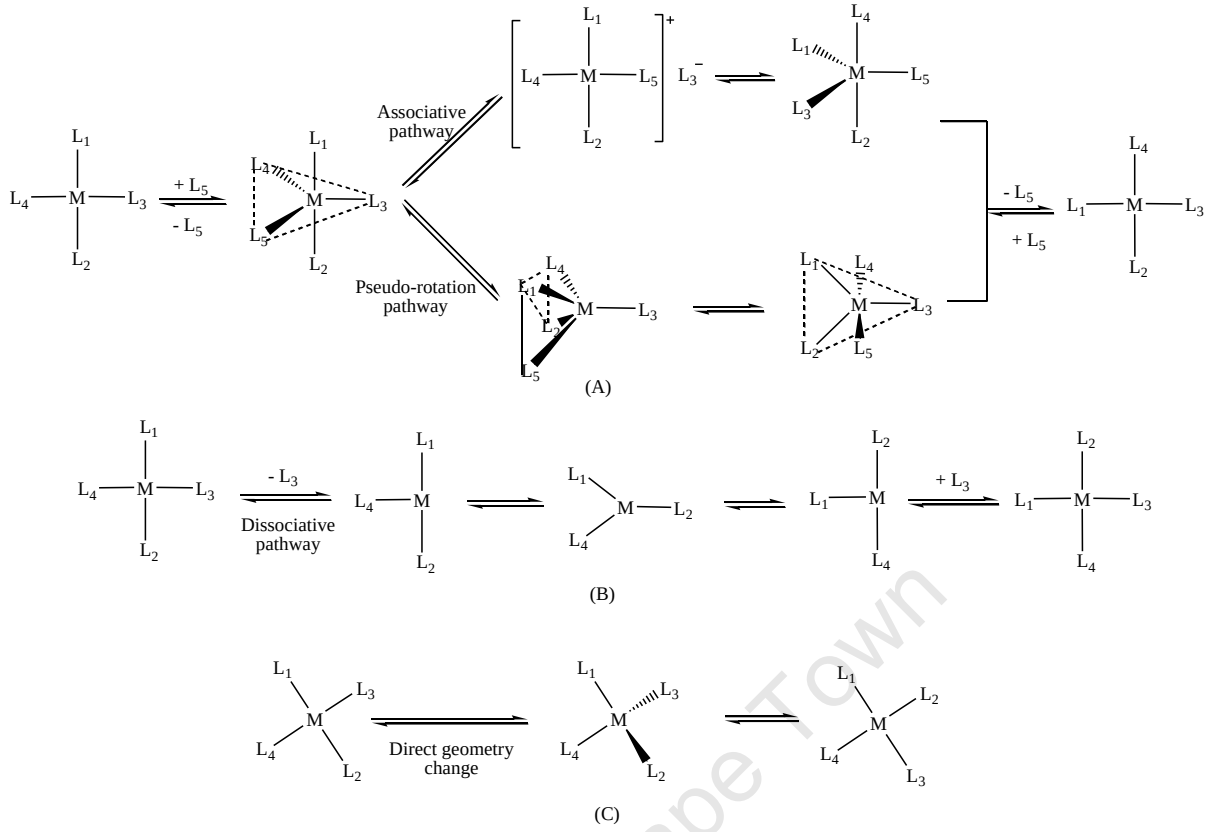

Scheme 4.6 Possible mechanisms considered for *cis*-to-*trans* isomerization in square-planar complexes.

Three possible isomerization routes were investigated. The energy profiles are shown in Figure 4.15 and the calculated activation parameters as well as the experimental values are given in Table 4.10 (Structure details in Supporting information). Our computational studies were initiated by performing DFT calculations on the isomerization of **C5a** through the dissociative pathway, involving the dissociation of the PPh_3 ligand, and the direct geometry change via a tetrahedral four-coordinate transition state. These two mechanisms are similar to those reported for *cis*-to-*trans* isomerization of the palladium complex bearing N^C ligand in Chapter 2 (Section 2.4.2.1). It is worth noting that both the "Y-shaped" three-coordinate transition state (TS-P) and the tetrahedral four-coordinate transition state (TS) are calculated to be extremely close in activation energy ($\Delta G^{\ddagger}_{298.15}$), in which TS-P is about 2 kcal/mol more stable than TS (see Table 4.9). On the other hand, TS-P is 10.6 kcal/mol higher in enthalpy ($\Delta H^{\ddagger}_{298.15}$) than TS, due to the very positive value of $\Delta S^{\ddagger}$ for TS-P (45.3 eu), which is expected for the dissociative mechanism.[36,39] Thus, the experimental value of $\Delta S^{\ddagger}$ obtained (1.2 ± 3.3 eu) is in contradiction with this mechanism and we can therefore rule it out.

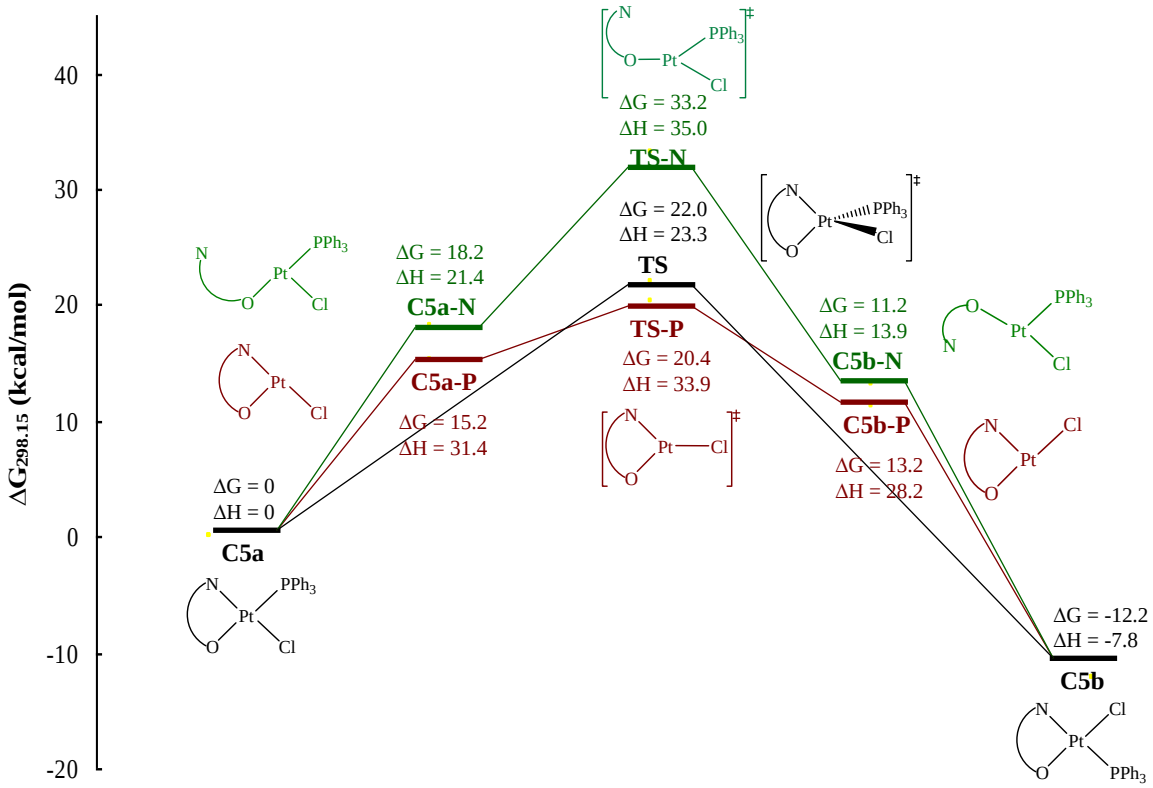

Figure 4.15 Isomerization routes: simple rotation via tetrahedral TS (black), dissociative route via the dissociation of PPh_3 (red) and dissociative route via the dissociation of N atom (green). ($\Delta G_{298.15}$/ $\Delta H_{298.15}$, kcal/mol at 1 atm relative to **C5a**).

Table 4.10 Summary of theoretical and kinetic data for the *cis*-to-*trans* isomerization of **C5a**

Entry	$\Delta H^{\ddagger}_{298.15}$ (kcal/mol)	$\Delta S^{\ddagger}_{298.15}$ (eu)	$\Delta G^{\ddagger}_{298.15}$ (kcal/mol)
1[a]	33.9	45.3	20.4
2[b]	35.0	-6.1	33.2
3[c]	23.3	4.1	22.0
4[d]	26.9±1.1	1.2±3.3	26.6±0.1

[a] Dissociative mechanism via the dissociation of the PPh_3 ligand
[b] Dissociative mechanism via the dissociation of the N-atom
[c] One-step, direct geometry change mechanism
[d] Experimental values

The third route proposed for isomerization of **C5a** is the dissociative pathway involving the dissociation of the N-atom. The dissociation of the labile N-atom from **C5a** affords a *cis*-like three-coordinate intermediate, **C5a-N**, with the agostic interaction between the Pt centre and the imine hydrogen (Pt···H distance is 2.467 Å). As shown in Figure 4.15, conversion of an agostic "*cis*-like" three-coordinate form to its *trans* form **C5b-N** requires a supplementary

consumption of energy. Our calculations find TS, the transition state for the one-step conversion of **C5a** to **C5b** to be *ca*. 11 kcal/mol lower in both enthalpy and activation energy than TS-N, which is the highest energy transition structure in the three isomerization routes.

Therefore, the calculated activation parameters of $\Delta H^{\ddagger}$ = 23.3 kcal/mol, $\Delta S^{\ddagger}$ = 4.1 eu for isomerization of **C5a** to **C5b** via the tetrahedral four-coordinate transition state (TS) are in good agreement with the experimental values of $\Delta H^{\ddagger}$ = 26.9 ± 1.1 kcal/mol, $\Delta S^{\ddagger}$ = 1.2 ± 3.3 eu (Table 4.10). This agreement provides support for the computational finding that the one-step, direct geometry change mechanism is really preferred to the three-step dissociative mechanisms. Similar DFT findings were reported for the *cis*-to-*trans* isomerization of a related palladium complex.[40]

4.3. Conclusions

The reactions of phosphines with Pt complexes containing both N^C and N^O ligands have been studied in the present work (Scheme 4.7).

The results obtained here show that the reaction of PPh_3 with the N^C complex **C1** leads to a *trans* isomer **C4** (where PPh_3 is *trans* to N atom), while the same reaction with N^O complex **C2a** or **C2b** leads to both *cis* and *trans* isomers **C5a** and **C5b**.

By reacting with the bidentate phosphine, dppe, in an equimolar ratio, the N^C complex **C1** formed a P^P chelated complex **C7**, in which dppe caused cleavage of the metallacycle, leading to a monodentate [N-C-κ^1*C*] system in the solid state, and extrusion of the chloride ligand, giving an ionic derivative in $CDCl_3$ or DCM. In contrast to this, ligand dissociation was observed for the N^O complexes **C2a** or **C2b** in the reaction with dppe.

When dppf was used as a spacer ligand (in a molar ratio = 1:2), the *trans* isomers with both N^C and N^O ligands gave diplatinum(II) complexes **C8** and **C9**, while no reaction occurred in the case of the *cis* isomer **C2a**.

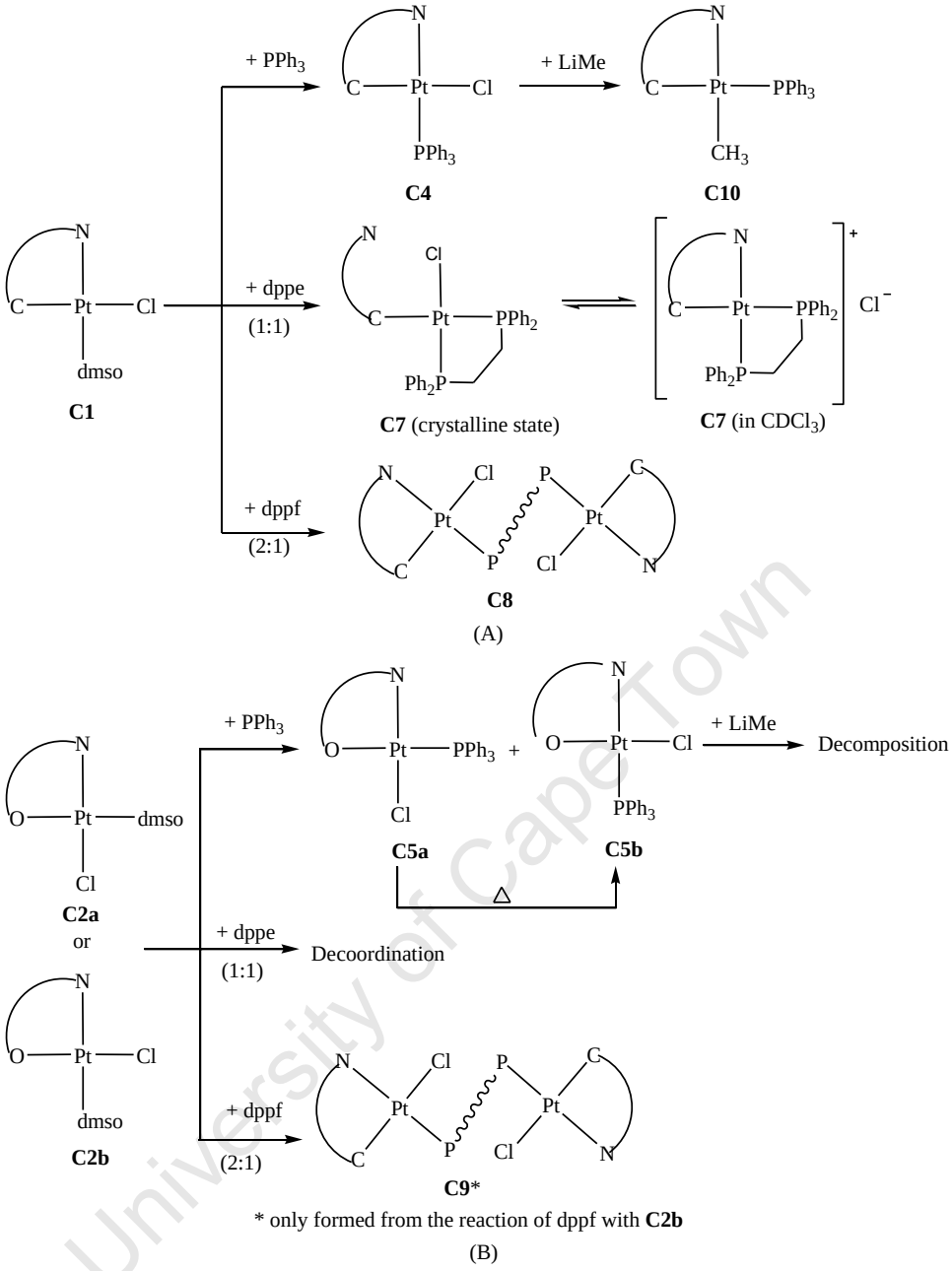

Scheme 4.7 Overall reactivities of dmso ligated complexes

Methylation reactions on the cyclometallated platinum complex **C4** using LiMe were studied as a model reaction to represent the methylation reaction by MAO on its palladium analogue in an actual catalytic process. The methylplatinum(II) complex with *cis* geometry (PPh_3 being *cis* to N atom), **C10**, was obtained as the predominant product due to the large *transphobia* of C-donor/C-donor ligands. This *transphobia* is generally more marked for Pd(II) complexes than for Pt(II) analogues. Thus, the formation of a methylpalladium(II) complex with *cis* geometry from the methylation by MAO should be feasible for the palladium precatalyst, and this agrees with the computational prediction.

Similar methylation reactions on the N^O complex **C5b** with LiMe were not successful, leading to a black decomposition product. This could be due to the relatively lower stability of the N^O chelate. The methylplatinum(II) complex containing the N^O ligand, **C11**, was obtained using an alternative synthetic route.

In the formation of both methylplatinum(II) complexes **C10** and **C11**, a spontaneous and rapid *cis*-to-*trans* isomerization should occur, leading to the more stable isomer, in which the pair of ligands with lower *transphobia* is mutually *trans* to each other, i.e., C-donor/P-donor for **C10** and N-donor/P-donor for **C11**, respectively.

The CV results of the diplatinum(II) complexes with dppf spacer ligands, **C8** and **C9**, in agreement with their $J_{Pt\text{-}P}$ coupling constants, indicate that the N^C ligand ($\mathbf{L_A}$) is a better electron-donating ligand compared to the N^O ligand ($\mathbf{L_B}$). Reductive elimination can be faster from the compounds with more electron-donating groups.[34,35] This could be a reasonable explanation for the DFT findings, i.e., the cyclometallated palladium-catalysed ethylene oligomerization reactions give mainly butenes as products.

The rate of conversion of the *cis* N^O complex **C5a** to its *trans* isomer **C5b** was measured in the temperature range of 313 – 336 K. The results of DFT calculations on this process show that both a dissociative mechanism (the dissociation of PPh_3) and a non-dissociative mechanism (direct geometry change) have very close energy barriers. The dissociative mechanism was calculated to have very positive entropy (45.3 eu), while the direct geometry change mechanism with small positive entropy (4.1 eu). Therefore, the small positive entropy (1.2 ± 3.3 eu) obtained experimentally supports the direct geometry change mechanism for the isomerization process and is in good agreement with the DFT prediction.

4.4. References

1. (a) J. Albert, M. Gómez, J. Granell, J. Sales and X. Solans, *Organometallics*, 1990, **9**, 1405; (b) J. Albert, J. Granell, J. Sales, M. Font-Bardía and X. Solans, *Organometallics*, 1995, **14**, 1393; (c) M. Crespo, X. Solans and M. Font-Bardía, *Organometallics*, 1995, **14**, 355; (c) M. Crespo, J. Granell, X. Solans and M. Font-Bardía, *J. Organomet. Chem*., 2003, **681**, 143.
2. A. Capapé, M. Crespo, J. Granell, M. Font-Bardía b and X. Solans, *Dalton Trans*., 2007, 2030.
3. (a) F. Canales, M. C. Gimeno, A. Laguna and P. G. Jones, *Organometallics*, 1996, **15**, 3412; (b) J. Diez, M. P. Gamasa, J. Gimeno, A. Aguirre, S. Garcia-Granda, J. Holubova and L. R. Falvello, *Organometallics* 1999, **18**, 662; (c) P. M. N. Low, A. L. Tan, T. S. A. Hor, Y.-S. Wen and L.-K. Liu, *Organometallics*, 1996, **15**, 2595.
4. J. Vicente, J. A. Arcas, E. Martínez-Viviente and P. G. Jones, *Organometallics*, 2002, **21**, 4454.
5. R. Martín, M. Crespo, M. Font-Bardia, T. Calvet, *Polyhedron*, 2009, **28**, 1369.
6. S. M. Nabavizadeh, H. Amini, H. R. Shahsavari, M. Namdar, M. Rashidi, R. Kia, B. Hemmateenejad, M. Nekoeinia, A. Ariafard, F. N. Hosseini, A. Gharavi, A. Khalafi-Nezhad, M. T. Sharbati and F. Panahi, *Organometallics*, 2011, **30**, 1466.
7. S. Jamali, S. M. Nabavizadeh and M. Rashidi, *Inorg. Chem*., 2008, **47**, 5441.
8. (a) J.-F. Ma and Y. Yamamoto, *Inorg. Chim. Acta*., 2000, **299**, 164; (c) R. Ares, M. López-Torres, A. Fernández, M. T. Pereira, G. Alberdi, D. Vázquez- García, J. J. Fernández and J. M. Vila, *J. Organomet. Chem*., 2003, **665**, 76; (d) D. R. Smyth, J. Hester, V. G., Jr. Young and E. R. T. Tiekink, *CrystEngComm.*, 2002, **4**, 517.
9. T. Karlen, P. Dani, D. M. Grove, P. Steenwinkel and G. van Koten, *Organometallics* 1996, **15**, 5687.
10. P. Bhattacharyya, J. Parr and A. M. Z. Slawin, *J. Chem. Soc., Dalton Trans*., 1998, 3609.
11. (a) J. Forniés, V. Sicilia, C. Larraz, J. A. Camerano, A. Martín, J. M. Casas and A. C. Tsipis, *Organometallics*, 2010, **29**, 1396; (b) P. D. Smith, T. Gelbrich and M. B. Hursthouse, *J. Organomet. Chem.*, 2002, **659**, 1; (c) C. A. Craig, F. O. Garces, R. J. Watts, R. Palmans and A. J. Frank, *Coord. Chem. Rev.*, 1990, **97**, 193; (d) M. M. Mdleleni, J. S. Bridgewater, R. J. Watts, P. C. Ford, *Inorg. Chem*., 1995, **34**, 2334; (e) A. Zucca, G. L. Petretto, S. Stoccoro, M. A. Cinellu, M. Manassero, C. Manassero and G. Minghetti, *Organometallics*, 2009, **28**, 215.

12. P. S. Pregosin and R. W. Kunz, in: P. Diehl, E. Fluck, R. Kosfeld (Eds.), *^{31}P and ^{13}C NMR of Transition Metal Phosphine Complexes*, Springer-Verlag, Berlin, 1979.
13. R. Munzenberg, P. Rademacher and R. Boese, *J. Mol. Struct*., 1998, **444**, 77.
14. R. Ares, D. Vázquez-García, M. López-Torres, A. Fernández, N. Gómez-Blanco, J. M. Vila and J. J. Fernández, *J. Organomet. Chem*., 2008, **693**, 3655.
15. D. Vázquez-García,A. Fernández, J. J. Fernández, M. López-Torres, A. Suárez, J. M. Ortigueira, J. M. Vila and H. Adams, *J. Organomet. Chem*., 2000, **595**, 199.
16. O. M. N Dhubhghaill, J. Lennona and M. G. B. Drew, *Dalton Trans*., 2000, 3213.
17. G. Bandoli and A. Dolmella, *Coord. Chem. Rev*., 2000, **209**, 161.
18. J.-F. Ma and Y. Yamamoto, *Inorg. Chim. Acta*., 2000, **299**, 164.
19. T. G. Appleton and M. A. Bennett, *Inorg. Chem*., 1978, **17**, 738.
20. S. S. Zumdahl, R. S. Drago, *J. Am. Chem. Soc*., 1968, **90**, 6669.
21. W. L. Steffen, G. J. Palenik, *Inorg. Chem*., 1976, **15**, 2432.
22. (a) F. R. Hartley, *The Chemistry of Platinum and Palladium*, Applied Science Publishers Ltd, London, 1973, pp. 331 – 334; (b) A. Garoufis, S. K. Hadjikakou and N. Hadjiliadis, *Metallotherapeutic Drugs and Metal-based Diagnostic Agents*; M. Gielen, E. R. T. Tiekink, Eds; John Wiley & Sons Ltd, England, 2005, pp. 339 – 415.
23. M. M. Mogorosi, PhD thesis, *Synthesis and Characterization of Nickel, Palladium and Chromium Complexes as Olefin Oligomerization Catalysts*, University of Cape Town, 2009.
24. C. Albrecht, C. Wagner, K. Merzweiler, T. Lis and D Steinborn, *Appl. Organometal. Chem*., 2005, **19**, 1155.
25. M. Crespo, M. Font-Bardía and X. Solans, *J. Organomet. Chem*., 2006, **691**, 444.
26. C. Anderson, M. Crespo, J. Morris and J. M. Tanski, *J. Organomet. Chem*., 2006, **691**, 5635.
27. Y. Murata, H. Ohgi, T. Fujihara, J. Terao and Y. Tsuji, *Inorg. Chim. Acta*, 2011, **368**, 237.
28. H. Makio, N. Kashiwa and T. Fujita, *Adv. Synth. Catal*., 2002, **344**, 477.
29. C. Anderson, M. Crespo, M. Font-Bardía, A. Klein and X. Solans, *J. Organomet. Chem*., 2000, **601**, 22.
30. M. Crespo, X. Solans and M. Font-Bardia, *J. Organomet. Chem*., 1994, **483**, 187.
31. N. C. Gonnell, C. Busacca, S. Campbell, M. Eriksson, N. Grinberg, T. Bartholomeyzik, S. Ma and D. L. Norwood, *Magn. Reson. Chem*., 2009, **47**, 461.
32. Similar mechanism: (a) Z. Shen and R. F. Jordan, *J. Am. Chem. Soc*., 2010, **132**, 52; (b) C. T. Burns, H. Shen and R. F. Jordan, *J. Organomet. Chem*., 2003, **683**, 240; (c) P. W. N. M.

van Leeuwen, C. F. Roobeek and R. Huis, *J. Organomet. Chem*., 1977, **142**, 233. (d) J. E. Hux, R. J. Puddephatt, *J. Organomet. Chem*., 1992, **437**, 251. (e) H. G. Alt, *Angew. Chem. Int. Ed. Engl*. 1984, **23**, 766. (f) A. Hudson, M. F. Lappert, P. W. Lednor and B. K. Nicholson, *J. Chem. Soc., Chem. Commun*., 1974, 966. (g) B. C. Ankianiec, D. T. Hardy, S. K. Thomson, W. N. Watkins and G. B. Young, *Organometallics*, 1992, **11**, 2591.

33. W. S. Knowles, B. D. Vineyard, M. J. Sabacky, G. L. Bachmann and D. J. Weinkauff, *J. Am. Chem. Soc*., 1977, **99**, 5946.
34. (a) J. J. Low and W. A. Goddard, III. *J. Am. Chem. Soc*., 1986, **108**, 6115; (b) K. Tatsumi, R. Hoffmann, A. Yamaoto, J. K. Stille, *Bull. Chem. Soc. Jpn*., 1981, **54**, 1857.
35. S. Shekhar and J. F. Hartwig, *J. Am. Chem. Soc*., 2004, **126**, 13016.
36. E. Guido, G. D'Amico, N. Russo, E. Sicilia, S. Rizzato, Alberto Albinati, A. Romeo, M. R. Plutino and R. Romeo, *Inorg. Chem*., 2011, **50**, 2224.
37. A. L. Casado and P. Espinet, *Organometallics* 1998, **17**, 954.
38. R. G. Wilkins, *Kinetics and Mechanism of Reactions of Transitions Metal Complexes*, 2nd ed.; VCH: Weinheim, 1991.
39. (a) G. Alibrandi, L. M. Scolaro and R. Romeo, *Inorg. Chem*., 1991, **30**, 4007 and references therein; (b) U. Frey, L. Helm, A. E. Merbach and R. Romeo, *J. Am. Chem. Soc*., 1989, **111**, 8161.
40. L. J. Goossen, D. Koley, H. L. Hermann, and W. Thiel, *Organometallics*, 2005, **24**, 2398.
41. F. Basolo and G. Pearson, *Mechanism of Inorganic Reactions*, 2nd ed.; Wiley: New York, 1967.
42. (a) G. K. Anderson and R. J. Cross, *J. Chem. Soc. Rev*., 1980, **9**, 185; (b) R. S. Berry, *J. Chem. Phys*., 1960, **32**, 933.
43. (a) F. Ozawa, T. Ito, Y. Nakamura and A.Yamamoto, *Bull. Chem. Soc. Jpn*., 1981, **54**, 1868; (b) R. S. Pavonessa and W. C. Trogler, *J. Am. Chem. Soc*., 1982, **104**, 3529.
44. S. Noda, A. Nakamura, T. Kochi, L. W. Chung, K. Morokuma and K. Nozaki, *J. Am. Chem. Soc*., 2009, **131**, 14088.
45. S. Sakaki, N. Mizoe, Y. Musashi and M. Sugimoto, *J. Mol. Struct. (THEOCHEM*), 1999, **461-462**, 533.

Chapter 5
Conclusions

5.1 Conclusions

Cyclometallated palladium complexes bearing *N*-benzylidenebenzylamines were previously synthesized and showed poor activity towards ethylene oligomerization.[1] In the present study, various factors which could possibly cause such low activity were investigated both theoretically and experimentally.

Theoretically, we studied i) the possible catalyst/co-catalyst interactions between the cyclometallated palladium pre-catalyst and three TMA-expanded MAO models, and ii) the possible mechanisms of their involvement in ethylene oligomerization.

The DFT-predicted Pd/MAO interactions suggest that a neutral MAO-dissociation process remains the major interaction that will take place as evident from all MAO models studied. The formal methyl abstraction process could also be feasible when more energy is providing by, for example, increasing the reaction temperature. Therefore, both Cossee-type (involving linear chain-growing intermediates) and metallacycle (involving cyclic chain-growing intermediates) mechanisms could be possible in the actual catalysis reactions.

Based on the energetic comparison of the two possible mechanisms, the Cossee-type mechanism was found to be kinetically favoured over the metallacycle mechanism. This kinetic favouring is not caused by significant differences in individual elementary step barriers or a single rate-determining step in either of the two mechanisms, but dictated by differences in thermodynamics. The Cossee-type mechanism is thermodynamically favoured with each uptake of ethylene, which results in a much lower overall kinetic barrier compared to that of the metallacycle mechanism.

Additionally, the chain-initiation, chain-growth and chain-transfer steps of a Cossee-type mechanism were studied. *Cis/trans* isomerization was considered for the alkylation of the palladium pre-catalyst by MAO. The so-called *cis*-methylpalladium(II) species **III'-s** (PPh_3

being *cis* to the N atom) was calculated to be thermodynamically more stable than the *trans* isomer **III-s** (where PPh_3 is *trans* to the N atom) and thus would be formed predominantly. On the other hand, the DFT-estimated LUMO of the three-coordinate (N^C)Pd(CH_3) species showed that the LUMO is localized on the imine fragment in the *cis* isomer **A1'**, while it is on the vacant site of the palladium centre in the case of the *trans* isomer **A1**. Therefore, **A1** is the active species for the uptake of ethylene to initiate the oligomerization cycle. Catalytic activity would thus possibly depend on the extent of the formation of the *trans*-methylpalladium(II) species **III-s**.

Furthermore, it was found that the incoming ethylene could only coordinate at the vacant site in the three-coordinate *trans*-alkyl palladium species. This is an unusual feature for the current Cossee-type mechanism involving a cyclometallated palladium catalyst system. Consequently, prior isomerization of the three-coordinate β-agostic *cis*-alkyl palladium species to its *trans* isomer would be required for chain propagation to commence. The energy barrier for the isomerization step, however, was predicated to be too high to overcome, leading only to the dimerization of ethylene.

From this theoretical study, we were able to conclude that the oligomerization of ethylene by cyclometallated palladium complexes has low activity and produces mainly ethylene dimers, and rationalize the observation of actual catalytic reactions.

Experimentally, cyclometallated platinum(II) complexes bearing *N*-benzylidenebenzylamine (N^C) were synthesized as model complexes of the palladium pre-catalysts. Their salicylaldimine (N^O) analogues were synthesized as well. Both the N^C and N^O chelate complexes have similar features and N^O ligands have previously been coordinated to transition metals and applied in ethylene oligomerization/polymerization.[2,3] The influence of these chelating ligands in platinum(II) complexes were thus investigated according to their spectroscopic and structural properties, as well as in various reactivity studies.

The N^C platinum complexes are generally more thermally stable than their N^O analogues. With regard to structural properties, there was no significant difference between the N^C complexes and the N^O analogues.

The reactions of various phosphines with dmso-ligated platinum(II) complexes containing both N^C and N^O chelating ligands were studied in the present work. The metal-containing-rings of the N^C complexes are more stable than those of the N^O analogues.

The methylplatinum(II) complex with a *cis* arrangement of PPh_3 and the N atom, **C10**, was obtained as the predominant product from the methylation reaction of its *trans* parent complex **C4** with LiMe. **C10** is therefore a thermodynamically controlled product. As a model reaction to represent the methylation step by MAO on the palladium analogue in an actual ethylene oligomerization process, it agrees quite well with the theoretical observation, i.e., the *cis*-methylpalladium(II) **III'-s** would be thermodynamically more stable than its *trans* isomer **III-s**.

The methyl-platinum and -palladium(II) complexes, **C11** and **C12**, were synthesized by an alternative route to methylation. *Cis/trans* rearrangement was also observed during the formation of stable products. Both platinum and palladium complexes showed similar spectroscopic properties, while the palladium complex is less stable both thermally and photolytically.

The CV results together with the ^{31}P NMR data of the diplatinum(II) complexes with a dppf spacer ligand, **C8** and **C9**, showed that the N^C ligand (**L_A**) is a better electron-donating ligand compared to the N^O ligand (**L_B**). From the complexes with more electron-donating groups, reductive elimination can be faster. [4] Due to the fact that the related N^O palladium complexes previously reported showed reasonable activities towards ethylene dimerization/oligomerization,[3,5] the ethylene oligomerization by N^C-cyclometallated palladium complexes would produce even shorter chain length oligomers. This is consistent with the DFT prediction of the formation of dimers as major products in cyclometallated palladium-catalysed ethylene oligomerization reactions.

The *cis*-to-*trans* isomerization of the N^O complex **C5a** was studied both experimentally and theoretically. The results of DFT calculations suggest that a direct geometry change mechanism would be the possible isomerization pathway amongst the three studied mechanisms. The computed activation parameters are in very good agreement with the experimental activation parameters obtained from kinetic studies.

Overall, this study has shown that the Cossee-type mechanism is the most likely mechanism for cyclometallated palladium-catalysed ethylene oligomerization. The catalysis reactions, however, show low activity and produce mainly butenes as products according to the DFT results. This confirms that DFT is a useful tool to interpret the experimental findings and to explore the crucial elementary steps of the entire catalytic reaction process. In conjunction with the experimental studies on platinum(II) model complexes, potential shortcomings existing in the currently studied cyclometallated palladium catalyst system have been identified. For example, we have shown that the *cis*-methylpalladium(II) species, which is not active for uptake of ethylene, could be formed as a major product in the MAO alkylation process, resulting in the low activity observed in the oligomerization reactions. We have also shown from the CV results that the N^C ligand is a better electron-donor ligand than the N^O ligand. This could result in the N^C complex undergoing fast reductive elimination and explain the production of butenes in the oligomerization reactions. The results presented here will contribute to the design of new palladium catalysts for oligomerization in the future.

5.2 References

1. (a) N. W. Mungwe, M.Sc. thesis, *The synthesis of the cyclometallated palladium complexes and their applications in olefin oligomerization and in phenylacetylene oligomerization/polymerization*, University of Western Cape, 2008; (b) N. Mungwe, A. Swarts, S. F. Mapolie and G. Westman, *J. Organomet. Chem*., 2011, **696**, 3527.
2. T. R. Younkin, E. F. Connor, J. I. Henderson, S. K. Friedrich, R. H. Grubbs and D. A. Bansleben, *Science*, 2000, **287**, 460.
3. (a) S. Budagumpi, Y. Liu, H. Suh and I. Kim, *J. Organomet. Chem*., 2011, **696**, 1887; (b)Y. Chen, S. Mandal and A. Sen, *Organometallics*, 2010, **29**, 3160.
4. (a) G. Alibrandi, L. M. Scolaro and R. Romeo, *Inorg. Chem*., 1991, **30**, 4007 and references therein; (b) U. Frey, L. Helm, A. E. Merbach and R. Romeo, *J. Am. Chem. Soc*., 1989, **111**, 8161; (c) E. Guido, G. D'Amico, N. Russo, E. Sicilia, S. Rizzato, Alberto Albinati, A. Romeo, M. R. Plutino and R. Romeo, *Inorg. Chem*., 2011, **50**, 2224; (d) X. Zhang, S. Kandala, L. Yang, W. H. Watson, X. Wang, D. A. Hrovat, W. T. Borden and M. G. Richmond, *Organometallics*, 2011, **30**, 1253.
5. M. M. Mogorosi, PhD thesis, *Synthesis and Characterization of Nickel, Palladium and Chromium Complexes as Olefin Oligomerization Catalysts*, University of Cape Town, 2009.

Chapter 6
Experimental Details

6.1 General Remarks

All reactions were carried out under a nitrogen or argon atmosphere using a dual vacuum/nitrogen line and standard Schlenk techniques unless stated otherwise. Solvents were dried and purified by heating at reflux under argon in the presence of a suitable drying agent. Hexane, pentane and methylcyclohexane were refluxed and distilled from calcium hydride (CaH_2); tetrahydrofuran (THF), diethyl ether (Et_2O), and toluene were dried over sodium-wire and benzophenone; dichloromethane was dried over P_2O_5 under nitrogen.[1] After the purification procedures, the solvents were transferred under vacuum into a Teflon-valve storage vessel. All reagents were purchased from Aldrich and used without further purification. (Benzylidene 2,6-diisopropylphenyl) amine (**L_A**),[2] $Pt(SOMe_2)Cl_2$,[3] Salicylaldimine ligands **L_B** and **L_C**[4] were prepared as reported elsewhere. Reaction progress and product mixtures were monitored by thin-layer chromatography (TLC) on precoated silica-gel F254 plates using a suitable solvent system, employing the ascending technique; the plates were viewed under a UV light. Column chromatography was carried out using 60 Å silica-gel (70-230 mesh ASTM).

6.2 Instrumentation

Melting points were recorded on a Kofler hotstage microscope (Reichert Thermovar). Elemental analyses were carried out on a Fisons EA 1108 CHNS Elemental Analyzer at the microanalytical laboratory of the University of Cape Town. IR absorptions were measured on a Perkin Elmer Spectrum One FT-IR spectrophotometer. Mass spectral analyses were carried out at Stellenbosch University on a Waters Q-TOF Ultima API or Waters Quattro Micro API mass spectrometer and using the electrospray ionization technique.

^1H, ^{31}P and ^{13}C NMR spectra were recorded on a Varian Mercury-300 MHz (^1H: 300 MHz; ^{13}C: 75.5 MHz; ^{31}P: 121 MHz) or Varian Unity-400 MHz (^1H: 400 MHz; ^{13}C: 100.6 MHz) spectrometer. ^1H NMR spectra were referenced internally using the residual protons in the

deuterated solvents ($CDCl_3$: δ 7.27; DMSO: δ 2.50 ppm; C_6D_6: δ 7.16 ppm) and values reported relative to the internal standard tetramethylsilane (δ 0.00). ^{13}C NMR spectra were referenced internally to the resonance ($CDCl_3$: δ 77.0; DMSO: δ 39.4, C_6D_6: δ 128.1 ppm) and the values reported relative to tetramethylsilane (δ 0.0). All chemical shifts are quoted in δ (ppm) and coupling constants, *J*, in Hertz (Hz).

6.3 Preparation of the Platinum(II) Complexes

***[PtCl{(C$_6$H$_4$)CH=N{2,6-(Me$_2$CH)$_2$(C$_6$H$_3$)}}(SOMe$_2$)]* (C1)**

C1 was obtained from *cis*-$[PtCl_2(SOMe_2)_2]$ (0.556 g, 1.32 mmol), imine ligand **L$_A$**, (0.0.350 g, 1.32 mmol) and sodium acetate (0.210 g, 2.65 mmol), which were allowed to react in dry methanol at 65 ^oC for 48 h. The reaction mixture was filtered through celite to remove metallic platinum. The solvent was removed on a rotary evaporator and the residue was recrystallized using dichloromethane-methanol, yielding a deep yellow crystalline solid which was isolated by filtration in *vacuo*. Yield 0.218 g (29%). m.p.: 194 – 196 ^oC. IR (KBr): ν (CH=N) 1601 cm^{-1}, (S=O) 1139 cm^{-1}. ^1H NMR (400 MHz, $CDCl_3$): δ = 8.31 [d, $^4J_{H\text{-}H}$ = 7.83 Hz, $^3J_{Pt\text{-}H}$ = 40.1, 1H, H^5], 7.95 [s, $^3J_{Pt\text{-}H}$ = 114.3, 1H, H^a], 7.41 [d, $^3J_{H\text{-}H}$ = 7.33, 1H, H^2], 7.31 [t, b, $^3J_{H\text{-}H}$ = 8.36 Hz, 1H, H^4], 7.27-7.22 [m, 1H, H^3], 7.21-7.16 [m, 1H, $H^{4'}$], 7.15 [d, $^3J_{H\text{-}H}$ = 7.77 Hz, 2H, $H^{3',5'}$], 3.52 (s, $^3J_{Pt\text{-}H}$ = 24.21, H^d), 3.29 (hept, 2H, H^b), 1.30 (d, $^3J_{H\text{-}H}$ = 6.79 Hz, 6H, H^c), 1.12 (d, $^3J_{H\text{-}H}$ = 6.87 Hz, 6H, $H^{c'}$). ^{13}C NMR ($CDCl_3$): δ = 181.05 [s, C^a], 179.94 [s, $C^{1'}$], 141.74 [s, $C^{2',6'}$], 133.94 [s, C^5], 133.58 [s, C^4], 131.58 [s, C^1], 129.64 [s, C^2], 128.11 [s, C^3], 124.24 [s, C^6], 124.73 [s, $C^{4'}$], 123.02 [s, $C^{3',5'}$], 46.78 [s, C^d], 28.17 [s, C^b], 24.44 [s, $C^{c'}$], 22.74 [s, C^c]. EI-MS: *m/z* 541.2 $[M\text{-}OMe]^+$, 500.02 $[M\text{-}^i Pr\text{-}2Me]^+$, 457.1 $[M\text{-}Cl\text{-}dmso]^+$. Anal. Found (calc. for $C_{21}H_{28}ClNOPtS$): C: 44.43 (44.01), H: 4.58 (4.92), N: 2.03 (2.44), S: 5.82 (5.60).

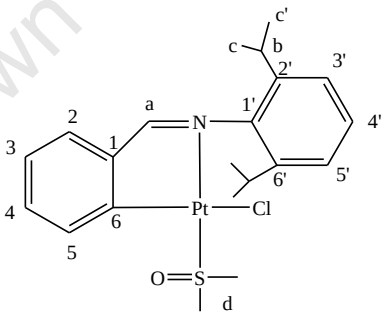

C1

***[PtCl{(OC$_6$H$_4$)CH=N{2,6-(Me$_2$CH)$_2$(C$_6$H$_3$)}}(SOMe$_2$)]* (C2)**

Cis-$[PtCl_2(SOMe_2)_2]$ (0.522 g, 1.24 mmol) and the imine **L$_B$** (0.348 g, 1.24 mmol) in the presence of sodium acetate (0.101 g, 1.24 mmol) were allowed to react in dry methanol (20

ml) under reflux for 2 h or 16 hr at room temperature. The solvent was removed on a rotary evaporator, and the residue obtained was dissolved in a minimum amount of CH_2Cl_2 and then passed through a SiO_2 column. Two isomeric forms of this product (**C2a** and **C2b**) were isolated. N-hexane/ethyl acetate (95:5) was used to elute the band of unreacted ligand and the second band was eluted by n-hexane/ethyl acetate (70:30), which produced complex **C2a**. The final band was eluted by n-hexane/ethyl acetate (50:50) solution to give isomer, **C2b**. These isomers differ in the conformation of the Cl^- ligand [*trans* to N atom (**C2a**) or O atom (**C2b**)].

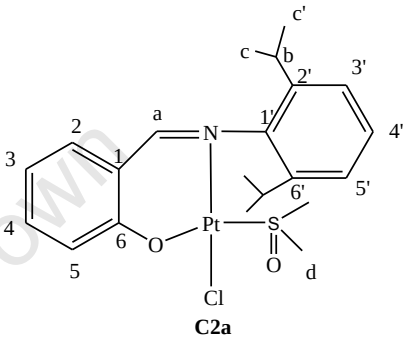

C2a

C2a, yield 0.550 g, 75 %. m.p.:164 – 167 ^oC. IR (KBr): ν (CH=N) 1606 cm^{-1}, (S=O) 1154 cm^{-1}. ^1H NMR (300 MHz, $CDCl_3$): δ = 7.73 [s, $^3J_{Pt\text{-}H}$ = 93.27 Hz, 1H, H^a], 7.43 [dd, $^3J_{H\text{-}H}$ = 8.53 Hz, $^4J_{H\text{-}H}$ = 1.60 Hz, 1H, H^2], 7.24 [t, $^3J_{H\text{-}H}$ = 7.74 Hz, 1H, H4'], 7.13 [d, $^3J_{H\text{-}H}$ = 8.34 Hz, 2H, $H^{3,4}$], 7.07 [d, $^3J_{H\text{-}H}$ = 7.74 Hz, 2H, $H^{3',5'}$], 6.63 [dd, $^3J_{H\text{-}H}$ = 7.33 Hz, $^4J_{H\text{-}H}$ = 1.86 Hz, 1H, H^5], 3.32 [s, 6H, H^d], 3.51 [hept, 2H, H^b], 1.28 [d, $^3J_{H\text{-}H}$ = 6.88Hz, 6H, H^c], 1.03 [d, $^3J_{H\text{-}H}$ = 6.79 Hz, 6H, $H^{c'}$]. ^{13}C NMR ($CDCl_3$): δ = 163.05 [s, C^a], 162.47 [s, $C^{1'}$], 148.19 [s, C^6], 141.78 [s, $C^{2',6'}$], 136.68 [s, C^2], 133.66 [s, C^3], 128.00 [s, $C^{4'}$], 123.37 [s, $C^{3',5'}$], 123.06 [s, C^6], 120.79 [s, C^4], 117.25 [s, C^5], 47.37 [s, C^d], 27.93 [s, C^b], 24.71 [s, $C^{c'}$], 22.54 [s, C^c]. EI-MS: *m/z* 590.12 $[M]^+$, 556.18 $[M\text{-}OMe]^+$, 553.15 $[M\text{-}Cl]^+$, 515.15 $[M\text{-}^i Pr\text{-}Me]^+$, 474.12 $[M\text{-}Cl\text{-}dmso]^+$. Anal. Found (calc. for $C_{21}H_{28}ClNO_2PtS$): C: 43.08 (42.82), H: 4.92 (4.79), N: 2.26 (2.59), S: 5.19 (5.43).

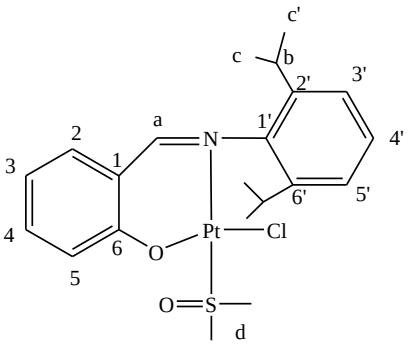

C2b

C2b, yield 0.164 g, 23 %. M.p.: 193 – 196 ^oC. IR: ν (CH=N) 1606 cm^{-1}, (S=O) 1140 cm^{-1}. ^1H NMR (300 MHz, $CDCl_3$): δ = 7.73 (s, $^3J_{Pt\text{-}H}$ = 59.47 Hz), 7.73 [s, $^3J_{Pt\text{-}H}$ = 93.27 Hz, 1H, H^a], 7.41 [dd, $^3J_{H\text{-}H}$ = 8.68 Hz, $^4J_{H\text{-}H}$ = 1.81 Hz, 1H, H^2], 7.20 [t, $^3J_{H\text{-}H}$ = 7.74 Hz, 1H, $H^{4'}$], 7.15 – 7.09 [m, 2H, $H^{3,4}$], 7.04 [dd, $^3J_{H\text{-}H}$ = 8.67 Hz, $^4J_{H\text{-}H}$ = 0.54 Hz, 2H, $H^{3',5'}$], 6.65 [dd, $^3J_{H\text{-}H}$ = 7.96 Hz, $^4J_{H\text{-}H}$ = 1.08 Hz, 1H, H^5], 3.32 [s, 6H, H^d], 3.26 [hept, 2H, H^b], 1.27 [d, $^3J_{H\text{-}H}$ = 6.80Hz, 6H, H^c], 1.03 [d, $^3J_{H\text{-}H}$ = 6.88 Hz, 6H, $H^{c'}$]. ^{13}C NMR ($CDCl_3$): δ = 162.83 [s, $C^{1'}$], 161.45 [s, C^a], 146.36 [s, C^6], 141.78 [s, $C^{2',6'}$], 136.09 [s, C^2], 134.38 [C^3], 127.66 [$C^{4'}$], 123.38 [s, C^1], 123.07 [$C^{3',5'}$], 120.62 [s, C^4], 117.11 [s, C^5], 42.31 [s, C^d], 28.09 [s, C^b], 24.40 [s, $C^{c'}$], 22.79 [s, C^c]. EI-MS: *m/z* 590.12 $[M]^+$, 556.18 [M-

OMe]$^+$, 553.15 [M-Cl]$^+$, 515.15 [M-^{i}Pr-Me]$^+$, 474.12 [M-Cl-dmso]$^+$. Anal. Found (calc. for $C_{21}H_{28}ClNO_2PtS$): C: 43.07 (42.82), H: 4.86 (4.79), N: 2.38 (2.59), S: 5.45 (5.43).

[PtCl{(OC$_6$H$_4$)CH=N(C$_6$H$_5$)}(SOMe$_2$)] (C3)

cis-[$PtCl_2(SOMe_2)_2$] (0.540 g, 1.28 mmol) and the imine $\mathbf{L_C}$ (0.252 g, 1.28 mmol) in the presence of sodium acetate (0.105mg, 1.28 mmol) were allowed to react in dry methanol (20 ml) for 16 hr at room temperature. A yellow precipitate **C3** formed. The product was collected by filtration in *vacuo*. Yield: 0.435 g, 67.2 %. M.p.: 170 – 172 ^{o}C. IR (KBr): ν (CH=N) 1607 cm^{-1}, (S=O) 1155 cm^{-1}. ^{1}H NMR (300 MHz, $CDCl_3$): δ = 7.83 [s, $^3J_{Pt\text{-}H}$ = 86.34 Hz, 1H, H^a], 7.47 [d, $^3J_{H\text{-}H}$ = 7.19 Hz, 2H, H$^{2',6'}$], 7.36 [m, 3H, H$^{3',4',5'}$], 7.27 [d, $^3J_{H\text{-}H}$ = 7.26 Hz, 1H, H^2], 7.21 [dt, $^3J_{H\text{-}H}$ = 8.08 Hz, $^4J_{H\text{-}H}$ = 1.30 Hz, 1H, H^4], 7.11 [t, $^3J_{H\text{-}H}$ = 8.60 Hz, 1H, H^3], 6.64 [d, $^3J_{H\text{-}H}$ = 7.42 Hz, 1H, H^5], 3.24 [s, 6H, H^d]. ^{13}C NMR (101 MHz, $CDCl_3$): δ = 163.47 [s, C$^{1'}$], 162.69 [s, C^a], 153.52 [s, C^6], 136.79 [s, C^2], 133.66 [s, C^4], 128.82 [s, C$^{2',6'}$], 128.00 [s, C$^{4'}$], 124.18 [s, C$^{3',5'}$], 121.06 [s, C^3], 120.08 [s, C^1], 117.58 [s, C^5], 46.36 [s, C^d]. EI-MS: *m/z* 506.03 [M]$^+$, 469.05 [M-Cl]$^+$, 391.04 [M-Cl-Ph]$^+$, 390.04 [M-Cl-dmso]$^+$. Anal. Found (calc. for $C_{15}H_{16}ClNO_2PtS$): C, 35.90 (35.68); H, 3.02 (3.19); N, 2.38 (2.77), S 5.98 (6.35).

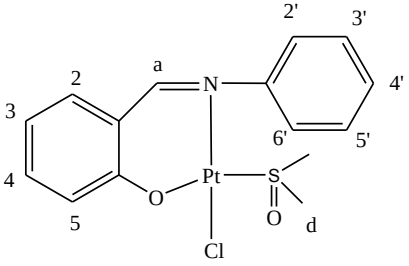

C3

[PtCl{(C$_6$H$_4$)CH=N{2,6-(Me$_2$CH)$_2$(C$_6$H$_3$)}}(PPh$_3$)] (C4)

C4 was obtained from compound **C1** (0.068 g, 1.12 mmol) and triphenylphosphine (0.031g, 0.12 mmol), which were allowed to react in acetone at room temperature for 2 h. The solvent was removed on a rotary evaporator and the residue was treated with dichloromethane-methanol, yielding a bright yellow crystalline solid which was dried in *vacuo*. Yield 70mg (78%). M.p.: 302 – 304 ^{o}C. IR (KBr): ν (CH=N) 1599 cm^{-1}. ^{1}H NMR (300 MHz, $CDCl_3$): δ = 8.28 [d, $^4J_{H\text{-}P}$ = 9.3 Hz, $^3J_{Pt\text{-}H}$ = 90.5 Hz, 1H, H^a], 7.68 - 7.63[m, 6H, Ph-H], 7.32 – 7.24 [m, 10H, H^2 and Ph-H], 7.11 – 7.06 [m, 3H, H$^{3',5'}$ and H$^{4'}$], 6.91 [t, $^3J_{H\text{-}H}$ = 7.26 Hz, 1H, H^4], 6.60 [dt, $^3J_{H\text{-}H}$ = 7.64 Hz, $^4J_{H\text{-}H}$ = 1.57

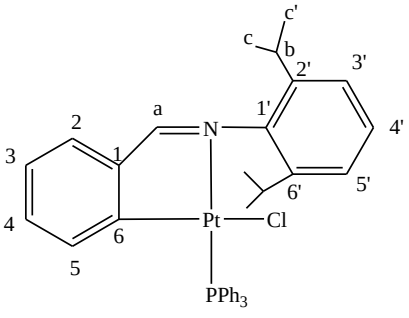

C4

Hz, 1H, H^3], 6.55 [dd, $^3J_{Pt\text{-}H}$ = 43.08 Hz, $^3J_{H\text{-}H}$ = 7.65 Hz, $^4J_{H\text{-}H}$ = 2.35 Hz, 1H, H^5], 3.35 [hept, 2H, H^b], 1.26 [d, $^3J_{H\text{-}H}$ = 6.80 Hz, 6H, H^c], 1.11 [d, $^3J_{H\text{-}H}$ = 6.88 Hz, 6H, $H^{c'}$]. ^{13}C NMR ($CDCl_3$): δ = 179.98 [d, $J_{P\text{-}C}$ = 3.22 Hz, $J_{Pt\text{-}C}$ = 85.13 Hz, C^a], 146.23 [s, $C^{1'}$], 141.55 [s, $C^{2',6'}$], 136.97 [d, $J_{P\text{-}C}$ = 5.68 Hz, $J_{Pt\text{-}C}$ = 85.13 Hz, C^5], 135.16 [d, $J_{P\text{-}C}$ = 11.13 Hz, 6C, Ph-C], 132.22 [s, C^3], 130.47 [s, $C^{3',5'}$], 129.84 [s, C^6], 128.92 [s, C^1], 127.73 [d, $J_{P\text{-}C}$ = 11.13 Hz, 9C, Ph-C], 127.13 [s, C^2], 122.72 [s, C^4], 122.55 [s, $C^{4'}$], 28.06 [s, C^b], 24.52 [s, $C^{c'}$], 22.92 [s, C^c]. ^{31}P NMR (121 MHz, $CDCl_3$): δ = 21.79 [s, $J_{P\text{-}Pt}$ = 4270.62]. EI-MS: *m/z* 762.25 $[M+5H]^+$, 721.22 $[M\text{-}Cl]^+$. Anal. Found (calc. for $C_{37}H_{37}ClNPPt$): C, 58.12 (58.69); H, 5.03 (4.93); N, 1.26 (1.85).

[PtCl{(OC$_6$H$_4$)CH=N{2,6-(Me$_2$CH)$_2$(C$_6$H$_3$)}(PPh$_3$)] **(C5)**

C2a or **C2b** or the mixture of **C2a** and **C2b** (0.666 g, 1.0 mmol) and triphenylphosphine (0.296 g, 1.0 mol) were allowed to react in dichloromethane at room temperature for 2 h. The solvent was removed using a rotary evaporator, and the residue obtained was dissolved in a minimum amount of CH_2Cl_2 and then passed through a SiO_2 column. Two isomeric forms of this product (**C5a** and **C5b**) were isolated. Elution with n-hexane/ethyl acetate (98:2) solution produced a yellow band, which yielded **C5b**; Elution with n-hexane/ethyl acetate (80:20) solution released second band that was collected and concentrated to give **C5a**. These isomers differ in the conformation of the PPh_3 ligand [*cis* to N atom (**C5a**) or *trans* to N atom (**C5b**)].

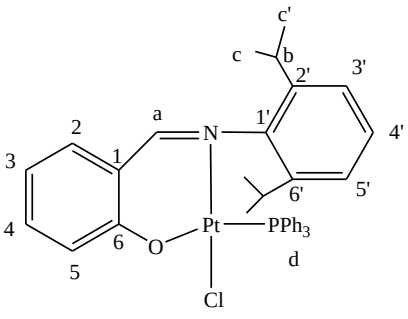

C5a

C5a, yield 0.294 mg, 34%. M.p.: 210 – 214 ^{o}C. IR: ν (CH=N) 1606.7 cm^{-1}. ^{1}H NMR (300 MHz, $CDCl_3$): δ = 7.61 [s, 1H, H^a], 7.49 [d, $^3J_{H\text{-}H}$ = 8.32 Hz, 1H, H^2], 7.48 – 7.43 [m, 6H, Ph-H], 7.29 – 7.25 [m, 3H, Ph-H], 7.19 [d, $^3J_{H\text{-}H}$ = 8.76 Hz, 1H, H^5], 7.16 – 7.12 [m, 6H, Ph-H], 7.09 [dt, $^3J_{H\text{-}H}$ = 8.07 Hz, $^4J_{H\text{-}H}$ = 1.48 Hz, 1H, H^4], 6.83 [t, $^3J_{H\text{-}H}$ = 7.77 Hz, 1H, $H^{4'}$], 6.64 [d, $^3J_{H\text{-}H}$ = 7.75 Hz, 2H, $H^{3',5'}$], 6.59 [t, $^3J_{H\text{-}H}$ = 7.29 Hz, 1H, H^3], 3.66 [hept, 2H, H^b], 0.94 – 0.92 [m, 12H, $H^{c,c'}$]. ^{13}C NMR (101 MHz, $CDCl_3$): δ = 163.94 [s, C^a], 163,22 [s, $C^{1'}$], 151.50 [s, C^6], 140.99 [s, $C^{2',6'}$], 136.17 [s, C^2], 134.92 [d, $J_{P\text{-}C}$ = 10.29, 6C, Ph-C], 133.48 [s, C^4], 129.83 [d, $J_{P\text{-}C}$ = 2.33 Hz, 3C, Ph-C], 128.50 [s, $C^{4'}$], 127.81 [d, $J_{P\text{-}C}$ = 11.05, 6C, Ph-C], 123.59 [s, $C^{3',5'}$], 122.05 [s, C^5], 118.85 [s, C^1], 116.25 [s, C^3], 27.78 [s, C^b], 25.48 [s, $C^{c'}$], 21.91 [s, C^c]. ^{31}P NMR (121 MHz, $CDCl_3$):

δ = -2.14 [s, $J_{P\text{-}Pt}$ = 4063.88]. EI-MS: *m/z* 774.2 $[M]^+$, 737.2 $[M\text{-}Cl]^+$. Anal. Found (calc. for $C_{37}H_{37}ClNOPPt$): C, 57.70 (57.47); H, 5.02 (4.82); N, 1.73 (1.81).

C5b, yield 0.423 g, 48%. M.p.: 236 – 239 ^oC. IR: ν (CH=N) 1609.8 cm^{-1}. ^1H NMR (300 MHz, $CDCl_3$): δ = 8.06 [d, $^4J_{P\text{-}H}$ = 13.92 Hz, 1H, H^a], 7.83 – 7.76 [m, 6H, Ph-H], 7.50 [d, $^3J_{H\text{-}H}$ = 13.92 Hz, 1H, H^2], 7.48 – 7.36 [m, 9H, Ph-H], 7.26 [t, $^3J_{H\text{-}H}$ = 1.82 Hz, 1H, H^4], 7.24 [t, $^3J_{H\text{-}H}$ = 1.80 Hz, 1H, $H^{4'}$], 7.20 [d, $^3J_{H\text{-}H}$ = 1.61 Hz, 2H, $H^{3',5'}$], 6.57 [dt, $^3J_{H\text{-}H}$ = 7.50 Hz, $^4J_{H\text{-}H}$ = 1.07 Hz, 1H, H^3], 6.31 [dd, $^3J_{H\text{-}H}$ = 8.57 Hz, $^4J_{H\text{-}H}$ = 0.49 Hz, 1H, H^5], 3.53 [hept, 2H, H^b], 1.41 [d, $^3J_{H\text{-}H}$ = 6.83 Hz, 6H, H^c], 1.14 [d, $^3J_{H\text{-}H}$ = 6.83 Hz, 6H, $H^{c'}$]. ^{13}C NMR (101 MHz, $CDCl_3$): δ = 163.46 [s, $C^{1'}$], 160.48 [s, C^a], 146.33 [s, C^6], 141.86 [s, $C^{2',6'}$], 135.13 [d, $J_{P\text{-}C}$ = 10.52 Hz, 6C, Ph-C], 134.89 [s, C^2], 134.48 [s, C^4], 130.63 [d, $J_{P\text{-}C}$ = 2.38 Hz, 3C, Ph-C], 128.71 [s, C^1], 127.85 [d, $J_{P\text{-}C}$ = 11.11 Hz, 6C, Ph-C], 126.98 [s, $C^{4'}$], 122.84 [s, $C^{3'\&5'}$], 121.10 [s, C^5], 116.10 [s, C^3], 28.18 [s, C^b], 24.73 [s, $C^{c'}$], 22.86 [s, C^c]. ^{31}P NMR (121 MHz, $CDCl_3$): δ = 8.87 [s, $J_{P\text{-}Pt}$ = 3818.82]. EI-MS: *m/z* 774.2 $[M]^+$, 737.2 $[M\text{-}Cl]^+$, Anal. Found (calc. for $C_{37}H_{37}ClNOPPt$): C, 57.78 (57.47); H, 4.93 (4.82); N, 1.72 (1.81).

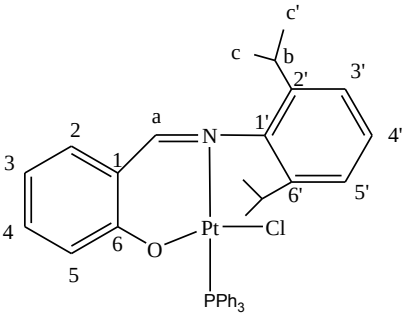

C5b

[PtCl{(OC$_6$H$_4$)CH=N(C$_6$H$_5$)}(PPh$_3$)] **(C6)**

C6 was obtained from **C3** (0.108 g, 0.21 mmol) and triphenylphosphine (56 mg, 0.21 mmol), which were allowed to react in dichloromethane at room temperature for 2 h. The solvent was removed on a rotary evaporator, and the residue obtained was dissolved in the minimum amount of CH_2Cl_2 and then passed through a SiO_2 column. Elution with n-hexane/ethyl acetate (90:10) solution gave a yellow band. Yield 0.102 g (69.3 %). M.p.: 210 – 212 ^oC. IR: ν (CH=N) 1608 cm^{-1}. ^1H NMR (300 MHz, $CDCl_3$): δ = 8.20 [d, $^4J_{P\text{-}H}$ = 13.39 Hz, 1H, H^a], 7.77 (m, 6H, Ph-H), 7.47 [d, $^3J_{H\text{-}H}$ = 6.84 Hz, 1H, H^2], 7.45 – 7.37 (m, 9H, Ph-H), 7.35 (m, 1H, H^4) 7.28 (d, $^3J_{H\text{-}H}$ = 7.48 Hz, 2H, $H^{2',6'}$), 7.22 (t, $^3J_{H\text{-}H}$ = 7.64 Hz, 2H, $H^{3',5'}$) 7.17 (t, $^3J_{H\text{-}H}$ = 8.60 Hz, 1H, $H^{4'}$), 6.55 (t, $^3J_{H\text{-}H}$ = 7.53 Hz, 1H, H^3), 6.16 (d, $^3J_{H\text{-}H}$ =8.62 Hz, 1H, H^5). ^{13}C NMR (101 MHz,

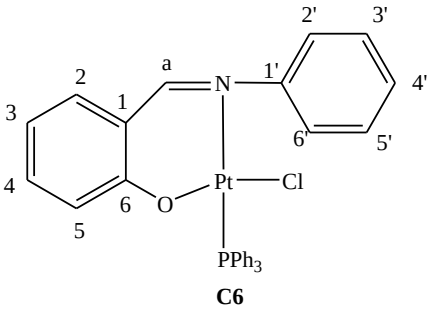

C6

$CDCl_3$): δ = 163.01 [s, $C^{1'}$], 160.89 [s, C^a], 151.12 [s, C^6], 135.06 [d, $J_{P\text{-}C}$ = 11.52 Hz, 6C, Ph-C], 134.96 [s, $C^{4'}$], 130. 67 [s, $C^{2,2',6'}$], 128.20 [d, $J_{P\text{-}C}$ = 2.42 Hz, 3C, Ph-C], 127.96 [d, $J_{P\text{-}C}$ = 10.32 Hz, 6C, Ph-C], 124.83 [s, $C^{3',5'}$], 121.86 [s, C^5], 119.64 [s, C^1], 116.52 [s, C^3]. ^{31}P NMR (121 MHz, $CDCl_3$): δ = 7.40 [s, $J_{P\text{-}Pt}$ = 3869 Hz]. EI-MS: *m/z* 688.2 $[M]^+$, 653.8 $[M\text{-}Cl]^+$. Anal. Found (calc. for $C_{31}H_{25}ClNOPPt$): C, 54.64 (54.04); H, 3.85 (3.66); N, 1.87 (2.03)

[Pt{(C$_6$H$_4$)CH=N{2,6-(Me$_2$CH)$_2$(C$_6$H$_3$)}}{Ph$_2$P(CH$_2$)$_2$PPh$_2$}]Cl **(C7** solution**)**
[PtCl{(C$_6$H$_4$)CH=N{2,6-(Me$_2$CH)$_2$(C$_6$H$_3$)}}{Ph$_2$P(CH$_2$)$_2$PPh$_2$}] **(C7** solid**)**

C7 was obtained from compound **C1 (**0.050 g, 0.087 mmol) and bis(diphenylphosphino)ethane (dppe) (0.035 g, 0.087 mmol) which were allowed to react in acetone at room temperature for 4 h. The solvent was removed on a rotary evaporator, and the residue obtained was dissolved in a minimum amount of CH_2Cl_2 and passed through a SiO_2 column. Elution with n-hexane/ethyl acetate (50:50) solution removed the impurities and the product band was eluted using methanol. The yellow solid obtained recrystallized from acetone giving an off white crystalline solid. Yield 33 mg (42%). M.p.: 320 – 323 ^oC. IR: ν (CH=N) 1631 cm^{-1} (KBr); 1602 cm^{-1} (DCM solution). ^{1}H NMR (300 MHz, $CDCl_3$): δ = 8.28 [d, $^4J_{H\text{-}P}$ = 8.09 Hz, $^3J_{Pt\text{-}H}$ = 83.82 Hz, 1H, H^a], 7.94 [dd, $^3J_{H\text{-}P}$ = 11.98 Hz, $^3J_{H\text{-}H}$ = 7.56 Hz, 4H, Ph-H], 7.60 - 7.52[m, 8H, Ph-H], 7.39 [m, 2H, Ph-H], 7.30 – 7.20 [m, 7H, H^3 and 6 Ph-H], 7.15 [t, $^3J_{H\text{-}H}$ = 7.69 Hz, 1H, H^4], 7.01 [t, $^3J_{H\text{-}H}$ = 7.77 Hz, 1H, $H^{4'}$], 6.98 – 6.88 [m, 2H, $H^{2,5}$], 6.78 [d, $^3J_{H\text{-}H}$ = 7.79 Hz, 2H, $H^{3',5'}$], 3.08 [hept, 2H, H^b], 2.58 [dt, $^2J_{P\text{-}H}$ = 27.06 Hz, $^3J_{H\text{-}H}$ = 14.78 Hz, 2H, H^e], 2.30 [dt, $^2J_{P\text{-}H}$ = 21.88 Hz, $^3J_{H\text{-}H}$ = 13.64 Hz, 2H, H^d], 0.79 [s, b, 12H, $H^{c,c'}$]. ^{13}C NMR ($CDCl_3$): δ = 184.92 [s, b C^a], 163.30 [dd, $J_{Pcis\text{-}C}$ = 5.62 Hz, $J_{Ptrans\text{-}C}$ = 105.58 Hz, C^6], 147.20 [d, $J_{Pcis\text{-}C}$ = 8.29 Hz, $C^{1'}$], 140.26 [s, $C^{2',6'}$], 138.51 [d, $J_{Pcis\text{-}C}$ = 3.19 Hz, $J_{Pt\text{-}C}$ = 90.59 Hz, C^5], 134.16 [d, $J_{P\text{-}C}$ = 13.67 Hz, Ph-C], 133.05 [d, $J_{P\text{-}C}$ = 11.12 Hz, Ph-C], 132.78 [d, $J_{P\text{-}C}$ = 2.03 Hz, C^3], 131.49 [d, $J_{P\text{-}C}$ = 1.96 Hz, Ph-C], 130.02 [d, $J_{P\text{-}C}$ = 4.00 Hz, C^1], 129.49 [dd, $J_{P\text{-}C}$ = 13.67, 22.46 Hz, Ph-C], 128.67 [s, P-C], 128.33 [s, $C^{4'}$], 128.21 [s, P-C], 126.23 [s, C^4], 125.92 [s, P-C], 125.31 [s, P-C], 123.74 [s, $C^{3',5'}$], 29.08 [m, $C^{e,d}$], 28.15 [s, C^b], 25.46, 21.80

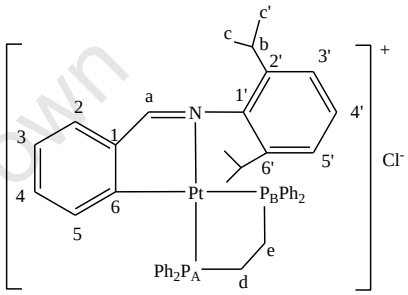

C7 in DCM or $CDCl_3$

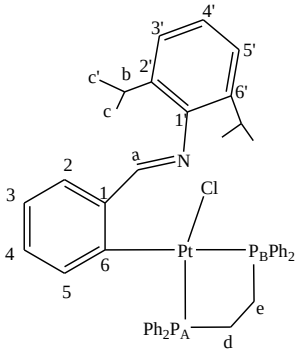

C7 in solid state

[ds, b, $C^{c,c'}$]. ^{31}P NMR (121 MHz, $CDCl_3$): δ = 43.30 [s, $J_{P\text{-}Pt}$ = 1900.91, P_B], 39.65[s, $J_{P\text{-}Pt}$ = 3711.14, P_A]. EI-MS: *m/z* 857.28 $[M\text{-}Cl]^+$. Anal. Found (calc. for $C_{45}H_{46}ClNP_2Pt$): C, 58.12 (58.69); H, 5.03 (4.93); N, 1.26 (1.85).

***[{PtCl(C$_6$H$_4$)CH=N{2,6-(Me$_2$CH)$_2$(C$_6$H$_3$)}}$_2$(μ-dppf)]* (C8)**

C8 was obtained from compound **C1** (0.062 g, 1.09 mmol) and 1,1'-bis(diphenylphosphino)-ferrocene (dppf) (0.030 g, 0.504 mmol) which were allowed to react in acetone at room temperature for 16 h. The solvent was removed on a rotary evaporator, yielding an orange solid which was dried in *vacuo*. Yield 65 mg (83%). M.p.: 184 -187 ^oC. IR (KBr): ν (CH=N) 1604 cm^{-1}. ^1H NMR (400 MHz, $CDCl_3$): δ = 8.17 (d, $^4J_{P\text{-}H}$ = 9.54 Hz, $^3J_{Pt\text{-}H}$ = 82.74 Hz, 2H, Ha), 7.62 – 7.57 [m, 8H, Ph-H], 7.35 [d, $^3J_{H\text{-}H}$ = 7.57 Hz, 2H, H^2], 7.29 [d, $^3J_{H\text{-}H}$ = 6.99 Hz, 4H, $H^{3',5'}$], 7.21 – 7.16 [m, 12H, Ph-H], 7.15 [t, $^3J_{H\text{-}H}$ = 5.61 Hz, 2H, $H^{4'}$], 6.97 [t, $^3J_{H\text{-}H}$ = 7.31 Hz, 2H, H^3], 6.66 [dd, $^3J_{H\text{-}H}$ = 7.94 Hz, $^4J_{H\text{-}H}$ =1.25 Hz, 2H, H^4], 6.45 [dd, $^3J_{H\text{-}H}$ = 7.92 Hz, $^4J_{H\text{-}H}$ = 2.31 Hz, 2H, H^5], 4.98 [s, 4H, H^e], 4.39 [s, 4H, H^d], 3.37 [hept, 4H, H^b], 1.30 [d, $^3J_{H\text{-}H}$ = 6.76 Hz, 12H, H^c], 1.12 [d, $^3J_{H\text{-}H}$ = 6.85 Hz, 12H, $H^{c'}$]. ^{13}C NMR (101 MHz, $CDCl_3$): δ = 179.47 [d, $J_{P\text{-}C}$ = 3.07 Hz, $J_{Pt\text{-}C}$ = 79.31 Hz,C^a], 146.60 [s, $C^{1'}$], 141.83 [s, $C^{2',6'}$], 137.36 [d, $J_{P\text{-}C}$ = 4.36 Hz, $J_{Pt\text{-}C}$ = 92.23 Hz, C^5], 134.33 [d, $J_{P\text{-}C}$ = 10.78 Hz, 8H, Ph-C], 132.00 [s, $C^{4'}$], 131.75 [s, C^1], 130.39 [s, $C^{3',5'}$], 129.17 [s, C^2], 127.57 [d, $J_{P\text{-}C}$ = 11.01 Hz, 12H, Ph-C], 127.28 [s, C^6], 122.92 [s, C^3], 122.63 [s, C^4], 76.73 [d, $J_{P\text{-}C}$ = 10.45 Hz,C^e], 75.48 [d, $J_{P\text{-}C}$ = 7.67 Hz,C^d], 28.12 [s, C^b], 24.79 [s, $C^{c'}$], 23.14 [s, C^c]. ^{31}P NMR (162 MHz, $CDCl_3$): δ = 9.42 [s, $J_{P\text{-}Pt}$ = 4239 Hz]. EI-MS: *m/z* 1549.4 $[M+5H]^+$, 1508.4 $[M\text{-}Cl]^+$, Anal. Found (calc. for $C_{72}H_{72}C_{l2}FeN_2P_2Pt_2$): C, 56.17 (56.46); H, 4.89 (4.70); N, 1.72 (1.81).

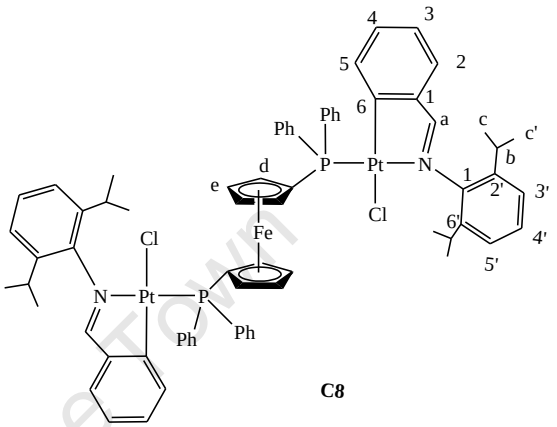

C8

***[{PtCl(OC$_6$H$_4$)CH=N{2,6-(Me$_2$CH)$_2$(C$_6$H$_3$)}}$_2$(μ-dppf)]* (C9)**

C9 was obtained from compound **C2b** (0.119 g, 20.28 mmol) and dppf (0.056g, 10.14 mmol) which were allowed to react in dichloromethane at room temperature for 16 h. The solvent

was removed on a rotary evaporator, and the residue obtained was dissolved in a minimum amount of CH_2Cl_2 and the passed through a SiO_2 column. N-hexane was used to elute the unreacted dppf, and the second band was removed by N-hexane/ethyl acetate (95:5) to produce complex **C9**. Yield: 68 mg, (75%). M.p.: decompose without melting at 281 – 285 ^oC. IR (KBr): ν (CH=N) 1610.5 cm^{-1}. ^1H NMR (400 MHz, $CDCl_3$): δ = 8.03 [d, $^3J_{H-H}$ = 14.16 Hz, 2H, H^a], 7.67-7.58 [m, 8H, Ph-H], 7.41 [d, $^3J_{H-H}$ = 6.63 Hz, 2H, H^2], 7.39 [d, $^3J_{H-H}$ = 6.59 Hz, 4H, Ph-H], 7.35-7.25 [m, 8H, Ph-H], 7.22 – 7.20 [m, 2H, H^4], 7.18 [d, $^3J_{H-H}$ = 7.43 Hz, 4H, $H^{3',5'}$], 7.17-7.14 [m, 2H, $H^{4'}$], 6.53 [t, $^3J_{H-H}$ = 7.12 Hz, 2H, H^3], 6.14 [d, $^3J_{H-H}$ = 8.60 Hz, 2H, H^5], 4.74 [d, $^3J_{H-H}$ = 0.98 Hz, 4H, H^e], 4.63 [d, $^3J_{H-H}$ = 1.55 Hz, 4H, H^d], 3.67 – 3.33 [hept, 4H, H^b], 1.33 [d, $^3J_{H-H}$ = 6.81 Hz, 12H, $H^{c'}$], 1.08 [d, $^3J_{H-H}$ = 6.84 Hz, 1H, H^c]. ^{13}C NMR (101 MHz, $CDCl_3$): δ = 163.26 [s, $C^{1'}$], 160.68 [s, C^a], 146.39 [s, C^6], 141.98 [s, $C^{2',6'}$], 134.93 [s, C^2], 134.53 [s, C^6], 134.27 [d, J_{P-C} = 10.41 Hz, 8C, Ph-C], 130.33 [s, $C^{4'}$], 127.54 [d, J_{P-C} = 11.15 Hz, 12C, Ph-C], 127.01 [s, C^4], 122.85 [s, $C^{3',5'}$], 120.98 [s, C^5], 119.68 [s, C^1], 116.07 [s, C^3], 76.51 [d, J_{P-C} = 10.52 Hz,C^e], 75.37 [d, J_{P-C} = 7.98 Hz,C^d], 28.16 [s, C^b], 24.79 [s, C^c], 23.05 [s, $C^{c'}$]. ^{31}P NMR (162 MHz, $CDCl_3$): δ = 1.98 [s, J_{P-Pt} = 3851 Hz]. EI-MS: *m/z* 1576.3 $[M]^+$, 1540.4 $[M-Cl]^+$. Anal. Found (calc. for $C_{72}H_{72}Cl_2FeN_2O_2P_2Pt_2$): C, 55.12 (54.86); H, 4.73 (4.60); N, 1.63 (1.78).

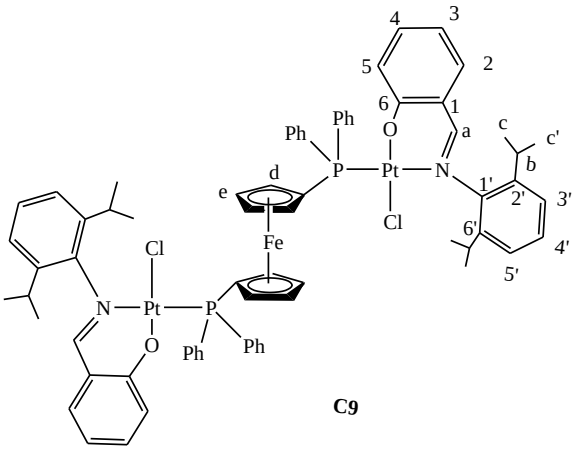

C9

[Pt(CH$_3$){(C$_6$H$_4$)CH=N{2,6-(Me$_2$CH)$_2$-(C$_6$H$_3$)}}(PPh$_3$)] **(C10)**

In a Schlenk flask, **C4** (96.3 mg, 0.127 mmol) in THF (15 ml) was cooled to T = -78 ℃, and methyllithium (0.3 mL of 1.6 M, 0.48 mmol) was added. The reactions mixture was allowed to warm to room temperature while stirring and stirred for 16 hrs until a clear orange solution was formed. The excess lithium reagent was removed by hydrolyzing the reaction mixture with 5 ml of saturated aqueous NH_4Cl at 0 ℃. The organic layer was separated and the aqueous layer was washed with 3 x 5 ml of THF. The combined organic layers were

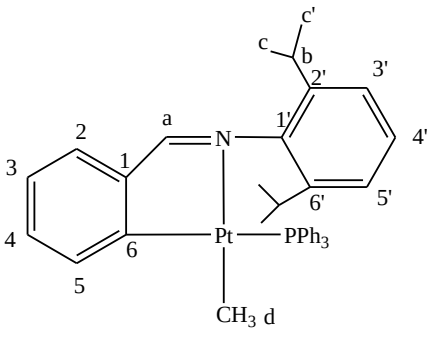

C10

dried over anhydrous $MgSO_4$ and all the volatiles were removed under reduced pressure. The residue was dissolved in a minimum of benzene and passed through a SiO_2 column. Elution with n-hexane gave a yellow band, which produced **C10**; which was recrystallized from a benzene/methanol mixture (5 ml: 10 ml) at -10 ℃ for 48 h. The orange powder solid was separated by decanting the mother liquor and dried under vacuum. Yield: 73mg (78%). M.p.: 232 – 236 ^{o}C. IR (KBr): ν (CH=N) 1599 cm^{-1}. ^{1}H NMR (300 MHz, C_6D_6): δ = 8.28 [t, $^{3}J_{H\text{-}H}$ = 6.44 Hz, $^{3}J_{Pt\text{-}H}$ = 48.07 Hz, 1H, H^5], 8.21 [s, $^{3}J_{Pt\text{-}H}$ = 57.11 Hz, 1H, H^a], 7.48 [m, 6H, Ph-H], 7.38 [t, $^{3}J_{H\text{-}H}$ = 7.58 Hz, 1H, H^4], 7.32 [d, $^{3}J_{H\text{-}H}$ = 7.59 Hz, 1H, H^2], 7.06 [t, $^{3}J_{H\text{-}H}$ = 7.35 Hz, 1H, H^3], 6.97 – 6.88 [m, 9H, Ph-H], 6.83 [t, $^{3}J_{H\text{-}H}$ = 7.57 Hz, 1H, $H^{4'}$], 6.69 [d, $^{3}J_{H\text{-}H}$ = 7.76 Hz, 2H, $H^{3',5'}$], 3.52 [hept, 2H, H^b], 1.31 [d, $^{3}J_{P\text{-}H}$ = 7.46 Hz, $^{2}J_{Pt\text{-}H}$ = 83.96 Hz 3H, H^d], 0.91 [d, $^{3}J_{H\text{-}H}$ = 6.76 Hz, 6H, H^c], 0.84 [d, $^{3}J_{H\text{-}H}$ = 6.85 Hz, 6H, $H^{c'}$]. ^{13}C NMR (101 MHz, C_6D_6): δ=180.28 [d, $J_{P\text{-}C}$ = 6.51 Hz, $J_{Pt\text{-}C}$ = 64.94 Hz, C^a], 147.82 [s, $J_{Pt\text{-}C}$ = 16.98 Hz, $C^{1'}$], 140.44 [s, $C^{2',6'}$], 134.65 (d, $J_{P\text{-}C}$ = 11.46 Hz, 6H, Ph-C), 134.12 [s, $J_{Pt\text{-}C}$ = 18.87 Hz, C^1], 133.70 [s, $J_{Pt\text{-}C}$ = 18.46 Hz, C^6], 132.19 [s, C^4], 131.94 [d, $J_{P\text{-}C}$ = 6.52 Hz, $J_{Pt\text{-}C}$ = 51.06, C^5], 128.90 [d, $J_{P\text{-}C}$ = 10.64 Hz, 9H, Ph-C], 127.78 [s, C^2], 126.38 [s, C^3], 123.83 [s, $C^{4'}$], 122.86 [s, $C^{3',5'}$], 27.30 [s, C^b], 24.96 [s, C^c], 21.63 [s, $C^{c'}$], -9.51 [d, $J_{P\text{-}C}$ = 5.97 Hz, $J_{Pt\text{-}C}$ = 744.06 Hz, C^d]. ^{31}P NMR (121 MHz, C_6D_6): δ = 31.11 [s, $J_{P\text{-}Pt}$ = 2166 Hz]. EI-MS: *m/z* 737.3 $[M]^+$, 513.1 [M-Ph-(2,6-2-^{i}Pr-Ph)]$^+$. Anal. Found (calc. for $C_{38}H_{40}NPPt$): C, 61.53 (61.95); H, 5.26 (5.47); N, 1.72 (1.90).

[Pt(CH$_3$){(OC$_6$H$_4$)CH=N{2,6-(Me$_2$CH)$_2$(C$_6$H$_3$)}}(PPh$_3$)] **(C11)**

To a methanol solution of imine $\mathbf{L_B}$ (0.206 g, 0.73 mmol) sodium acetate (0.06 g, 0.73 mmol) was added. The reaction mixture was allowed to stir at room temperature for 30 min. This mixture was slowly added to a methanol solution (10 mL) of Pt(COD)MeCl (0.258 g, 0.73 mmol) at room temperature giving a clear yellow solution. PPh_3 (0.192 g, 0.73 mmol) was then added and a yellow precipitate was obtained. The reaction mixture was left to stir at room temperature for 16 h. The reaction mixture was then filtered through Celite, and the solvent was removed in *vacuo* to give a light yellow solid. The crude product was dissolved in a minimum amount of CH_2Cl_2 and the passed through a SiO_2 column. Elution with an n-hexane/ethyl acetate (95:5) solution

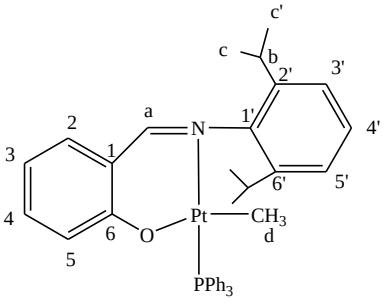

C11

produced a yellow band that was collected and concentrated to give **C11**. Yield 0.472 g (86%). M.p.: 254 - 257 ^{o}C. IR (KBr): ν (CH=N) 1608 cm^{-1}. ^{1}H NMR (300 MHz, $CDCl_3$): δ = 8.11 [d, $^{4}J_{P\text{-}H}$ = 12.25 Hz, $^{3}J_{Pt\text{-}H}$ = 70.88 Hz, 1H, H^{a}], 7.73 – 7.67 (m, 6H, Ph-H), 7.44 – 7.33 (m, 9H, Ph-H), 7.27 [dt, $^{3}J_{H\text{-}H}$ = 8.62 Hz, $^{3}J_{H\text{-}H}$ = 1.81 Hz, 1H, H^{4}], 7.21 – 7.16 [m, ^{3}H, H$^{3',4',5'}$], 7.10 [dd, $^{3}J_{H\text{-}H}$ = 7.92 Hz, $^{4}J_{H\text{-}H}$ = 1.86 Hz, 1H, H^{2}], 6.45-6.42 [m, 2H, H^{3,5}], 3.59 [hept, 2H, H^{b}], 1.37 [d, $^{3}J_{H\text{-}H}$ = 6.87 Hz, 6H, H$^{c'}$], 1.14 [d, $^{3}J_{H\text{-}H}$ = 6.85 Hz, 6H, H^{c}], -0.29 [d, $^{3}J_{P\text{-}H}$ = 3.19 Hz, $^{2}J_{Pt\text{-}H}$ = 73.34 Hz, 3H, H^{d}]. ^{13}C NMR (101 MHz, CDCl3): δ = 166.74 [s, C$^{1'}$], 162.12 [s, C^{a}], 146.76 [s, C^{6}], 141.54 [s, C$^{2',6'}$], 135.00 [s, C^{2}], 134.89 [Ph-C], 134.64 [s, C^{4}], 130.25 [d, $J_{P\text{-}C}$ = 2.08 Hz, Ph-C], 129.73 [s, C^{1}], 127.75 [d, $J_{P\text{-}C}$ = 10.80 Hz, Ph-C], 126.65 [s, C$^{4'}$], 123.15 [s, C$^{5,3',5'}$], 113.95 [s, C^{3}], 27.56 [s, C^{b}], 25.13 [s, C^{c}], 22.54 [s, C$^{c'}$], -18.93 [d, $J_{P\text{-}C}$ = 8.97 Hz, C^{d}]. ^{31}P NMR (121 MHz, $CDCl_3$): δ = 20.43 [s, $J_{P\text{-}Pt}$ = 4399.74 Hz]. EI-MS: *m/z* 753.3 [M]$^{+}$, 513.1 [M-(O-Ph)-(2,6-2-^{i}Pr-Ph)]$^{+}$. Anal. Found (calc. for $C_{31}H_{25}ClNOPPt$): C, 60.04 (60.63); H, 5.66 (5.36); N, 1.63 (1.86).

[Pd(CH$_3$){(OC$_6$H$_4$)CH=N{2,6-(CH$_3$CH$_3$CH)$_2$(C$_6$H$_3$)}}(PPh$_3$)] **(C12)**

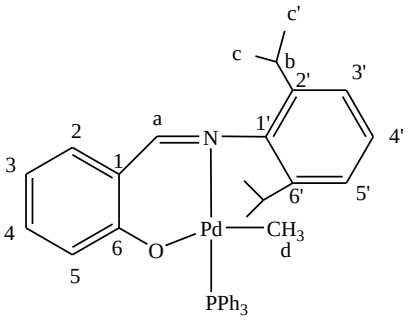

C12

To a methanol solution of imine **L$_B$** (0.225 g, 0.80 mmol) sodium acetate (0.10 g, 1. 5 mmol) was added. The reaction mixture was allowed to stir at room temperature for 30 min. This mixture was slowly added to a methanol solution (10 mL) of [Pd(COD)MeCl] (0.212 g, 0.80 mmol) at room temperature giving a clear yellow solution. PPh_3 (0.209 g, 0.80 mmol) was then added, giving a light orange precipitate **C12**. Yield 0.456 g (91%). M.p.: 203 - 208 ^{o}C. IR (KBr): ν (CH=N) 1608 cm^{-1}. ^{1}H NMR (300 MHz, $CDCl_3$): δ = 7.95 [d, $^{4}J_{P\text{-}H}$ = 11.47 Hz, 1H, H^{a}], 7.67 – 7.60 (m, 6H, Ph-H), 7.46– 7.34 (m, 9H, Ph-H), 7.21 – 7.15 [m, 4H, H$^{4,3',4',5'}$], 7.07 (dd, $^{3}J_{H\text{-}H}$ = 7.99 Hz, $^{4}J_{H\text{-}H}$ = 1.68 Hz, 1H, H^{2}), 6.44-6.38 (m, 2H, H^{3,5}), 3.59 [hept, 2H, H^{b}], 1.33 [d, $^{3}J_{H\text{-}H}$ = 6.88 Hz, 6H, H$^{c'}$], 1.13 [d, $^{3}J_{H\text{-}H}$ = 6.83 Hz, 6H, H^{c}], -0.43 [d, $^{3}J_{H\text{-}H}$ = 3.05 Hz, 3H, H^{d}]. ^{13}C NMR (101 MHz, $CDCl_3$): δ = 168.98 [s, C$^{1'}$], 165.41 [s, C^{a}], 147.31 [s, C^{6}], 141.02 [s, C$^{2',6'}$], 135.64 [s, C^{2}], 134.86 [d, $J_{P\text{-}C}$ = 11.76 Hz, Ph-C], 134.67 [s, C^{4}], 130.60 [s, C^{1}], 130.22 [d, $J_{P\text{-}C}$ = 2.08 Hz, Ph-C], 127.75 [d, $J_{P\text{-}C}$ = 10.80 Hz, Ph-C], 126.02 [s, C$^{4'}$], 123.21 [s, C$^{3',5'}$], 122.95 [s, C^{5}], 112.78 [s, C^{3}], 27.92 [s, C^{b}], 25.02 [s, C^{c}], 22.54 [s, C$^{c'}$], -0.14 [d, $J_{P\text{-}C}$ = 10.78 Hz, C^{d}]. ^{31}P NMR (121 MHz, $CDCl_3$): δ = 39.22 [s]. EI-MS: *m/z* 686.19 [M+Na]$^{+}$, 650.12 [M-CH$_3$]$^{+}$,

645.11 [M-CH_3 -5H]$^+$. Anal. Found (calc. for $C_{31}H_{25}ClNOPPt$): C, 68.12 (68.72); H, 6.66 (6.07); N, 2.03 (2.11).

6.4 Isomerization Kinetics (C5a→C5b)

NMR tubes (5 mm) were charged with 15 mg of **C5a**, which was dissolved at room temperature (293 K) in chloroform-d to a fixed volume of 600±5 μl. The tube was placed in a thermostated probe. The conversion **C5a→C5b** was then followed by the conventional ^{31}P NMR technique. All reactions obeyed a first-order rate law until over 90% of the reaction. Relative concentration of **C5a** vs. time data were acquired from ^{31}P NMR signal areas of **C5a** and **C5b** and fitted to the equation $\ln(a_0/a_t)$ vs. t (a_0 = relative concentration of **C5a** before heating = 100%; a_t = relative concentration of **C5a** at completion of the reaction) to obtain first-order rate constants k_{obs} from least-squares slopes (standard error are also given). Activation parameters were derived from a linear least-squares analysis of $\ln(k_{obs}/T)$ vs. T^{-1} data according to the linear expression of the Eyring equation:[5]

$$\ln\frac{k}{T} = \frac{-\Delta H^*}{R} + \ln\frac{k_B}{h} + \frac{\Delta S^*}{R} \qquad \text{(Eq. 5.1)}$$

where: R = 1.986 cal $mol^{-1}K^{-1}$, k_B = 8.62 x 10^{-5} eV K^{-1}, h = 4.14 x 10^{-15} eV S

and are listed in Table 4.9.

6.5 X-ray Structure Analysis

X-ray single crystal intensity data for structures were collected on a Nonius Kappa-CCD (**C1**, **C2a**, **C2b**, **C3**, **C4** and **C9**) or a Bruker KAPPA APEX II DUO (**C5a**, **C5b**, **C7** and **C13**) diffractometers using graphite monochromated MoKα radiation (λ = 0.71073 Å). Temperature was controlled by an Oxford Cryostream cooling system (Oxford Cryostat). The strategy for the data collections was evaluated using the Bruker Nonius "Collect" program. Data were scaled and reduced using DENZO-SMN software.[6] An empirical absorption correction using the program SADABS[7] was applied.

The structure was solved by direct methods and refined employing full-matrix least-squares with the program SHELXL-97[8] refining on F^2. Packing diagrams were produced using the

program PovRay and graphic interface X-seed.[9] All the non-hydrogen atoms were refined anisotropically. The hydrogen atoms were placed in idealised positions in a riding model with U_{iso} set at 1.2 or 1.5 times those of their parent atoms and fixed C-H bond lengths. The structure was refined successfully with final R = 0.0330. The parameters for crystal data collection and structure refinements, the bond lengths, angles, torsion angles and other molecular parameters (data sets 1 – 13) and the CIF files are given in Support Information.

6.6 Computational Methods

6.6.1 Hardware

The hardware used for the molecular modelling is the "Sun Hybrid System" based at the Centre of High Performance Computing (CHPC) in Cape Town.[10]

6.6.2 Software

All computational results in this study were calculated using the DMol^3 density functional theory (DFT) code[11] as implemented in Accelrys MaterialsStudio (Version 5.5). DFT was used since it usually gives realistic geometries, relative energies and vibrational frequencies for transition metal compounds. The nonlocal generalized gradient approximation (GGA) exchange-correlation functional was employed in all geometry optimizations, viz., the PW91 functional of Perdew and Wang.[12] DMol^3 utilizes a basis set of numeric atomic functions, which are exact solutions to the Kohn-Sham equations for the atoms.[13] These basis sets are generally more complete than a comparable set of linearly independent Gaussian functions and have been demonstrated to have small basis set superposition errors. In the present study an all-electron polarized split valence basis set, termed double numeric polarized (DNP), has been used. All geometry optimizations employed highly efficient delocalized internal coordinates.[14] The use of delocalized coordinates significantly reduces the number of geometry optimization iterations needed to optimize larger molecules compared to the use of traditional Cartesian coordinates. The tolerance for convergence of the self-consistent field (SCF) density was set to 1×10^{-5} hartrees, while the tolerance for energy convergence was set to 1×10^{-6} hartrees. Additional convergence criteria include the tolerance for converged gradient (0.002 hartrees/ Å) and the tolerance for converged atom displacement (0.005 Å).

Self-consistent-field (SCF) convergence problems are frequently encountered for open shell organometallic systems. To enhance SCF convergence efficiency during optimization of stationary points, a small electron thermal smearing value of 0.005 Ha was specified for all calculations unless explicitly stated to the contrary. The thermal smearing option in MaterialsStudio makes use of a fractional electron occupancy scheme at the Fermi level according to a finite-temperature Fermi function.[12,15]

In selected cases optimized geometries were subjected to full frequency analyses at the same GGA/PW91/DNP level of theory to verify the nature of the stationary points. Equilibrium geometries were characterized by the absence of imaginary frequencies. Preliminary transition state geometries were obtained by either the DMol3 PES scan functionality in Cerius[16] (Version 5.5, Accelrys, Inc.) or the integrated linear synchronous transit/quadratic synchronous transit (LST/QST) algorithm[17] available in MaterialsStudio. These preliminary structures were then subjected to full TS optimizations using an eigenvector following algorithm. All transition structure geometries exhibited only one imaginary frequency in the reaction coordinate.

All calculations were performed without the incorporation of solvent effects; motivated by the fact that Pd-catalysed ethylene oligomerization is commonly performed in nonpolar solvents such as toluene and cyclohexane. All results were mass balanced for the isolated system in the gas phase. The reported energies refer to Gibbs free energy corrections to the total electronic energies at 298.15 K and 1 atm, unless explicitly stated to the contrary.

The following aspects were investigated with the use of molecular modelling:

- The role of MAO in the precatalyst activation, i.e. the Pd/MAO interactions according to Scheme 2.7 in Chapter 2. This approach was investigated to gain insight into the possible active species obtained from Pd/MAO interactions (in Chapter 2).
- The possible mechanisms of Pd-catalysed ethylene oligomerization based on the active species resultant from Pd/MAO interactions, i.e., the Cossee-type and metallacycle mechanisms. At GGA/PW91/DNP level, the complete geometry optimization and full frequency analysis were performed (in Chapter 2).
- Three possible mechanisms of geometry isomerization **C5a→C5b** (in Chapter 4).

6.7 References

1. D. D. Perrin and W. L. F. Araregо, *Purification of Laboratory Chemicals*, 1988, Pergamon Press, Oxford.
2. (a) N. W. Mungwe, M.Sc. thesis, University of Western Cape, **2008**; (b) N. Mungwe, A. Swarts, S. F. Mapolie and G. Westman, *J. Organomet. Chem*., 2011, **696**, 3527.
3. (a) J. H. Price, A. N. Williamson, R. F. Schramm and B. B. Wayland, *Inorg. Chem*., 1972, **11**, 1280; (b) V. Y. Kukushkin, A. J. L. Pombeiro, C. M. P. Ferreira and L. I. Elding, *Inorg. Synth*., 2002, **33**, 189.
4. C. Wang, S. Friedrich, T. R. Younkin, R. T. Li, R. H. Grubbs, D. A. Bansleben and M. W. Day, *Organometallics*, 1998, **17**, 3149.
5. B. K. Carpenter, *Determination of Organic Reaction Mechanisms*; Wiley-Interscience: New York, 1984.
6. Z. Otwinowski and W. Minor, *Methods in Enzymology, Macromolecular Crystallography*, d. Carter Jr, C. W. & Sweet, R. M., part A, 1997, 276, 307-326, Academic Press
7. G. M. Sheldrick, SADABS, University of Göttingen, Germany, 1996.
8. G. M. Sheldrick, SHELXL-97 and SHELXS-97, University of Göttingen, Germany, 1997.
9. L. J. Barbour, *J. Supramol. Chem*., 2001, **1**, 189.
10. www.chpc.ac.za.
11. (a) B. Delley, *J. Chem. Phys*. 1992, **92**, 508. (b) B. Delley, *J. Phys. Chem*. 1996, **100**, 6107. (c) B. Delley, *J. Chem. Phys*. 2000, **113**, 7756.
12. J. P. Perdew and Y. Wang, *Phys. ReV. B*, 1992, **45**, 13244.
13. B. Delley, In Modern Density Functional Theory: A Tool for Chemistry; Seminario, J. M., Politzer, P., Eds.; Theoretical and Computational Chemistry, Vol. **2**; Elsevier: Amsterdam, The Netherlands, 1995.
14. J. Andzelm, R. D. King-Smith and G. Fitzgerald, *Chem. Phys. Lett*., 2001, **335**, 321.
15. M. Weinert and J. W. Davenport, *Phys. Rev. B*, 1992, **45**, 13709.
16. D. Vogt, In Applied Homogeneous Catalysis with Organometallic Compounds; Cornils, B., Herrmann, W. A., Eds.; VCH: Weinheim, Germany, 1996; p. 245.
17. N. Govind, M. Petersen, G. Fitzgerald, D. King-Smith and J. Andzelm, *Comput. Mater. Sci*., 2003, **28**, 250.